Interaction of Biologically Relevant Nanoparticles with Cells Studied by Cryo Soft X-Ray Tomography

DISSERTATION

zur Erlangung des akademischen Grades

doctor rerum naturalium

(Dr. rer. nat.)

im Fach Chemie

eingereicht an der

Mathematisch-Naturwissenschaftlichen Fakultät

der Humboldt-Universität zu Berlin

von

M.Sc. Burcu Kepsutlu

Präsident der Humboldt-Universität zu Berlin

Prof. Dr.-Ing. Dr. Sabine Kunst

Dekan der Mathematisch-Naturwissenschaftlichen Fakultät

Prof. Dr. Elmar Kulke

Gutachter/innen: 1. Prof. Dr. Matthias Ballauff

2. Prof. Dr. Gerd Schneider

3. Prof. Dr. Helge Ewers

Tag der mündlichen Prüfung: 16.07.2018

Abstract

Nanoparticles are endocytosed and trafficked within cells by selecting one or more of the cell's intrinsic processing pathways. However, general rules which drive this selection have not yet been defined. Therefore, each nanoparticle has to be investigated separately to determine its endocytosis and intracellular trafficking pathways. In this thesis, such an analysis was performed for two different biologically relevant nanoparticles, namely dendritic polyglycerol sulfate (dPGS) coated gold nanoparticles (dPGS nanoparticles) and polyethyleneimine (PEI) coated gold nanoparticles (PEI nanoparticles), each with the same 50 nm core size and each used at the same concentration (0.13 nM). These nanoparticles were designed by our collaborators for therapeutic use. Specifically, dPGS nanoparticles are good candidates for the diagnosis and treatment of inflammation, and PEI nanoparticles are promising agents for targeted gene delivery. Neither nanoparticle has been used in clinical studies yet, since there are many unknowns about their behaviour in the human body including their cellular interactions. Specifically, the intracellular trafficking pathway of dPGS nanoparticles is unknown, and how PEI nanoparticles escape to the cytoplasm and whether they enter into the nucleus are highly controversial. To address these unknowns and controversies, cryo soft X-ray tomography was used which provides the ability to image endocytic compartments of near-native state cells in 3D and to track nanoparticles relative to these compartments at 40 nm spatial resolution without a need for staining, chemical fixation or slicing. Both dPGS nanoparticles and PEI nanoparticles were found to be endocytosed predominantly via macropinocytosis, and most nanoparticles became localized to endosomes, multivesicular bodies and lysosomes. Despite these similarities in trafficking, there were also key differences, demonstrating that the nanoparticle coat influences cellular trafficking. Some dPGS nanoparticles were also found in lipid droplets, a rarely observed destination for nanoparticle targeting, but no PEI nanoparticles were found in this compartment. At a concentration of 0.13 nM, PEI nanoparticles were observed to induce extensive rupture of lysosomes, leading to significant levels of cytoplasmic escape and nuclear entry. In contrast, no evidence for lysosomal rupture with dPGS nanoparticles was detected, and concomitantly very low levels of cytoplasmic escape and no nuclear entry were found. Interestingly, when the PEI nanoparticles concentration was reduced by ten-fold, a switch in the endocytosis pathway from macropinocytosis to a putative caveolae-mediated

endocytosis was observed. Importantly, under these conditions, PEI nanoparticles no longer induced lysosomal rupture, but nevertheless still yielded significant cytoplasmic escape and nuclear entry. This lack of lysosomal rupture at the lower concentration was correlated with reduced cellular damage, and so has important implications for use of PEI in gene delivery. Most surprisingly, both nanoparticle types were found to induce previously unreported global cytoplasmic alterations in the cells. Specifically, after incubation with either nanoparticle, consistent and significant changes in the number of endosomes, multivesicular bodies, mitochondria and lipid droplets were detected, as well as significant changes in lipid droplet size. These cytoplasmic alterations could reflect important physiological changes, but further work is required to determine this. In sum, a number of similar patterns were found in endocytosis, intracellular trafficking and morphological effects with the two types of nanoparticles analyzed. The differences, which were observed between the two nanoparticles, were consistent with their specific coating, and were therefore not surprising. These observations suggest that the behavior of biologically relevant nanoparticles might become more predictable in the future by further application of systematic studies such as this thesis in which the independent variable is restricted to only one, such as the surface coat or the concentration.

Kurzzusammenfassung

Nanopartikel werden von Zellen durch Endozytose aufgenommen und auf unterschiedlichen intrazellulären Transportwegen im Zytoplasma weiterverarbeitet. Allgemeine Regeln zur Voraussage der Transportwege wurden jedoch bisher noch nicht definiert. Derzeit muss jedes Nanopartikel separat untersucht werden, um seine Endozytose und seine intrazellulären Transportwege zu bestimmen. In dieser Arbeit wurde eine solche Analyse für zwei verschiedene biologisch relevante Nanopartikel durchgeführt, nämlich für dendritisch Polyglycerolsulfat (dPGS) beschichtete Goldnanopartikel (dPGS-np) und für Polyethylenimin (PEI) beschichtete Goldnanopartikel (PEI-np), welche jeweils die gleichen Nanopartikeldurchmesser von 50 nm haben und jeweils in der gleichen Konzentration (0,13 nM) eingesetzt wurden. Diese Nanopartikel wurden von unseren Kollegen für therapeutische Zwecke entwickelt. Insbesondere sind dPGS-np vielversprechend hinsichtlich Diagnose und Behandlung von Entzündungen, und PEI-np sind vielversprechende Partikel zur gezielten Genabgabe. Diese Nanopartikel wurde bisher nicht in klinischen Studien verwendet, da ihr Verhalten im menschlichen Körper einschließlich ihrer zellulären Wechselwirkungen noch weitgehend unbekannt ist. Insbesondere ist der intrazelluläre Transportweg von dPGS-np unbekannt. Wie PEI-np in das Zytoplasma entweichen und ob sie in den Zellkern gelangen ist ebenfalls umstritten. Um einen Beitrag zum Verständnis der Wechselwirkung dieser Nanopartikel mit Zellen zu leisten, wurden die Transportwege mittels Kryo-Röntgentomographie untersucht. Diese Mikroskopie mit weicher Röntgenstrahlung ermöglicht es, Zellen und gleichzeitig die Nanopartikel im nahezu nativen Zustand in 3D mit einer räumlichen Auflösung von 40 nm abzubilden. Es besteht dabei nicht die Notwendigkeit einer Färbung, einer chemischen Fixierung oder eines Aufschneidens der Probe. Diese 3D Untersuchungen zeigten, dass sowohl dPGS-np als auch PEI-np vorwiegend über Makropinozytose endozytiert werden und dass die meisten Nanopartikel in Endosomen, multivesikulären Körpern und Lysosomen lokalisiert sind. Trotz dieser Ähnlichkeiten im Verhalten beider Partikel gab es auch maßgebliche Unterschiede die zeigten, dass die jeweilige Beschichtung der Nanopartikel den intrazellulären Transport beeinflusst. Im Gegensatz zu PEI-np, wurden einige dPGS-np in Lipidtröpfchen gefunden, in welchen Nanopartikel im Allgemeinen eher selten beobachtet werden. Weiterhin verursachen die PEI-np bei einer Konzentration von 0,13

nM ein Zerplatzen von Lysosomen in erheblichem Ausmaß wodurch die Nanopartikel in das Zytoplasma entweichen und teilweise in den Zellkern eindringen. Im Unterschied dazu konnte kein Nachweis für ein Zerplatzen von Lysosomen durch dPGS-np erbracht werde und gleichzeitig konnten nur sehr wenige dPGS-np im Zytoplasma und keine dPGS-np im Zellkern gefunden werden. Interessanterweise wurde ein Wechsel des Endocytose-Weges von der Makropinozytose zu einer mutmaßlichen Caveolae-vermittelten Endozytose beobachtet, wenn die PEI-np-Konzentration um das Zehnfache reduziert wurde. Unter diesen Bedingungen induzierten PEI-np kein Zerplatzen von Lysosomen mehr, aber es wurde eine signifikante Zahl von Nanopartikeln im Zytoplasma und im Zellkern nachgewiesen. Das Ausbleiben von zerplatzten Lysosomen bei dieser niedrigeren Konzentration korreliert mit einer verringerten Zellschädigung und hat somit wichtige Auswirkungen auf die Verwendung von PEI beim Gentransfer. Überraschenderweise stellte sich heraus, dass beide Nanopartikelarten eine bisher nicht beobachtete umfassende zytoplasmatische Veränderungen in den Zellen induzierten. Insbesondere wurden nach der Inkubation mit beiden Nanopartikeln konsistente und signifikante Veränderungen in der Anzahl an Endosomen, an multivesikulären Körper, an Mitochondrien und an Lipidtröpfchen sowie signifikanten Veränderungen der Lipidtröpfchengröße festgestellt. Diese zytoplasmatischen Veränderungen könnten wichtige physiologische Veränderungen widerspiegeln, jedoch ist hierzu zusätzliche Forschung erforderlich. Zusammenfassend wurden zahlreiche ähnliche Mustern in der Endozytose, im intrazellulärem Transport und in morphologischen Effekten mit den zwei analysierten Nanopartikelarten gefunden. Die Unterschiede, die zwischen beiden Nanopartikelarten beobachtet wurden, passen wie zu erwarten zu ihrer spezifischen Beschichtung. Diese Beobachtungen deuten darauf hin, dass das Verhalten biologisch relevanter Nanopartikel in Zukunft vorhersehbarer werden kann durch weitere systematische Studien entsprechend der vorliegende Arbeit, in der sich auf eine unabhängige Variable beschränkt wurde, wie die Oberflächenbeschichtung oder die Konzentration.

TABLE OF CONTENTS

1. MOTIVATION AND PROBLEM STATEMENT

People are constantly exposed to nanoparticles (1 - 100 nm) in daily life. These nanoparticles either arise as by-products of various industrial processes or they are specifically developed for use by humans. For instance, nanoparticles are incorporated into a variety of consumer products in order to improve their quality, such as personal-care products, cosmetics, sporting goods and filtration devices [1].

Nanomedicine is another field in which nanoparticles are used [1, 2]. Based on their targeting capabilities, nanoparticles are being used to increase the efficiency of drug delivery and/or diagnosis of diseases. This is a very active area of current research, but the field is still in an embryonic state [2-4].

Many nanoparticles of various sizes, shapes, materials and surface functionalities have been synthesized so far, including ones with simple surface chemistries as well as much more complicated chemistries that are biologically relevant. The biologically relevant nanoparticles are designed to specifically target cells and sometimes even organelles by exploiting the environmental cues of the desired target site, such as pH, temperature or ionic content. Most of these nanoparticles are being tested for use in medical applications. Specifically, tests are performed to evaluate their physicochemical properties, their cellular interactions, their cytotoxicity, and their physiological effects on cells, their bio-distribution and their biocompatibility within animals. If the nanoparticles can pass these tests, they can be used in clinical trials [2, 3].

In order to synthesize nanoparticles specifically targeted to diseased cells or organelles, it is essential to understand the cellular interactions of the nanoparticle. Such an investigation is also vital to determine whether the nanoparticles reach their target, whether they localize to other unintended locations, whether they are eventually excreted, and whether they will induce unwanted side effects. For all of these reasons, the behavior and fate of nanoparticles in biological systems have been studied intensely.

This extensive investigation of nanoparticle - cell interactions has led to a number of important findings. The early systematic studies usually focused on nanoparticles with simple surface chemistries and demonstrated that the size, shape and surface charge of nanoparticles influence their uptake rates, cytotoxicity and their cellular destinations [3].

Specifically, 50 nm spherical nanoparticles are endocytosed most efficiently by cells compared to other sizes [5-7], and positively charged nanoparticles are preferentially endocytosed compared to negatively charged nanoparticles [8]. Additionally, proteins in biological fluids attach to nanoparticle surfaces and form a so-called protein corona, which typically alters the behavior of nanoparticles on and within cells [9, 10]. Furthermore, these early studies showed that nanoparticles are endocytosed via different endocytosis pathways and trafficked within the cell using various intrinsic cellular pathways [9, 11]. However, in the current literature [11], there are conflicting reports concerning the effect of a nanoparticle's physicochemical properties on its endocytosis and intracellular trafficking pathway. These conflicts and contradictions have only grown worse with the development of biologically relevant nanoparticles. It has become obvious that it is not possible to directly transfer the already conflicting knowledge about the endocytosis and intracellular pathways obtained from nanoparticles with simple surface chemistries to those with biologically relevant chemistries. Therefore, most studies of biologically relevant nanoparticles have usually focused on one particular type of coating and examination of its trafficking pathway in detail. Since these nanoparticles often present a wide variability in their physicochemical properties, it is very difficult to compare published studies in order to derive general rules about nanoparticle interactions, since multiple variables defining the nanoparticle properties change between one study to the next.

The focus of this thesis, like many other current studies, is individual, biologically relevant nanoparticles, namely dPGS-coated gold nanoparticles and PEI-coated gold nanoparticles. dPGS nanoparticles are designed for simultaneous diagnosis and treatment of inflammation [12]. PEI nanoparticles are designed for targeted gene delivery [13, 14]. Note that neither of these nanoparticles has been used in clinical trials yet, since there are many unknowns about their effects on biological systems. Therefore, in this thesis, some of the unknowns about the cellular interactions of these nanoparticles will be addressed in order to contribute to their future development for potential clinical use.

Furthermore, in contrast to current practice in the literature, the effect of the biological coating on nanoparticle – cell interactions will also be systematically and simultaneously analyzed by comparing the cellular interaction of dPGS and PEI nanoparticles. This

systematic analysis was possible since these nanoparticles differed only in their coat, but contained the same core, namely a citrate stabilized 50 nm spherical gold nanoparticles, and were applied at the same concentration to the same cell type. Note that gold nanoparticles are selected here since they can be easily functionalized and observed via various imaging techniques due to gold nanoparticles' unique light absorption and scattering properties [15-17].

dPGS is an anionic polysulfated analogue of dendritic polyglycerol [18]. dPGS compounds accumulate at inflammation sites due to their high affinity towards two cell-surface molecules, L-selectin and P-selectin, which are enhanced at inflammation sites [19, 20]. According to published studies, dPGS can exert its diagnostic and therapeutic effects against inflammation simply by binding to these cell surface molecules on the plasma membrane, and therefore dPGS nanoparticles would not need to enter into the cells. However, previous studies have shown that dPGS is internalized by cells [21-26], and this raises questions about the effect of this internalized dPGS on the cells. Current studies report that dPGS does not exert significant cytotoxicity according to evaluations of mitochondrial metabolic activity and nuclear membrane integrity [21, 27-31]. However, many important aspects of dPGS interactions with cells remain unknown, including the endocytosis pathway, the intracellular trafficking pathway and the end-points of this compound within the cell. The cellular distribution of nanoparticles is important for understanding potential side-effects and the mode-of-function of the nanoparticles. Therefore, answering these questions about the cellular interaction of dPGS compounds, which is one goal of this thesis, is important for the further development of dPGS-based therapeutic and diagnostic agents for inflammation.

The other compound analyzed in this thesis, PEI, is a cationic polymer with a high content of unprotonated amines. PEI is used as a targeted gene delivery tool in order to carry exogenous genes to the cytoplasm and nucleus of cells to treat genetic diseases [32-34]. Specifically, RNA molecules need to be delivered to the cytoplasm and DNA molecules need to be delivered into the nucleus. However, targeting the cytoplasm or nucleus is not straightforward, since most nanoparticles enter cells by endocytosis, and then may remain within membrane-bound endocytic vesicles. PEI was reported to enhance the efficiency of gene delivery probably due to its ability to destabilize these

membrane vesicles, thereby facilitating the cytoplasmic escape of genetic material into the cytoplasm [13, 35]. Conjugation of PEI on gold nanoparticles was also reported to enhance the efficiency of gene delivery [13, 36]. However, the cytoplasmic escape mechanism together with the endocytosis pathway and intracellular trafficking of PEI nanoparticles are still controversial topics in the literature [37-42]. Specifically, it is still not clear whether PEI ruptures vesicles or instead creates temporary pores on these vesicles in order to escape to the cytoplasm [33, 43]. Moreover, whether PEI nanoparticles escape to the cytoplasm through lysosomes or some other organelle remains a critical, unanswered question [42, 44-50]. Additionally, whether PEI can enter into the nucleus to deliver DNA is still a controversial issue [33]. Answering these questions, which is another goal of this thesis, is important for the development of more efficient PEI-based gene delivery tools. Related to these questions, is the role of PEI nanoparticle concentration in cytoplasmic escape. According to previous studies, the number of unprotonated amines is proportionally correlated with the gene delivery efficiency and the cytotoxicity of the nanoparticles [51]. However, the reason for this observation has not been studied before. In this thesis, a hypothesis is proposed that the concentration of PEI nanoparticles may affect the cytoplasmic escape mechanism, hence altering the efficiency and cytotoxicity of PEI nanoparticles.

In the past, nanoparticle - cell interaction studies were usually performed by transmission electron microscopy (TEM) and fluorescence microscopy (FM) [52-56]. However, these techniques have some limitations. For instance, previous nanoparticle - cell studies by TEM are based on the observation of only a very limited number of 2D sections from the cell. Therefore, the 3D nature of nanoparticle - cell interactions cannot be completely observed. Hence, rare nanoparticle events such as cytoplasmic escape and nuclear entry can be easily missed [57, 58]. Additionally, these TEM studies often relied on samples which were chemically fixed, stained and embedded in plastic. These non-native procedures can alter the ultrastructural details of cells and also yield artefactual data [59-61]. In contrast, FM can provide 3D information from live cells. However, this technique requires fluorescence labeling of features of interest. This requirement almost always limits the number of features that can be simultaneously observed in the cell to three or four. Therefore, the unlabeled features cannot be observed, and a complete picture of nanoparticle - cell events cannot be gathered [59].

In this thesis, cryo soft X-ray tomography will be used to examine nanoparticle - cell interactions. Cryo soft X-ray tomography is a 3D technique which allows simultaneous detection at 40 nm spatial resolution of both membrane-bound organelles and gold nanoparticles without a need for slicing, staining or chemical fixation [62, 63]. Therefore, with this technique, rare events including cytoplasmic escape and nuclear entry can be observed free of sample preparation artefacts.

Cryo soft X-ray tomography will also be used to analyze the effect of nanoparticles on the global ultrastructural content of the cells. There have been limited studies of the effects of nanoparticles on cell morphology, even though this morphology can provide significant insights into the functional state of the cell [64, 65]. Recently, it has been shown that nanoparticles can alter the morphology of individual organelles [66]. However, an analysis to investigate the global ultrastructural effects of nanoparticles on cells has not been performed before. Therefore, in this thesis, the global ultrastructural effects of dPGS and PEI nanoparticles on cells will also be analyzed. In this thesis, a hypothesis is proposed that this morphological analysis could reflect important physiological alterations within the cell which are not easy to detect with simple biochemical assays.

In sum, this thesis will provide new information on the cellular interactions of dPGS and PEI nanoparticles that will be important for their further development as potential therapeutic agents. Key areas of focus will be the cellular trafficking pathways and the global cytoplasmic organization observed after treatment with either nanoparticle. For PEI nanoparticles, an additional focus will be on the mechanism of cytoplasmic escape and the impact of PEI nanoparticles concentration on this mechanism. Finally, because only one variable has been changed at a time in this thesis, it will also be possible to compare the cellular behaviors of dPGS and PEI nanoparticles in order to understand the effect of either the coating or the concentration on cellular behavior. The results of this comparison will suggest how it may be possible to define some general rules about nanoparticle - cell interactions that may one day make it easier to design nanoparticles tailored for specific treatments.

2. NANOPARTICLES FOR SPECIFIC BIOMEDICAL APPLICATIONS IN NANOMEDICINE

As explained in the Introduction, the cellular interactions of biologically relevant gold nanoparticles will be investigated in this thesis. The field of nanomedicine includes various types of nanoparticles used to treat and diagnose diseases. Therefore, this chapter will first introduce nanomedicine as a biomedical field which utilizes nanoparticles. Later, the chapter will provide examples of some of these nanoparticles for various biomedical applications.

2.1 Nanomedicine aims to improve drug delivery and diagnostics via use of nanoparticles

Nanomedicine is application of nanoparticles in order to diagnose, prevent and treat diseases or to investigate the patho-physiology of diseases in order to improve the quality of life [67]. Nanoparticles are materials which have at least one dimension in the nanometer regime between 1 - 100 nm [68]. They have enormous potential in biomedical applications, including the ability to improve the sensitivity, effectiveness and efficacy of not only current drugs but also biomedical imaging systems. As a consequence, there is great interest in their development. Indeed, each hour of every day at least one article is being published about nanomedicine with an aim to create better tools for targeted drug delivery, diagnosis, *in vivo* imaging, *in vitro* probing and theranostics, which is a clinical field aiming to combine therapeutic and diagnostic capabilities into one biomedical tool by using nanoparticles [67, 69].

Compared to current drugs, nanoparticles have many advantages. One of these advantages is the reactivity and the ease of functionalization with polymers or biologically relevant targeting molecules such as antibodies and receptor specific proteins. Therefore, nanoparticles can target specific sites and deal with the health problems at the same scale as the biomolecules involved. Also, by changing the size and shape of nanoparticles, their transport kinetics can be altered. This may provide higher stability and hence increase blood circulation times compared to bulk drugs. Additionally, nanoparticles show many unique and size-dependent optical properties which make them promising candidates for *in vivo* and *in vitro* imaging tools [4].

In nanomedicine, nanoparticles are first designed and synthesized. Then, they are characterized at the cell, tissue and organismal level. First, their cellular interactions are

analyzed to ensure that nanoparticles reach their targets without causing adverse effects on the cells. Then, some animal studies are performed to understand the biocompatibility and bio-distribution of nanoparticles. If nanoparticles can pass these characterization tests, nanoparticles enter clinical trials. The eventual success of a medical product to be able to enter into a phase I clinical trial is estimated to be only 10%. Even though nanoparticle characterization is a very tedious procedure, more than 200 nanomedicine products have already entered into clinical trials and some of them have been approved by the Food and Drug Administration (FDA) [15]. This outcome shows the potential and the reality of nanomedicine.

However, nanomedicine is still at its infancy and more time is required to reach its potential. For instance, a few previously FDA-approved iron-oxide nanoparticles have been discontinued [70], and the FDA has also published some safety announcements about previously approved gadolinium nanoparticles. These events suggests that both nanoparticles designs and their characterization techniques still needs to be improved [71].

2.2 Organic, inorganic or hybrid nanoparticles are used for various biomedical applications

In nanomedicine, many nanoparticles are used for various biomedical applications. These nanoparticles can be classified according to their chemical composition, size, shape, porosity, surface charge, surface functionality, hydrophobicity/hydrophilicity and opti-electronic properties. They can be composed of organic or inorganic material or both. Any of these nanomaterials can be conjugated with macromolecules such as targeting peptides and polymers to enhance their targeting and delivery efficiencies and contrast agents to enhance their imaging. These nanoparticles are designed for various applications such as *in vivo* diagnosis, *in vitro* and *ex-vivo* molecular probing and drug delivery [15, 68]. In this thesis, biologically relevant gold nanoparticles will be used. These nanoparticles will be reviewed in the next Chapter (Chapter 3). The purpose of this chapter is to provide an overview of the different kinds of nanoparticles currently used in nanomedicine, and some examples of how they are being used.

2.2.1 High atomic number nanoparticles for *in vivo* computed tomography (CT)

In vivo computed tomography (CT) is used to image the structure of hard and soft tissue. This imaging technique is based on the difference of the linear absorption coefficient for different material. The X-ray absorption of low atomic number elements found in soft tissue is not high enough for direct imaging. Therefore contrast agents, which are composed of high atomic number elements such as iodine and barium, are often used. However, their blood circulation times are short, since they are easily absorbed by tissues before they reach the disease site. In order to obtain high contrast at the disease site, a large amount of iodine and barium must be administered to the patient, and this induces undesirable side effects. To reduce the amount of contrast agent required for CT, hence the side effects, high atomic number nanoparticles such as gadolinium oxide nanoparticles and gold nanoparticles have been suggested [72]. These nanoparticles can be used at lower concentrations compared to conventional contrast agents because their blood circulation time is higher and also because they can be targeted to diseased soft tissues by functionalization with targeting moieties and thereby create the required contrast exactly where it is needed [73]. For instance, heparin functionalization of gold nanoparticles increases their localization in both Kupffer cells and endothelial cells lining the liver. This increased localization has the potential to enhance liver-specific CT imaging and at much lower concentration levels compared to conventional procedures [74]. Similarly, folic acid conjugation to gold nanoparticles was found to enhance tumor targeting [73, 75], and high-density-lipoprotein-coated nanoparticles enhanced atherosclerosis targeting [76]. Therefore, usage of high atomic number nanoparticles can enhance *in vivo* imaging via CT.

2.2.2 Quantum dots for *in-vitro* and *ex vivo* diagnostics

Diagnostics can also be done *ex vivo* by analyzing specimens taken from the patients for the presence of inflammation or cancer biomarkers. One technique to detect these biomarkers is labeling them with organic fluorophores. However, these analyses are limited by the low concentrations of biomarkers, especially at the early stages of the diseases, thereby lowering the chances of early prevention. In addition, fluorescent labels are relatively inefficient and insensitive, since they suffer from short fluorescence lifetimes and auto fluorescent signals of organic tissue may interfere with the fluorescence signal of the label [77]. Additionally, fluorescent labeling cannot be used for

simultaneous imaging of multiple different markers, since fluorescence labels have broad bandwidths which overlap with each other [78]. These disadvantages of fluorescence labeling in *ex vivo* diagnostics can be addressed by using quantum dots as molecular probes.

Quantum dots (QDs) offer a viable alternative for labeling by organic fluorophores. Compared to organic fluorophores, QDs are 20 times brighter and resistant to photo-bleaching even at corrosive conditions, highly acidic or basic conditions and at various salt concentrations. Additionally, QDs have a broad absorption band. Therefore, multiple QDs can be excited simultaneously by a single wavelength of light [77, 79]. These properties make QDs ideal candidates for multiplex analysis to detect multiple proteins and genes simultaneously down to 1 pM [79, 80]. QDs are also reported for *in vivo* molecular probes after polymer coating [81, 82] and coupling to targeting moieties such as biotin [81], oligonucleotides [82, 83] and antibodies [84].

2.2.3 Surface-enhanced Raman spectroscopy (SERS) nanoparticles as nanoprobes and labels

SERS nanoparticles are plasmonic nanoparticles, more precisely gold and silver, coupled to a reporter which presents a characteristic Raman spectrum. Depending on the type of reporter, SERS nanoparticles can be used as molecular probes for *in vitro* pH measurements, quantification of reactive oxygen species [85], and as labels for *in vivo* diagnosis [86] and cell phenotyping [78]. As molecular labels and probes for biomedical detection, SERS nanoparticles have various advantages over fluorescence labels such as stability against photobleaching and multiplexing ability [78, 87]. They also minimize autofluorescence effects since SERS nanoparticles are effective at near-infrared (NIR) light which is not absorbed by tissues. Since penetration depth of NIR light to tissue is high (up to several hundred microns) noninvasive *in vivo* measurements become possible, as demonstrated by the detection of an inflammation marker in an animal model system [86].

2.2.4 Plasmonic nanoparticles for induction of site specific cell death

Some nanoparticles can be stimulated via external conditions such as pH, temperature, metabolites, ions and light. This enables targeted activation at specific sites in the body for different therapeutic purposes [88]. Plasmonic nanoparticles are one type of

activatible nanoparticle. They can be stimulated by NIR light which is not absorbed by tissue. When a tumor with targeted plasmonic nanoparticles is illuminated with NIR light, the nanoparticles will absorb this light and transform it to heat. This heat, then, will kill the tumor cells which have internalized these nanoparticles [89]. Plasmonic nanoparticles, therefore, constitute an example of inorganic nanoparticles for targeted therapeutics.

2.2.5 Lipid based nanoparticles for targeted drug delivery

Lipid based nanoparticles have attracted great interest as targeted drug delivery agents because they can be loaded with drugs, conjugated with targeting moieties, stabilize therapeutic compounds and provide increased blood circulation time compared to conventional drugs. Additionally, their physicochemical properties such as size, shape and surface charge can be manipulated to address many biomedical problems.

Liposomes are phospholipid based nanoparticles. More than 30 liposomal nanoparticles are under clinical investigation [15]. Many liposomes such as polyethylene glycol-conjugated liposomes and cationic liposomal-based drugs are FDA approved [90]. This success of liposomes is due to their phospholipid content and unique structures. Their phospholipid content is important because phospholipid is the main component of both the cell's plasma membrane and cellular vesicles that the nanoparticles are targeting. Due to their phospholipid content, liposomes can easily incorporate into phospholipid bilayers of these various cellular membranes and thereby aid in drug delivery. Furthermore, the structures of liposomes are suitable for delivery of both hydrophilic and hydrophobic materials. This is because liposomes are composed of an outer phospholipid layer which encapsulates an aqueous space. The lipid bilayer entraps the hydrophobic materials and the aqueous center entraps the hydrophilic ones [91].

Exploiting these various advantages, liposomes have been loaded so far for preclinical studies with contrast agents for simultaneous diagnosis and treatment, anticancer drugs to treat cancer, natural products such as curcumin to treat inflammation [92], nucleic acids for gene therapy and many other biomedical agents such as antibiotics, antifungals and anesthetics to address various biomedical conditions. Liposomes are also coupled to targeting moieties to enhance their targeting ability [93, 94].

2.3 Summary

Nanomedicine is application of nanoparticles to solve various biomedical problems such as treating and diagnosing diseases. Nanoparticles have the potential to improve current biomedical imaging techniques and targeted drug delivery. However, the field is at an early stage and requires time and effort to reach its promised potential.

3. GOLD NANOPARTICLES: OPTICAL PROPERTIES, SYNTHESIS and FUNCTIONALIZATION FOR TARGETED DELIVERY OF ANTI-INFLAMMATORY AGENTS AND GENES

The preceding chapter provided an overview of nanoparticles now in use or under development for nanomedicine. In this chapter gold nanoparticles will be described in detail since gold nanoparticles are used in this thesis. This chapter will discuss the properties which make gold nanoparticles promising tools, their synthesis, and the significance of functionalization in nanomedicine. In this chapter, specifically, two functional coatings of gold nanoparticles that are investigated in this thesis will be introduced: specifically dPGS-coated gold nanoparticles to target inflammation and PEI-coated gold nanoparticles for targeted gene delivery. Finally, some of the key unanswered questions about these two functional coatings and their behavior within cells will also be introduced. The experimental part of this thesis, will then address these unanswered questions.

3.1 Gold nanoparticles are promising candidates for treatment and diagnosis of diseases

Gold nanoparticles are being developed for diagnostics, biosensing, targeted drug delivery and theranostics. There are many reasons for this interest in gold nanoparticles [15-17]. Due to their high atomic number and localized surface plasmons, gold nanoparticles possess unique absorption and scattering properties making them especially useful for diagnostics. Additionally, these optical properties can easily be altered for a specific application through a wet chemical reduction method [15-17, 95, 96]. Gold nanoparticles are also preferred for targeted drug delivery since they can be easily functionalized with moieties to enhance their targeting abilities and with various coating materials to address biomedical issues such as the protein corona (i.e. proteins associated with the nanoparticle surface) and cytoplasmic escape [15-17]. Moreover, by combining the unique optical properties and targeting abilities of nanoparticles, theranostic agents can be developed to image and treat diseases simultaneously. However, no gold nanoparticles have yet to be approved by the FDA. Even though they are promising tools and some gold nanoparticles are under clinical studies, they need to be optimized and tested for their effects in biological systems until the intended results are obtained [15-17].

As already discussed in Chapter 2, gold nanoparticles are promising candidates for *in vivo* and *in vitro* diagnosis via X-ray tomography since they have high atomic number (Z = 79) and large X-ray attenuation coefficients. Therefore, gold nanoparticles absorb X-rays more than surrounding organic molecules and this generates greatly improved contrast in images obtained by X-ray tomography [15, 17].

Gold nanoparticles are also special due to their surface plasmon resonance. When gold nanoparticles are illuminated with an electromagnetic field at certain frequencies, the conduction electrons of gold nanoparticles undergo collective oscillations along the direction of the electric field. These oscillations are called localized surface plasmons and resonate with the frequency of incident light. Gold nanoparticles exhibit localized surface plasmons usually in the visible region [17, 95]. These plasmons provide gold nanoparticles unique light absorption and scattering properties which are utilized in many biomedical applications.

First, localized surface plasmon resonance (LSPR) of gold nanoparticles offers great potential for bio-sensing applications such as molecule identification via surface-enhanced Raman spectroscopy. With Raman spectroscopy, Raman active molecules can be identified via their unique vibrational energy levels through corresponding Raman scattering fingerprints. In surface enhanced Raman spectroscopy, these molecules adsorb on or position in close proximity to a plasmonic nanoparticle (like gold nanoparticles) and their Raman scattering is enhanced up to a factor between 10^6 and 10^{14}. As a result, molecules can be identified with higher specificity and sensitivity [97]. This enhancement is reported to be highly reproducible with gold nanoparticles since their size and shape can be controlled to yield a monodisperse solution. This enhancement is useful for the *in vivo* and *in vitro* localization of specific molecules, and also for *in vivo* pH and temperature measurements which can be accomplished by using pH and temperature sensitive Raman active molecules in the vicinity of the gold nanoparticles [85, 98, 99].

Second, due to LSPR, gold nanoparticles strongly absorb and scatter light, dependent on their physiochemical properties such as size, shape and surface modification [95]. These tunable absorption and scattering properties of gold nanoparticles are exploited in both photothermal therapy and biomedical imaging. In photothermal therapy, the absorption property of gold nanoparticles is exploited. According to Mie light scattering theory, light

is primarily absorbed by a small gold nanoparticle (~20 nm) when illumination is in the visible to NIR range [96]. This absorbed light is converted into heat, which is the basis for photothermal therapy. In this therapy, gold nanoparticles can be targeted using a variety of strategies to bind specifically to cancer cells. When the cancerous tissue is illuminated with NIR light, the gold nanoparticles absorb the light, and transform it to heat which kills the cancer cells [89]. For example, Auroshell® is a 20 nm silica nanoparticle coated with a gold layer that has been developed for phototherapy against head and neck cancer [15].

For biomedical imaging applications, the scattering of light by gold nanoparticles is exploited. Scattering of the incident light increases with nanoparticle size [96]. As a consequence, larger gold nanoparticles are usually selected for real-time optical imaging of both cells and tissues via dark field microscopy, multiphoton resonance microscopy and photoacoustic tomography [12]. These techniques detect the scattered light from the gold nanoparticles to localize them on cells and tissues. The shape of gold nanoparticles also changes their scattering properties. Gold nanorods, for example, scatter ten-fold more light than nanospheres, and therefore yield higher contrast for detection per micron [96]. Therefore, dependent on the application, gold nanoparticles may be employed with different sizes and shapes.

As the discussion above shows, gold nanoparticles of different sizes and shapes have different potential applications. Fortunately, the size and shape of gold nanoparticles can be easily controlled by using different top-down or bottom-up techniques [100, 101]. The top-down techniques usually depend on subdividing bulk material into smaller units, while the bottom-up techniques depend on controlled growth of metal ions into gold nanoparticles, and include procedures such as wet chemical reduction, thermal decomposition and sol-gel synthesis [101].

A widely used chemical technique for nanoparticle synthesis is wet chemical reduction [100]. In this approach, a metal salt is reduced with a reducing agent such as sodium borohydride, ascorbic acid, trisodium citrate or alcohols in the presence of a stabilizing agent such as sodium citrate and cetrimonium bromide (CTAB), or polymers. Stabilizing agents attach on the nanoparticle surface and provide electrostatic or steric stabilization [100]. For instance, in the Turkevich method, gold nanoparticles are produced by

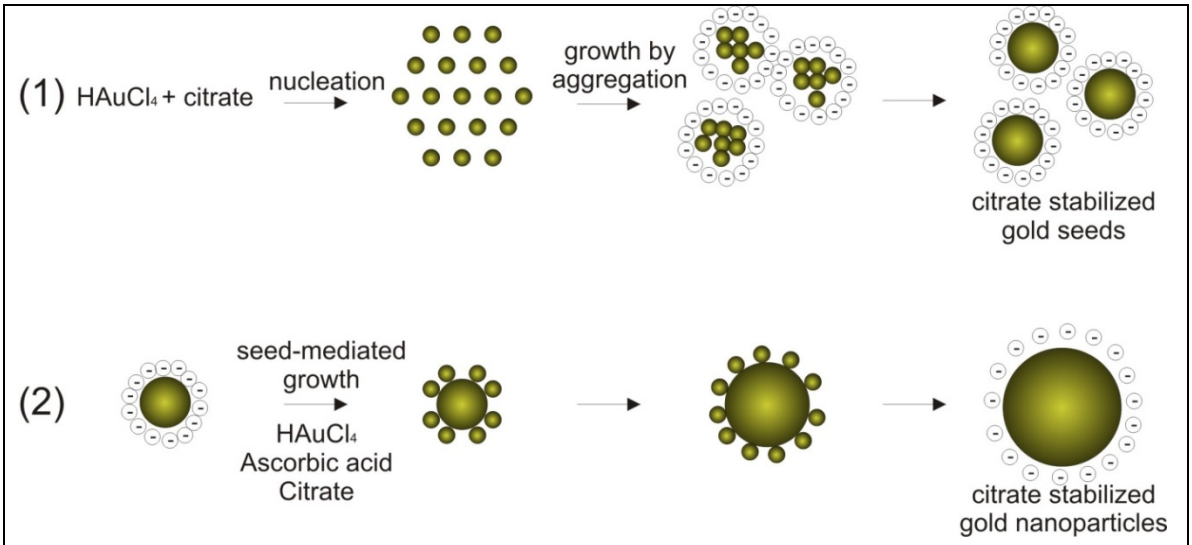

Figure 3.1 Synthesis of gold nanoparticles via a citrate-mediated seed-growth mechanism. At the first step, chloroauric acid ($HAuCl_4$) is reduced by citrate to generate citrate stabilized gold seeds through nucleation and growth by aggregation. At this step, gold ions (Au^{3+}) are reduced to gold atoms (Au^0) by the following formula $2AuCl_4^- + C_6H_5O_7^{-3} + 2H_2O \rightarrow 2Au + 3CH_2O + 3CO2 + 8Cl^- + 3H^+$ (1). Then, gold salts are reduced on citrate stabilized gold seeds via ascorbic acid to produce citrate stabilized gold nanoparticles of a desired size. Ascorbic acid is selected since it is a weak reducing agent which would prevent further nucleation and promote anisotropic growth of gold nanoparticles. Citrate acts as the stabilizing agent to obtain monodispersed nanoparticles (2).

chemical reduction of chloroauric acid ($HAuCl_4$) using citrate in which gold ions (Au^{3+}) is reduced to gold atoms (Au^0) in water (Fig. 3.1.1) [102]. The Turkevich method yields citrate stabilized monodisperse spherical gold nanoparticles with a diameter of around 10 - 20 nm (Fig. 3.1.1). Larger gold nanoparticles can be produced by modifications of this technique, and this can yield a monodisperse size distribution up to 120 nm. For example, a seed-mediated growth approach can be used to control both the shape and size of gold nanoparticles (Fig. 3.1.2) [103].

The cores of the nanoparticles that are used in this thesis (which are dPGS-coated and PEI-coated gold nanoparticles) were synthesized by our collaborators using this seed-mediated growth procedure. Specifically dPGS nanoparticles were designed by the group of Prof. Rainer Haag at the Free University of Berlin and PEI nanoparticles were synthesized by the group of Prof. Miriam Breunig at Regensburg University. As exemplified by Vonnemann et al. [103], at the first step of this procedure, 16 nm citrate-stabilized gold nanoparticles were prepared by reducing gold salt via trisodium citrate at 110 ºC. The formation of these seed nanoparticles was monitored by observing a color

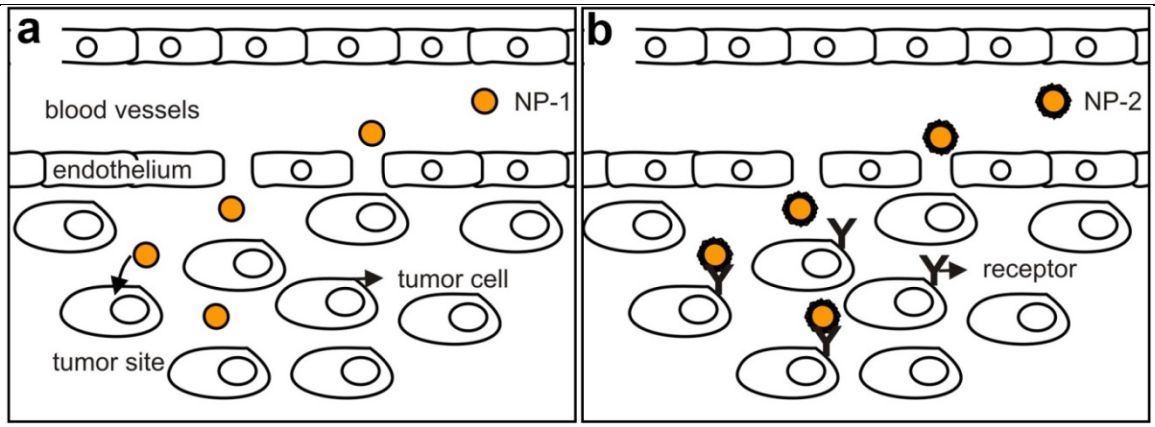

Figure 3.2 Passive accumulation of nanoparticles and targeted delivery of nanoparticles via targeting moieties. The nanoparticles (NP - 1) can accumulate at the disease site due to leaky vessels during passive accumulation (a). However, if nanoparticles are coupled with targeting moieties (NP - 2), they are targeted to specific cell surface receptors or proteins (b).

change of the solution from pale yellow to deep red. Then, to induce seed-mediated growth, the 16 nm seed nanoparticles were transferred to a new solution, and the reducing agents ascorbic acid and citrate were added to achieve a controlled growth via gold salt deposition on the seed nanoparticle surface. This reaction yielded monodispersed 50 nm citrate-stabilized gold nanoparticles [14, 103].

3.2 Functionalization and coating of gold nanoparticles for targeted drug delivery

Gold nanoparticles, lipid based and polymeric nanoparticles can all be targeted to disease sites to diagnose and treat tumors or inflammation and they can also be used for delivery of genes to diseased cells for gene therapy. The delivery of these different nanoparticles to a specific target cell or tissue may occur via either passive accumulation (Fig. 3.2a) [104] or active targeting (Fig. 3.2b) [105, 106]. Passive accumulation relies on relatively higher accumulation of nanoparticles at the disease sites compared to other healthy tissue due to the enhanced permeation and retention (EPR) effect (Fig. 3.2a) [104, 107]. Active targeted delivery is designed to increase the specificity of passive accumulation by coupling nanoparticles to targeting moieties or to biologically relevant polymers (Fig. 3.2b) [105-107]. These targeting moieties and biologically relevant polymers can direct the nanoparticles to specific cell-surface receptors or to other biomolecules which are overexpressed at the disease sites [105-107]. Once localized to these sites, biologically relevant biomolecules on the nanoparticle can react to physical

and chemical cues such as temperature, light and pH at the disease site, and produce some desired effect, such as localized cell death or specific release of a drug at the site [108].

In this thesis, nanoparticles, which are actively targeted to their target cells and organelles, are utilized. The first one is dPGS nanoparticles and they are designed to accumulate at inflammation sites due to their high affinity to cell surface molecules, namely L- and P-selectins, which are overexpressed at inflammation sites [19, 20, 109]. The second one is PEI nanoparticles and they are designed to deliver exogenous genes into the cell cytoplasm by facilitating their cytoplasmic escape [13, 14, 35].

Coupling of nanoparticles with these targeting moieties or biologically relevant polymers is done through either physical [14] or chemical interactions between them [109, 110]. Physical interactions include spontaneous electrostatic and hydrophobic attraction [14]. Chemical interactions include [109, 110] covalent binding of targeting moieties and polymers to the nanoparticle surface via thiol derivatives and bifunctional linkers [105, 111]. For instance, a folic acid coupled gold nanoparticle was synthesized by Zhang et al. through chemical interactions [112]. These nanoparticles target folate receptors which are overexpressed in cancer cells. To couple folic acid on gold nanoparticles, they used glutathione as a bifunctional linker. Glutathione was conjugated to the gold nanoparticle via Au-thiol bonds using the thiol groups from cysteine moieties in glutathione. Then to conjugate folic acid to glutathione, the carboxyl group of glutathione was activated to react with the amine groups of folic acid [112]. In this thesis, dPGS- and PEI-coated gold nanoparticles are used. To couple dPGS and PEI on gold nanoparticles, chemical and physical interactions are used and these will be explained later in Chapter 3.3 and Chapter 3.4 respectively.

3.3 Targeting inflammation

One targeting site that has attracted great interest in nanomedicine is inflamed tissue. In this thesis, dPGS nanoparticles, which are designed to be targeted to inflammation sites, are investigated. Therefore, in this section, inflammation will be shortly defined and the nanomedical techniques to target inflammation will be described including dPGS nanoparticles.

Acute inflammation is a natural response of the body against tissue damage. However, if acute inflammation cannot be terminated, it can lead to chronic inflammation which

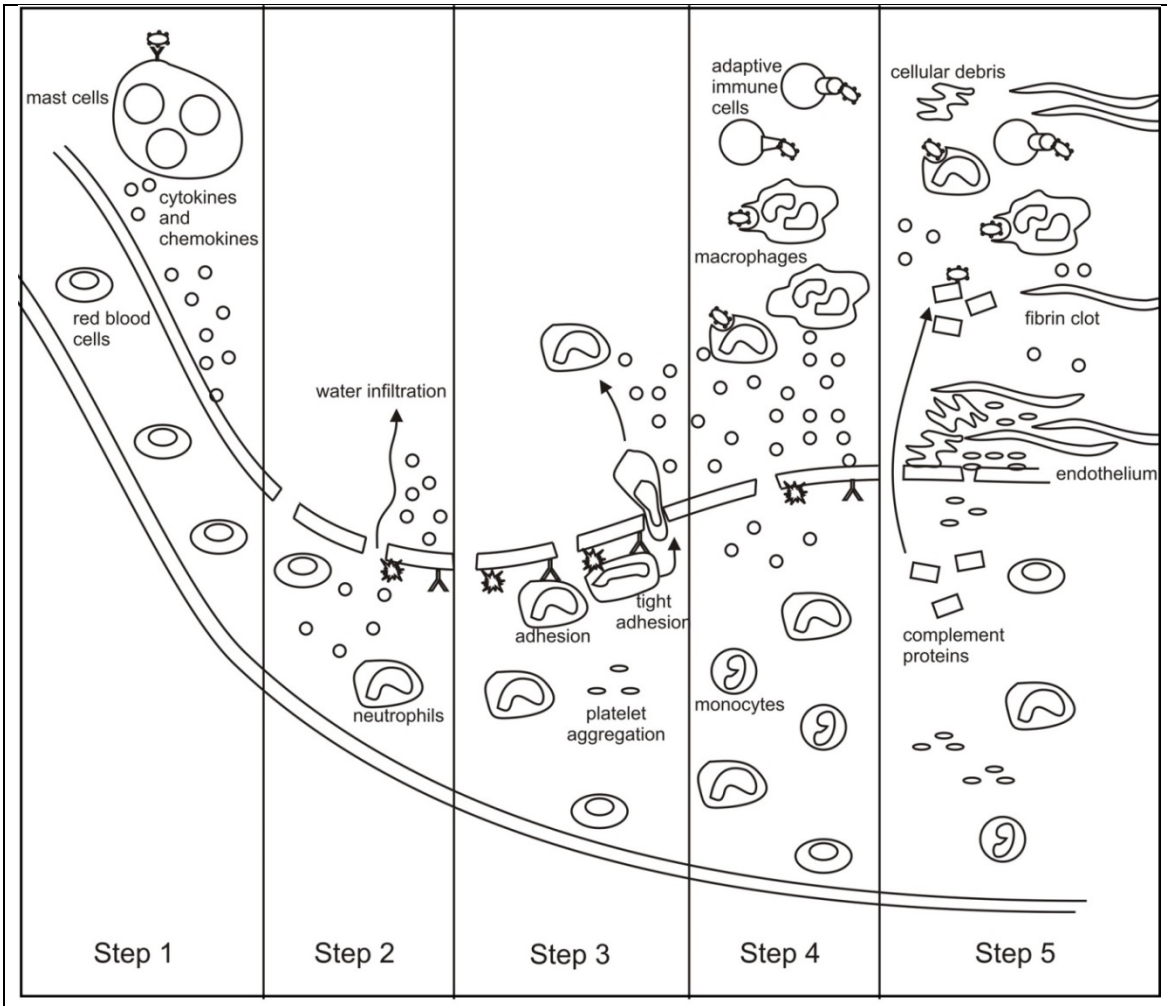

Figure 3.3 The key steps of inflammation. At Step 1, mast cells are activated via foreign factors and start to excrete histamine, cytokines and chemokines to activate endothelial cells (a). At Step 2, with activation of endothelial cells, the mast cells start to release cytokines and chemokines and express adhesion molecules on their plasma membrane. The tight junctions of endothelium are opened. Blood vessels expand, blood flow increases and vessels become more permeable (b). At Step 3, leukocytes are attracted to inflamed sites due to released chemokines from endothelial cells. Leukocytes adhere on endothelial cells and are recruited to inflamed tissue. Leukocytes release more cytokines and chemokines (c). At Step 4, due to increased cytokines and chemokines, macrophages are also recruited to inflamed tissue which releases more cytokines and chemokines. Leukocytes and macrophages engulf the foreign factor. Specific antigens from this foreign factor are then presented on the macrophage surface, which leads to the activation of adaptive immune cells which then kill the pathogen in an antigen specific manner (d). At Step 5, collagen and complement system is also activated. Complement system further assists in destruction of the foreign factor. Fibrin clot and cellular debris start to accumulate at the inflamed tissue which further damages the tissue together with water infiltration from the blood vessels (e).

damages tissues and ultimately results in inflammatory diseases such as colitis, Crohn's disease, atherosclerosis, rheumatoid arthritis and asthma [106, 113]. Inflammation is also

linked to diabetes, obesity, Alzheimer's disease and cancer [114-116]. Therefore, it needs to be diagnosed and treated.

To better understand how inflammation can be diagnosed and treated, the inflammatory response will now be briefly explained. Acute inflammation occurs against either infection or physical, chemical or traumatic injury. The goals of this inflammation are to remove the damaging agent and to limit the tissue damage via a complex cascade of vascular, molecular and cellular events which are regulated by inflammatory mediators. Key steps in this cascade are described below and shown in the schematic in Fig. 3.3. However, it is worth noting that in reality, it is difficult to separate inflammation into steps. It is in reality an intertwined cascade of events [113, 117-119].

In the first step, mast cells are attracted to the inflammation site. In the case of an infection, the invading pathogens express pathogen specific molecules, which are called pathogen associated molecular patterns (PAMPs), on their surface. PAMPs are recognized by the membrane bound pattern-recognition receptors of mast cells in the tissue. Then, these mast cells are activated and start to release proinflammatory mediators such as histamine, leukotrienes, proteases, cytokines and chemokines (Fig. 3.3 / Step1) [113, 117-119].

In the second step of the cascade, these proinflammatory mediators activate endothelial cells which line the blood vessels. This induces opening of the tight junctions of these endothelial cells causing the vessels to expand and become more permeable. The activated endothelial cells start to release chemokines, proinflammatory cytokines and express cell adhesion molecules such as selectins, vascular cell adhesion molecule-1 (VCAM1) and intercellular adhesion molecule-1 (ICAM1) (Fig. 3.3 / Step 2) [113, 117-119].

In the third step, as blood vessels expand, more leukocytes are carried to the inflamed sites. The chemokines and cytokines attract leukocytes and they adhere to cell adhesion molecules on the surface of the epithelial cells and infiltrate to the inflamed site from the open junctions of endothelial cells. The infiltrated leukocytes also release cytokines and chemokines (Fig. 3.3 / Step 3) [113, 117-119].

In the fourth step, the cytokines and chemokines are released by the leukocytes which result in recruitment of macrophages to the site of inflammation. The macrophages (as well as the leukocytes) phagocytose pathogens at the site of inflammation. Specific antigens from pathogens phagocytosed by the macrophages are then presented on the macrophage surface, which leads to the activation of adaptive immune cells which then kill the pathogen in an antigen specific manner. In the inflamed region, cellular debris starts to accumulate (Fig. 3.3 / Step 4) [113, 117-119].

In the fifth step, a series of cellular response mechanisms are activated. This includes the activation of both the collagen system and complement system. In addition, a fibrin coating starts to form at injury sites within the tissue. Furthermore, complement proteins in the blood vessels infiltrate the tissue and further assist in destruction of the pathogen. This includes opsonization of the pathogen for degradation by macrophages, and creation of a membrane attack complex to destroy the pathogen. Blood vessels further expand to facilitate access of these inflammatory cells, clotting agents, complement molecules, inflammatory mediators and oxygen. With this expansion, more inflammatory cells reach the area, and this in turn increases the production of new proinflammatory mediators in the site and vessels expand even more (Fig. 3.3 / Step 5) [113, 117-119].

The progressive expansion of the vessels enables increasing fluid infiltration at the inflamed site causing swelling of the tissue. This fluid carries metabolic waste, lactic acid and uric acid. The presence of this excess fluid, the infiltration of inflammatory cells and the accumulated cellular debris all lead unintentionally to tissue damage during the healing process [113, 117-119].

Thus, although inflammation is necessary to eliminate the pathogen, it is at the same time harmful to the surrounding healthy tissue. Therefore, when the inflammatory stimulus is eliminated, the inflammation should enter a resolution phase with a timely and adequate suppression of inflammatory mediators, apoptosis of acute inflammatory cells and removal of the cellular debris by macrophages. If the resolution process is not adequate, chronic inflammation occurs [113, 120, 121]. Chronic inflammation occurs either because the inflammatory response cannot eliminate the initial stimulus or due to a defect in the regulation of inflammation. The chronic inflammation continues without the requirement for an external stimulus. The continuous infiltration of fluid with metabolic

waste, infiltration of many cells to the inflamed region, high amounts of reactive oxygen species and accumulated cellular debris start to destroy the surrounding tissue which leads to inflammatory diseases [113, 122].

Inflammatory diseases are widespread in modern society and associated with many other diseases. However, the detection and treatment of these diseases is not straightforward. As a result, inflammatory diseases can yield fatal outcomes [123, 124]. Thus, there is an immediate need for both reliable detection and treatment procedures for inflammation. To achieve the best therapy, it is critical to detect and treat inflammation at an early stage [122] in which the signs of inflammation such as biomarkers and physiological changes are rather mild. Unfortunately, current techniques do not allow reliable detection of either small amounts of biomarkers or mild physiological changes at sites of inflammation [125].

A number of biomedical imaging techniques are currently being used for noninvasive detection of inflammation. These include medical ultrasound, single-photon emission computed tomography (SPECT), positron-emission tomography (PET), magnetic resonance imaging (MRI) and computed tomography (CT). Ultrasound is the safest technique among them. However, it provides low tissue penetration, low resolution and low sensitivity, all of which reduce the success of diagnosis. SPECT and PET provide high sensitivity and high penetration into deep tissue. However, it is still low resolution and requires usage of radioactive agents. MRI and CT address resolution problems [125]. However, both require contrast agents for imaging. These contrast agents are not specific enough and have a low blood circulation time. To obtain sufficient contrast, high doses of contrast agents are required which may cause long term accumulation at the healthy tissue and adverse side effects [122].

The treatment of inflammation is another hurdle since the underlying cause of the inflammatory stimulus is often unknown and difficult to identify. Therefore, theraupeutics often target the inflammation itself to alleviate it rather than to eliminate the inflammatory stimulus. However, the inflammatory response should not be completely suppressed since acute inflammation is a natural defense mechanism to prevent tissue damage. Therefore, to avoid complete suppression of the inflammatory response, therapeutics should be carefully designed. The currently used inflammation therapeutics

such as nonsteroidal anti-inflammatory drugs and glucocorticoids are unsatisfactory and nonspecific [113], and can lead to serious side effects such as non-specific colitis, relapse of the inflammation, fistula, large intestinal ulcers, bleeding perforation, thin and fragile skin, disturbed wound healing, ocular hypertension, risk of hyperglycemia, adrenal insufficiency, growth failure, osteoporosis and adverse effects on central nervous system and muscle myopathy [126, 127]. Thus, the inflammation field is in need of better drugs as well as contrast agents to diagnose and treat inflammation. Ideally, to minimize side effects, the agents should be targeted to inflamed tissue. For this, nanoparticles are promising candidates since they can be modified with targeting moieties to target disease sites and they provide unique absorption and scattering properties for biomedical imaging [122].

Many nanoparticles are currently designed to exploit the unique physiological and molecular features of inflammation, such as increased vascular permeability and vast amounts of inflammatory cells, signaling molecules, inflammatory mediators and cell adhesion molecules. The anti-inflammatory nanoparticle types include liposomes, polymer based nanoparticles or inorganic nanoparticles such as quantum dots, iron oxide nanoparticles and gold nanoparticles. They often combine targeting, drug delivery and contrast agents for simultaneous treatment and diagnosis [128]. In the following sections, the common inflammatory features that nanoparticles exploit will be reviewed, with specific examples using gold nanoparticles to better target and diagnose inflammation.

One target to treat and diagnose inflammation is the increased permeability of vasculature at the inflamed tissue due to opening of junctions between endothelial cells. The junction size increases from 12 - 20 nm up to 0.2 - 1.2 μm. Therefore, nanoparticles larger than 20 nm have been designed to target inflammation via passive accumulation without a need of targeting moieties (Fig. 3.2a) [129].

Macrophages have been another important target of inflammation diagnosis since macrophages are important elements in both the activation and the resolution of inflammation. Additionally, they can be easily targeted since they can phagocytose nanoparticles. For instance, gold nanoparticles coupled with high density lipoprotein were used for detection of macrophages in atherosclerosis by CT. High density lipoproteins attached to the gold nanoparticle surface facilitated the internalization of the nanoparticles

by the macrophages. The ingested nanoparticles provided much better contrast compared to bulk contrast agents, enabling a more sensitive detection of the inflammation [130, 131].

Another common target of nanoparticles is reactive oxygen species (ROS). These are an important factor in the progression of inflammatory diseases both as signaling molecules and inflammatory mediators. High amounts of ROS are produced by leukocytes at inflamed sites. These increased levels of ROS have been used to trigger the release of either anti-inflammatory drugs or imaging agents attached to nanoparticles. For instance, a 600 nm ROS-responsive nanoparticle has been targeted to inflamed tissue via passive accumulation. When these nanoparticles encounter ROS, they undergo a conformational change and release their drug which suppresses innate cytokine production [132]. The increased levels of ROS at inflammation sites in a mouse model system have also been exploited in the diagnosis of arthritic inflammation via near-infrared fluorescence (NIRF) dye coupled hyaluronic acid immobilized gold nanoprobes. NIRF dye was quenched when it was in close proximity to gold nanoparticles. At the target site, when hyaluronic acid is cleaved by ROS, NIRF dye was released from the gold nanoparticles thereby creating a strong fluorescence signal to enable imaging of the inflamed site [133]. Finally, gold nanoparticles by themselves have been found to catabolize redox reactions and hence reduce ROS production. Gold nanoparticles also induced overexpression of Glutathione peroxidase 1 (Gpx-1), an antioxidant enzyme, by inhibiting the receptor activator of Nuclear Factor-κB (NF- κB) ligand which suggests that gold nanoparticles reduce oxidative stress during inflammatory processes [134]. In sum, by using such smart designs, high levels of ROS at inflamed sites can be reduced or exploited both for targeted anti-inflammatory drug delivery and targeted imaging of inflammation.

Another feature of inflammation that nanoparticles target is the proinflammatory cytokines such as tumor necrosis factor alpha (TNFα), interleukin 6 (IL-6) and vascular endothelial growth factor (VEGF), all of which play important roles in enhancement of inflammation. With 21 nm gold nanoparticles, the production of mRNA IL-6 and TNFα were reported to be reduced in the abdominal fat which indicates that gold nanoparticles can alleviate inflammatory response by reducing proinflammatory cytokine production [135]. Gold nanoparticles were also found to reduce inflammation by binding to VEGF at

inflammatory sites [136]. Multifunctional hyaluronate coupled gold nanoparticles loaded with Tocilizumab, which is a humanized monoclonal antibody against IL 6, was generated to treat inflammation [137]. Hyaluronate was used to increase the targeting ability of the nanoparticles since it was reported to enhance targeting [138]. According to a study performed on a mouse model with arthritis, the gold nanoparticle core bound to VEGF to inhibit angiogenesis which in turn reduced the infiltration of further inflammatory cells, blood proinflamatory mediators and extra fluid into the inflamed sites. The drug, Tocilizumab, bound to IL-6 receptors on inflammatory cells to inhibit the interaction of this receptor with the proinflammatory cytokines. Therefore, the cell cannot be activated and the inflammation is alleviated [137]. In sum, bare gold nanoparticles or gold nanoparticles with biologically relevant coatings can bind to proinflammatory cytokines or their receptors to inhibit the production of further proinflammatory cytokines and hence reduce the inflammation. However, contradictory studies are also available about gold nanoparticles. Gold nanoparticles with diameters of 10 nm and 50 nm were found to increase the gene expression of cytokines in the liver [139]. Therefore, size-, shape- and coating-dependent studies must continue to be performed to understand the potential of gold nanoparticles to treat inflammation.

Cell adhesion molecules expressed on endothelial cells are another target of inflammation. Since these molecules are overexpressed at inflamed sites, nanoparticles can be targeted to these sites if they carry molecules which will bind cell adhesion molecules such as E-selectin [140, 141], VCAM-1 [142] and ICAM-1 [143, 144].

Leukocytes are another target of inflammation diagnosis and treatment as a direct therapeutic delivery tool to inflamed sites [145]. For instance, leukocytes loaded with nanotherapeutics in *vitro* were administrated to the sites of inflammation and released their therapeutic contents at the inflammatory sites [145]. Alternatively, nanoparticles made from albumin were administrated to eliminate leukocyte infiltration. Gold nanoparticles coated with hyperforin (which is a phytochemical produced by plants that has been reported to have anti-inflammatory and anti-carcinogenic properties [146]) were shown to reduce the inflammatory cell infiltration at inflamed sites in multiple sclerosis. However, the exact mechanism of hyperforin inhibition remains to be investigated [128, 147]. Some nanoparticles are specifically designed to reduce leukocyte recruitment by

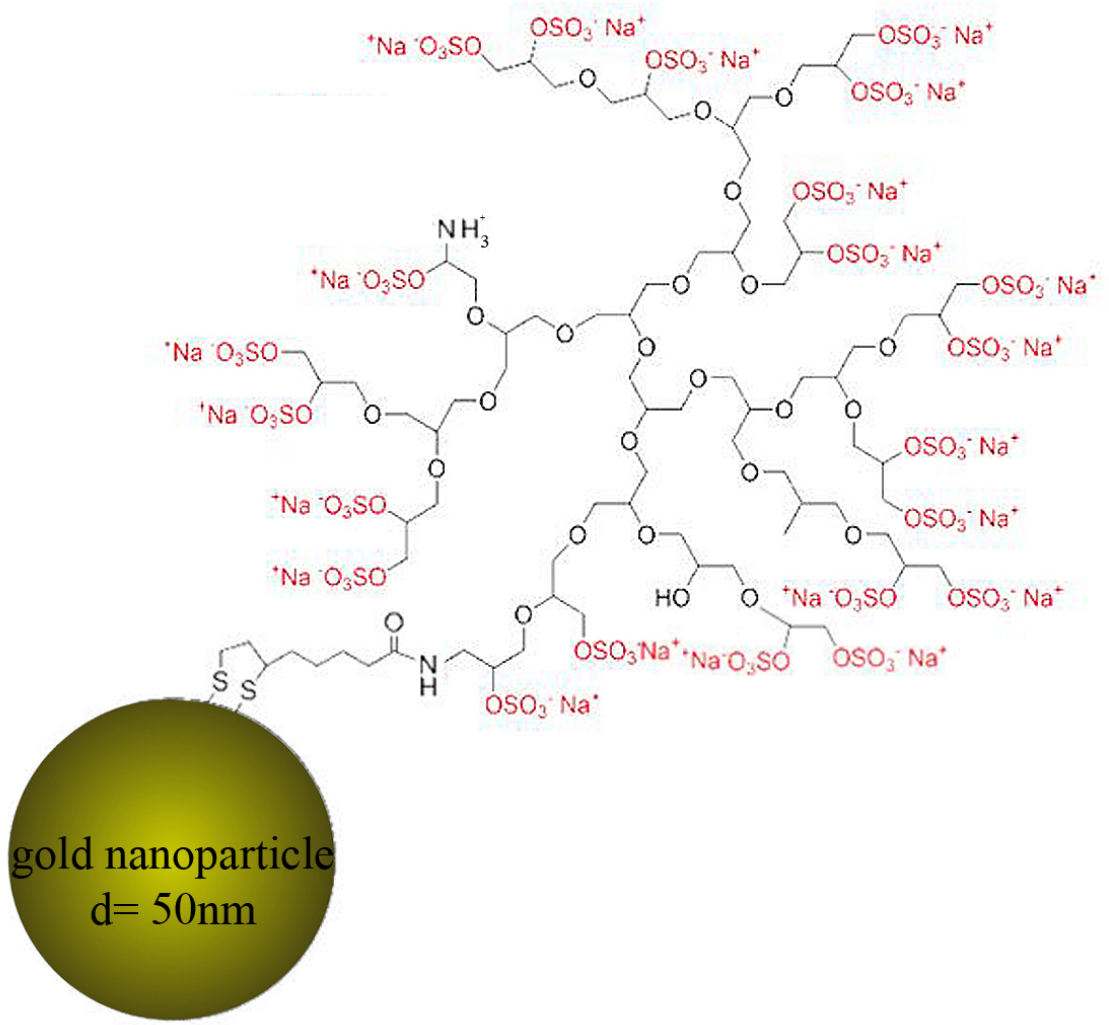

Figure 3.4 Conjugation of thioctic acid modified dendritic polyglycerol sulfate to a gold nanoparticle via Au-thiol binding. Modified from [148].

reducing the adhesion of leukocytes to endothelial cells [149]. There are various ways to do this. One strategy is to target activated leukocytes to block their movement and inhibit their adhesion to endothelial cells. For instance, albumin based nanoparticles can deliver drugs either to eliminate proinflammatory kinase production or to eliminate production of signaling molecules which take part in leukocyte adhesion on endothelial cells [150]. Albumin can be coupled to gold nanoparticles too. However, the effect of albumin-coated gold nanoparticles on inflammation has not been studied [151]. Additionally, leukocyte infiltration can be eliminated by targeting nanoparticles to cell adhesion proteins on endothelial cells. In this approach, nanoparticles compete with leukocytes to adhere to

endothelial cells, which eventually reduce leukocyte infiltration and alleviate inflammation [152, 153].

Dendritic polyglycerol sulfate (dPGS), which is investigated in this thesis, is an example of a nanoparticle designed to treat inflammation by inhibiting leukocyte recruitment. The coupling of dPGS to metal nanoparticles, including gold nanoparticles, has yielded theradiagnostic agents which provide sufficient contrast for diagnosis by imaging and simultaneously provide an anti-inflammatory therapy by competing with leukocyte adhesion at the site of inflammation [12, 154]. dPGS nanoparticles were created by conjugating thioctic acid (TA) modified dendritic polyglycerol sulfate to gold nanoparticles via Au-thiol binding (Fig. 3.4) [12]. This creates a stable binding of dPGS to gold nanoparticles and ensures that the dPGS is not released from the nanoparticles during diagnostic imaging or therapy. However, these dPGS compounds are also known to be internalized by cells, which could have further beneficial therapeutic effects, but might also have unwanted consequences. This latter possibility has stimulated various investigations of the cellular and whole organism behavior of dPGS compounds [12] which will be reviewed in the following section.

3.3.1 Polyglycerol sulfate dendrons (dPGS) to target inflammation

Dendritic polyglycerol sulfate (dPGS) is a potential diagnostic and therapeutic agent for inflammatory diseases [23, 148, 155, 156]. This compound, which was synthesized as a polysulfated analog of dendritic polyglycerol (dPG) in 2004, has lower anticoagulative and enhanced anti-inflammatory activity compared to common inflammatory drugs such as heparin [157]. dPGS is a 13 kDa, nanosized agent with a 5 nm hydrodynamic diameter. According to *in vitro* studies, dPGS binds to L-selectin and P-selectins on cell surfaces to compete with leukocytes and therefore inhibit the extravasation of leukocytes into inflamed tissues [148, 158].

In order to utilize dPGS for *in vivo* or *in vitro* imaging studies, it has been coupled to fluorescence tags [159-161], radiolabels [162, 163] or nanoparticles [12, 154]. In all of these forms, dPGS has been found to accumulate at inflammation sites in various inflammatory disease models, such as rheumatoid arthritis [164], acute asthma [165] and osteoarthritis [166]. In addition, to this diagnostic potential, dPGS has also been shown to exert therapeutic effects. Specifically, dPGS treatment reduces edema formation in

mouse model systems [166]. In preclinical animal studies, the cytotoxicity of dPGS compounds has been assessed in rat models after systemic delivery and the results demonstrated the biocompatibility of dPGS compounds for clinical applications [167]. The blood half-life of the compound has been found to be 12 days. The major route of elimination was found to be via bile and feces. Liver and spleen were late target organs where dPGS amine was found to accumulate in phagocytic cells [162].

Several preclinical studies suggest that cells internalize dPGS by endocytosis. The evidence for this comes from the punctate cellular uptake patterns of fluorescently tagged dPGS [21-26]. Many studies suggest that dPGS does not exert substantial cytotoxicity [23-26, 168]. However, several key questions about dPGS cellular delivery remain unanswered. First, does dPGS reach the cytoplasm and nucleus of cells where it might exert therapeutic effects on intracellular molecules involved in regulating inflammation? This question is important in order to understand how dPGS may exert its therapeutic effects. Second, what sub-cellular compartments does dPGS enter following delivery to cells? This question is critical to determine how dPGS is processed by cells, whether its targeting might be improved in the future and whether it may ultimately be released from cells. Third, does dPGS uptake influence cell structure? This question is significant since cell structure directly reflects cell function, and so an analysis of cell structure provides a very sensitive assay of cell physiology during nanoparticle delivery [169].

3.4 Targeted gene delivery

In this thesis, PEI-coated gold nanoparticles, which are designed for targeted gene delivery to the cell cytoplasm and nucleus, will be used. Therefore, in this section, targeted gene delivery will shortly be defined and the common nanomedical techniques utilized for targeted gene delivery will be described, including PEI-coated gold nanoparticles. Targeted gene delivery is another area that has attracted great interest in nanomedicine. Gene based therapy is the introduction and intentional expression of exogenous nucleic acids such as DNA, mRNA, small interfering RNA (siRNA), microRNA (miRNA) or antisense oligonucleotides to treat pathological conditions. By using these nucleic acids, almost any part of the cell genome can be intentionally expressed or repressed. For instance, a tumor suppressor gene can be delivered to the target area to inhibit tumor growth. This possibility to treat genetic diseases by exogenous gene delivery has created great excitement [106].

However, there are a number of issues that must be addressed in order to ensure safe and effective delivery of genes. Exogenous nucleic acids can only be delivered rarely with reasonable efficiency to cells without a carrier, since they are quickly cleared from the blood within ~30 min [36, 170]. This is typically not enough time to reach the target cell. Additionally, nucleic acids are hydrophilic and negatively charged, and hence cannot bypass the plasma membrane of cells in order to reach the cytoplasm or nucleus and exert a therapeutic effect. Therefore, many studies have been done to design vectors that can carry exogenous nucleic acids to their cellular target. One widely studied vector is based on viruses. Some adenoviruses and retroviruses can deliver exogenous nucleic acids to target cell nucleus efficiently, however, viral vectors were reported to cause random insertional mutagenesis. If this mutagenesis occurs at a gene which involves in programmed cell death or cell proliferation, the mutagenesis may yield cell death and tumor formation due to uncontrolled cell proliferation. For instance, a young boy developed a leukemia-like condition after gene therapy which was applied to treat his severe combined immune deficiency (SCID) [36]. Another drawback of viral vectors is their immunogenicity. For instance, a young patient died due to a rare metabolic disorder of the liver which was suspected to be caused by an immune response to the adenovirus used for gene therapy [36]. Finally, viral vectors have limited DNA packing capacity and a low yield production which limit the efficiency of the treatment [171, 172].

These disadvantages of viral vectors can be addressed by using synthetic non-viral vectors such as liposomes, polymeric nanoparticles and metal nanoparticles [171, 172]. Many nanoparticles are currently under investigation as non-viral vectors and are not reported to yield random insertional mutagenesis and immunogenicity. Additionally, these non-viral vectors can be easily produced in large quantities and they can be loaded with large amounts of target DNA [36, 171, 172]. However, the design and synthesis of effective non-viral vectors are challenging.

One of the biggest challenges in using nanoparticles for gene delivery is targeting the cytoplasm and nucleus. Specifically, the final desired target site depends on the nucleic acid: RNA molecules need to reach the cell cytoplasm and DNA molecules need to reach the cell nucleus. However, after internalization by cells, most of these nanoparticles end up in membrane-bound organelles. Moreover, the membrane-bound organelles in which

the exogenous nucleic acid is usually trapped during delivery are often acidic and contain degradative enzymes. Both of these features can damage the nanoparticle's nucleic acid cargo. Therefore, nanoparticles carrying nucleic acids must escape from the membrane-bound compartments into the cytoplasm and nucleus before the nucleic acids are degraded. A number of techniques have been developed to facilitate escape of nanoparticles from membrane-bound organelles [172-174].

Traditional synthetic vectors for nucleic acid delivery are cationic liposomes [175, 176] and cationic polymers [177, 178]. Some of the cationic liposomes have been commercialized, such as Transfectam and Lipofectaime. However, these liposome vectors have a number of disadvantages. They cannot be stored stably for extended periods. They lack specific targeting ability and they cannot be tracked via *in vivo* imaging techniques. Therefore, the search for more efficient and specific non-viral vectors is still underway [34].

Gold nanoparticles are promising tools to address the limitations of the cationic liposome vectors, since the gold surface is easily and stably functionalized with targeting moieties and because, as noted above, gold provides an excellent contrast agent. By themselves, gold nanoparticles are reported to enhance gene therapy when they are coupled to DNA [179] and siRNA [180]. Gene delivery was found to be further enhanced when gold nanoparticles were coupled with oligonucleotides [181], since the oligonucleotide coating facilitated the coupling of the nucleic acid to the gold nanoparticles. Additionally, it protected the nucleic acid from the acidic and degradative conditions of the membrane-bound organelles in the cell [181].

An alternative approach to enhance gene delivery by nanoparticles is to add a coating to the nanoparticle which facilitates the rapid escape of nanoparticles from membrane-bound organelles, which has been referred to as cytoplasmic escape. One such compound that facilitates cytoplasmic escape is poly(lactic-co-glycolic acid) (PLGA), which is cationic only in acidic conditions. After internalization into acidic vesicles, PLGA interacts with the inner side of the membrane and destabilizes it. This allows the nucleic acid cargo to escape from the membrane bound organelle [182].

Another approach to enhance cytoplasmic escape is to synthesize nanoparticles whose shape leads to membrane breakdown. So-called prickly gold nanodiamonds facilitate cytoplasmic escape via rapid vesicle rupture due to their irregular surface structures [183].

A third approach to enhance cytoplasmic escape is to coat gold nanoparticles with polyethyleneimine (PEI), which also leads to membrane destabilization [13, 14, 184]. Recently, this approach has been extended by synthesizing nanoparticles with the nucleic acid sandwiched in between two layers of PEI. Synthesis of these nanoparticles is done using the layer-by-layer technique of Elbakry et al [14]. First, a citrate stabilized 50 nm gold nanoparticle core is synthesized via a seed-mediated growth mechanism as explained in Chapter 3.2. Then, the citrate ions on 50 nm gold nanoparticles are replaced with 11-mercaptoundecanoic acid (11-MUA) which acts as a linker and enables coating of gold nanoparticles with PEI via electrostatic interactions (Fig. 3.5). According to the layer-by-layer technique, layers of PEI and nucleic acids are added on the gold nanoparticle consecutively via electrostatic interactions, since the adjacent layers have opposite charges with PEI being positively charged and nucleic acids being negatively charged. At the first step, a layer of PEI with a molecular weight of 25 kDa is formed. In this thesis, the PEI-coated gold nanoparticles, which are obtained as a result of this first step, are used. At the following steps, the genetic material, DNA or a double-stranded 21-mer siRNA, can be added. Finally, another layer of PEI can be added to form a shell over the nucleic acids [14]. This final PEI shell is designed to both protect DNA and siRNA from degradation while simultaneously facilitating cytoplasmic escape from the vesicle. In the following section, PEI and the suggested mechanisms of how it enhances cytoplasmic escape and nuclear entry of the exogenous nucleic acids will be reviewed.

3.4.1 Polyethyleneimine (PEI) for targeted gene delivery

Polyethyleneimine (PEI) is the most studied polymeric material for nucleic acid delivery purposes. PEI is a cationic polymer with multiple unprotonated amino groups which can be protonated under acidic conditions [185, 186]. Due to its cationic structure, PEI is rapidly attracted to negatively charged nucleic acids and forms complexes, called polyplexes. Polyplexes can be conjugated with liposomes[187], other polymers[188, 189], cell adhesion ligands [190] and gold nanoparticles[13] to enhance gene delivery.

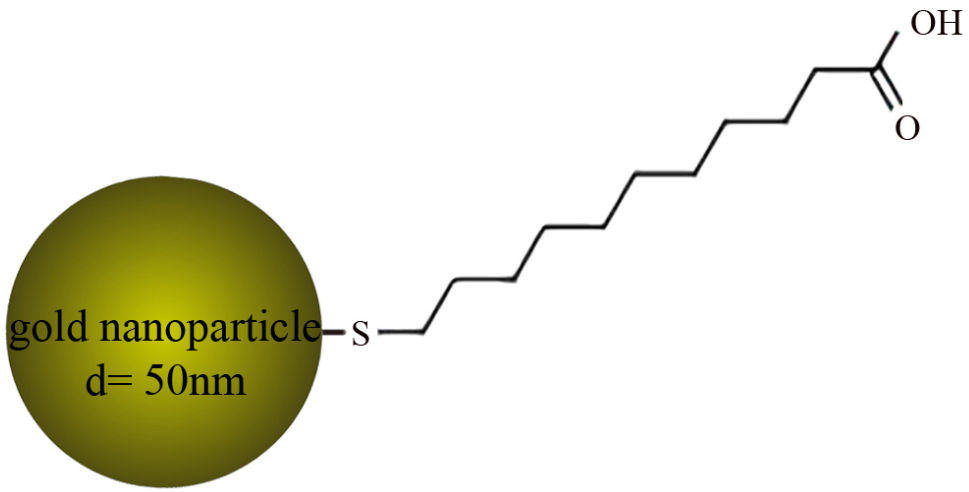

Figure 3.5 Conjugation of 11-mercaptoundecanoic acid (11-MUA) to gold nanoparticles through Au-thiol binding.

Even though PEI has been tested extensively in preclinical and clinical studies, some questions still remain to be answered about the cellular trafficking of these nanoparticles. Addressing these questions will be important to enhance PEI-mediated gene therapy and to develop better delivery tools.

First, the specific endocytosis pathway used for PEI internalization is debated. The reported endocytosis pathways are numerous, including macropinocytosis and clathrin- and/or caveolae-mediated endocytosis [37-42]. This variability is attributed to the physiochemical properties of the nanoparticles and the cell type [37-42]. This may be true, but it is nevertheless important to better understand the endocytosis pathway of PEI nanoparticles and the factors which alter the selection of these pathways, since the endocytosis pathway strongly influences nanoparticle localization, and hence the end-points of these nanoparticles in the cell, all of which influences their side effects and mode-of-function [191-193].

Moreover, what happens to PEI nanoparticles after internalization remains another controversial point. Specifically, it is not known whether PEI nanoparticles are trafficked to lysosomes or not. Some studies suggest that PEI localizes and escapes from lysosomes [42, 44-47], whereas other studies suggest that PEI never localizes to lysosomes and

instead accumulates in endosomes from which it may escape into the cytoplasm [48-50]. Clearing up these ambiguities is critical because endosomes are a relatively safe location for nucleic acids, whereas lysosomes are not. This is because lysosomes contain digestive enzymes, so if a PEI - nucleic acid complex enters lysosomes, then the nucleic acids can be easily degraded [194]. Thus, PEI would be most effective as a gene delivery agent if it could reliably cause cytoplasmic escape from endosomes rather than lysosomes.

Furthermore, the cytoplasmic escape mechanism of PEI nanoparticles has also not been defined. According to current hypotheses, PEI may create temporary pores in the membranes of cellular vesicles to escape to the cytoplasm [43, 45]. Alternatively, PEI may rupture the vesicles that it is localized to. The cause for such a rupture is explained by the "proton sponge" hypothesis. According to this hypothesis, PEI exhibits a buffering capacity within acidic compartments due to its unprotonated amines. These amines act like a proton sponge and attract protons to the membrane-bound organelles, together with Cl^- and water. As a result, the membrane-bound organelle swells and ruptures [35]. However, this hypothesis has not been directly tested so far [44].

Finally, whether PEI nanoparticles enter into the nucleus or not is another contested issue [33]. According to one hypothesis, PEI nanoparticles can enter into the nucleus together with DNA [42, 195] either via activation of the nuclear import machinery while the cell is in interphase (i.e. not dividing) or during mitosis when the nuclear envelope temporarily disappears [33]. An alternative possibility is that PEI nanoparticles do not enter into the nucleus. Rather, it has been suggested that DNA dissociates from the PEI nanoparticles, and these DNA molecules then diffuse through the cytoplasm eventually entering into the nucleus [42, 195]. Which of these hypotheses may be correct is uncertain. However, the nuclear entry of PEI was reported to depend on the size and shape of nanoparticles [196-198]. Also, the presence of nuclear localization signals on the nanoparticle surface is reported to facilitate nuclear entry in some cases [199, 200], but not all cases [198]. Therefore, there is presently no consensus on how PEI reaches the nucleus when delivered via nanoparticles.

3.5 Summary

Gold nanoparticles have many advantages for nanomedicine, most notably their ease of synthesis and relatively lower cytotoxicity compared to other metallic nanoparticles.

Their surface plasmon resonance offers an added benefit for a number of biomedical applications providing unique light absorption and scattering properties to these nanoparticles. Gold nanoparticles can be easily modified with targeting moieties to target inflammation sites and for targeted delivery of genes. In this thesis, two biomedically relevant gold nanoparticles have been examined, namely dPGS-coated and PEI-coated 50 nm gold nanoparticles. dPGS is proposed for use as a diagnostic and therapeutic agent for inflammation, while PEI is proposed as a gene delivery agent for inducing cytoplasmic escape of genes from vesicle compartments in the cell. The unknown questions about these nanoparticles will be addressed. Specifically, the endocytosis and intracellular trafficking of dPGS nanoparticles will be investigated. Additionally, whether these nanoparticles escape to the cytoplasm, enter into the nucleus and whether they are excreted from the cell will be observed. For nanoparticles, the endocytosis and intracellular trafficking pathway including lysosomal localization of these nanoparticles will be investigated. Additionally, the cytoplasmic escape mechanism of PEI nanoparticles and the effect of nanoparticle concentration on this mechanism will be investigated. Furthermore, whether PEI nanoparticles enter into the nucleus and whether they are excreted from cells will be investigated. Answering these questions will help understanding whether these nanoparticles reach their intended targets within the cell. This work should contribute to the development of more efficient dPGS nanoparticles for diagnosis and treatment of inflammation and more efficient PEI based targeted gene delivery tools.

4. INTERACTION OF NANOPARTICLES WITH BIOLOGICAL SYSTEMS: AGGREGATION, PROTEIN CORONA, INTERNALIZATION AND TRAFFICKING OF NANOPARTICLES, MORPHOLOGICAL EFFECTS OF NANOPARTICLES ON CELLS

The preceding chapter has introduced gold nanoparticles in general, and in particular gold nanoparticles with the two coatings studied in this thesis: dendritic polyglycerol sulfate (dPGS) as a tool in inflammation and polyethyleneimine (PEI) as a tool for gene delivery. In this thesis, the cellular interactions of these nanoparticles were investigated. Therefore, in this chapter, the key concepts about how other nanoparticles interact with cells are provided. First, how nanoparticle stability and surface are altered when suspended in biological fluids is discussed. Then, how nanoparticles interact with cells including their internalization mechanisms and trafficking pathways will be considered. Finally, what is known about the physiological effects of nanoparticles on cells will be discussed.

4.1 Nanoparticles interact with biological fluids during *in vitro* studies of nanoparticle - cell interactions

As discussed in Chapter 2 and Chapter 3, nanoparticles are designed to diagnose and treat diseases. However, at present, there is no common protocol defined by the Food and Drug Administration (FDA) to standardize nanoparticles before use in biomedical applications [201]. Nevertheless, a series of different analyses are typically performed to assure the safety and efficacy of nanoparticles before they are used in biomedical applications. These tests of nanoparticles usually include a detailed characterization of their physicochemical properties, followed by an analysis of their effects on cells and tissues *in vitro* via various biochemical assays and microscopic techniques [201, 202], and followed by studies of their *in vivo* compatibility via animal tests and finally clinical tests. After laboratory, animal and clinical tests, the successful compound can be used in the clinic if the FDA permits this [15].

In this thesis, the *in vitro* interaction of gold nanoparticles with two different coats on cells is studied. Therefore, the focus will be on *in vitro* studies in the following paragraphs and during the chapter. In *in vitro* studies, nanoparticles are first prepared as a colloidal suspension and characterized. Then, nanoparticles are transferred in cell culture medium to interact with cells [203]. Once a nanoparticle interacts with a cell, a series of

events typically ensue. First, the nanoparticles attach to the cell's plasma membrane, then they usually enter the cell where they typically become entrapped within cytoplasmic vesicles and finally they are trafficked to their cellular targets [204]. During such a study, the nanoparticles are always submerged in fluids, either fluids with simple electrolytes or biological fluids which contain both electrolytes and macromolecules including proteins. When nanoparticles encounter biological fluids, nanoparticles may aggregate or a protein corona may form around the nanoparticles. Both nanoparticle aggregation and the protein corona are reported to alter the interaction of nanoparticles with cells [205, 206]. Therefore, these processes are important to understand. Thus the fluids, which a nanoparticle encounters at various steps of an *in vitro* study, and their possible effects on nanoparticle aggregation and protein corona will be introduced in the following paragraphs.

At the first step of an *in vitro* study, nanoparticles are synthesized usually as a stable and monodispersed colloidal suspension within a fluid with simple electrolytes and characterized for their physicochemical properties and stability. Stability is one important criterion for nanoparticle suspensions since nanoparticle properties greatly depend on size. This is not straightforward since nanoparticles have a high surface to mass ratio, hence a large surface which is energetically unfavorable in terms of thermodynamics. Therefore, nanoparticles can easily aggregate. Hence, before use, the stability of nanoparticles should be characterized together with their other physicochemical properties. The most common characterization techniques are dynamic light scattering (DLS), gel electrophoresis, zeta potential analysis and microscopic imaging including scanning electron microscopy (SEM) and transmission electron microscopy (TEM) [202, 205]. Other techniques that are also utilized in nanoparticle characterization, although less frequently, are cellular interaction studies, including fluorescence correlation spectroscopy (FCS), thermogravimetric analysis (TGA), inductively coupled plasma mass spectrometry (ICP-MS), atomic force microscopy (AFM) and atomic absorption spectroscopy (AAS) [201, 202, 207, 208]. Nanoparticles can then be used in *in vitro* studies only if this initial physicochemical analysis demonstrates their expected physiochemical properties and the stability of the nanoparticle suspension.

Before considering the second step of *in vitro* studies, the stability of a nanoparticle suspension will first be described in some detail in the following paragraphs. The stability of a colloidal suspension is defined by Derjaguin, Landua, Vervey, and Overbeek (DLVO) theory. This theory states that the nanoparticle stability can be approximated by the delicate balance of van der Waals forces and double layer interactions [203, 209, 210].

van der Waals attractive forces are caused by the dipole-dipole interactions between nanoparticles. These attractive forces are a function of the physiochemical properties of nanoparticles and the distance between nanoparticles (Fig. 4.1a) [203, 209, 210].

The electric double layer interactions represent repulsive forces and are especially important for charged nanoparticles (Fig. 4.1b) [203, 209, 210]. Note that the electric double layer interactions are a function of the physiochemical properties of both nanoparticles and the surrounding fluid. These interactions arise due to the electric double layer around the nanoparticles. The electric double layer is an ion cloud around a nanoparticle which forms when a nanoparticle is exposed to a fluid with simple electrolytes, since some counter ions from the fluid are collected around the nanoparticle (Fig. 4.1b,c). The first layer of this electric double layer is called the stern layer. At this layer, counter ions are found strongly anchored on the nanoparticle surface. The second layer is called the diffuse layer in which, as its name suggests, counter ions are more diffuse (Fig. 4.1c) [211]. This charge cloud becomes a part of the nanoparticle since the cloud moves with the nanoparticle. As a result, the electric double layer shields the real surface charge of a nanoparticle and provides a new charge which is called the effective surface charge. The electric double layer, hence the effective surface charge of nanoparticles, depends on the physicochemical properties of the nanoparticles as well as the pH, temperature, ionic and molecular composition of the surrounding liquid. Therefore, once nanoparticles are submerged in different fluids, the electric double layer of the nanoparticles can change [203, 210].

Therefore, nanoparticles are attracted to each other due to van der Waals forces and repulsed from each other due to double layer interactions. In a symmetrical situation, in which the nanoparticles are identical or at least very similar, the energy profiles of attractive and repulsive interactions between two nanoparticles are depicted in Fig. 4.1d.

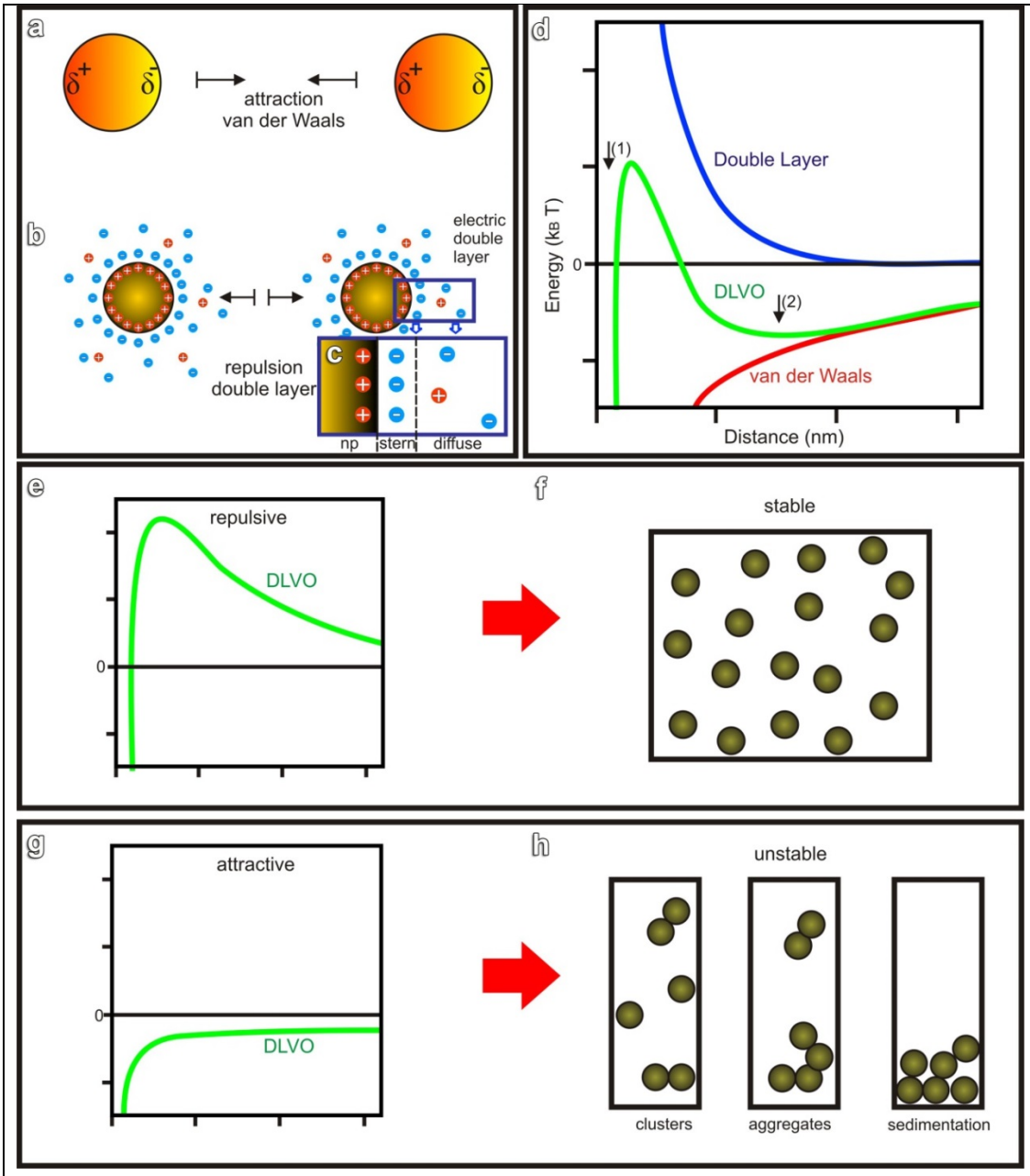

Figure 4.1 The stability of a nanoparticle suspension. According to DLVO theory, the stability of a nanoparticle suspension is determined by van der Waals and double layer interactions. Van der Waals interactions are attractive and caused by the dipole-dipole interactions between nanoparticles (a). Double layer interactions are repulsive forces between charged nanoparticles (b) which contain an electric double layer around them. The electric double layer is an ion cloud which is composed of a stern and a diffuse layer (c). The potential energy profile describing the interaction between two identical nanoparticles, namely its DLVO potential energy profile, as inspired by [203, 210] (d). When the nanoparticles are in close proximity, an attractive well forms in the DLVO energy profile (d, 1). At larger distances, the DLVO energy profile reaches a maximum and later presents a shallow minimum (d, 2). The DLVO energy profile is very useful for understanding the stability of a nanoparticle suspension with identical nanoparticles. When the DLVO energy profile is repulsive (e), nanoparticles repulse each other to form a stable nanoparticle suspension (f). When the DLVO energy profile is attractive (g), nanoparticles attract each other to form an unstable nanoparticle suspension in which nanoparticles first form clusters, then aggregates. Then, nanoparticles sediment at the bottom of the container (h).

The combination of these attractive and repulsive energy profiles yields the DLVO energy profile which provides information about the stability of the colloidal solution.

According to this profile, when the nanoparticles are in close proximity, a deep attractive well forms which is also referred to as a primary minimum. At larger distances between the nanoparticles, the DLVO energy profile reaches a maximum. As the separation distance further increases, the DLVO energy profile presents a shallow minimum which is called a secondary minimum. When the DLVO energy profile is repulsive (Fig. 4.1e), the double layer repulsive forces dominate the interactions of nanoparticles. Therefore, the nanoparticles repel each other and form a stable suspension (Fig 4.1f). When the profile is attractive (Fig. 4.1g), the interactions are dominated by van der Waals attractive forces. Therefore, the nanoparticles will form an unstable suspension. In an unstable suspension, nanoparticles attract each other and stick to form clusters and aggregates. Eventually, nanoparticles may sediment to the bottom of the container (Fig. 4.1h) [209]. In a symmetrical situation in which the nanoparticles are identical or at least very similar, the nanoparticles are attracted to each other due to van der Waals forces and repulsed from each other due to double layer interactions as shown in the potential energy profiles.

Having described the stability of a nanoparticle suspension, it is time to return to the steps of an *in vitro* study following nanoparticle synthesis and characterization, and specifically now to focus on the second step. Here, nanoparticles are transferred to a protein-supplemented cell culture medium which is an electrolyte rich fluid which usually has a different ionic composition than the fluid in which the nanoparticles were suspended. Now the nanoparticles start to interact with this new fluid. The interaction of nanoparticles with various cell culture media has been extensively studied. This interaction is suggested to be a function of the physicochemical properties of the nanoparticles as well as the physicochemical properties of the cell culture medium. With this interaction, the electric double layer around the nanoparticles is altered, which causes repulsive forces between the nanoparticles to be altered while van der Waals forces remain the same. Therefore, the stability of the nanoparticle solution can be disturbed and the nanoparticles can aggregate [203, 210].

During this aggregation process, dispersed particles stick to each other and spontaneously form irregular particle clusters. In early stages of aggregation, the suspension mainly contains particle monomers and some dimers. In later stages, larger clusters form. As the clusters grow in size to reach more than around 1 μm, they may settle down to the bottom of the container (Fig. 4.1h) [209].

Particle aggregation is usually an irreversible procedure [209], which changes the properties of the nanoparticles, since these properties are very sensitive to size. Therefore, aggregated nanoparticles will behave differently than monodispersed nanoparticles, and this may lead to unintended consequences. For instance, aggregation of nanoparticles in many *in vivo* studies was reported to alter their biodistribution, reduce their therapeutic effects and increase systemic toxicity of nanoparticles [203, 210]. In many *in vitro* studies, nanoparticle aggregation within cell culture medium was reported to alter the uptake efficiency and toxicity of these nanoparticles [205, 212].

Therefore, the stability of monodispersed nanoparticles in the intended biological system must be assured before the nanoparticles can be used in a biomedical application [213, 214]. To increase the repulsion between nanoparticles, and hence to increase their stability, nanoparticle surfaces have been modified with charge or polymer brushes [214].

At the final step of an *in vitro* study, the nanoparticle suspension is added to the cell. Once nanoparticles interact with the cell, nanoparticles are usually internalized by the cell. This exposes nanoparticles to cellular fluids which are usually electrolyte rich suspensions of various macromolecules including proteins, lipids, carbohydrates and inorganic matter. Each sub-cellular compartment such as cytoplasm, nucleus, endosomes, lysosomes, and other organelles have their specific ionic and macromolecular composition. Therefore, as nanoparticles progress through various sub-cellular compartments, they are exposed to various biological fluids. Even though the interaction of nanoparticles with cellular fluids is not well studied, a few studies have suggested that nanoparticles aggregate within the cell and some cellular compartments [215, 216]. Researchers suspect that such an aggregation within the cell may have an effect on the cellular behavior of nanoparticles. Specifically, how these nanoparticles interact with macromolecules and how they are trafficked within the cell may be altered. However, this issue is not very well studied in the field yet [215, 216]. In this thesis, the interaction of

dPGS nanoparticles in the absence and presence of serum proteins will be analyzed to understand the effect of serum proteins on the cellular uptake rate and the intracellular trafficking pathway of these nanoparticles. This study will provide some information about the effect of the protein corona on intracellular trafficking of nanoparticles.

Nanoparticle aggregation is not the only consequence of the interaction between nanoparticles with biological fluids. With this interaction, nanoparticles are exposed to various types of proteins which may attach on the nanoparticle surface to form a protein-corona. This is a widespread phenomenon since biological fluids typically contain high concentrations of proteins and other biomolecules [214]. For instance, blood contains up to 60 - 80 g/L protein under normal conditions [217]. When nanoparticles are exposed to such biological fluids, the proteins and biomolecules adhere on the surface of the nanoparticle. As proteins start to attach to the surface of the nanoparticles, a protein corona is formed around nanoparticles, and this alters the characteristics of the nanoparticle [210, 218-220]. The protein corona will change depending on what molecules are found in the extracellular environment. This environment changes in different parts of the cell. Thus the same type of nanoparticle may have different protein coronas in different parts of the cell.

These different protein coronas can alter the properties of the nanoparticles and their interaction with cells. For example, the protein corona was reported to alter the internalization efficiency of nanoparticles [5, 221-224], although whether the protein corona helps or hinders internalization depends on the specific situation. Some studies report protein adsorption to the nanoparticle decreases cellular internalization because the increased surface free energy reduces the contact of the nanoparticle with the cell membrane, thereby inhibiting cellular uptake [5, 219, 225, 226]. However, other studies report that protein adsorption can increase cellular internalization [227, 228]. Not surprisingly, the type of protein adsorbed to the nanoparticle surface can change the outcome. For instance, attachment of either Apolipoprotein A-IV (ApoA4) or Apolipoprotein C-III (ApoC3) proteins reduced cellular uptake, while attachment of Apolipoprotein H (Apo-H) increased cellular uptake [229]. Moreover, the protein corona was also reported to affect the cytotoxicity, immunogenicity, targeting ability, cellular internalization pathway and behavior within cells [222, 230, 231]. In addition, once

nanoparticles are inside the cell, nanoparticles can absorb proteins and alter their properties, and this can induce unintended processes within the cell. For instance, negatively charged polyacrylic-acid-conjugated nanoparticles result in fibrinogen folding, which enhances the production of inflammatory cytokines and which in turn leads to inflammation [232]. This is a clearly a very undesirable consequence of the protein corona of these polyacrylic-acid-conjugated nanoparticles. Therefore, the interaction of nanoparticles with the surrounding biological media is critical to analyze in order to understand the behavior of a nanoparticle within the cellular environment.

However, so far, these changes of nanoparticles within the cellular environment, namely the formation of the protein corona, have not been extensively investigated although protein corona formation within cell culture medium is extensively studied [214]. The main effort in the literature is to try to prevent protein corona formation in general. Analogous to preventing nanoparticle aggregation by modifying the nanoparticle surface, it would also be generally useful to reduce protein corona formation on nanoparticles, since this can also modify the behavior of the nanoparticles. Currently, PEGylation of nanoparticles is the most common method which reduces protein binding. As a consequence, this increases the blood circulation times of the nanoparticles and provides invisibility against the phagocytic system, which might otherwise engulf the nanoparticles and remove them from the blood stream. On the other hand, PEGylation may also reduce the interaction of nanoparticles with the intended target cells, and thereby reduce the therapeutic efficiency of the treatment [233, 234]. Thus, there is still a great need for improved nanoparticle design to prevent nonspecific binding of proteins without interfering with nanoparticle binding to the intended biological target sites.

4.2 The efficiency of nanoparticle internalization depends on physicochemical properties of nanoparticles

As described in the previous section, nanoparticle aggregation and the protein corona have been reported to alter the efficiency of nanoparticle internalization. In the initial studies performed in the nanomedicine field using nanoparticles with simple surface modalities, the efficiency of nanoparticle internalization was correlated to some other physicochemical properties of the nanoparticles such as size [235, 236], shape [237] or surface charge [228]. In addition, the uptake of nanoparticles was also affected by a

number of cell-specific factors, including the cell type [238], the cell phenotype [237], the cellular density and the cell cycle phase [239]. It is important to consider currently known factors which affect nanoparticle - cellular interactions in order to evaluate the cellular interactions of dPGS- and PEI-coated gold nanoparticles, which are utilized in this thesis. Therefore, some of these factors will be described in the following paragraphs.

One factor that clearly affects nanoparticle uptake is the nanoparticle surface charge. For instance, positively charged nanoparticles are internalized more than neutral or negatively charged nanoparticles. Uptake of positively charged nanoparticles is favored due to the electrostatic interactions of these nanoparticles with the negatively charged plasma membrane [8], but negatively charged particles can also be internalized. In addition to the favorable effects of positive charges, uptake of nanoparticles is also enhanced if they are either hydrophobic or amphiphilic, since these features help embed the nanoparticles in the plasma membrane [233, 240, 241].

In addition to their surface properties, the size of nanoparticles will also affect their internalization efficiency. Nanoparticle size influences the plasma membrane wrapping geometry. This geometry allows the cellular uptake of nanoparticles over a very wide range of diameters spanning between 10 nm and 500 nm. A size of 50 nm is suggested to be the optimal for the most efficient uptake of nanoparticles, according to various systematic studies with different types of nanoparticles [5-7].

Shape is another factor which affects the internalization rate of nanoparticles. For instance, above 100 nm, rod-shaped nanoparticles are found to be internalized best followed by spheres, cylinders and cubes, respectively [242]. However, below 100 nm, the spherical nanoparticles are internalized with higher efficiency compared to rod-shaped nanoparticles [6, 243, 244].

Although the results discussed above demonstrate that charge, size and shape alter the internalization rate [245], it should be emphasized that the literature on this topic is often complex and contradictory. Also, these kinds of systematic studies which investigate the effect of charge, size and shape are usually performed on simple nanoparticles which cannot address the needs of nanomedicine in which nanoparticles need to target specific cells and subcellular compartments. However, all these initial studies have provided

valuable insight about nanoparticle - cell interactions in order to prepare more sophisticated nanoparticles. Using the knowledge gained from the initial studies, biologically relevant nanoparticles have been prepared which are conjugated to targeting moieties, ligands and biologically relevant proteins. These nanoparticles often formed specific interactions with cells and exploited certain intrinsic cellular processes due to their biologically relevant functionalization [246], such as endocytosis and intracellular membrane trafficking. In this thesis, two biologically relevant nanoparticles, dPGS- and PEI-coated gold nanoparticles with 50 nm core gold size will be used. First, their cellular interactions such as their endocytosis pathway, intracellular trafficking pathway, end-points and excretion tendencies will be individually analyzed. Then, these interaction patterns of these two differently-coated nanoparticles will be compared to determine if it might be possible to extract general rules about cellular interactions of nanoparticles.

4.3 Cells internalize nanoparticles mostly via endocytosis

In many biomedical applications, biologically relevant nanoparticles are targeted to cells and even more specifically to subcellular organelles. As discussed before, as the nanoparticle - cell interaction occurs, the nanoparticle first attaches on the plasma membrane, then is internalized into the cell, then reaches its subcellular target. These different cellular processing events are important to characterize for several reasons. First, for any nanoparticle that is targeted to a specific cellular location, it is critical to determine what fraction of nanoparticles arrives at the target and what fraction arrives at other cellular locations. This provides key information about the efficiency of delivery, and also the potential side effects if many nanoparticles arrive at other cellular sites. Second, even for nanoparticles that are not targeted to a specific site (for example nanoparticles that are used for imaging), it is still important to determine where these nanoparticles go in the cell to understand the possible effects of the nanoparticle on the cell. Now, each of these cellular processing steps will be described.

The plasma membrane, which is the first step of nanoparticle entry, is a lipid bilayer covered by a carbohydrate coat, namely the glycocalyx, which gives the plasma membrane its negative charge. When a nanoparticle encounters the plasma membrane, it can attach on the membrane via either nonspecific and/or specific binding interactions. Non-specific interactions are formed due to intrinsic nanoparticle properties such as

roughness, hydrophobicity, surface charge and surface modifications [247]. For example, due to the negative charge of the outer glycocalyx coat, as discussed in the previous section, cationic nanoparticles can form better non-specific interactions with the plasma membrane than anionic nanoparticles. Nanoparticles interact specifically with the plasma membrane when they are functionalized with molecules designed to interact with specific proteins present on the outer surface of the lipid bilayer. For example, nanoparticles functionalized with either ligands, antibodies [245], protein or aptamer specific to a cell membrane bound receptor will form specific interactions with that cell surface receptor on the plasma membrane [210]. In this thesis, such nanoparticles are called biologically relevant nanoparticles.

The function of the plasma membrane is to separate and maintain the chemical environment of the cell interior and to allow a selective and continual material exchange between the cell and its environment. This material exchange is done via either passive diffusion, active transport or endocytosis depending on both the osmotic pressure across the plasma membrane and the charge, size, and hydrophobicity of the material to be transported [248]. Passive penetration has been suggested as one route of nanoparticle internalization [249, 250] that is strongly dependent on nanoparticle size [251, 252]. However, in general, this passive route is only rarely exploited by nanoparticles and when it occurs it can also result in membrane disruption [253, 254], which is detrimental to the cell. Endocytosis is actually the most common form of nanoparticle internalization by cells. Therefore, this route will be discussed extensively below.

Endocytosis of nanoparticles may occur due either to specific or non-specific binding of nanoparticles to the plasma membrane. After non-specific attachment, the plasma membrane wraps around the nanoparticle eventually forming a bud to engulf the nanoparticle when the cell has sufficient energy reserves for membrane wrapping. Later, the bud is pinched off from the plasma membrane to form a cytoplasmic vesicle containing the nanoparticle in its interior. The vesicle may then be transported to other locations in the cell or it may fuse with other vesicles and/or it may change and mature into other types of cellular vesicles. The process of endocytosis is somewhat different when nanoparticles bind to specific receptor molecules on the plasma membrane. Binding of a ligand molecule on the nanoparticle to a specific cell surface receptor usually leads to

the recruitment of more receptor molecules to this binding site, typically via passive diffusion of receptors through the plasma membrane. When a critical number of receptor molecules are bound, then the energy of these chemical bonds contributes to the elastic energy of the plasma membrane and this initiates the membrane wrapping process. The total time required for wrapping depends on specific nanoparticle properties [255, 256]. As with non-specific wrapping, the nanoparticle is eventually engulfed within a cytoplasmic vesicle, which can migrate and mature in various ways within the cytoplasm.

Endocytosis of foreign material, whether it is specifically or non-specifically attached to the plasma membrane, can occur via two different pathways: phagocytosis and pinocytosis. Phagocytosis is the process whereby cells normally engulf either pathogens or dead cells. Phagocytosis can only be performed by a specific category of cells, namely phagocytes, which include cell types such as macrophages, neutrophils and monocytes. These cell types engulf foreign material such as a pathogen or a dead cell when they contain certain molecular markers, known as opsonins. The opsonins indicate that this material is a target for removal. Phagocytosis therefore can lead to the engulfment of relatively large objects exceeding microns in size [257]. Phagocytosis of nanoparticles will occur when they are either intentionally coated with opsonins including immunoglobulins, complement proteins and blood serum proteins, or when they inadvertently acquire opsonins in the extracellular environment. In either case, phagocytes will recognize these nanoparticles due to these opsonins. Nanoparticles will adhere on the plasma membrane of these phagocytes through specific receptors including the Fc receptor, complement receptors and scavenger receptors. This receptor-ligand binding then rearranges actin filaments to phagocytose the nanoparticles into specialized cytoplasmic vesicles known as phagosomes [258].

The more widespread form of endocytosis is the process of pinocytosis, which is normally used by cells to uptake fluid material from their extracellular environment. Virtually all cell types are capable of pinocytosis, and this therefore forms the primary pathway for endocytosis of nanoparticles. Pinocytosis can be divided into three categories: 1) clathrin-dependent endocytosis, 2) caveolae-dependent endocytosis, 3) clathrin- and caveolae- independent endocytosis [258, 259]. Now, these different forms of

pinocytosis pathways, which are known to be involved in nanoparticle uptake, will be discussed below.

Clathrin-dependent endocytosis is a dynamin-dependent pathway and involves a coat. In this endocytosis, the cargo is internalized via clathrin-coated pits when a ligand forms specific interactions with some receptors on the plasma membrane (e.g the transferrin receptor and the low-density lipoprotein (LDL) receptor) [260]. Upon ligand-receptor binding, cytosolic adaptor proteins bind to the cytosolic tails of these receptors and to clathrin at the same time to link clathrin to the plasma membrane. Clathrin-coated pits are pinched off via dynamin-dependent process to enclose the cargo within clathrin-coated vesicles of 100 - 140 nm diameter. Later, this clathrin coat is removed and they are sorted to the endo/lysosomal pathway. Here, they can be either recycled back to the plasma membrane by recycling endosomes, transported to the retrograde pathway, degraded in lysosomes or excreted to the extracellular environment by multivesicular bodies (Fig. 4.2a) [260-262]. Since some selective molecular markers were defined for clathrin including LDL and transferrin, a good amount of knowledge has accumulated about this endocytosis pathway in the literature [263]. Many nanoparticles have been reported to be internalized via clathrin-mediated endocytosis [236, 264, 265].

Caveolae-dependent endocytosis is a dynamin-dependent endocytosis and involves a coat. In this pathway, cargo is internalized via caveolin-coated flask-shaped pits of 60 - 80 nm in diameter, namely caveolae. According to transmission electron microscopy (TEM) studies, the caveolin coat is very thin in contrast to the thick coat around clathrin-coated pits [266]. When the cargo interacts with caveolae, the caveolae is then pinched off via a dynamin-dependent process to enclose the cargo within caveolar vesicles which are coated with caveolin [257]. The intracellular fate of caveolar vesicles is altered dependent on the internalized cargo. For example, different intracellular fates for caveolar vesicles have been suggested for cholera toxin and albumin respectively [259, 266]. Cholera toxin, endocytosed by the caveolae-dependent pathway, is trafficked to endosomes, Golgi and then to the ER [267]. In another study, cholera toxin was also reported to be recycled back to the plasma membrane concomitantly by caveolar vesicles [268]. Albumin, however, was found in multivesicular bodies. Interestingly, albumin could not be found in lysosomes [269], providing a case of escape from lysosomal

degradation [270]. In sum, caveolae-mediated endocytosis is involved in internalization of many cargos and traffics these cargos to different locations dependent on the cargo. Some of these trafficking routes bypass lysosomal degradation (Fig. 4.2b).

In the nanomedicine field, caveolae-mediated endocytosis has been viewed with great interest for several reasons. First, the pathway may provide direct recycling (as in the one case of cholera toxin mentioned above) of nanoparticles back to the extracellular environment without interacting with other cellular components. Such a pathway would be desirable for nanoparticles designed purely for imaging purposes. Second, the caveolae endocytosis pathway may provide a pathway in which nanoparticles can bypass lysosomes (as in the case of albumin mentioned above). Such a pathway would prevent nanoparticles from exposure to the harsh conditions of lysosomes in which the organic parts of the nanoparticles can be degraded.

Due to the preceding reasons, some effort has been devoted to direct nanoparticles to the caveolae-dependent pathway. However, it is not a straightforward procedure. For instance, folate was used to direct nanoparticles to this pathway, since folate is reported to be internalized via caveolae-dependent endocytosis. Folate was conjugated to nanoparticles with different sizes ranging from 50 nm to 250 nm. It was found that nanoparticles below 250 nm were internalized via both clathrin- and caveolae-dependent endocytosis. Only, nanoparticles around 250 nm were internalized purely with caveolae-mediated endocytosis [39, 271]. Such a study suggests that nanoparticles can be directed to this route. However, this individual case is not very well suited for biomedical purposes since 250 nm is simply too large to enable passive accumulation at disease sites.

In sum, clathrin- and caveolae-dependent endocytosis are dynamin-dependent pathways which involve a coat formation around invaginations and resulting endocytic vesicles. These pathways are involved in uptake and trafficking of many cargo including nanoparticles in a cargo-dependent manner.

Unlike clathrin and caveolae-dependent endocytosis, other identified forms of endocytosis do not include coat formation around the membrane invaginations. Together, these alternate forms are known as the clathrin- and caveolae-independent pathways. They include the CLIC/GEEC pathway, the flotilin-mediated pathway and

macropinocytosis [272]. To date, only a limited number of nanoparticles were reported to be internalized via the first two pathways. In contrast, many nanoparticles have been suggested to be internalized via macropinocytosis. In the following paragraphs, these pathways will be explained in some detail.

The CLIC/GEEC pathway is a clathrin- and caveolae- independent pathway [262]. The cargo is internalized through 40 nm wide uncoated tubular invaginations. Internalized cargo is first enclosed within distinct and elongated uncoated clathrin-independent carriers (CLICs) which arise directly from the plasma membrane. From CLIC, the cargo is transported to glycophosphatidylinositol-anchored-protein enriched endosomal compartments (GEECs) from which the cargo is sorted to the endo/lysosomal pathway (Fig. 4.2c) [272-275]. It is reported that cholesterol and actin polymerization are critical for this pathway. However, experimental analysis of this pathway is still ongoing. Transmembrane proteins including CD44 and dysferlin are reported to be selectively internalized through this pathway as well as extracellular fluids [272]. To date, not many nanoparticles were reported to be internalized with these routes. In one rare example, polystyrene nanoparticles were reported to be internalized through this pathway when they are not covered with a protein corona [276].

Flotillin-mediated endocytosis is another clathrin- and caveolae- independent pathway which was defined recently. Flotillins are membrane proteins which form microdomains in the plasma membrane. Growing evidence links flotillin microdomains to a clathrin- and caveolae-independent pathway. The flotillin microdomains are reported to bud from the plasma membrane to enclose the cargo into endocytic vesicles which contain flotillin, but are distinct from clathrin- and caveolin-coated vesicles. So far, experimental data suggest that the budding and pinching off can be either dynamin-dependent or -independent. Endocytosis of GPI-anchored protein CD59 and cholera toxin B subunit were associated with flotilin-dependent endocytosis. The vesicles containing the cargo are suspected to traffic to multivesicular bodies and lysosomes (Fig. 4.2d) [277, 278]. Recently, silica nanoparticles with sizes of 30 nm, 70 nm and 300 nm were reported to be internalized via the flotillin-dependent pathway [279].

Macropinocytosis is an actin regulated and dynamin-independent clathrin- and caveolae- independent endocytosis pathway. It involves a nonspecific internalization of

surrounding material via membrane ruffles [273]. These ruffles are plasma membrane protrusions which close back on the plasma membrane to enclose the cargo into macropinosomes. The resulting macropinosomes do not contain a coating like clathrin- and caveolin-coated endocytic vesicles [259]. The macropinosomes are usually bigger than 200 nm in diameter and their size can reach up to 5 μm [280]. Macropinosomes are believed to mature eventually via homotypic and heterotypic fusion events, acquire late endosome markers and eventually fuse with lysosomal compartments (Fig. 4.2e). However, studies to understand the fate of macropinosomes are still ongoing [273, 281]. Cells make use of the macropinocytosis pathway to engulf objects larger than 100 nm, including both pathogenic and non-pathogenic mycobacteria [282, 283]. Accordingly, this pathway is known to be involved in the uptake of larger nanoparticles. For example, an increase in the size of mesoporous silica nanoparticles is known to enhance their internalization via macropinocytosis both in Hela and A549 cells [284]. Another example is 350 nm chitosan nanoparticles. They were also internalized via macropinocytosis in Hela cells [285]. However, smaller nanoparticles can also be taken up by macropinocytosis. For example, lipidopeptide nanoparticles containing siRNA with approximately 60 nm size are found to be internalized via macropinocytosis, although clathrin-mediated endocytosis is also involved [286, 287]. These results demonstrate that the same nanoparticle may be internalized via several different endosomal pathways.

In sum, there are multiple ways for nanoparticles to enter into a cell. Understanding the rules which govern the selection of the endocytosis pathways by nanoparticles will be important for predicting their intracellular trafficking and whether or not they will reach their target end-point. To contribute to the formulation of general rules which govern this selection, in this thesis two different biologically relevant polymer-coated nanoparticles with the same size and in the same cell type will be used, and their endocytosis pathways will be identified.

4.4 Nanoparticle identity affects the internalization pathway of nanoparticles

The preceding discussion has shown that there are a variety of different endocytosis pathways for nanoparticles. These different pathways have evolved to enable cells to effectively process an assortment of different materials found in their extracellular environment. One or more of these uptake pathways will be triggered when a cell detects

a nanoparticle on its surface. The pathway(s) triggered partly depend on a number of nanoparticle properties, including the surface charge, size, shape and specific surface functionalization of the nanoparticle.

Understanding the endocytosis pathway utilized by a nanoparticle is critical to understand whether nanoparticles will efficiently reach their target and what other locations in the cell they may also reach, which could induce side effects. Therefore nanoparticle uptake has mostly been studied on a case-by-case basis. The following paragraphs will review what is currently known about the uptake of nanoparticles, with a focus on how the physicochemical properties of the nanoparticle influence the internalization pathway. Currently, there are no clear-cut rules about which nanoparticle properties direct nanoparticles to specific endocytosis routes. In particular, there is not much consensus about how surface charge, size, shape and surface functionality of nanoparticles affect their internalization pathway.

Many reports suggest that positively charged nanoparticles are internalized via clathrin-mediated endocytosis and macropinocytosis [285, 288]. For instance, positively charged aminoacid functionalized 100 nm polystyrene nanoparticles were internalized via clathrin-mediated endocytosis, while plain polystyrene nanoparticles were internalized through clathrin-independent pathways into mesenchymal stem cells (MSCs) [289]. In another report, a similar positively charged polystyrene nanoparticle around 100 nm was reported to be internalized via macropinocytosis into Hela cells [290]. Similar experiments were also performed for biologically relevant nanoparticles such as chitosan nanoparticles and poly(lactic-co-glycolic acid) (PLGA) nanoparticles and similar outcomes were observed. Positively charged 200 nm chitosan nanoparticles were internalized via clathrin-mediated endocytosis in A549 cells [291]. Their 350 nm counterparts were internalized mainly via macropinocytosis into Hela cells [285].

Despite the preceding reports, there are also many contradictions to the theory that positively charged nanoparticles are internalized via clathrin-mediated endocytosis and micropinocytosis. For instance, according to one study, 60 nm positively charged polystyrene nanoparticles were internalized instead via caveolae-dependent endocytosis in BEAS-2B cells [292], even though as noted in the preceding paragraphs other

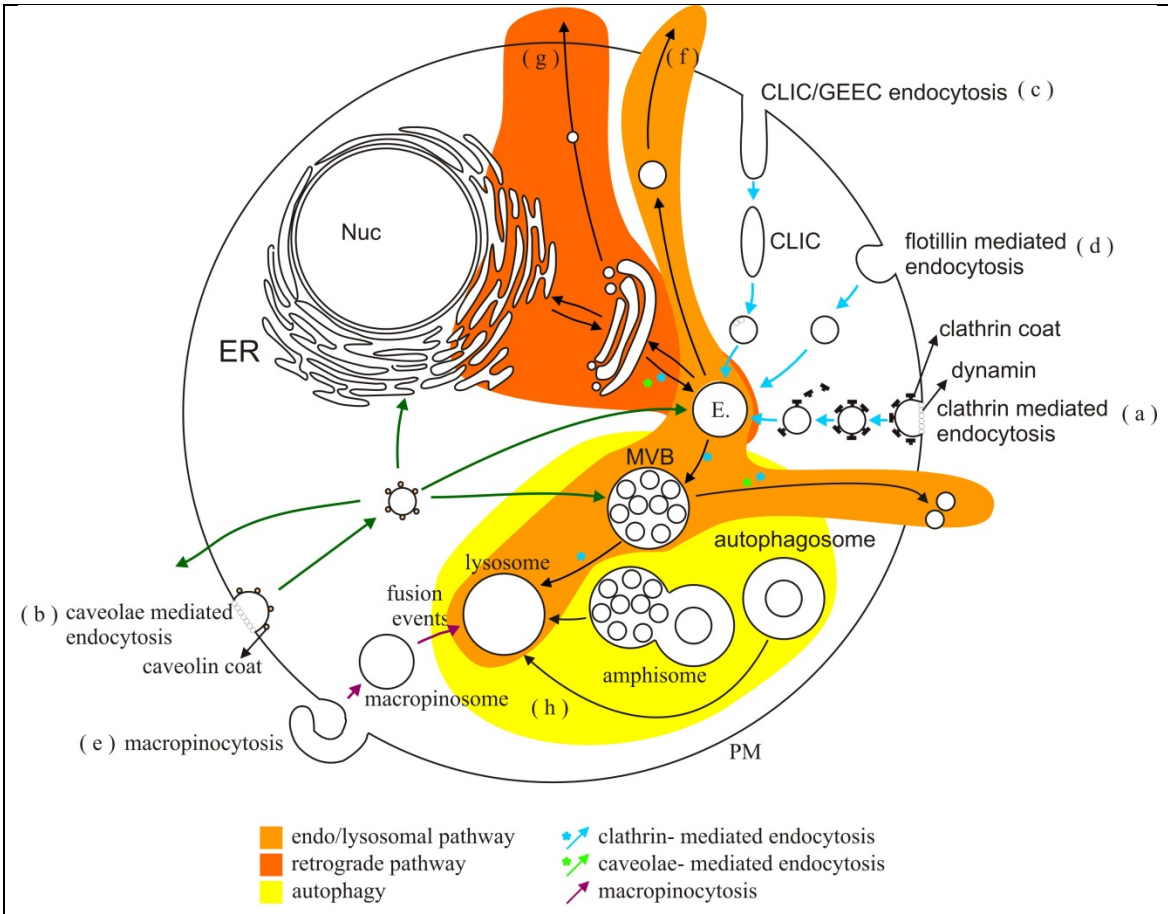

Figure 4.2 Schematic illustrating different types of endocytosis and intracellular trafficking of cargo in cells. A cargo can be endocytosed via clathrin-mediated endocytosis (a), caveolae-mediated endocytosis (b), CLIC/GEEC endocytosis (c), flotilin-mediated endocytosis (d) and macropinocytosis (e). The endocytosed cargo is often trafficked to endosomes to be sorted to other organelles (a,b,c,d). In macropinocytosis, the endocytosis cargo is reported to be directly trafficked to macropinosomes and sorted to other destinations from these macropinosomes (e). The cargo is then trafficked within the cell through various trafficking pathways such as the endo/lysosomal pathway (f), the retrograde pathway (g) and/or autophagy (h).

polystyrene-coated nanoparticles behaved according to the general rule for positively-charged nanoparticles. Similar contradictory outcomes were obtained with some biologically relevant nanoparticles. For instance, strikingly, transferrin conjugated PLGA nanoparticles below 100 nm were found to be internalized by caveolae-mediated endocytosis into BBB endothelial cells, even though the nanoparticles are positively charged and conjugated to transferrin, which is known to be specific for clathrin-mediated endocytosis [293]. Many PEI based polyplexes, which are cationic, were reported to be internalized through a combination of endocytosis pathways which include caveolae-

mediated endocytosis [192, 193]. And, from a different perspective, some negatively charged nanoparticles were found to be internalized via clathrin-mediated endocytosis. For instance, 50 nm cerium oxide nanoparticles were also reported to involve clathrin-mediated endocytosis in HaCat cells, even though these nanoparticles are not cationic [294].

Clearly, the surface charge has contradictory effects on the endocytosis pathway of nanoparticles. Such a contradiction may be caused from the usage of different cell types in these studies. Additional reasons for the conflicting results could be protein corona formation over these nanoparticles, which as explained in Chapter 4.1, is dependent upon the physicochemical properties of the nanoparticles and the fluid that the nanoparticles are suspended in. Additionally, differences in the size and shape of these nanoparticles in some cases may override the surface charge effect.

In the field, it is believed that clathrin-dependent endocytosis has a certain upper size limit of 200 nm, suggesting that any nanoparticle above 200 nm cannot enter via clathrin-dependent endocytosis [9]. For instance, one study using folate conjugated methoxy-poly(ethylene glycol)-b-polycaprolactone (mPEG-b-PCL) nanoparticles suggests that as nanoparticle size decreases from 250 nm to below 200 nm, the uptake pathway switches from a clathrin- and caveolae- mediated pathway to solely a caveolae-mediated pathway in ARPE-19 cells [271]. For the mesoporous silica nanoparticle, the increase in size instead enhances internalization via macropinocytosis both in Hela and A549 cells [284]. However, there are also contradictory studies against this 200 nm upper size limit. For instance, 360 nm hydrophobically-modified cationic-glycol-chitosan nanoparticles were internalized through a combination of endocytosis pathways, which included clathrin-dependent endocytosis in Hela cells [295]. According to these studies, it is clear that size has an effect on the nanoparticle internalization pathway. However, no simple rule exists to correlate size with the internalization pathway.

Another factor which affects the internalization pathway of nanoparticles is surface functionality. For instance, gold nanoparticles, which were reported to be internalized by macropinocytosis in one study, were instead internalized via clathrin-mediated endocytosis when they were conjugated with the RGD peptide [296]. In some cases, it was reported that surface functionalization can even override the size and shape effect.

For instance, surface functionalization was reported to override the effect of size and shape on internalization pathway, based on the analysis of polystyrene polymer carriers of different sizes (0.1 - 10 μm) and shapes (spheres and elliptical disks). These nanoparticles were all coated with an antibody against a transmembrane glycoprotein, and they were all found to be internalized by clathrin- and caveolae- independent endocytosis, regardless of the shape and size of the nanoparticles [245]. This shows that surface functionalization is a very important factor which affects the internalization pathway of nanoparticles.

In sum, it is clear that there are many different factors that can influence the internalization pathway of nanoparticles. Unfortunately, to date, there are no clear-cut rules about how nanoparticle identity and cell-specific factors may combine to determine the internalization of nanoparticles. This is because nanoparticle properties and cells themselves are simply too diverse and complicated, and furthermore nanoparticle characteristics can change with changing environmental conditions that arise during nanoparticle treatment [297, 298]. Therefore, wide variations in laboratory conditions, usage of different cells, usage of different sizes, shapes and surface chemistries of nanoparticles, plus differences in the techniques used to characterize nanoparticles and the lack of appropriate tools to fully investigate these cellular pathways may alter the outcomes of the experiments. Especially, for biologically relevant nanoparticles which contain many application-specific surface functionalizations, the number of factors affecting the internalization pathways is even larger than for simple nanoparticles. Therefore, extracting general rules about the nanoparticle internalization pathway can be extremely difficult. Note that this complexity is only at the cell level. When these nanoparticles are used at the organismal level, which contains various cells, biological fluids in between them and various barriers at the organismal level, trying to create general rules can be extremely difficult. Therefore, this thesis proposes that the most efficient technique is to focus on a specific type of nanoparticle for a specific application and carefully investigate this nanoparticle for each characterization step. This can lead to optimization for the specific type of nanoparticle to be used in a specific biomedical application. Perhaps later, by collecting information gathered from these specific nanoparticles, some general rules might be constructed. Therefore, in this thesis will separately investigate both the endocytosis pathway and the intracellular trafficking pathway of two different biologically relevant polymer-coated gold nanoparticles, namely

dPGS- and PEI- coated gold nanoparticles with a core gold size of 50 nm. Later, these pathways will be compared to identify similarities and differences in order to contribute to the generation of more general rules about cellular interactions of nanoparticles.

4.5 Intracellular trafficking of nanoparticles

As discussed in Chapter 2 and Chapter 3, nanoparticles used in medicine are designed for treatment and diagnosis of diseases. In many of these applications, intracellular and subcellular delivery of nanoparticles is the key in order to achieve the desired effect [2, 299].

Chapter 4.2 and Chapter 4.3 explained that defining the endocytosis pathway of nanoparticles can suggest where nanoparticles will end up in the cell because previous studies have already defined some intracellular routes for various ligands internalized by cells. However, endocytosis routes are complex and involve trafficking of nanoparticles to various organelles in a cargo-dependent manner. Therefore, even though endocytosis pathways can be identified and thereby suggest organelles through which nanoparticles will be processed, they cannot define these organelles with 100% certainty [258]. Intracellular trafficking of the nanoparticles must therefore still be investigated after identification of the endocytosis pathway.

Moreover, some nanoparticles are intentionally designed to escape from these cellular routes to localize in the cytoplasm, mitochondria, lysosomes or nuclei and exert specific activities there [2, 299-305]. This combined process is called targeting. It is usually achieved by adding different moieties to the nanoparticle, one responsible for localization such as a peptide that sends the nanoparticle to a specific organelle and another responsible for the specific therapeutic activity that is to be localized to that organelle, such as a buffering activity in the acidic environment of the lysosome, or gene delivery activity within the DNA of the nucleus [2, 299].

In either case, it is important to understand how nanoparticles are trafficked to their targets, whether they reach their targets, where else these nanoparticles are found in the cell and whether they will eventually be excreted from the cells. Hence, many studies have investigated the intracellular trafficking of nanoparticles.

Therefore, each nanoparticle should be separately investigated for its endocytosis pathway, intracellular trafficking and end-points. Thus a number of trafficking studies have been performed to define where nanoparticles localize inside of cells. To date, at least some types of nanoparticles have been found in the following sub-cellular compartments: recycling endosomes [306, 307], early endosomes [308], late endosomes [308, 309], fusion vesicles (which exhibit properties of both early [310, 311] and late endosomes [53]), lysosomes [308, 312, 313], autophagosomes [314], endoplasmic reticulum [311, 313], Golgi [311] and mitochondria [300, 313]. In some cases, nanoparticles are also found in the cytoplasm [182, 310-312, 315] and the nucleus [316, 317].

Although the preceding list is extensive and diverse, there are some underlying rules that should be discussed. Regardless of their initial endocytosis pathway, many nanoparticles enter into some well-defined intracellular trafficking routes, namely the endo/lysosomal pathway, the retrograde pathway or autophagy. Note that these pathways are not completely separate, since they are all known to interconnect for various cellular processes. In the following, each of these pathways will be explained in some detail, focusing on nanoparticle trafficking.

The first and most common suggested route for nanoparticles is the endo/lysosomal pathway (Fig. 4.2f). The endo/lysosomal pathway is a dynamic, interconnected network of four membrane bound organelles, namely the early endosomes, recycling endosomes, multivesicular bodies and lysosomes. In cells, the main function of this endo/lysosomal pathway is to internalize extracellular cargo and some components of the plasma membrane, and sort them to lysosomes for degradation, or to the retrograde pathway, or to the plasma membrane for reuse [318]. In this endo/lysosomal pathway, nanoparticles are first sorted to early endosomes. From here, they may be sorted to recycling endosomes to be trafficked back to the extracellular environment. Note that this recycling step may be either desirable or undesirable dependent on the nanoparticle application. For nanoparticles designed for medical imaging, recycling of nanoparticles is desirable since these nanoparticles are not designed to exert any effects on the cells. However, for therapeutic nanoparticles, recycling is a limitation since the nanoparticles may need to reach certain sub-cellular locations to exert their effect [306].

While recycling is one pathway from the early endosomes, alternatively nanoparticles can be sorted from early endosomes to either late endosomes or to lysosomes. Late endosomes, in turn, can traffic the nanoparticles again to the extracellular environment or to lysosomes for degradation [314]. Lysosomal degradation of therapeutic nanoparticles is often not desirable and nanoparticles which follow this route need to be designed to escape from the endo/lysosomal pathway, presumably from endosomes, before they finally reach the lysosomes. Many nanoparticles have been designed for endosomal escape using a variety of strategies [319]. However, the escape efficiencies of these nanoparticle platforms are still low, and their precise endosomal escape mechanism is still not entirely known [33, 44].

The second, and rarely suggested, route for nanoparticles is the retrograde pathway (Fig. 4.2g) [320]. In cells, the main function of the retrograde pathway is to receive secretory cargo from the endo/lysosomal pathway, modify this secretory cargo in the Golgi or ER, and then distribute it to other organelles and the extracellular space [318]. Consistent with this pathway, nanoparticles have been found in the Golgi and ER. They are thought to arrive at these destinations by sorting from the endosomes, and therefore this trafficking pathway can also avoid endo/lysosomal degradation, as demonstrated for example with PLGA nanoparticles with an average size of 95 nm [311]. With regard to nanoparticles in the retrograde pathway, two key questions remain to be answered. The first unknown is how nanoparticles are sorted to the Golgi. Does this occur by endosomal fusion with the Golgi or do the nanoparticles first escape into the cytoplasm and then enter the Golgi? Does this occur by endosomal fusion with the Golgi or do the nanoparticles first escape into the cytoplasm and then enter the Golgi? The second unknown is whether or not these nanoparticles are excreted to the extracellular environment by using the secretory vesicles of the Golgi apparatus. A hint supporting this possibility was found almost 20 years ago using 40 - 120 nm colloidal gold nanoparticles labeled with fumaric and sebacic acid copolymers. These nanoparticles were found to localize into secretory vesicles of the Golgi near the lateral edge of the cell, suggesting that they might be secreted to the extracellular space [321]. This older result has drawn more recent attention now with the goal of using these secretory vesicles as a new nanoparticle target [299].

The third, and another rare, route for nanoparticles is autophagy (Fig. 4.2h). This is a degradative pathway in which autophagosomes deliver their components to lysosomes. To do this delivery, autophagosomes can first fuse with multivesicular bodies to form amphisomes. Then, both amphisomes and autophagosomes fuse with lysosomes for degradation of the cargo. Autophagy has been suggested for nanoparticle trafficking since some nanoparticle trafficking studies report nanoparticle localization in autophagosomes [322]. However, the exact role of autophagy in nanoparticle trafficking studies still has many unanswered questions, such as whether the nanoparticle uptake into autophagosomes is a specific or a non-specific process and whether autophagic engulfment of these nanoparticles causes stress within the cells. Thus, further careful investigation is required [323] to fully understand the autophagosome pathway for nanoparticles.

Endosomes: After internalization, nanoparticles are enclosed within endocytic vesicles which mostly fuse with early endosomes. Depending on the cell type, the size of early endosomes can reach up to 500 nm. They are mostly spherical, but some may exhibit tubulation [324], and all are moderately acidic (~pH 6.5). Endosomes sort nanoparticles to other organelles within the cytoplasm [324-326].

Multivesicular bodies: Multivesicular bodies (MVB's) mature from early endosomes within 4 - 30 min after endocytic uptake [327]. As the name implies these organelles are comprised of a larger vesicle which contains a series of smaller, so-called luminal vesicles. MVB's are formed by inward invagination of the early endosome membrane, which then pinches off into the interior of the endosome in a process known as scission to form a luminal vesicle [327]. The luminal vesicles are around 50-100 nm in diameter, and up to 30 or more can form. The entire MVB is typically round or oval with a diameter of 250 - 1000 nm [328]. MVB's can be easily recognized using electron microscopy which reveals the multivesicular body phenotype. Alternatively, these compartments can be recognized based on their molecular composition, for example by fluorescent tagging with specific antibodies. Multivesicular bodies contain markers such as Rabs, LAMPs and mannose 6-phosphate receptor (M6PR). Interestingly, the protein composition of the outer, so-called limiting membrane, and the intraluminal vesicles differ [329].

The cargo endocytosed into an early endosome typically ends up inside of the luminal vesicles of the MVB. How this happens is still uncertain, although it is known that this cargo is present within the luminal vesicle as soon as it is formed. This localization of the cargo to the site of luminal vesicle formation might be regulated by ubiquitination [329].

Following their formation, MVB's are typically trafficked in one of two ways: fusion with the plasma membrane or fusion with lysosomes [329]. In the first case, the fusion of an MVB with the plasma membrane leads to excretion of its cargo via release of a subset of the luminal vesicles to the extracellular space. The luminal vesicles that are excreted are known as exosomes, and they exhibit molecular differences from the other luminal vesicles. Specifically, the membrane of exosomes is high in cholesterol, sphingomyelin, ceramide and detergent-resistant membrane domains which stabilize the exosome vesicles in the extracellular space [330]. Excretion of exosomes by MVB's plays a role in a number of different biological processes, including the immune response [331, 332], the inflammatory response [333], cell-cell communication [334] and maternal-fetal communication [335].

Alternatively, MVB's may fuse with lysosomes thereby releasing the luminal vesicles into this organelle. Note that early endosomes may bypass the MVB step, and fuse directly with lysosomes.

Lysosomes: Lysosomes are the degradative organelle of both the cellular endo/lysosomal pathway and autophagy. By electron microscopy, the lysosomes appear as large vacuoles containing electron or X-ray dense material with whorls of internal membranes. The lysosomes maintain a strongly acidic environment (pH ~5.5) due to the proton pumping activity of vacuolar protein ATPases attached on their membranes. The lysosomes contain a large number of digestive enzymes, namely more than ~60 different soluble acid hydrolases such as peptidases, proteinases and nucleases. Lysosomes are therefore involved in the digestion of all internalized cargo, including obsolete components of the cell itself [194, 336, 337].

The lysosome has a 7 - 10 nm thick single phospholipid bilayer membrane which is covered with glycoproteins. This creates a continuous carbohydrate layer at the luminal side of the membrane to prevent its self-degradation [338]. These glycoproteins have

been used as markers of lysosomes [339] and are named lysosome associated membrane proteins (LAMP1/LAMP2) and lysosomal integral membrane proteins (LIMP 1/2) [338].

Autophagosomes: Autophagosomes are double membraned vesicles which are formed by three sequential steps. These steps are nucleation of an isolation membrane, namely the phagophore, elongation of this isolation membrane and then finally sealing to generate the immature autophagosome. The origin of the isolation membrane is still debated. However, most studies suggest that it may originate from either mitochondria or ER. During their formation, immature autophagosomes already engulf a part of the cytoplasm. [340, 341].

Through fusion with endocytic components, autophagosomes are involved in sequestration of cargo within the cell [342]. The initial, immature autophagosomes do not contain either lysosomal membrane proteins or enzymes, and they are not acidic. These initial autophagosomes then fuse with endocytic components, such as early endosomes and MVB's, to form hybrid organelles, namely amphisomes. These fusion events are interpreted to be a degradative cross-talk between endocytic and autophagic processes [342].

4.6 Targeting of nanoparticles to specific organelles

As explained in Chapter 4.5, for therapeutic purposes, it is often desirable to engineer a nanoparticle such that it will localize within a specific sub-cellular organelle and exert a particular function there. This is referred to as nanoparticle targeting, a term that includes both the localization as well as the specific localized activity engineered into the nanoparticle. Targeting is done either to treat or diagnose diseases or to induce controlled cell death.

Typical locations for nanoparticle targeting are the lysosomes, mitochondria, cytoplasm or nucleus [2, 299-305]. Most of these destinations are not part of the typical trafficking pathways. As explained in Chapter 4.5, nanoparticles are internalized via endocytosis and often stay enclosed within membrane bound organelles of the endocytosis pathway and subsequent intracellular trafficking routes [259, 299]. Since the lysosome is a part of most of these pathways, nanoparticles can easily reach lysosomes. However, to reach either mitochondria, the cytoplasm or nucleus, nanoparticles must be engineered to escape from

their intracellular trafficking routes. This localization of nanoparticles to the mitochondria, cytoplasm or nucleus is an ongoing challenge in nanomedicine. Next, some of the strategies to deliver nanoparticles to these specific locations and why this organelle delivery is required will be discussed.

Mitochondria are one of the subcellular targets of nanoparticles [301]. These organelles are involved in cellular energy regulation, and so play a role in many different diseases, including diabetes, obesity and Alzheimer's. Thus, it might be possible to detect and treat these diseases by targeting nanoparticles to the mitochondria. One way to achieve such mitochondrial targeting is by conjugating thiamine pyrophosphate (TPP) to the surface of a nanoparticle. TPP is a cation, which is then electrostatically attracted to mitochondria due to their negative membrane potential. If TPP nanoparticles are also conjugated with a therapeutic agent, then this agent can be specifically delivered to the mitochondria [301].

TPP targeting strategy has been tested as a potential treatment for Alzheimer's disease, in which the overproduction of reactive oxygen species (ROS) from the mitochondria might be a causative factor which ultimately leads to neuronal cell death. To reduce ROS levels, ceria (CeO_2) nanoparticles were used. These act as scavengers for ROS by shuttling between Ce^{3+} and Ce^{4+}. By attaching TPP to these ceria nanoparticles, the nanoparticles could be localized to mitochondria [300], where they protected cells against ROS species (specifically superoxide and hydrogen peroxide). The same nanoparticles also suppressed neuronal death in a mouse model system [300].

The lysosome is another commonly targeted organelle in cells in order to treat either dysfunctional lysosomes or to induce controlled cell death [299]. Here, the targeting is different than for mitochondria, since most nanoparticles already reach lysosomes naturally through either the endolysosomal route or autophagy without the need for a targeting peptide. Thus nanoparticles targeted to lysosomes only require a moiety that can be specifically activated once the lysosome is reached. To date, these moieties are either pH or light sensitive. Light sensitive nanoparticles can be activated once the nanoparticles reach lysosomes by exposure of the cells to light while pH sensitive nanoparticles are activated by the highly acidic conditions in lysosomes. As an example of light sensitive nanoparticles to target lysosomes, nanoparticles have been targeted specifically to dysfunctional lysosomes which arise under conditions such as lipotoxicity in which the

high levels of fatty acids alter the acidic condition of lysosomes. Regulation of the proper acidity in lysosome was achieved by targeting photoactivatable nanoparticles to lysosomes, which are then induced to release hydrogen ions through rapid photolysis after illuminating cells with light at 365 nm wavelength [302]. Alternatively, controlled cell death can also be induced by exploiting the acidic conditions of lysosomes. For instance, acid-activatable amphiphilic nanoparticles exploit the acidic environment of lysosomes for selective drug delivery in cancer targeting. Here, cancer cells are targeted due to their higher metabolism rates yielding higher nanoparticle internalization compared to healthy cells [303]. In another study, magnetic nanoparticles were also utilized to exploit the corrosive conditions of lysosomes in order to selectively kill cancer cells. When magnetic nanoparticles localize to lysosomes of the cells within a cancerous tissue, a localized magnetic field is applied to the therapeutic site. With the magnetic field, the nanoparticles rupture the lysosomes causing release of their corrosive content to the cytoplasm which kills the cancer cells [304]. This magnetic drug targeting has been used in the experimental treatment of cancer patients. It was found to reduce the cancer and extend the life of the patients without damaging healthy organs [343].

One of the most common and widely studied targeting sites of nanoparticles is the cytoplasm, since nanoparticles often carry therapeutics such as siRNA, which exert its effect in the cytoplasm. Furthermore, the cytoplasm is often the first destination for nanoparticles designed to ultimately reach the mitochondria or the nucleus [299]. To reach the cytoplasm, nanoparticles must first escape from the membrane-bound endosomes that arise upon nanoparticle endocytosis where the endosome membrane is a barrier. A number of strategies have been developed to enable nanoparticles to either bypass or escape from endosomes such as microinjection, lipid-mediated membrane fusion and destabilization of endosome membranes via prickly nanoparticles, cationic-polymer based nanoparticles and pH-responsive nanoparticles [319]. These strategies will be explained in the following paragraphs.

Microinjection is the mechanical delivery of nanoparticles directly into the cytoplasm via nano-needles [344]. More generally, this technique is also used to evaluate the intracellular fate of nanoparticles which are outside of membrane-bound organelles. For instance, diffusion of 20 nm quantum dots within the cytoplasm and nucleus was

evaluated after microinjection of nanoparticles into the cytoplasm and nucleus. In the cytoplasm, 70% of quantum dots diffused freely [344]. The remaining portion either moved within restricted corrals or was stationary. The diffusion coefficients of quantum dots ranged from 0.1 to 4 $\mu m^2/s$. These results were used to calculate the local biophysical properties of the cytoplasm using the Stokes-Einstein relation for diffusion. The viscosity of the cytoplasm was estimated to range between 4 to 200 cP dependent upon the specific region of the cytoplasm. This heterogeneity was attributed to the effect of the cytoskeleton and the endoplasmic reticulum on the diffusion of nanoparticles. In the nucleus, most quantum dots were immobilized after delivery. This was suggested to arise because nanoparticles were trapped in chromatin-dense domains of the nucleus. However, some nanoparticles within the nucleus could diffuse over an extended distance of ~10 μm before they became immobilized, which could reflect diffusion through interchromatin domains [344].

Lipid-mediated membrane fusion is another technique to target the cytoplasm. For this purpose, cationic liposomes are usually preferred. Once a cationic liposome is inside the endosome, electrostatic interactions are suggested to form between these liposomes and the luminal side of the endosomal membrane. Upon this interaction, anionic lipids of the endosomal membrane are suggested to laterally fuse with the liposome, which eventually results in fusion of these liposomes with the endosomal membrane to expose the material inside the liposomes to the cytoplasm [345]. Cationic liposomes can be loaded with nucleic acids, drugs or proteins to deliver therapeutics to the cytoplasm [346].

Destabilization of the endosomal membrane is another technique to target the cytoplasm. This has been accomplished by several different strategies. Recently, prickly nanoparticles were used to mechanically destabilize endosomes to enhance cytoplasmic escape of the nanoparticles. However, these nanoparticles have not been extensively studied yet. In contrast, cationic nanoparticles are very popular in the nanomedicine field to enhance endosomal escape of therapeutics through membrane destabilization. So far two different mechanisms for cationic-nanoparticle-mediated destabilization of endosomes were reported: temporary pore formation or endosomal rupture [347]. These will be explained in some detail in the following paragraphs. Note that the experiments in this thesis utilize a cationic polymer-based nanoparticle, namely a PEI-coated gold

nanoparticle, which is designed to escape to the cytoplasm from endocytic vesicles for gene delivery purposes.

According to the pore formation theory, some cationic nanoparticles including cationic PLGA, PEI and polynucleotides create a temporary pore on the endosomal membrane due to the electrostatic interaction between cationic nanoparticles and the luminal side of the endosomal membrane once nanoparticles are inside endosomes. From the opened pores, nanoparticles can then escape to the cytoplasm [347].

According to the endosomal rupture theory, nanoparticles permanently rupture endosomes to escape to the cytoplasm. Two different mechanisms have been suggested for endosomal rupture. First, cationic nanoparticles can rupture endosomes through electrostatic interactions between nanoparticles and the endosomal membrane. Secondly, cationic nanoparticles, which have amino groups, can rupture endosomes due to their buffering abilities via a phenomenon called the proton-sponge mechanism. According to this mechanism, once these nanoparticles are inside the endosomes, their unprotonated amino groups act like a proton pump attracting hydrogen and water molecules inside the endosomes. As water molecules continue to enter into the endosomes, the endosomes swell and eventually rupture. This rupture releases nanoparticles into the cytoplasm [44, 347].

The exact mechanism of endosomal escape by nanoparticles remains controversial [347]. One of the possible mechanisms, namely pore formation, is quite difficult to study because the pores are thought to be small and transient. Thus the pores might be detected by a high resolution technique like electron microscopy, but their transient formation greatly reduces the number of pores present at the moment when the cells are fixed. Alternatively, a live cell microscopy method increases the odds for finding a pore, but here the resolution is too low to visualize the pore. Instead to date, the investigation of pore opening has been done by a careful engineering of the experimental setup. In one such experimental design, a polymer-based nanoparticle was synthesized using a combination of poly (lactic-co-glycolic acid) (PLGA) and a copolymer, which is consists of 2-Propylacrylic acid (PAA), butyl methacrylate (BMA) and 2-(dimethylamino) ethyl methacrylate (DMAEMA), and evaluated for its endosomal escape mechanism. These polymer-based nanoparticles were then incubated with fluorescently tagged dextran

particles with different molecular weights such as 4, 40, 150 and 2000 kDa. Once both the polymer-based nanoparticles and the dextran particles were inside the endosomes, then only small dextran particles were found in the cytoplasm. This result suggested that the polymer based nanoparticles caused pore formation on the endosomal membrane letting only the small dextran out into cytoplasm, since dextran particles which were bigger than the opened pore on the membrane would stay enclosed within the endosomes [348]. In this thesis, the cytoplasmic escape mechanism of PEI-coated gold nanoparticles will be investigated to contribute to the literature on escape mechanisms.

Another example of nanoparticles used for destabilizing endosomal membranes is pH responsive nanoparticles which swell in acidic conditions. One example of such a nanoparticle is 2-diethylamino ethyl methacrylate core crosslinked with poly(ethyleneglycol) dimethacrylate and a 2-aminoethyl methacrylate shell. These nanoparticles were reported to expand 2.8-fold in diameter when they are transferred from pH 7.4 to pH 5.0 because the polymer chains were ionized in acidic conditions and repelled each other to cause the nanoparticle to swell. Once nanoparticles were inside the acidic compartments of the cell, the nanoparticle swelling is reported to disrupt endosomes and nanoparticles could escape into the cytoplasm [349].

In sum, the cytoplasm is targeted by nanoparticles through various techniques including microinjection, lipid-based membrane fusion and endosomal membrane destabilization via prickly nanoparticles, cationic nanoparticles and pH responsive nanoparticles. The membrane destabilization methods are controversial. Two main destabilization mechanisms have been suggested so far, namely pore opening and endosomal rupture.

Cytoplasmic escape from vesicles is often a prerequisite for targeting nanoparticles to another important site in the cell, namely the cell nucleus. Nuclear targeting is critical for example in many forms of gene therapy where DNA delivery is required [350]. However, targeting nanoparticles to the nucleus is a significant challenge since the nucleus is separated from the cytoplasm by a double membrane which contains nuclear pore complexes. According to morphological studies of nuclear pore complexes performed by cryo-electron tomography, these complexes are found to be 125 nm in diameter with an inner diameter of 40 nm [351, 352]. According to various studies, proteins can either freely diffuse into the nucleus or dilate the nuclear pore complex if they have nuclear

localization signals. The size limit for a protein to be able to enter into the nucleus in eukaryotes was defined as 60 kDa. However, proteins with higher masses (~150 kDa) were also reported to localize to the nucleus [353, 354]. In another study, fluorescent molecules were traced to visualize the steps of nuclear entry via fluorescence microscopy, and molecules up to 40 nm were found to enter into the nucleus via nuclear pore complexes. However, any size larger than 40 nm can enter into the nucleus only if the central channel of the nuclear pore complex is disrupted [355].

This intrinsic cellular process of nuclear entry via a nuclear localization signal has been translated into nanomedicine (and also used as a tool to understand the general nuclear entry mechanism). Nanoparticles have been conjugated with various nuclear localization signals such as TAT, HA2 and GALA [316]. With this strategy, microscopic studies have suggested that gold nanoparticles up to 28 nm can enter into the nucleus through nuclear pores [356, 357]. In another study providing evidence for nanoparticle entry through nuclear pores, the nuclear entry of gold nanoparticles was compared in dividing and non-dividing cells using electron microscopy [200]. Gold nanoparticles were conjugated with nuclear localization signals and their size ranged between 4 nm and 25 nm. Results suggested that in dividing 3T3-L1 cells, the size distribution of nanoparticles within the cytoplasm and nucleus was similar and ranged between 4 nm to 25 nm. However, in nondividing 3T3-L1 cells, the number of nanoparticles inside the nucleus was less than in dividing cells and furthermore only a subset of nanoparticles was found in the nucleus, namely those less than 20 nm. This suggested that in non-dividing cells entry into the nucleus was through the nuclear pore, and consistent with this the authors could detect many nanoparticles on the nuclear envelope with some localized at pores [200]. Also, in this thesis, 50 nm gold nanoparticles were detected inside the nucleus, but only if they were coated with PEI polymers, as will be explained in Chapter 8. Additionally, the effect of the concentration of PEI-coated gold nanoparticles in nuclear entry efficiency will be investigated in Chapter 11. In this thesis, rare events like nuclear entry can easily be detected since a high resolution 3D technique, cryo soft X-ray tomography, is used instead of a 2D technique like transmission electron microscopy.

4.7. Physiological effects of nanoparticles on cells

Nanoparticles have been shown to have a number of different physiological effects on cells [358-360] including promotion or suppression of cell growth [359, 361-366], inhibition of cell migration [360], induction of reactive oxygen species [367-369] and alterations in protein expression [359-361, 365, 370]. Furthermore, nanoparticles may induce cells to differentiate or to undergo either apoptosis or caspase-independent cell death. A few studies also suggest that nanoparticles may induce changes in cell morphology [66], including changes at the cell surface [66, 371] and changes in microtubules [372], mitochondria [372], lysosomes [372], ER [373-375] or nuclei [358, 364]. In the subsequent paragraphs, a number of these reported changes induced by nanoparticle treatment will be discussed in more detail.

Nanoparticles were found to exert oxidative stress on cells, as detected by measuring the levels of reactive oxygen species within cells [367-369]. Reactive oxygen species are oxidative radicals, which are formed by incomplete reduction of oxygen [376]. Such oxidative stress induced by nanoparticles has been reported to produce a long list of cellular modifications and damage, including loss of plasma membrane integrity [372], cytoskeleton reorganization [377], chromatin reorganization and condensation [358, 364, 372], DNA damage [367], mitochondrial damage, alterations in mitochondrial morphology [368, 372], lysosome impairment [378], alterations in lysosome morphology [379, 380] and increases in the size and number of lipid droplets [380]. Nanoparticle-mediated oxidative stress was also shown to promote an inflammatory response in primary dendritic cells by increasing the expression of proinflammatory cytokines, even though cytotoxic effects were not observed in the cells [381].

Importantly, increased levels of reactive oxygen species can be fatal especially at high nanoparticle concentrations. This has been exploited in cancer treatment or for anti-bacterial purposes by using some nanoparticles such as gold nanoparticles, silver nanoparticles and titanium dioxide nanoparticles to induce reactive oxygen species production in a size-dependent manner [376, 382].

Nanoparticles were also reported to alter protein and gene expressions in cells. This resulted in altered cell-cell signaling or differentiation of progenitor cells into specific lineages [359-361, 365, 370, 383-386]. For example, in hen ovarian granulosa cells zinc

oxide nanoparticles increased the expression of over three hundred genes associated with a variety of processes including human T-cell lymphotropic virus type 1 (HTLV-I) infection, natural-killer-cell-mediated cytotoxicity, cell adhesion, hepatitis, cancer and apoptosis. Protein expression was also greatly altered as a consequence. Some of the proteins expressed were found to localize to extracellular regions or cell junctions, suggesting that the nanoparticle treatment may alter the signaling properties of the cells [365].

The nanoparticle-induced protein expression changes have been linked to differentiation of various progenitor cell lines. For example, both gold and titanium oxide nanoparticles were found to promote differentiation of mesenchymal stems cells into adipocytes and then eventually osteoblasts. This differentiation pathway was tracked by measuring cell morphology, lipid droplet size and the levels of adipogenic and osteogenic gene expression [359, 383]. The extent of differentiation along this pathway could be adjusted by altering the concentration of gold nanoparticles [359, 360, 383]. It has been suggested that these changes in gene expression might arise due to the mechanical stress induced by the nanoparticles on the mesenchymal cells [359, 383]. Another example of nanoparticle induced differentiation comes from treatment of bone marrow cells with extracellular vesicle-mimetic nanovesicles. These induced differentiation into insulin-producing cells. This approach has been used to treat diabetes mellitus in animal models [384].

Several studies have reported that nanoparticles can alter the cell surface. For example, polymer-coated gold nanoparticles reduced the number of filopodia in HUVEC cells [66]. Moreover, TiO_2 nanoparticles (below 100 nm) led to alteration of microvilli structures in intestinal epithelial cells [371].

Nanoparticles also induced some alterations at sub-cellular sites. One site was the cytoskeleton [377]. For instance, 20 nm silver nanoparticles caused loss of some cytoskeleton components such as ß-tubulin and filamentous actin, as detected by fluorescence microscopy measurements. Furthermore, reduced viability of the cells was observed [387]. However, with 37 nm gelatin nanoparticles, even though similar cytoskeleton changes were observed as in fibroblasts, the viability of the cells was not reduced. However, the gelatin nanoparticles resulted in increased vacuolization and produced membrane abnormalities that were observed by fluorescence, TEM and SEM

imaging [388]. Interestingly, other nanoparticles have different effects on the cytoskeleton. Silica nanoparticles (50 nm or 100 nm) induced the formation of long and thick filamentous actin fibers [389].

Nanoparticles have also been reported to have effects on mitochondria. Both cerium dioxide nanoparticles and amine modified polystyrene nanoparticles caused elongation of mitochondria and loss of mitochondrial membrane potential in human peripheral blood monocytes [390]. TiO_2 nanoparticles had different effects. They caused swelling of mitochondria and disruption of the inner and outer mitochondrial membranes [373].

Many nanoparticles are known to cause autophagosome accumulation in cells [379, 391-394]. This has been detected by a variety of approaches including fluorescence labeling of autophagosomes via fluorescence microscopy or by assessing the upregulation of autophagosome markers in the cells by western blot assay [379, 391-394]. A rapid increase in autophagosome numbers is a morphological hallmark of autophagy. Under stress conditions such as nutrient deprivation or pathogen invasion, which sometimes occurs after nanoparticle internalization, autophagy is induced to maintain cell homeostasis. These autophagosomes can engulf and sequester damaged organelles, aggregated proteins, foreign materials or parts of the cytoplasm via either selective or non-selective processes [341, 395]. By sequestering harmful cytoplasmic contents to lysosomes, autophagosomes postpone or slow-down apoptosis. If autophagy fails to remove enough harmful content from the cell interior, then apoptosis takes over and programmed cell death is induced. In some studies, it is also reported that autophagy itself may induce cell death, which is called autophagic cell death. The autophagic cell death pathway is still debated. However, current theories suggest that when overstimulated, autophagosomes mistakenly engulf vital organelles and proteins. This can lead to self-digestion. Such an improper regulation of autophagy may lead to cancer or neurodegenerative diseases. Therefore, increase in autophagosome numbers upon nanoparticle incubation should be carefully monitored and nanoparticle properties should be tuned to reduce the autophagic response if controlled cell death is not the aim of the treatment [341, 395].

Additionally, titanium nanoparticles and silica nanoparticles were reported to lead to ER stress through disruption of the calcium homeostasis and protein folding in the cells

[373-375] and titanium oxide nanoparticles were reported to disrupt contact sites of ER and mitochondria [373].

In sum, nanoparticles may exert many physiological effects on cells including formation of reactive oxygen species, alterations at the cell surface, in the cytoskeleton or in protein and gene expression, induction of cellular differentiation and autophagy, and disruption of the function and morphology of mitochondria. One powerful approach to understand these physiological effects has been morphological studies of cells exposed to nanoparticles, but so far these studies are fairly limited. In particular, all have focused on the changes within a specific organelle of interest, and to date no studies have examined the global sub-cellular changes induced by nanoparticles. Such an overview of sub-cellular morphology would provide a much more comprehensive view of the potential physiological effects induced by nanoparticles on cells.

4.8 Summary

This chapter has discussed the importance of characterizing nanoparticles for their interactions with biological systems via *in vitro* studies, *in vivo* studies, animal studies and clinical trials before their use in biomedical applications. Since an *in vitro* analysis was performed in this thesis, this chapter has focused on *in vitro* studies, including the main steps of performing an *in vitro* study to analyze cellular interactions of nanoparticles. First, nanoparticles are synthesized and characterized for their physicochemical properties. The stable and monodisperse solutions of nanoparticles within cell culture mediums are then incubated with cells. Upon incubation, the cells endocytose nanoparticles thorough different endocytosis pathways and traffic the cargo within the cell through different trafficking pathways. Recently, some strategies have been developed to direct nanoparticles to either the mitochondria, nucleus, lysosomes or cytoplasm. However, these targeting strategies are not specific enough yet. In the literature, the driving factors of how nanoparticles select their endocytosis and trafficking routes remains unclear. The aim of this thesis is to contribute toward a better understanding of these driving factors by analyzing the endocytosis and trafficking pathway of dPGS and PEI nanoparticles and comparing them to each other. Only when it is understood how nanoparticles select specific endocytosis and trafficking routes can these nanoparticles then be efficiently directed to specific pathways to reach specific end-

points. Additionally, as described in this chapter, besides improving biomedical applications, nanoparticles can also yield unwanted physiological effects on cells and these need to be tested before nanoparticles are used in biomedical applications. In the literature, the morphological effects of nanoparticles on cells are greatly ignored even though morphology has strong correlations with function. Therefore, in this thesis, the focus will be on the morphological effects of nanoparticles on cells by examining two different nanoparticles, namely dPGS nanoparticles and PEI nanoparticles.

5. MICROSCOPY TECHNIQUES TO STUDY NANOPARTICLE - CELL INTERACTIONS

To be able to design a nanoparticle which provides the safest and most efficient treatment and diagnosis, it is critical to understand the interaction between nanoparticles and cells. The accumulated knowledge about these cellular effects, however, is still very limited. Certainly, many rules, which help define the interactions of nanoparticles with cells, are not known. For example, the reasons why certain nanoparticles select a specific pathway to enter the cell, how nanoparticles escape to the cytoplasm, which nanoparticles localize to which organelles, why some nanoparticles enter the nucleus and some do not, or how nanoparticles, once they perform their function, can be completely eliminated from cells are not known. This is partly because of the complexity of biological systems, partly because of the wide variety of nanoparticles and the reactivity of their surfaces, and partly because of the lack of appropriate imaging techniques to analyze nanoparticle - cell interactions.

For understanding nanoparticle - cell interactions, the ideal imaging tool needs to provide a high contrast for both nanoparticles and cell compartments. In addition, a sufficiently high 3D resolution is needed to resolve both individual nanoparticles and the cell ultrastructure. Other important capabilities for the optimal imaging tool would include 3D dimensional label-free imaging, high throughput and finally live-cell imaging capabilities [59].

In this chapter, the most common imaging techniques that are being used for cellular studies at the nanoscale are reviewed: light microscopy, fluorescence microscopy and electron microscopy [396]. Super resolution fluorescence microscopy [397], Raman spectroscopy [398], electron tomography [399] and X-ray tomography [400] are other emerging techniques for cellular studies. As summarized in Fig. 5.1 and described in the following sections, each technique has its advantages and disadvantages. Therefore, some combination of these techniques will be required to understand nanoparticle - cell interactions.

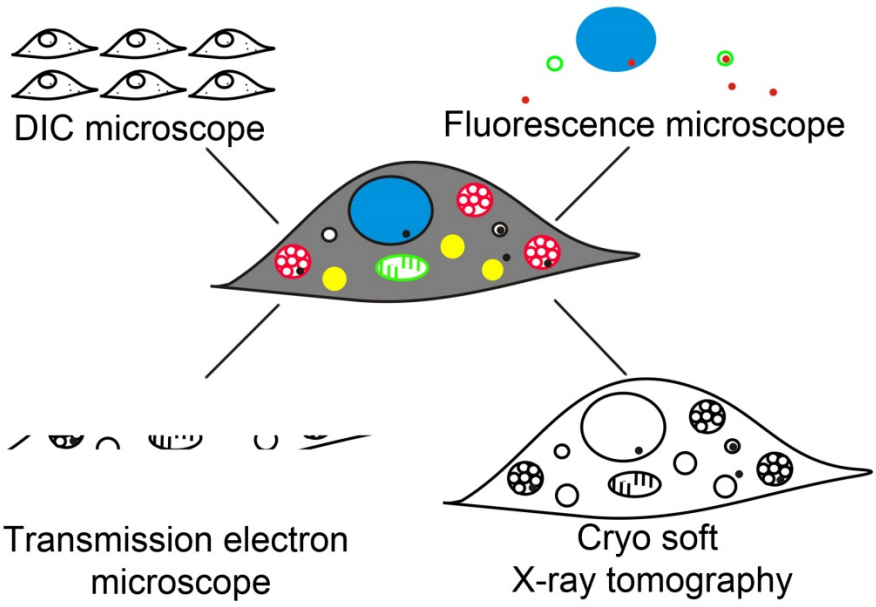

Figure 5.1 Comparison between microscopy techniques to study nanoparticle - cell interactions. The DIC microscope can provide statistical information. However, it cannot resolve the ultrastructure of cells and the location of nanoparticles relative to these cellular features. Fluorescence microscopy can provide high resolution if super resolution techniques are used. However, the features need to be tagged fluorescently. This requirement limits the number of features which can be simultaneously imaged. TEM also provides high resolution for all features of the cell and nanoparticles can also be resolved. However, with this technique only a thin section of the cell can be imaged, which makes it difficult to detect rare events such as cytoplasmic escape and nuclear entry. Cryo soft X-ray tomography can image cells in 3D in their near native state with high resolution. This can reveal nanoparticle - cell interactions, although cryo-fixed cells must be used.

5.1. Light microscopy to investigate nanoparticle - cell interactions

Light microscopes, such as transmitted or fluorescence light microscopes, provide the capability to image cell and nanoparticle interactions within either live or fixed cells and with a minimal amount of sample preparation. This enables high throughput imaging.

The nanoparticle - cell interaction can be studied by various transmitted light microscopes, such as bright field, phase contrast, dark-field, and differential interference contrast (DIC). For each of these microscopes, the resolution is limited to ~200 nm due to by the wavelength of light used for imaging [401]. Thus these microscopes cannot resolve two adjacent nanoparticles, but single nanoparticles or clusters of nanoparticles can be detected if they have sufficient contrast. Bright-field light microscopy relies on the absorption of light by the specimen. It can detect overall morphological changes in the

cell, but in general does not provide sufficient contrast to detect nanoparticles. Phase contrast relies on refractive index differences in the cells which is useful for detecting many sub-cellular features. However, the dark field and DIC modes in the light microscope are better suited to detect highly scattering nanoparticles within label-free cells [401]. Since DIC microscopy has been used in some of the experiments performed in this thesis, DIC microscopy will be described in more detail in the following chapters.

DIC microscopy detects optical path differences in a specimen by splitting the light beam into two parts and then recombining them after passing through the specimen. This greatly enhances the contrast of typical biological specimens. It also enhances the contrast of small nanoparticles making them visible by DIC. Thus a variety of nanoparticles have been detected by DIC, including 25 nm nuclear-peptide-conjugated gold nanoparticles [402], 100 nm mesoporous silica [403] and silver, polystyrene, silica and poly (methyl methacrylate) nanoparticles of different sizes ranging between 20 nm to 400 nm [404]. Although DIC can detect these nanoparticles, due to the 200 nm resolution limit of light microscopy, it cannot determine whether a single nanoparticle or a cluster is being visualized [404]. DIC has been used to study the kinetics of nanoparticle uptake [403], and to track the localization of nanoparticles within organelles such as the nucleus [402]. Another advantage of DIC is that it has a small depth of focus which provides good axial resolution thereby enabling optical sectioning of a thicker specimen. In bioimaging, DIC is often used as a template on which to overlay fluorescence images [405, 406].

One important consideration in the analysis of DIC images is that due to the contrast mechanism, the images take on a 3D appearance with the presence of peaks and troughs in the image. These peaks or troughs reflect optical gradients within the specimen. Thus a peak may either be a raised feature or it may be an area of high refractive index. And similarly, a trough may either be a hollow feature or an area of low refractive index such as a vacuole.

Fluorescence microscopy provides the best contrast among the light microscopy methods. The contrast is achieved by labeling structures of interest with fluorophores. When fluorophores absorb photons, electrons are promoted from their ground state to an excited state. When they return to their ground state, the molecule emits fluorescent light which has a lower energy than the exciting photon since some amount of the excitation

energy is transferred into vibrational energy. Different kinds of fluorophores exist, including quantum dots and organic fluorophores such as FITC or fluorescence proteins such as GFP [407, 408].

The labeling with fluorophores is used in several different kinds of fluorescence microscopes, such as wide-field and confocal laser scanning microscopy. These microscopes typically operate in epifluorescent mode, meaning that the same lens is used as both the condenser to shine excitation light on the specimen and as the objective to collect the emitted fluorescence. Filters are typically inserted in both the excitation and emission paths to select the appropriate wavelengths. The wide-field microscope illuminates the entire specimen within one field of view, usually with light from an ultraviolet or xenon arc lamp. In contrast, confocal laser scanning microscopy utilizes a laser beam which is focused to a point in the specimen and raster scanned over the area of interest. At each point in the raster scan, the focal point in the specimen is then imaged by the objective lens to a pinhole in front of the detector. This reduces out-of-focus fluorescence arising from regions above or below the focal point. Therefore, the confocal imaging configuration increases axial resolution and enables optical sectioning, hence, 3D imaging [408].

Fluorescence microscopy has been used extensively to study nanoparticle - cell interactions. For example, the internalization of nanoparticles by cells can be evaluated using fluorescently tagged nanoparticles. To confirm whether these fluorescent nanoparticles are endocytosed or not, the plasma membrane of cells can be labeled either with a fluorophore of another color or the cell can be visualized directly by transmitted light microscopy and overlaid onto the image of the fluorescent nanoparticles [409]. Moreover, similar fluorescent double-labeling strategies can be employed to follow the trafficking of nanoparticles within the cell [410]. For example, different organelles can be tagged with fluorescent labels to see if nanoparticles colocalize with them. These analyses can be combined with experiments in which specific inhibitors are used for different steps in the endocytosis pathway in order to help define the trafficking pathway [39, 411]. Additionally, some functionality assays can also be performed by fluorescence microscopy. For instance, the efficacy of a gene delivery agent, which carries a DNA encoding for a fluorescent protein such as GFP, can be assessed by the amount of GFP

expressed within the cell [286]. Therefore, light microscopy provides valuable and high-throughput data about cellular interactions of nanoparticles from living cells.

However, light microscopy has some disadvantages. First, conventional light microscopy provides low resolution. Nanoparticles are smaller than 100 nm and tracing these small structures requires higher resolution. The resolution limitations of conventional light microscopy can now be overcome by super-resolution fluorescence microscopy [412]. This approach can bypass the diffraction-limited resolution of conventional fluorescence microscopy by using stimulated emission, photo-switchable fluorophores, structured illumination or some combination of these strategies. With these super-resolution techniques, 10 nm resolution can be achieved under optimal circumstances, and these approaches are now beginning to be used to investigate interactions of nanoparticles with cells [413]. However, in fluorescence microscopy, the labeling of both nanoparticles and cell components are required. This labeling may alter the physicochemical identity of the nanoparticles and/or the behavior of the labeled cellular components [59]. Additionally, by fluorescence microscopy only labeled features can be studied and this may result in the loss of information related to unlabeled components. Therefore, in this thesis, to overcome these disadvantages of conventional light microscopy, cryo soft X-ray tomography was selected to investigate cellular interactions of nanoparticles. Cryo soft X-ray tomography is a high resolution technique. With this technique, both nanoparticles and cellular features can be resolved without the need for labeling.

5.2 Electron microscopy to investigate nanoparticle - cell interactions

In principle, TEM can resolve atoms in samples with a spatial resolution of 0.1 nm. Therefore, TEM can be used to determine the size, the shape and the number of nanoparticles internalized by cells. At the same time, TEM also provides detailed information about the morphology of cellular structures which provides the opportunity to investigate the morphological features of cell. Therefore, TEM can study nanoparticle internalization, nanoparticle localization within cell compartments and also nanoparticle distribution after nanoparticle treatment [414, 415].

When electron beams interact with a sample, they undergo elastic and inelastic scattering [416]. The number of scattering events increases as the thickness of the sample

increases. In practice, the inelastic scattering of the electrons in the TEM limits the sample thickness to a few hundred nanometers. Note that scattering of the electron beam is stronger for heavier atoms (with high Z) than for light elements (with low Z), hence, a contrast between the heavy and the light material occurs [416]. Therefore, the high Z materials of the nanoparticles enable their detection by TEM with high contrast within the cellular environment.

Although TEM provides high resolution imaging, the technique is not suitable for direct imaging of whole cells due to their thickness of many microns. Therefore, the cells need to be sectioned into thin sections. To address these limitations of TEM, the biological sample needs to be carefully prepared through two established techniques which are described in the following paragraphs [417, 418].

The conventional TEM sample preparation technique requires chemical fixation, dehydration and plastic embedding steps [417, 419]. With this conventional TEM sample preparation technique, the cell is stabilized against vacuum conditions and hardened for sectioning. Therefore, the sample can be serially sectioned into slices of 40-100 nm thickness which then can be imaged to analyze cell structures and nanoparticle locations. These serial slices can be combined to obtain a 3D image of the cell. However, the sample preparation steps are reported to alter the ultrastructural features of the samples. For instance, chemical fixation is often performed by aldehydes which are reported to cause artefactual findings. Additionally, aldehydes cannot effectively fix all of the lipids within the cell. Therefore, to stabilize lipids, an additional chemical fixation by osmium tetroxide is required which is reported to cleave proteins and alter their structures upon long incubation times. After chemical fixation, the sample is dehydrated by ethanol or acetone in which these organic solvents are replaced with the water inside the cell. Unfortunately, these organic solvents cause aggregation of proteins and nucleic acids which were not successfully immobilized by the prior chemical fixation step. After dehydration, the plastic resin is infiltrated within the cells and polymerized through heat or UV light. During plastic embedding, the size of the sample is reported to be shrunken considerably. Therefore, the native state of the cell cannot be preserved and the acquired 2D and 3D images can be misleading [417, 419].

During this conventional sample preparation technique, staining of the sample is another requirement to be able to create contrast of the biological sample compared to the plastic resin that has been infiltrated and polymerized. The staining usually utilizes different heavy metals such as uranyl acetate, uranyl formate or lead citrate , which create a shell of heavy metal atoms around different cellular structures, thereby creating the amplitude contrast needed [419]. However, staining may cause loss of some ultrastructural details since the obtained images map the affinity of stains to the different regions of the biological sample [417, 419]. Additionally, it is also reported that heavy metal staining can be easily misinterpreted as nanoparticles, a result which would further complicate the analysis of cellular interactions with real nanoparticles [420].

A more modern TEM sample preparation technique requires cryo-fixation of the living cell. This can be done by plunge freezing, slam freezing or high pressure freezing [421, 422]. As in conventional TEM, the sample still needs to be sectioned, which must be performed under cryo conditions using a diamond knife [417, 419]. This sectioning has some drawbacks such as knife marks and deformation of the section in the direction of cutting [417, 423]. These artefacts caused by the cutting process make it impossible to acquire a 3D image of the whole cell by serial sectioning.

However, obtaining 3D information from the cell is extremely important especially during analysis of nanoparticle interactions since these interactions occur throughout the 3D native environment. To obtain 3D images of the cells, electron tomography has been developed in which projection images from a thin slice of a cell can be obtained over a tilt angle series. The projection images are later reconstructed into 3D images of this cell slice. Electron tomography provides high contrast images for stained samples that have also been chemically fixed, dehydrated and plastic embedded. However, for cryo-fixed, unstained cells, the contrast is low and furthermore only thin sections of the cell (<500 nm) can be examined [419].

Another 3D electron microscopy technique that has been developed is focused ion beam (FIB) – scanning electron microscopy (SEM). This technique uses a scanning electron microscope to image the surface of a specimen, and then uses a focused ion beam to mill away a thin layer on the specimen surface to expose a somewhat deeper layer of the specimen. This layer can then be imaged with the scanning electron microscope. Iteration

of this process produces a 3D image of the specimen. FIB – SEM has been primarily used for samples which have been chemically fixed, stained and embedded and so also suffers from potential artefacts [424].

In sum, none of the widely used forms of microscopy provide a high resolution technique which generates a 3D image from an intact, native cell. Such a capability is provided by cryo soft X-ray tomography, which is used in this thesis. This technique will be described in more detail in the next section.

5.3 Cryo soft X-ray tomography for nanoscale imaging of cells

As described above and as summarized in Fig. 5.1, conventional methods for imaging nanoparticle - cell interactions have some serious limitations. None of these approaches can provide a complete 3D ultrastructural image of a native cell.

To overcome the drawbacks of light microscopy and electron microscopy, an imaging technique based on soft X-rays is utilized in this thesis [62, 425]. Soft X-rays are electromagnetic waves with short wavelengths in the range from 1 - 10 nm. According to the Rayleigh resolution criterion, due to their short wavelengths, soft X-rays can potentially provide high resolution to resolve cell ultrastructure. Moreover, the penetration depth of soft X-rays into a biological specimen is much larger than that of electrons. Therefore, soft X-rays provide the ability to image whole cells (~10 μm) without slicing. Since soft X-rays provide high resolution, elemental specific imaging and high penetration into biological samples, they can be used for studying nanoparticle - cell interactions by high resolution 3D imaging [62, 425].

However, to utilize soft X-rays to image hydrated biological samples is not straightforward. First, the refractive index of all materials in the soft X-ray region is close to unity. Therefore, focusing X-ray beams by using conventional refractive optics is not possible. Instead, special diffractive or total reflection X-ray optics need to be utilized. Second, similar to the TEM, X-rays cause radiation damage to cells. To prevent this, cryo-fixation must be used to embed whole cells into a vitrified ice layer [62].

In the following sections, the interaction of X-rays with matter which leads to the natural contrast mechanism used in soft X-ray imaging will be described. In addition, the currently existing X-ray imaging techniques will be introduced and compared. Finally,

cryo soft X-ray tomography (cryo-SXT) will be described in detail since this method was utilized in this thesis to study nanoparticle - cell-interactions.

5.3.1 Interaction of soft X-rays with the matter

Upon interaction with a material, incoming X-rays are attenuated and phase shifted. The absorption and phase shift of X-rays in a given material can be described by the complex refractive index for that material:

$$n = 1 - \delta - j\beta \qquad \text{Eq. 5.1}$$

where δ represents the phase shift and β represents the attenuation of X-rays while passing through the material. δ and β values of all materials are very small ($\leq 10^{-3}$) in the X-ray range, rendering the refractive index of all materials slightly less than unity for X-rays.

The electric field corresponding to monochromatic X-ray light propagating along the positive z-axis can be written as $A(z) = A_o e^{(-jkz)}$, where $k = 2\pi/\lambda$ and λ is the wavelength of the X-ray light. When these soft X-rays pass through matter with a defined thickness (d) and a defined refractive index (n), the electric field of the X-rays after passage through the material can be written as:

$$A(d) = A_o \cdot e^{(-jkn(\lambda)d)} = A_o \cdot e^{(-jkd)} \cdot e^{(jk\delta(\lambda)d)} \cdot e^{(-k\beta(\lambda)d)} \qquad \text{Eq. 5.2}$$

The intensity of an electromagnetic wave is proportional to the square of the amplitude of the light ($I = \alpha A^2$). The transmission of X-rays passing through the material is calculated by the quotient of the transmitted and incoming light. Therefore, the transmission is given by Beer's law:

$$T = \frac{I_d}{I_o} = \frac{|A_d|^2}{|A_o|^2} = e^{(-2k\beta(\lambda)d)} = e^{-\mu d} \qquad \text{Eq. 5.3}$$

The transmission of X-rays passing through matter depends on the element, the density of the material and the photon energy of the X-rays. Depending on the element, the X-ray transmission shows absorption edges at certain photon energies (Fig. 5.2). These energies correspond to the binding energies of the inner-shell electrons of the elements.

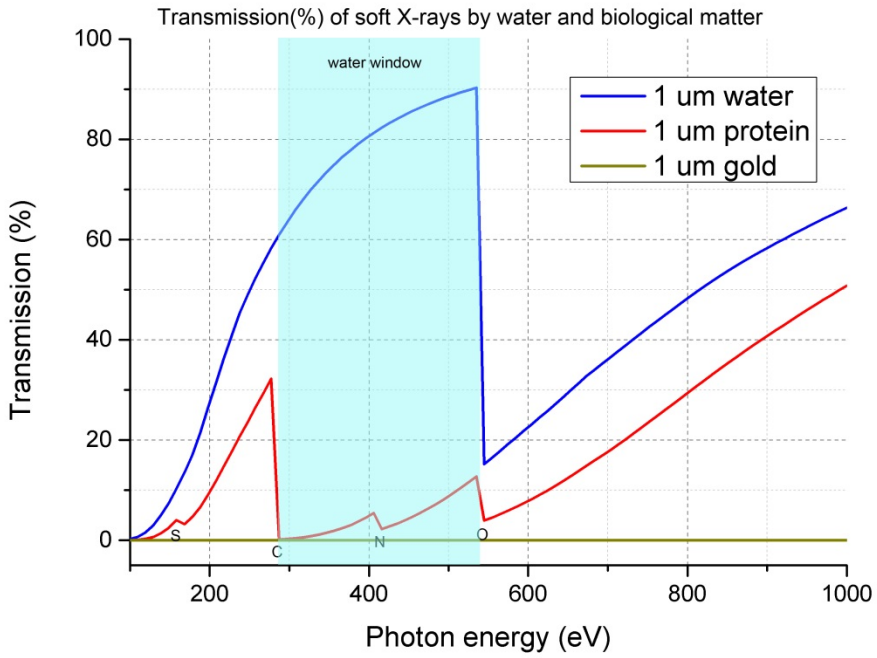

Figure 5.2 Transmission of soft X-rays at different X-ray photon energies by water, or a typical protein or gold, each of 1 μm thickness. The region between the K-adsorption edge of carbon and oxygen (290 eV-540 eV) is called the water window. In this water window, protein absorbs significantly stronger than water yielding a natural absorption contrast that can be used to distinguish organic matter from water without a need for chemical staining. In this same water window, gold absorbs even more strongly than protein, and so gold nanoparticles can also be easily discerned.

5.3.2 Contrast mechanism for imaging cells in cryo soft X-ray tomography

Soft X-rays are frequently used to image hydrated cells in their near native state. In this state, the mass fraction of intracellular water with respect to total cell mass is ~70% for E.coli [426] and ~65% for yeast [427]. In the soft X-ray energy range organic matter can be distinguished from water (or ice) through natural absorption contrast within a photon energy region from 282 eV (carbon K-absorption edge) to 533 eV (oxygen K-absorption edge) - the so-called water window energy range [428]. In this region, organic matter which contains elements such as carbon and nitrogen absorbs X-rays significantly stronger than water (Fig. 5.2). Therefore, cellular ultra-structures can be visualized with high contrast in their near-native state without the necessity of staining [428, 429].

In this thesis, the ultimate aim is to image both cellular ultrastructure and gold nanoparticles. This can be accomplished in the water window because gold absorbs X-

rays stronger than water and protein. Therefore, 50 nm gold nanoparticles can be tracked within the cells.

5.3.3 Lens-based and lens-less X-ray imaging techniques

So far the interaction of X-rays with matter was discussed. Now the techniques which utilize X-rays for imaging will be described. These techniques can be roughly classified as lens-based and lens-less X-ray imaging methods. X-ray imaging techniques which do not utilize X-ray lenses for image formation and therefore require reconstruction of image information from reciprocal space include coherent diffraction imaging (CDI), Fourier transform holography (FTH) and ptychography [430]. In contrast, scanning transmission X-ray microscopy (STXM) and full-field transmission X-ray microscopy (TXM) are real space imaging techniques using suitable X-ray lenses [431].

Coherent diffraction imaging (CDI) is a lens-less X-ray imaging technique for 2D and 3D imaging of nanoscale structures (Fig. 5.3a) [430]. In this technique, a monochromatic, coherent X-ray beam is used to illuminate the object. The X-ray photons are scattered by the object and produce a far-field diffraction pattern which is collected by an X-ray detector (Fig. 5.3a). The X-ray detector only records the intensity of the scattered X-ray beam. Hence the phase information is lost (this is known as the phase problem [430]), and so prior knowledge of the specimen is required to reconstruct the image from the reciprocal space diffraction pattern through iterative feedback algorithms. In particular, the sample has to be isolated and small. So far, CDI experiments provided reliable imaging results only on artificial samples and high resolutions for biological samples could not be attained [432].

Ptychography is a similar technique to CDI. However, in contrast to CDI in ptychography a coherent, focused X-ray beam is scanned over an extended sample (Fig. 5.3b) [433-435]. Thereby, for each position a diffraction pattern is recorded on an X-ray detector including an overlap of the single illumination patches. The overlap of the regions generates the required oversampling to solve the phase problem and avoids ambiguity as in CDI experiments [433-435]. Ptychography has been demonstrated to be well suited for analyzing strongly scattering extended samples. However, higher resolutions are more difficult to obtain for specimens that are not strongly scattering such

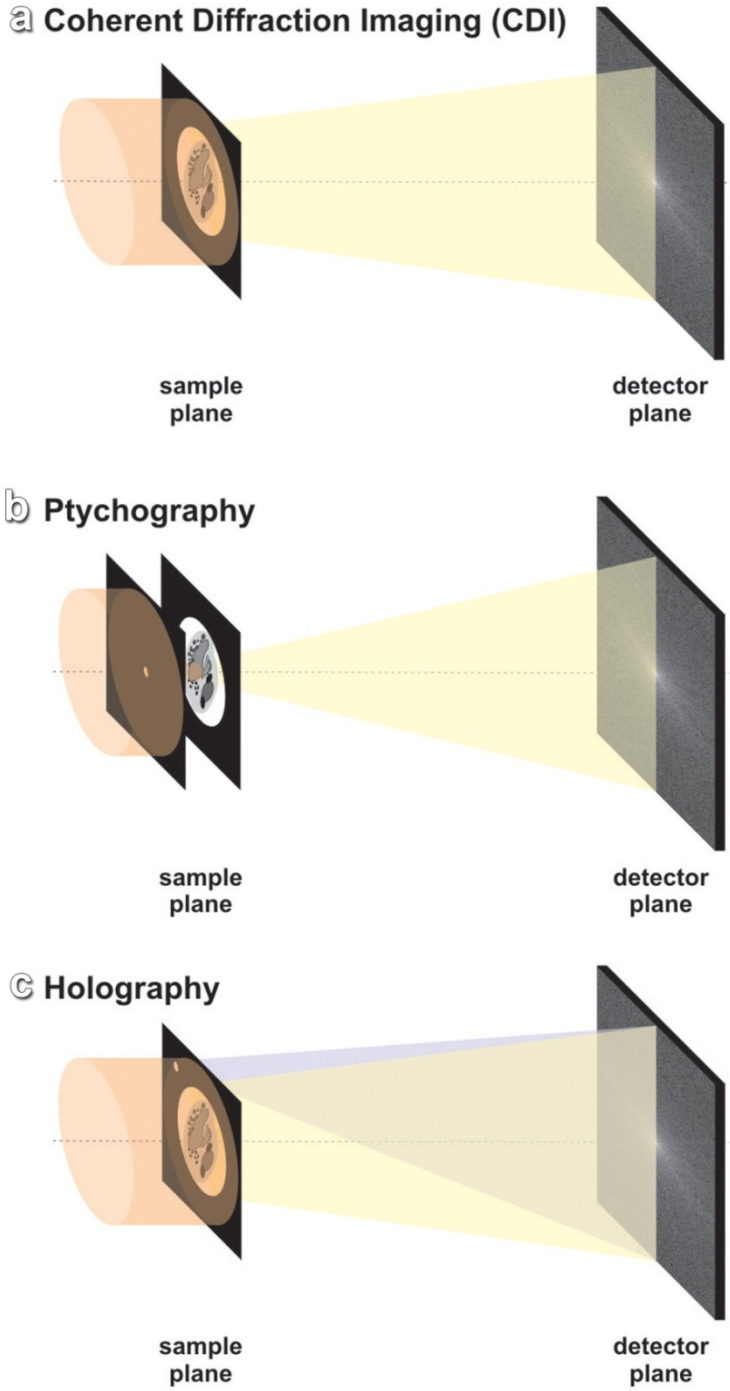

Figure 5.3 Optical setup of lens-less X-ray imaging techniques: coherent diffraction imaging (a), ptychography (b) and Fourier transform holography (c).

as biological samples. Recently, 2D reconstructions of a biological sample have been obtained that reveal some higher resolution structures [436].

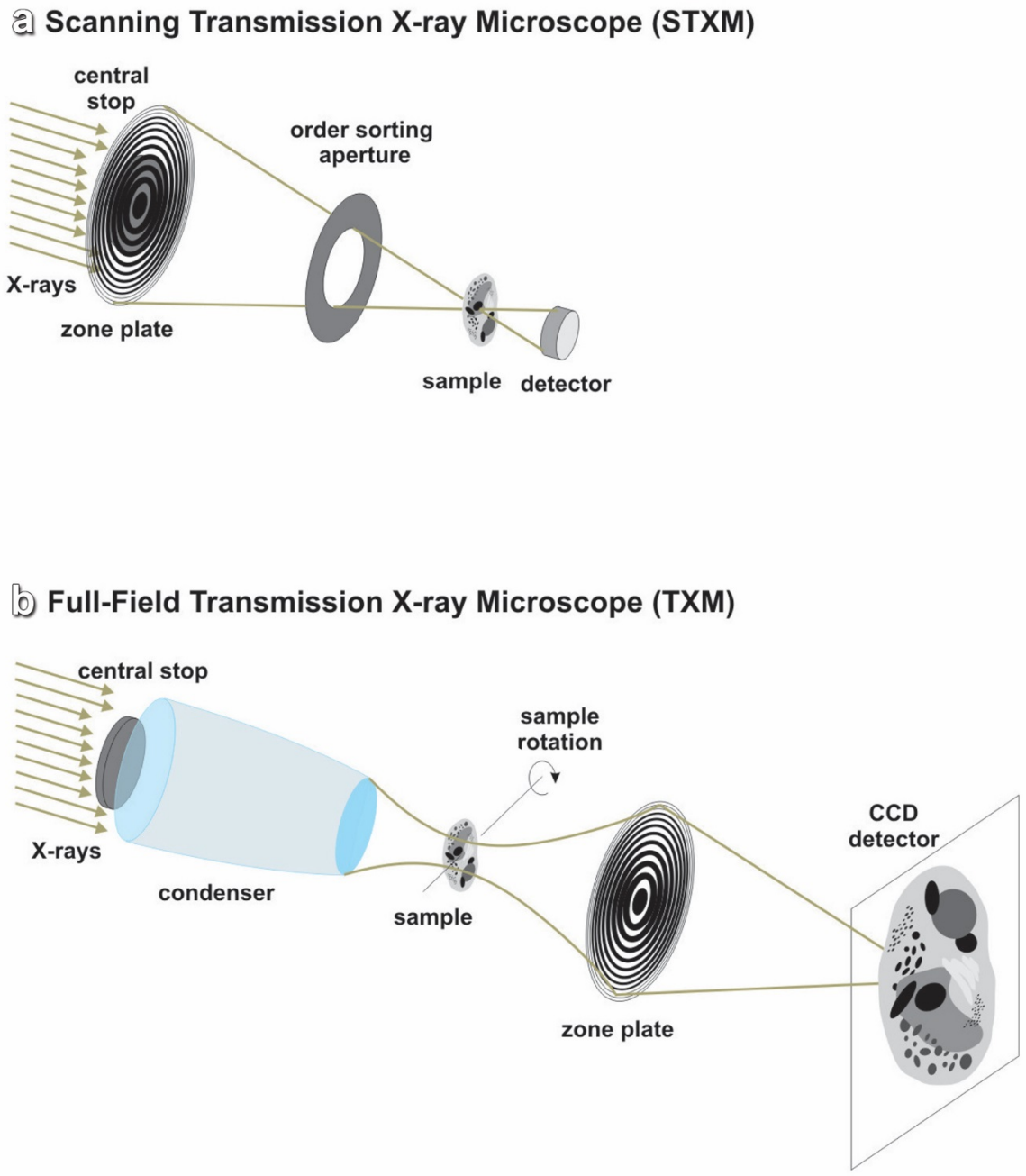

Figure 5.4 Optical setup of lens-based X-ray imaging techniques: scanning transmission X-ray microscopy (a) and full-field transmission X-ray microscopy (b).

In Fourier transform holography the sample area and a separate, small reference are illuminated with a coherent X-ray beam [354-358]. The diffraction pattern resulting from the interference between the scattered light from the sample and the scattered light from the reference pinhole is recorded on an X-ray detector (Fig. 5.3c). Using this setup a

Fourier transformation reconstructs the image information from the reciprocal space diffraction pattern. However, this technique requires a high degree of spatial coherence.

Lens-less X-ray imaging techniques have been quickly evolving in the past few years. However, so far these techniques did not demonstrate the potential to visualize 3D cellular ultrastructure with high spatial resolution. In contrast, lens-based X-ray imaging methods are well established for a wide range of applications, in particular in life sciences [10, 437-440].

In scanning transmission X-ray microscopy, a high-resolution Fresnel zone plate focuses a monochromatized X-ray beam onto a diffraction limited spot which is raster-scanned over the sample (Fig. 5.4a). The image of the sample is obtained by detecting the transmitted light at each scan position. Therefore, the image represents the distribution of the local absorption coefficient in the imaged object. Since Fresnel zone plates are diffraction optics and have multiple diffraction orders, an order sorting aperture is required to block light from diffraction orders not used for imaging [431].

In this thesis, a full-field transmission X-ray microscope was utilized for the investigation of biological specimens. Similar to classical light microscopes, full-field transmission X-ray microscopes utilize an X-ray condenser to illuminate the sample area. A highly resolving X-ray objective is used to form the image of the sample on an X-ray detector. Details on the optical setup of state-of-the-art full-field transmission X-ray microscopes will be given in the next section.

5.3.4 Optical setup for cryo soft X-ray tomography at BESSYII and ALBA

A number of cryo soft X-ray transmission microscopes are installed at synchrotron sources worldwide. Two of these microscopes were used for investigations during this thesis, one at the undulator U41 [425] at the BESSYII electron storage ring and the other at the undulator MISTRAL09 [441] at the ALBA electron storage ring. Both of these full-field transmission X-ray microscopes (TXM) share the same principle optical setup, which will be discussed in detail now focusing on the U41-TXM at BESSY II (Fig. 5.4b).

In electron storage rings, X-ray beams are produced by the acceleration of quasi-relativistic electrons in a magnetic field. For the TXM at BESSY II, this is done by the undulator U41 which acts as an X-ray source for the soft X-ray microscope. The emitted

X-ray beam is monochromatized by using a spherical grating monochromator in combination with a horizontal exit slit which also defines the achievable energy resolution. The monochromatized X-ray beam is focused onto the sample plane using an ellipsoidal mono-glass-capillary condenser by total reflection inside the optics [442, 443]. To achieve a homogenous illumination on the sample the condenser spot is scanned helically over an area of approximately 13 x 13 µm. A high-resolution Fresnel zone plate objective collects the X-rays which have been diffracted by the sample and generates an enlarged image of the sample on an X-ray detector. Commonly a directly illuminated, back-thinned charge coupled device (CCD) is utilized as soft X-ray detector. For 3D X-ray imaging the sample is mounted on a tilt stage (FEI compustage) to permit tomographic imaging. The sample stage is capable of working under cryo conditions (using Gatan cryo-holders) for biological applications. Partly for this reason, the TXM works under vacuum conditions, but also because the mean free path of soft X-rays in air is short [444].

The key optical elements for nanoscale soft X-ray imaging are the Fresnel zone plate objectives. These are nanofabricated radial gratings with decreasing grating width at increasing radius. The width of the so-called zones is critical to focus the light to the desired focal point. The spatial resolution achievable with these optics depends on the outermost zone width of the zone plate [445]. At the soft X-ray microscopes at BESSYII and ALBA, zone plates with 25 nm and 40 nm outermost zone widths are utilized for biological imaging. 25 nm zone plates contain 900 zones resulting in a focal length of 0.925 mm at 510 eV. 40 nm zone plates contain 560 zones resulting in a focal length of 1.5 mm at 510 eV. The next section will describe how the TXM setup was used to generate 3D volume information from whole vitrified cells.

5.3.5 Cryo soft X-ray tomography: 2D projections of the vitrified cell are recorded from various tilt angles and reconstructed into 3D volumes

As described before, full-field cryo soft X-ray transmission microscopy works in the water-window energy region of the X-ray spectrum to image whole cells via natural absorption contrast using Fresnel zone plates. Furthermore, cryo soft X-ray tomography can provide 3D volume information of the cells with approximately 40 nm spatial

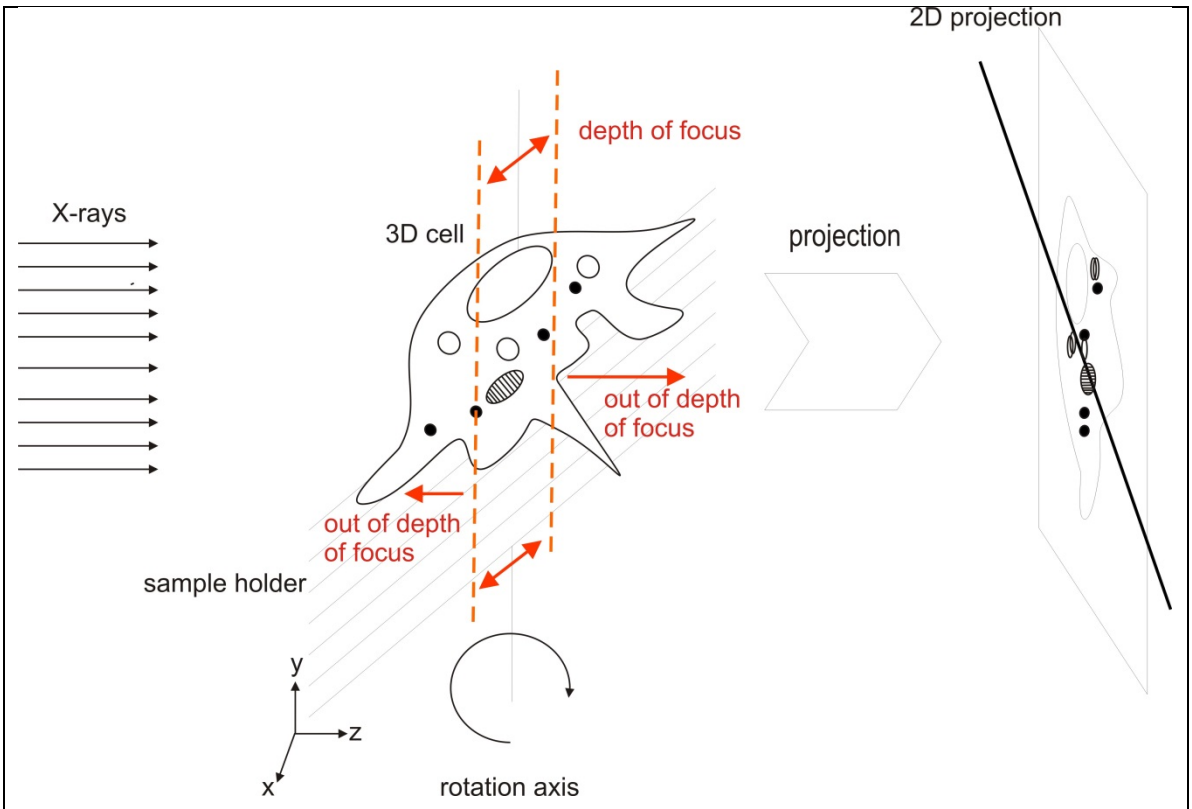

Figure 5.5 Rotation of the sample to obtain 2D projections from the sample via cryo soft X-ray tomography. X-rays illuminate the cell and they are diffracted by the cellular features. The diffracted wave field is collected by the zone plate which forms an enlarged real-space projection image. The sample holder rotates from -70° to +70° with 1° increments to obtain 141 projections from the cell. These projections will then be used to reconstruct a 3D volume.

resolution [62, 63]. Now, how this 3D volume information is reconstructed from 2D projections of a cell obtained from different tilt angles will be described.

For soft X-ray tomography the specimen is placed on a cryo sample holder on a stage which can be tilted perpendicular to the optical axis. First a region of interest on the sample is selected (field of view typically 12 x 12 µm) by moving the sample holder in a plane (xy) perpendicular to the optical axis (z). Then the sample holder is moved in the z direction to obtain the best focus. After focusing on the area of interest, a tilt series of images is recorded by rotating the sample holder in an angular range from -70° to +70° at 1° increments. At each tilt angle, the image produced is to a reasonable approximation a 2D projection of the sample. This is because the X-ray objectives have relatively large depths of field at the energies used. Acquisition of such a 2D projections of the sample at each tilt angle results in a tomographic data set that can be used for the reconstruction of

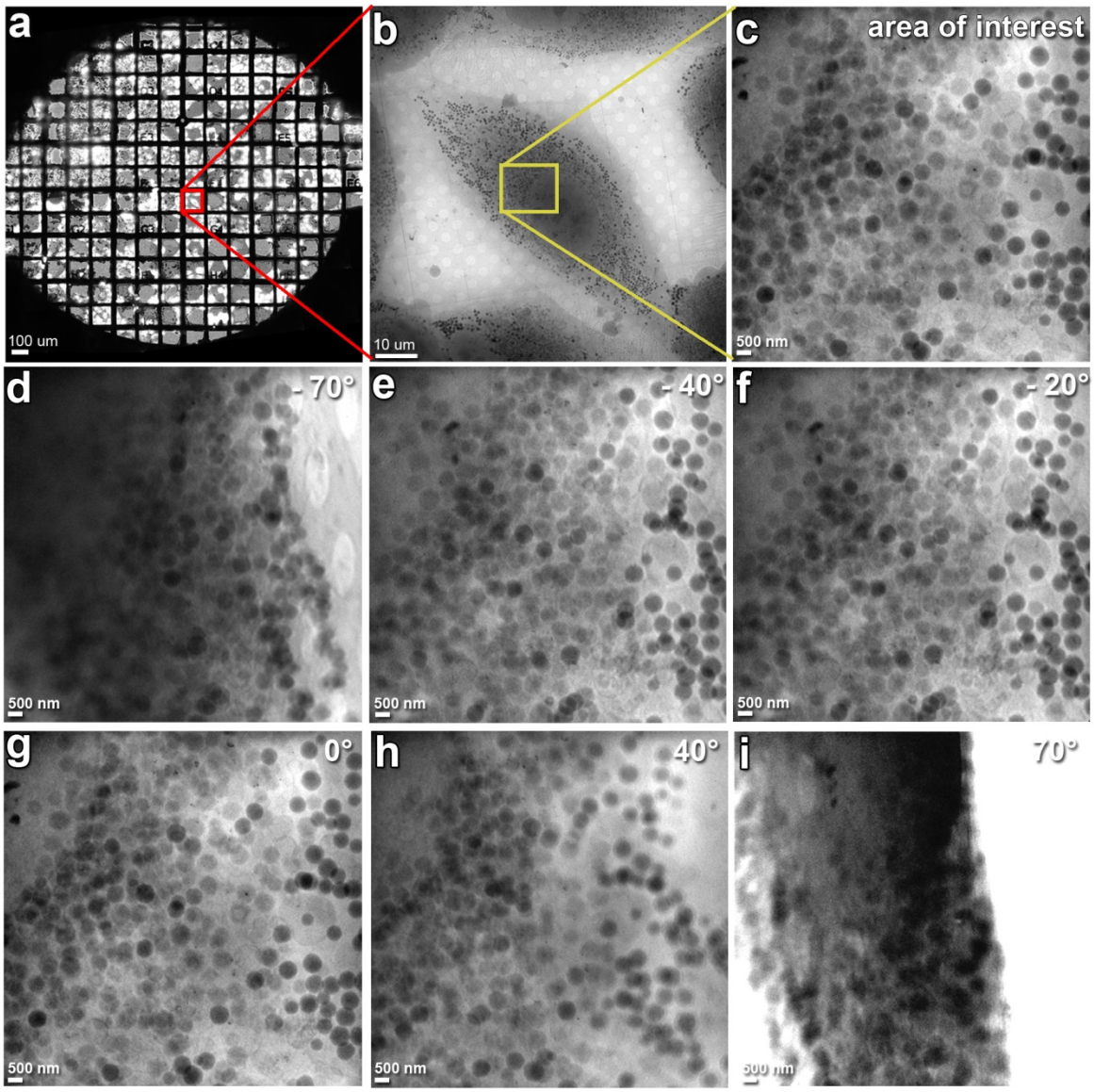

Figure 5.6 Sample selection and data acquisition via cryo soft X-ray tomography. First, a grid hole which presents good ice quality is selected from the grid by using fluorescence microscopy (a). Then, a cell, an isolated cell near the middle of this grid hole, will be found (b). Then, the area of interest will be focused on (c). The sample is then rotated from -70° to 70° with 1° increments and a 2D projection is obtained from the area of interest at each angle. Shown are representative 2D projections from tilt angles of -70° (d), -40° (e), -20° (f), 0° (g), 40° (h) and 70° (i). Scale bars = 500 nm.

the 3D cell volume (Fig. 5.5, Fig. 5.6). To minimize missing wedge artifacts in the reconstruction, the tilt series should contain 2D projections from an angular range of at least 120° [440, 444, 446].

During sample rotation and data acquisition two important events occur which influence the achievable resolution of the 3D reconstruction [447]. First, as the sample holder is rotated, some parts of the cell remain out of the depth of focus of the zone plate, which at 510 eV is 2 μm for the 25 nm zone plate and 5.4 μm for the 40 nm zone plate. Second, the sample holder experiences slight mechanical shifts while the sample holder is rotated. These shifts may result in displacements of the projection image by as much as 5 - 30 pixels (Fig. 5.7b). Since the pixel size is typically about 13 nm, 5 - 30 pixel shifts can cause significant loss of information in the final 3D reconstruction, especially for investigations on endocytosis and intracellular trafficking of nanoparticles dealing with features as small as 40 nm (Fig. 5.7). Therefore, these shifts need to be corrected by an alignment of the projections according to a common frame of reference to obtain an accurate 3D reconstruction. In soft X-ray tomography, fiducial-marker-based alignment is preferred guaranteeing a consistent alignment for each tilt angle, although marker-less alignment is also possible [447].

Fiducial markers can be either gold nanoparticles of about 200 nm in size, or highly absorbing round structures within the cells such as lipid droplets. Fiducial-marker-based alignment is done by measuring the coordinates of the fiducial markers through the image series and fitting them to an appropriate 3D model [447]. In this thesis, the software package BSoft was utilized for fiducial-marker-based alignment of tilt series and the procedure will be described below [448-450].

In Bsoft, tomographic tilt series are represented as a stack of 2D images. The stack usually shows a contrast variation due to the increased thickness that the X-ray beam must traverse at higher tilt angles. These variations are first normalized by fitting the central part of the histogram of each 2D image to a Gaussian function to estimate average intensity and then rescaled by this value. Then, at the zero-degree tilt image, the fiducial markers with a defined marker size are selected. As the sample is tilted, a marker will rotate around the tilt axis to different degrees depending on the z-coordinates of the marker within the sample. In addition, marker location will also change due to mechanical shifts and vibrations. Therefore, while trying to align these markers at each projection, there are two unknowns, the z-coordinates of the markers and the shift. To

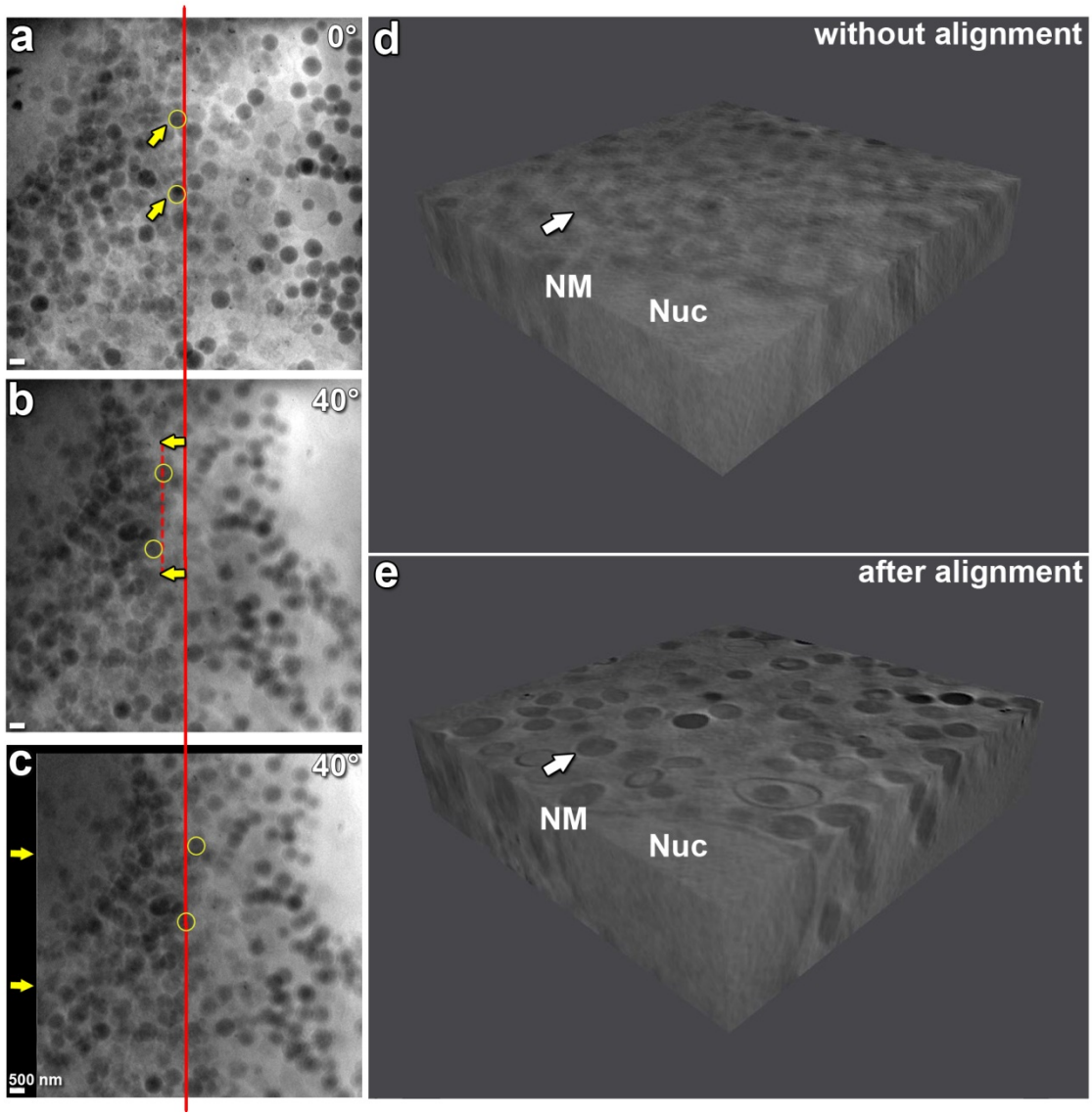

Figure 5.7 Alignment of 2D projections before reconstruction. The fiducial markers are defined at the 0° tilt angle (a). The same fiducial markers are then found at every tilt angle (b), and then the image is shifted to align the fiducial markers (c). If this alignment is not performed, the resultant reconstruction suffers from low resolution: for example the nuclear membrane (NM) and cellular organelles (arrow) cannot be resolved (d). However, if alignment is properly performed, the 3D reconstruction provides significantly more 3D information about the nuclear membrane (NM) and cellular organelles (arrow) (e). Scale bars = 500 nm for (a-c).

obtain the z coordinates, an iterative procedure is used. First, an estimate of the z coordinates of each marker is calculated for each projection from different tilt angles by real space correlations along a line determined by tilt angle and direction. Then, a projection image from the whole marker set is formed. This projection of markers is

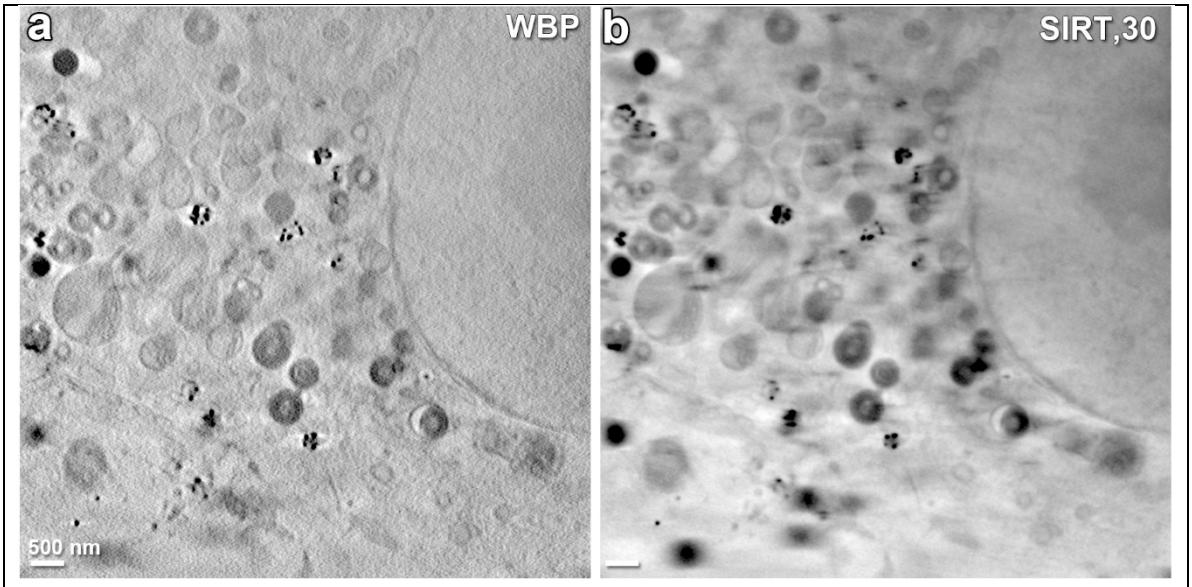

Figure 5.8 Reconstruction of cryo-SXT data via WBP (a) and SIRT with 30 iterations (b). Scale bars = 500 nm.

cross-correlated with the image to find the degree of shift. The process is iterated until the shift at the z-coordinates is lower than one pixel. Then, the exact positions of the markers in each 2D projection are refined according to the tilt axis.

Once this aligned stack of 2D projections is produced, the 3D volume of the cell can then be computed by using different tomographic reconstruction algorithms [447], such as weighted back-projection (WBP) or iterative techniques, such as the simultaneous iterative reconstruction technique (SIRT). A representative example of reconstructions obtained by weighted back projection and SIRT can be seen in Fig. 5.8. In the following, the reconstruction algorithms will be briefly introduced and the WBP algorithm will be explained in some detail since it was mainly utilized in this thesis.

3D reconstruction methods are classified into Fourier reconstruction methods or iterative real space methods. In Fourier reconstruction methods, Fourier transforms of the projections are used for reconstruction, and then the real space distribution of the sample is calculated through inverse Fourier transformation. Modified back-projected methods work on the real space data as well as Fourier transform data of the projections. They include convolution back-projection and weighted back-projection techniques. In iterative real-space methods, all calculations are carried out in real space [447].

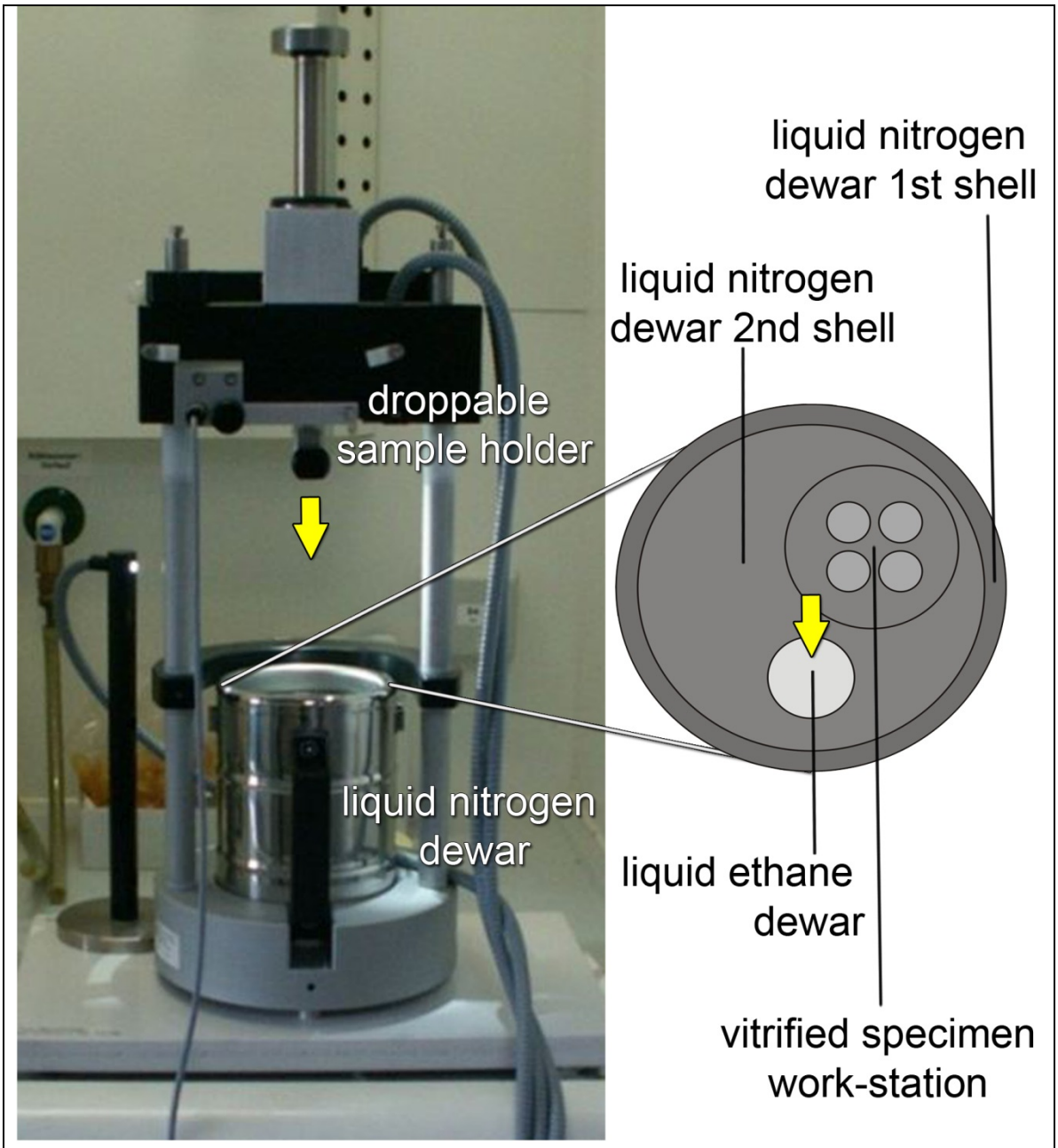

Figure 5.9 A plunge freezer. The manual plunge freezer contains four components including a specimen holder which can be dropped rapidly, a liquid nitrogen dewar which is composed of two shells in order to maintain the plunge freezer at cryogenic conditions, a liquid ethane dewar inside the liquid nitrogen dewar to dip the sample in for cryo-fixation and a vitrified specimen work-station to temporarily store the cryo-vitrified samples. The two shells of the liquid nitrogen dewar are filled with liquid nitrogen to maintain the cryogenic temperature of the plunge freezer. Then, the liquid ethane dewar is filled with liquid ethane. The sample will be dipped into liquid ethane.

All algorithms require a set of projections of the sample recorded at different tilt angles. The data collection is determined by the properties of the sample such as radiation sensitivity (which may limit the number of tilt angles that can be collected) and

orientation preferences of the objects in the sample (which may require tilting of the specimen along a preferred axis). The data collection preferences also affect the selection of the reconstruction algorithm.

In this thesis, samples were typically tilted in the range of -60° to +60° with 1° increments around a single tilt axis. The image of the same region (12 μm x 12 μm) was recorded at each tilt angle with a typical exposure time of 2 - 4 sec. This produced no sign of radiation damage throughout the tilt series. Then a WBP algorithm for single axis tilt geometry with equal angular increments was used to perform reconstructions, since WBP algorithms are very efficient. Specifically, they are fast and provide good enough results to resolve membrane bound organelles and nanoparticles. Moreover, the WBP algorithms involve linear operations and are faster for reconstructing large data sets. Therefore, the outcome is entirely determined by the experimental data. In contrast, iterative techniques are very slow and require prohibitively large amounts of computer memory due to Fourier interpolation and associated inversion [447].

5.3.6 Sample preparation: during soft X-ray illumination, cells must be vitrified to eliminate radiation damage

Soft X-ray tomography depends on the measurement of attenuation of X-rays by the sample dependent on its specific elemental distribution. Therefore, this elemental distribution needs to stay constant during the data acquisition.

However, once the sample is illuminated by X-rays, the dose of the X-rays applied to the sample is in the range of 10^6 - 10^9 Gy. Such a dose is high enough to break atomic bonds which will lead to an alteration of the elemental distribution inside the sample [425].

To avoid the resulting disintegration of biological samples, cryo-fixation is used [451, 452]. During cryo-fixation water within and surrounding cells is transformed into amorphous ice without inducing nucleation of ice crystals, so that the biological material is embedded within a thin layer of amorphous ice (Fig. 5.10) [452].

Ice crystallization destroys cellular structures and therefore induces artifacts (Fig. 5.11). To avoid such problems, the total thickness of the cell and the ice layer should not surpass 10 μm [452].

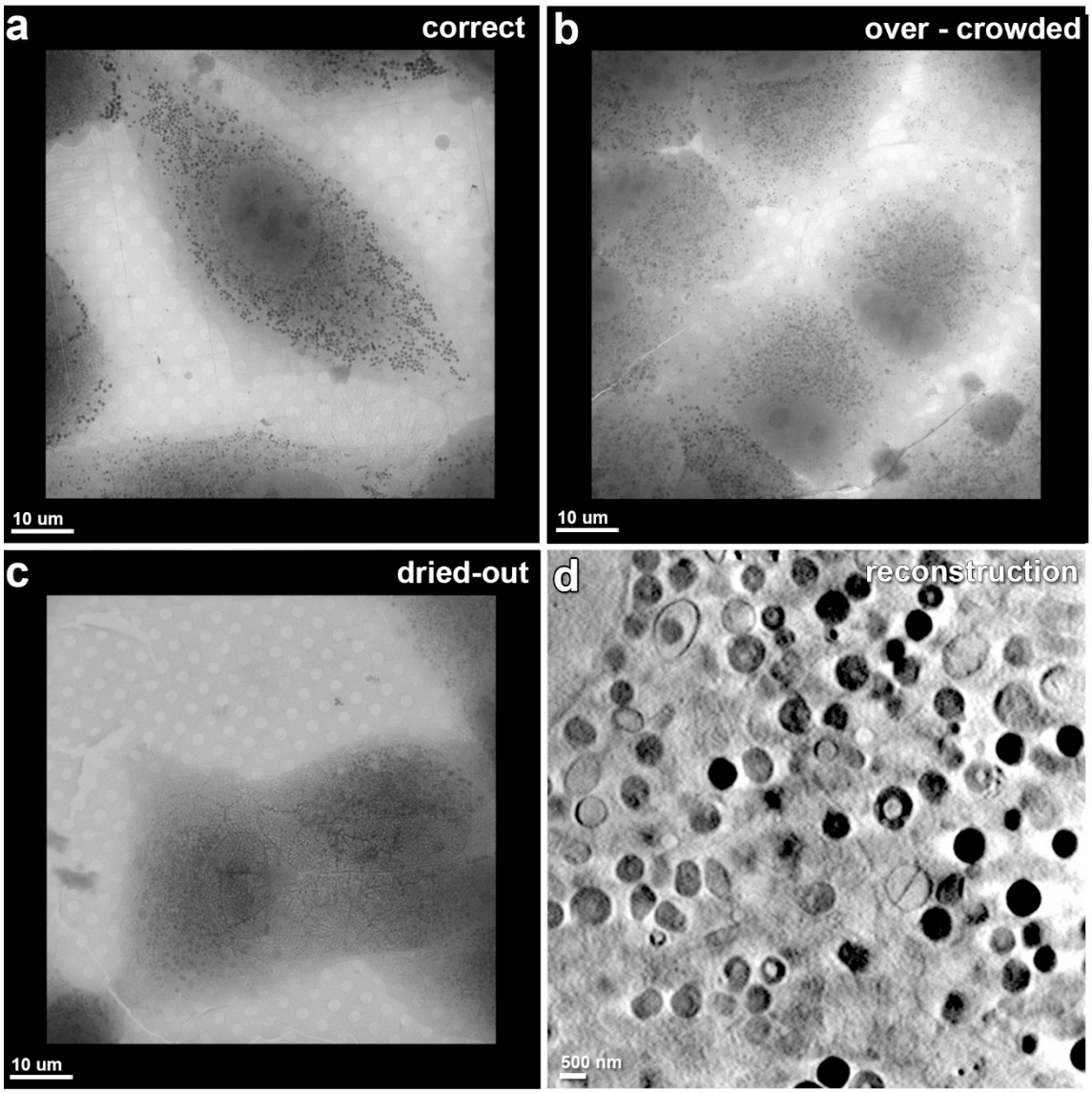

Figure 5.10 Vitrified cells via plunge freezing. Before plunge freezing, the cells need to be blotted in a way that the resultant ice layer just covers the top of the cell (a). Cell density should not be too high (b), since adjacent cells can enter the field of view during the tilt series. Cells should not be blotted for too long, otherwise they will be dried out (c). If freezing is successful, a good reconstruction from the area of interest can be obtained after serial data acquisition at different tilt angles (d). Scale bars = 10 μm in (a-c), 500 nm in (d).

The transition of water from the liquid phase to amorphous ice requires rapid cooling with an approximate rate of 10^7 K/s [453]. This can be achieved by plunge freezing using cryogenic liquids such as liquid nitrogen and liquid ethane. A manual plunge freezer, as it was used for cryo-fixation in this thesis, is shown in Fig. 5.9. It contains a liquid nitrogen dewar which is composed of two shells in order to maintain the plunge freezer at

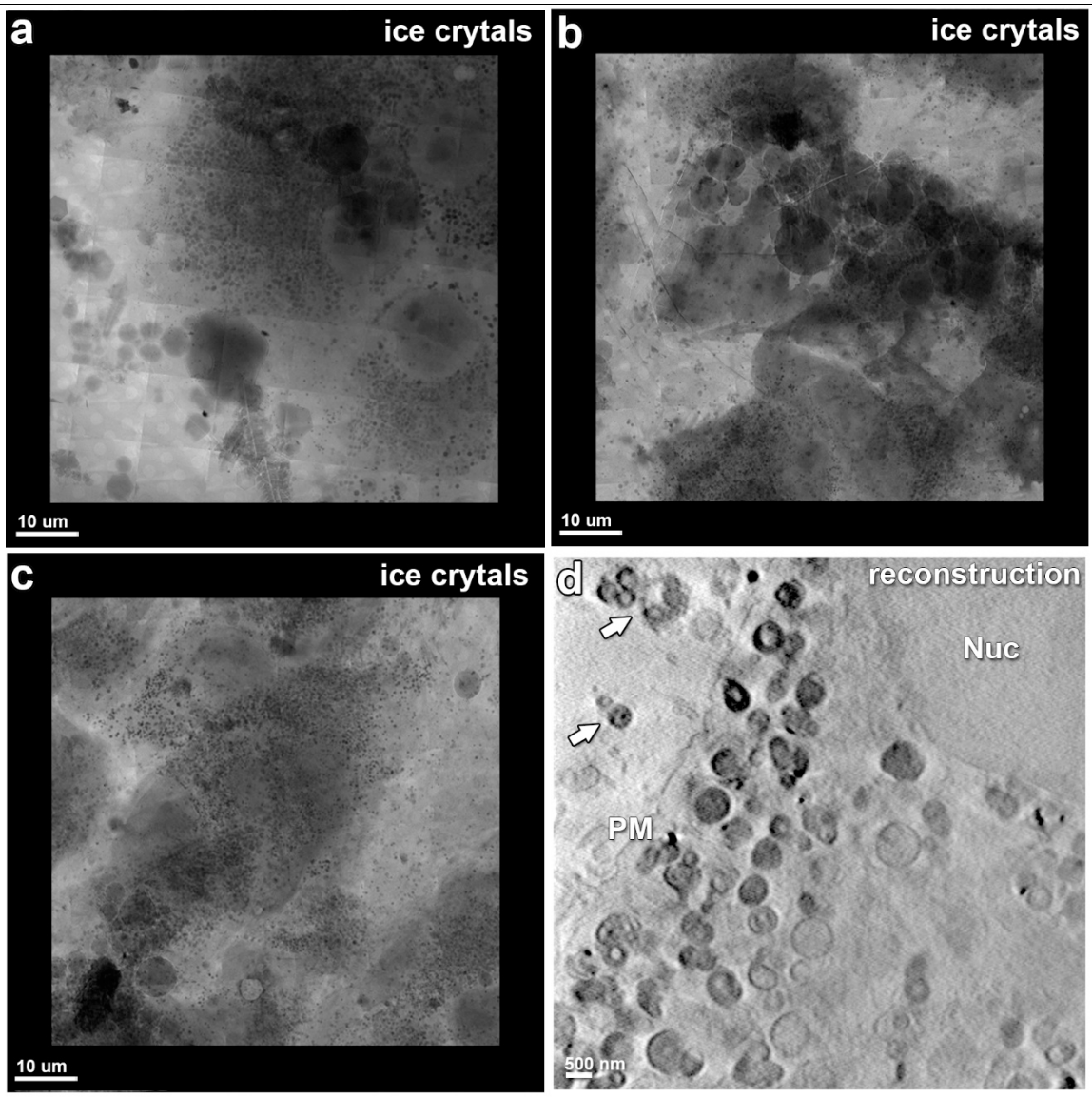

Figure 5.11 Vitrified cells via high pressure freezing. Many ice crystals were found and ice layer thickness was too thick, which could reduce data quality (a-c). After reconstruction, some cells were destroyed during the procedure (arrows point to cell fragments) (d). Scale bars = 10 μm in (a-c), 500 nm in (d).

cryogenic conditions, a liquid ethane dewar inside the liquid nitrogen dewar to dip the sample in for rapid cryo-fixation, a specimen holder which is dropped into the liquid ethane dewar and a vitrified specimen work-station to temporarily store the cryo-vitrified samples (Fig. 5.10). The vitrification is performed by immediately dipping the sample within liquid ethane after blotting.

Another way to transform water into amorphous ice is high pressure freezing through rapid cooling under high pressure. High pressure reduces the nucleation temperature and

this slows down ice crystal formation [454]. However, in the high pressure freezing experiments, which were performed in this thesis, a high amount of ice crystallization and cell disintegration were observed. Additionally, the ice layers produced by this technique were often too thick for soft X-ray tomographic imaging (Fig. 5.11). Therefore, for A549 cells, which are investigated in this thesis, plunge freezing was much better suited.

5.4 Summary

There are various techniques to image nanoparticle - cell interactions (Table 1). With light microscopy, it is possible to obtain high-throughput data from living cells. However, the resolution is limited by 200 nm and so ultra-structural features cannot be resolved. Fluorescence microscopy also provides high-throughput data from living cells with 200 nm resolution. Additionally, by using confocal setups, 3D information can be obtained from fluorescence tagged samples and with super-resolution setups, the resolutions down to 20 nm can be achieved. However, only a small subset of fluorescence markers can be imaged simultaneously, which makes it difficult to observe more than a few structures in the cell. With TEM, very high resolution imaging is possible down to 3 nm or better on biological samples. With this technique, even ribosomes can be resolved. However, this imaging method is limited to thin samples which prohibit observation of the whole cell in 3D. In conventional TEM setups, cell preparation requirements such as dehydration and plastic embedding can disturb cellular features. Also heavy metal staining used for contrast enhancement as well as chemical fixation can yield artificial structures. For cryo-TEM, embedding and staining is no longer required. However, this technique still requires thin sectioning (typically < 500 nm) of the sample. Cryo soft X-ray tomography also utilizes cryo samples, but without chemical staining and slicing requirements. This tomographic technique can generate 3D volume information from whole cells making it ideal for the investigation of the cellular environment during nanoparticle cell interactions. Therefore, in this thesis, soft X-ray tomography was utilized to investigate cellular interactions of nanoparticles.

In the future, combining several different microscopic techniques to image the same sample will become more important. At present, a correlative fluorescence light and high-resolution X-ray microscope is installed at the BESSYII electron storage ring. This system will be upgraded to obtain super-resolution fluorescence images of the same sample imaged by soft X-ray tomography. This will enable the combined imaging at

similar resolution of molecular markers by fluorescence microscopy with the ultrastructural features revealed by cryo soft X-ray microscopy.

	Classical LM	Super - resolution LM	Conventional TEM / cryo-EM	cryo-SXT
Sample thickness	several microns	several microns	~200 nm	~10 µm
Resolution	200 nm	20 nm	2 - 5 nm	30 - 40 nm
Sample statistics	high - throughput	medium-throughput	low-throughput	low-throughput
Preparation requirements	no	fluorescence tags	heavy metal staining and plastic embedding / cryo	cryo
Live - cell imaging	possible	possible	not possible	not possible
3D information	from whole cells	from thin regions of whole cells	from thin sections	from whole cells

Table 1 There are various techniques to investigate nanoparticle - cell interactions including the light microscope (LM), the fluorescence microscope (FM), the transmission electron microscope (TEM) and cryo soft X-ray tomography (cryo-SXT). With LM and FM, high-throughput data can be obtained from living cells. However, the resolution of LM is limited to 200 nm and only fluorescently tagged features can be observed by FM. TEM can reach very high resolution. However, only thin slices can be obtained and heavy metal staining, chemical fixation, plastic embedding requirements may interfere with the final image or disturb the cellular features. Cryo-SXT provides high resolution 3D image of the cell which is ideal for observation of nanoparticle - cell interactions. However, cryo-preservation requirements slow the sample preparation time, and user time is limited since these microscopes operate at synchrotron sources which are limited in number.

6. UPTAKE KINETICS AND TRAFFICKING PATHWAY OF dPGS NANOPARTICLES IN A549 CELLS STUDIED BY DIC MICROSCOPY AND CRYO-SXT

As discussed before in Chapter 4, cells can internalize and traffic nanoparticles which then can exert functional and morphological effects on the cells. These changes may include not only the intended effect of the drug, but also unintended side effects. In either case, the changes need to be determined in order to analyze whether the nanoparticles are exerting their design effect or creating undesirable effects on the cells.

The focus of this chapter will be dPGS nanoparticles, which are designed as tools for diagnosis and treatment of inflammation. Specifically, the uptake rate, uptake mechanism, cellular localization and excretion of dPGS nanoparticles will be investigated.

6.1 Motivation to study the uptake rate, uptake mechanism and the trafficking of dPGS nanoparticles

As discussed before in Chapter 3, chronic inflammation causes many deaths and has connection to many diseases such as cancer, heart attack and Alzheimer's. However, its diagnosis and treatment are not straightforward. A potential approach for providing improved diagnosis and treatment of inflammation is provided by the compound dPGS, which is a hyperbranched polymer approximately 5 nm in size. dPGS compounds were found to accumulate at inflamed sites in animal models, which could be valuable for early diagnosis of inflammation [109, 164-166]. At the same time, dPGS can also reduce the inflammation, which could be valuable for treatment of inflammation [166].

The underlying mechanisms for dPGS action are as follows. dPGS binds to L-and P-selectins on the plasma membrane which are known to be enhanced at inflamed sites [148, 158]. Thus dPGS accumulates at the inflamed site, which is valuable for diagnosis, and in addition dPGS competes with leukocytes to inhibit their binding to endothelial cells, thereby also reducing inflammation [148, 158]. To accomplish these goals, dPGS should attach to the plasma membrane until the inflammation is alleviated. However, previous studies did not investigate the interaction of dPGS nanoparticles with the plasma membrane in situ. Additionally, these previous studies have shown that dPGS is internalized by cells in contrast to its design purpose. Fluorescent dPGS nanoparticles

were detected in punctated pattern within cells [21-26], which typically reflects entry into into cellular vesicles that are presumably involved in the endocytic pathway. This cellular internalization of dPGS does not appear to be toxic to cells, according to assays of mitochondrial activity and plasma membrane integrity [23-26, 168]. However, dPGS nanoparticles could be localizing to various organelles, or to the cytoplasm or the nucleus in the cell and cause physiological effects on the cell which need to be defined. Therefore, in this thesis, the interaction of dPGS nanoparticles with cells will be inspected. This analysis includes determining the exact localization of dPGS nanoparticles in the cell. Specifically, it will be determined which membrane bound vesicles contain dPGS, and whether dPGS remains within these vesicles or escapes into the cytoplasm, or if dPGS enters other organelles not part of the conventional endocytosis and trafficking pathways, such as mitochondria and the nucleus. A knowledge of which parts of the cell contains dPGS is important for understanding what cellular functions might be impacted by dPGS. Furthermore, it is important to understand whether dPGS might be eventually excreted from cells, and this can also be evaluated by determining its sub-cellular distribution.

To answer these questions, cryo soft X-ray tomography was utilized since it provides a 3D image of a cell at 40 nm spatial resolution without a need for slicing, fixation or staining [62, 63]. With this technique, rare events such as cytoplasmic escape and nuclear entry can potentially be detected. To be able to track dPGS in the cell, dPGS was attached to the surface of 50 nm gold nanoparticles. The nanoparticles were incubated with A549 cells for different incubation time points (1 h, 3 h and 6 h) and then the cellular locations of nanoparticles at each time point were determined from the 3D images.

In this study, A549 cells were selected as a model system because they have been reported to interact with dPGS compounds before [23-26]. Additionally, A549 cells are relatively large cells (~40 μm diameter) with a relatively small nucleus compared to other mammalian cells. This provides an extended volume of cytoplasm to investigate the ultrastructural localization of dPGS within organelles.

6.2 Using DIC microscopy, dPGS nanoparticles are found to be internalized into A549 cells in a time-dependent manner

As a first step, it was determined if the dPGS nanoparticles would be internalized by cells analogous to what had been previously reported for fluorescent forms of dPGS [21-26]. To do this, cells were incubated with 0.13 nM dPGS nanoparticles and nanoparticle - cell interaction was imaged via DIC microscopy.

DIC microscopy was used since the sample preparation and data acquisition by this technique are faster than cryo-SXT. DIC also provides statistical information by allowing imaging of many cells. DIC microscopy was selected over other high-throughput light microscopy imaging techniques because DIC microscopy allows detection of materials with sizes lower than the diffraction limit and provides a relatively narrow depth of field which enables optical sectioning (Fig. 6.1) [455, 456]. With this optical sectioning ability, dPGS nanoparticles could be searched in each optical slice of the cell to understand the location of dPGS nanoparticles relative to cellular structures such as the plasma membrane and nucleus (Fig. 6.1). With this approach, dPGS nanoparticles were found to be internalized by cells after 1 h incubation (Fig. 6.1, Fig 6.2a).

Then, DIC microscopy was used to perform a control, namely to investigate the role of the sulfate moieties of dPGS on the uptake of dPGS nanoparticles. To do this, cells were incubated for 1 h and 6 h with control dendritic polyglycerol coated gold nanoparticles (dPG nanoparticles), which lack the sulfate moiety but are otherwise identical. No dPG control nanoparticles could be detected within the cytoplasm and on the plasma membrane (Fig. 6.2g,h). These cells looked similar to control cells (Fig. 6.2f), demonstrating that dPG nanoparticles are not internalized by cells. This shows that the sulfate moieties of dPGS play a critical role in the internalization of the dPGS nanoparticles, and it also shows that the interactions, which are described in this and subsequent chapters are likely to be specific to dPGS.

Even though dPGS nanoparticles are demonstrated to be internalized by cells using DIC microscopy, the exact location of the dPGS nanoparticles relative to membrane-bound organelles was impossible to discern by DIC since these structures are not easily visible by this technique. Therefore, a technique with a higher resolution, namely cryo soft X-ray tomography was utilized. In order to identify useful time points for analysis by cryo-SXT,

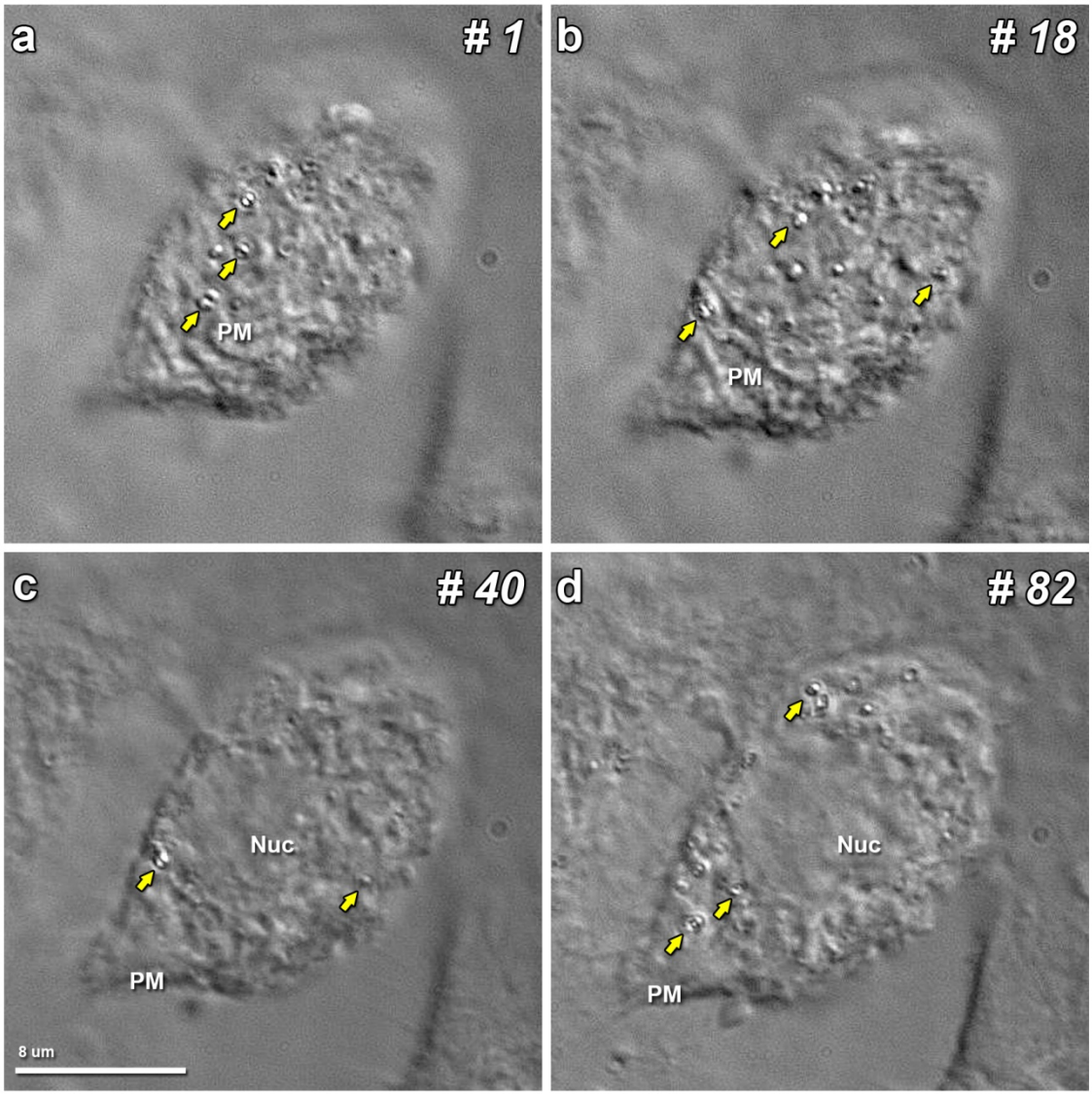

Figure 6.1 Selected optical sections obtained by DIC microscopy. A549 cells were incubated with dPGS nanoparticles for 1 h and then imaged. Shown is a series of optical sections along z (a-d) enabling examination of nanoparticle (arrows) localization relative to the plasma membrane (PM) and nucleus (Nuc). At optical section #1, nanoparticles are seen on top of the cell and not internalized (a). At optical sections #18, 40 and 82 the microscope is focused at different planes within the cell. These show that nanoparticles are internalized and localize within the cytoplasm, namely the region between the nucleus and plasma membrane (b-d). Scale bar = 8 μm.

a time-lapse study of dPGS nanoparticle uptake was performed via DIC microscopy. Specifically, A549 cells were incubated with a fixed concentration (0.13 nM) of dPGS nanoparticles for 1 h, 3 h, 6 h, 12 h and 48 h. The amount of nanoparticles within the cell was observed to increase as the incubation time increased from 1 h to 48 h (Fig. 6.2a-d, i).

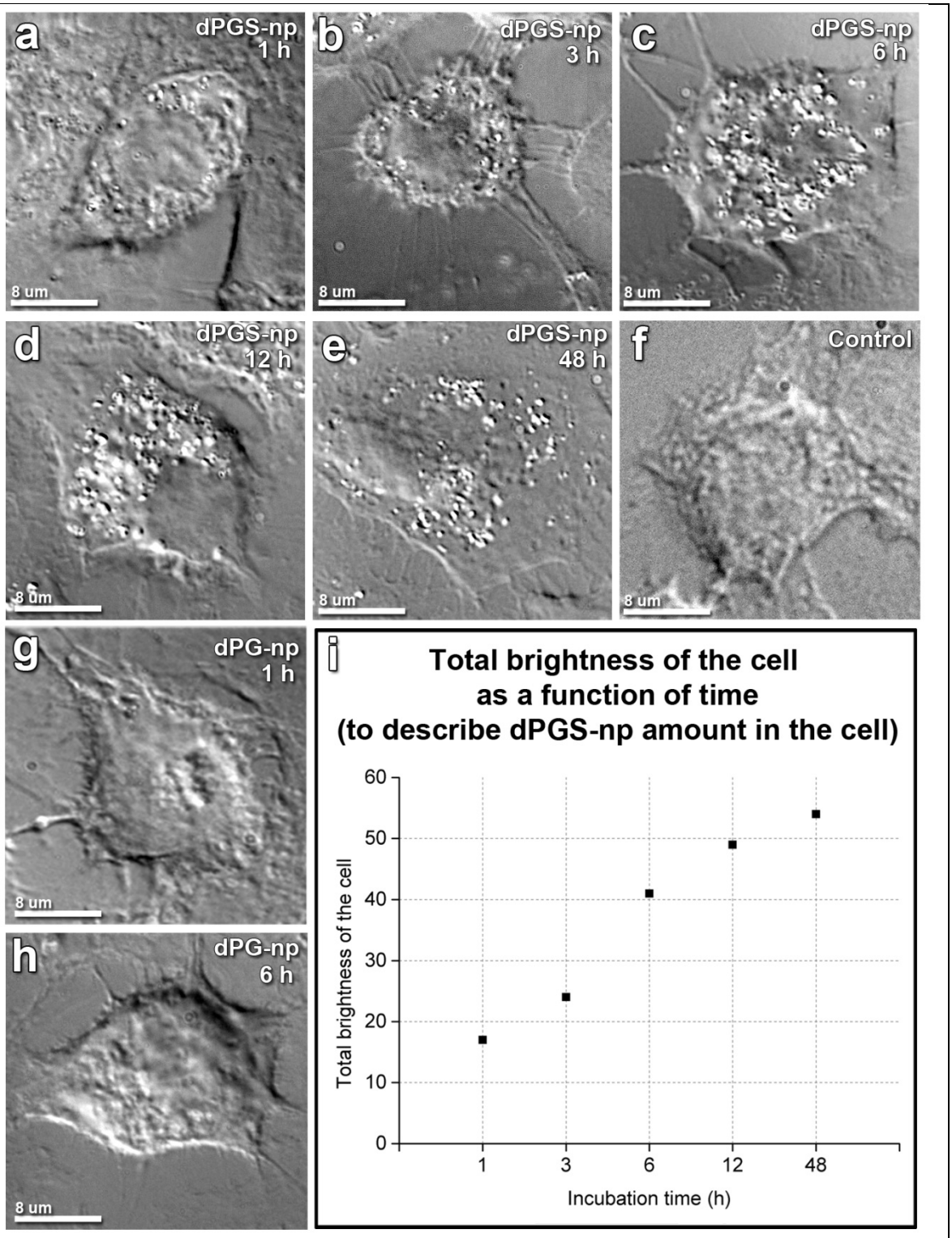

Figure 6.2 Cellular uptake of dPGS nanoparticles by DIC. Cells were examined after 1 h (b), 3 h (c),6 h (d), 12 h (e) and 48 h (f) of incubation with dPGS nanoparticles. Nanoparticles (visible as small white dots by DIC) were present in cells throughout this period, but control cells incubated with dPG nanoparticles showed no uptake (h). For quantification, cell intensities were thresholded such that only the nanoparticles were visualized, and then total intensity per cell was measured to estimate the number of nanoparticles per cell at different time points (i). Scale bar = 8 μm.

Based in part on the DIC images of dPGS nanoparticle uptake, 6 h was selected as the optimum incubation time point for cryo-SXT studies, since at this time point the cells contained a sufficiently large number of nanoparticles to facilitate investigation of nanoparticle localization (Fig. 6.2c). Another reason for selecting the 6 h time point is that the 4 - 6 h incubation time span has been widely used in many other nanoparticle trafficking studies [6, 14, 457].

In sum, these DIC microscopy studies indicate that dPGS nanoparticles are internalized by A549 cells in a time-dependent manner and that 6 h is a reasonable time point to investigate the cellular location of dPGS nanoparticles. However, the resolution of DIC was not enough to understand whether dPGS nanoparticles stay enclosed within the endo-membrane system or reach the cytoplasm, nucleus or unintended organelles. Additionally, sufficient information about excretion of dPGS nanoparticles could not be collected due to the dilution effect arising upon cell division. For these reasons, cryo-SXT was utilized for cells incubated with dPGS nanoparticles.

6.3 Cryo-SXT can resolve membrane bound organelles within A549 cells

Cryo-SXT could resolve membrane bound organelles in the A549 cells. Specifically, in A549 cells, it was possible to recognize the plasma membrane, various endosomal compartments including endosomes, multivesicular bodies, lysosomes and autophagic vacuoles, plus other organelles such as mitochondria, Golgi, endoplasmic reticulum (ER) and lipid droplets (Fig. 6.3a). These organelles could be identified through comparison with previous studies performed by electron microscopy, X-ray tomography alone, and correlative fluorescence and X-ray tomography [63, 458]. Thus cryo-SXT provides a powerful technique to visualize cellular organelles in 3D and so determine where the dPGS nanoparticles localize.

6.4 Cryo-SXT demonstrates that dPGS nanoparticles attach to the plasma membrane and are internalized in a time-dependent manner

As mentioned in Chapter 3.3.1 and Chapter 6.1, dPGS nanoparticles are designed to attach on L- and P- selectins on the plasma membrane [148, 158]. Therefore, it was important to understand if this happens or not. To answer this question, the cells were incubated with dPGS nanoparticles for 1 h, 3 h and 6 h. And then at each time point cryo-SXT was used to determine the locations of the nanoparticles relative to cellular

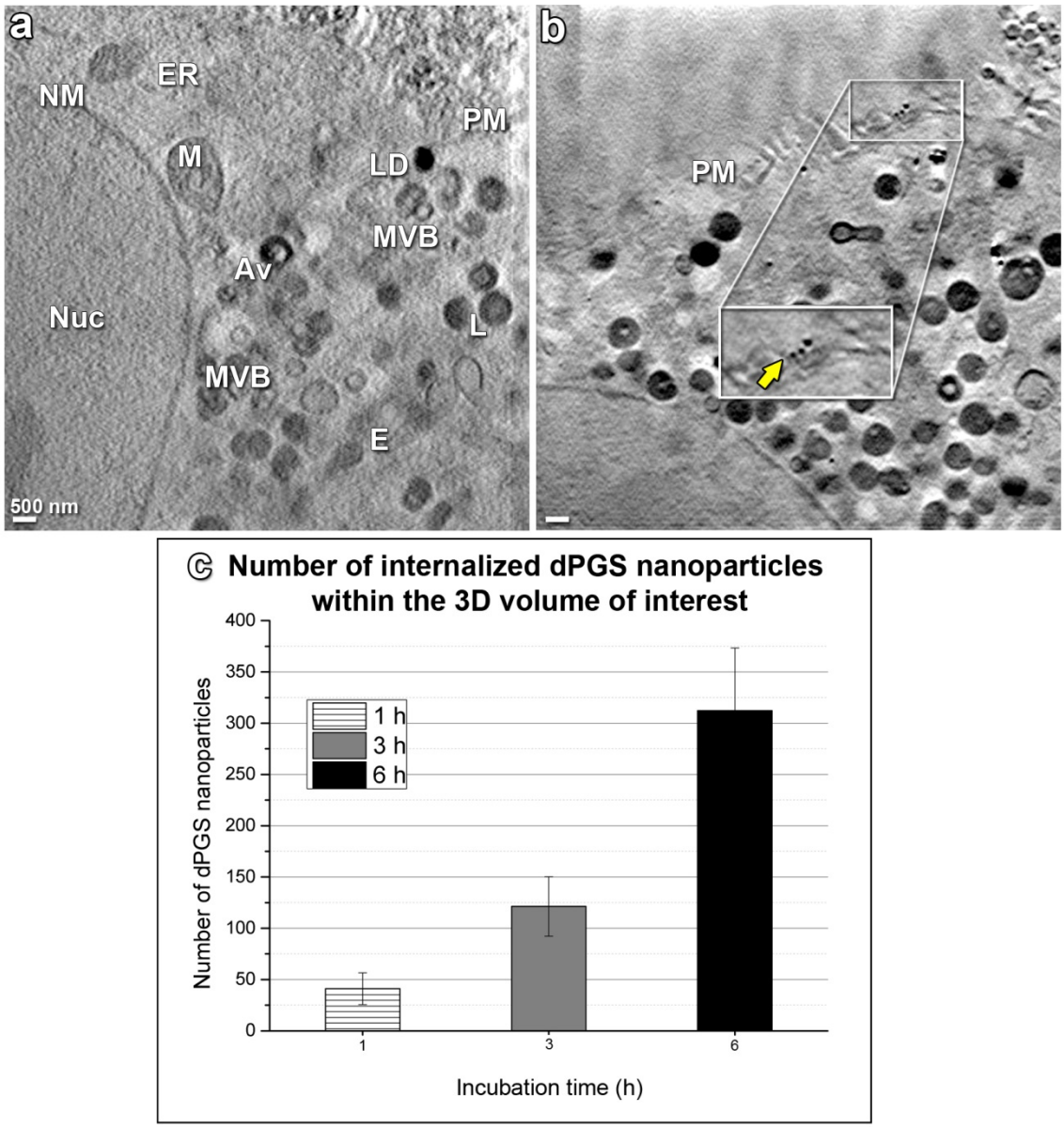

Figure 6.3 Control A549 cells and interaction of dPGS nanoparticles with the plasma membrane in A549 cells via cryo SXT. Control cells do not contain nanoparticles. Frequently detected organelles in A549 cells are mitochondria (M), Golgi (G), endosomes (E), lysosomes (L), lipid droplets (LD), multivesicular bodies (MVB), endoplasmic reticulum (ER), autophagic vacuoles (Av) and a nucleus (Nuc) enclosed within the nuclear envelope (NM) (a). After nanoparticle incubation, dPGS nanoparticles were found to associate with the plasma membrane (PM) as can be seen in the white box as a zoomed in view (b). Quantification of these cryo-SXT images showed dPGS nanoparticles were internalized into cells in a time-dependent manner (c).

membranes. According to this analysis, dPGS nanoparticles were found to attach to the plasma membrane at apparently random and widely spaced locations (Fig. 6.3b). These attachment patterns could be detected at 1 h, 3 h and 6 h. Even by 6 h, the nanoparticles

on the plasma membrane were so widely spaced that more than three nanoparticles in close proximity could never be observed (Fig. 6.3b).

According to cryo-SXT studies in this thesis, after attachment to the plasma membrane, the dPGS nanoparticles were also found to be internalized by cells in a time-dependent manner (Fig. 6.3c). Typically, 3D images were acquired from 8 - 15 cells per time point, and by examining these it was clear that the number of nanoparticles in the cytoplasm was increasing over time. To quantify this, a manual counting of nanoparticles was performed in a 3D sub-volume of the cell (Fig. 12.2). A sub-volume was used because a single field of view in the X-ray microscope is not large enough to include the entire cell (Fig. 12.3). Furthermore, for consistency, this sub-volume was always located at the same relative position within the cell (Fig. 12.2), namely midway between the plasma membrane and the nucleus, since the composition of the cytoplasm changes somewhat as a function of distance from the plasma membrane. (For example, the fraction of endosomes is higher near the plasma membrane). For most of the quantitative measurements in this thesis, manual counts were performed in this 3D sub-volume (typically containing ~200 focal planes per cell). This was a laborious procedure which limited the number of cells that could be counted. For most of the measurements in this thesis, four cells were counted which usually yielded reasonably small standard deviations. For details of this measurement procedure, please consult the Methods section in Chapter 12 (Fig. 12.2, Fig. 12.3). For the counts here of nanoparticles in the cytoplasm, an average of 60 nanoparticles were found per cell at the 1 h incubation time point, 121 nanoparticles at 3 h, and 312 nanoparticles at 6 h. Thus, compared to the 1 h time point, the average number of nanoparticles in this sub-volume had doubled by 3 h and almost quintupled by 6 h (Fig. 6.3c).

6.5 dPGS nanoparticle internalization in A549 cells appears to occur via two different routes

As described in the previous section, dPGS nanoparticles are internalized into cells after attaching to the plasma membrane. The pathway by which the nanoparticles are internalized is an important factor to define which cellular organelles the dPGS nanoparticles are likely to enter, and whether or not the nanoparticles will eventually be excreted. Therefore, the internalization pathway of dPGS nanoparticles was investigated

to obtain clues about the potential cellular trafficking pathways. This analysis was performed using cryo-SXT 3D images obtained from 8 - 15 cells at each of the three incubation time points. From this collection of cells, dPGS nanoparticles were consistently found within membrane pits (Fig. 6.4a-c), suggesting that dPGS nanoparticles were internalized through endocytosis.

Then, the morphology of these membrane pits with attached nanoparticles was analyzed (Fig. 6.4a-c), as well as the morphology of endocytic vesicles containing nanoparticles (Fig. 6.4d-f). The dPGS nanoparticles were observed to be present in two different types of membrane pits. One type appeared to be membrane ruffles, which are defined as membrane protrusions formed to internalize a foreign cargo (Fig 6.4a,c). The other type of membrane pit was an omega-shaped invagination that contained a coating along the invagination (Fig. 6.4b). These two different types of membrane invaginations may have led to the formation of two different types of endocytic vesicles. Specifically, dPGS nanoparticles were found in larger endocytic vesicles with a diameter of 200 nm or more, but lacking any coat. These vesicles contained a mixed interior of X-ray lucent and X-ray dense material. Such vesicles could have arisen from the membrane ruffles, since the ruffles also lacked a coat (Fig. 6.4c,e). dPGS nanoparticles were present in smaller vesicles of 100 - 150 nm that contained a coat. Such vesicles could have arisen from the coated omega-shaped invaginations (Fig. 6.4d,f).

Thus, the data suggest that dPGS can enter cells via at least two distinct endocytic pathways. This morphological data also suggest what these pathways might be. Membrane ruffles which pinch off to form large, uncoated vesicles are characteristic of macropinocytosis [259], whereas omega-shaped invaginations are characteristic of either caveolae- or clathrin-mediated endocytosis [266]. The morphological data do not clearly distinguish between these latter two pathways. According to the morphological analysis, the membrane coat of the coated vesicles did not disappear and was thinner than the coating typically seen for clathrin, features that would support caveolae-mediated endocytosis [260]. Furthermore, some of these vesicles looked like a cluster of small vesicles, which is also characteristic of caveolae-mediated endocytosis [266]. However, the size of these coated vesicles (100 - 150 nm) was larger than typical caveolin-coated vesicles (60 - 80 nm) [266], and more in the range of clathrin-coated vesicles (100 - 150

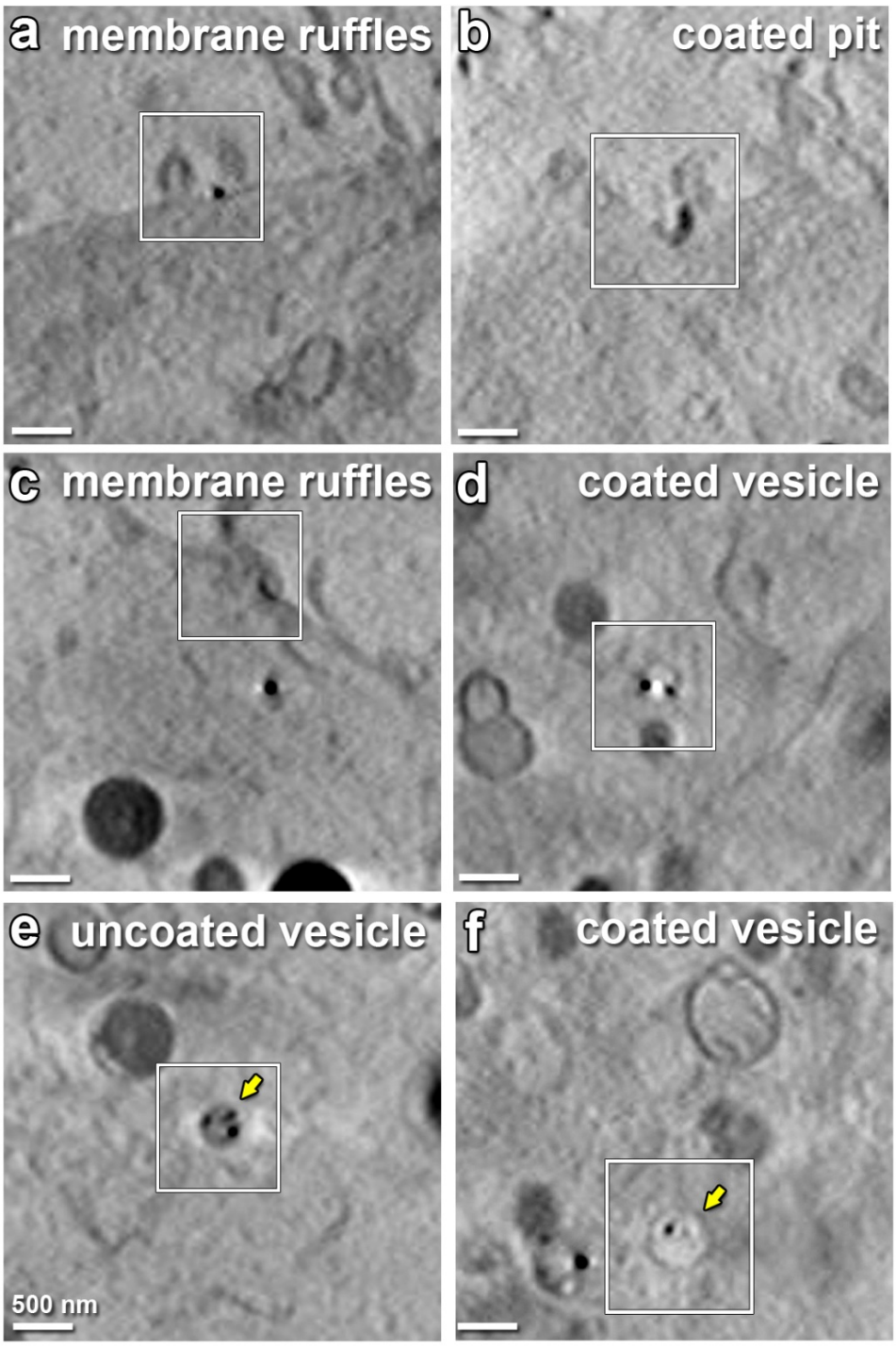

Figure 6.4 Endocytosis of dPGS nanoparticles in A549 cells by cryo SXT. dPGS nanoparticles were found in membrane ruffles (a,c) and in coated pits (b) on plasma membrane. dPGS nanoparticles were also found in uncoated vesicles (e) which may arise from membrane ruffles and within coated vesicles (d,f) which may arise from the coated pits. The yellow arrows point out uncoated and a coated vesicle containing nanoparticles. Note that uncoated vesicles contain an interior which is a mixture of an X-ray dense and X-lucent material (e). The coated vesicles contain a relatively clear X-ray lucent interior (d,f). Scale bars = 500 nm.

nm) [261]. Clearly, fluorescent microscopy analyses using established molecular markers for these pathways are required in the future to definitively identify the different endocytosis pathways for dPGS.

In order to determine how often these two different endocytosis pathways were used, the number of coated and uncoated vesicles that contained the dPGS nanoparticles from 12 cells was quantified by using a counting technique as explained in Chapter 12 (Fig. 12.2, Fig. 12.3). According to this morphological analysis, 85% $\pm$ 10 of the vesicles were of the larger, uncoated variety characteristic of the macropinocytosis pathway. Thus these measurements suggest, that macropinocytosis accounts for about 85% of nanoparticle uptake, whereas the putative caveolae- or clathrin- mediated endocytosis accounts for about 15% of the nanoparticle uptake.

In sum, through a careful morphological analysis of membrane invaginations and vesicles within which dPGS nanoparticles localize, it was concluded that dPGS nanoparticles are likely to be internalized via two different endocytic pathways which are likely to be macropinocytosis and either caveolae- or clathrin-mediated endocytosis. These observations should be tested in the future by performing fluorescence microscopy with established molecular markers for these different pathways. Interestingly, the current conclusions of this thesis are partially consistent with two previous studies of dPGS uptake in which inhibitors against different endocytosis pathways were used and the reduction in the uptake of fluorescently tagged dPGS was measured [168, 457]. These studies also found evidence for uptake of dPGS by macropinocytosis [168] and by clathrin- and caveolae-mediated endocytosis [457]. However, the proportional contribution of each pathway was different, which could reflect the fact that different cell types were examined in these inhibitor studies (human monocytic cells [457] and microglial cells [168]). Nevertheless, these previous observations provide some support for the current morphological findings of this thesis.

6.6 The majority of dPGS nanoparticles stay enclosed within membrane bound organelles of the endo/lysosomal pathway and autophagy

After this investigation of how dPGS nanoparticles enter the A549 cells, the next step was to examine how they were trafficked within the cell cytoplasm. Recall that entry of the dPGS nanoparticles into the cell is probably not required for either their diagnostic or

therapeutic action, since diagnosis and therapy of inflammation are thought to occur via interactions of dPGS with cell-surface receptors [148, 158] as explained in Chapter 3.3.1 and Chapter 6.1. However, fluorescent dPGS compounds were reported to enter into cells [21-26]. Additionally, dPGS nanoparticles were shown to be internalized by cells in Chapter 6.2. In this case, dPGS nanoparticles should stay enclosed within the endomembrane system and have minimal contact with the cytoplasm, nucleus and other organelles to not interfere with other cellular processes. Ideally, dPGS nanoparticles should then be excreted from the cells as soon as possible. To determine if this was occurring, dPGS nanoparticles were tracked in the 3D volumes of cells obtained by cryo-SXT. As described in detail below, it was found that the majority of dPGS nanoparticles (~90%) localize to compartments in the endo/lysosomal pathway and autophagy, namely within endosomes, lysosomes, multivesicular bodies and autophagic vacuoles.

dPGS nanoparticles were found inside of endosomes, which probably arise from the membrane invaginations as discussed in the previous section through at least two different endocytosis pathways (Fig. 6.5). At 1 h, 1 - 5 nanoparticles are found in these endosomes (Fig. 6.5a). The nanoparticles were located both at the perimeter of the inner membrane and also within the luminal space inside of the endosomes (Fig. 6.5a). At later incubation time points, the size of endosomes containing nanoparticles increased up to 450 nm, and this was accompanied by an increase in nanoparticle number (up to 15) inside the endosomes (Fig. 6.5c-d, Fig. 6.6a). This suggests that dPGS nanoparticles induce fusion events between endosomes during trafficking of dPGS nanoparticles. Indeed, such fusion events could be found, although mostly between uncoated vesicles (i.e the putative macropinosomes) (Fig. 6.5b).

Also, dPGS nanoparticles were detected in multivesicular bodies (MVB's). MVB's were identified as clusters of small vesicles enclosed in a surrounding outer membrane (Fig. 6.6b) [459, 460]. The dPGS nanoparticles that are associated with MVB's were found either on the outer surface of the enclosed vesicles or free within the lumen of the surrounding outer membrane. MVB's are known to excrete some of their cargo to the extracellular space [330, 332, 461]. Therefore, localization of dPGS nanoparticles to MVB's suggests that the nanoparticles may eventually be excreted from the cells.

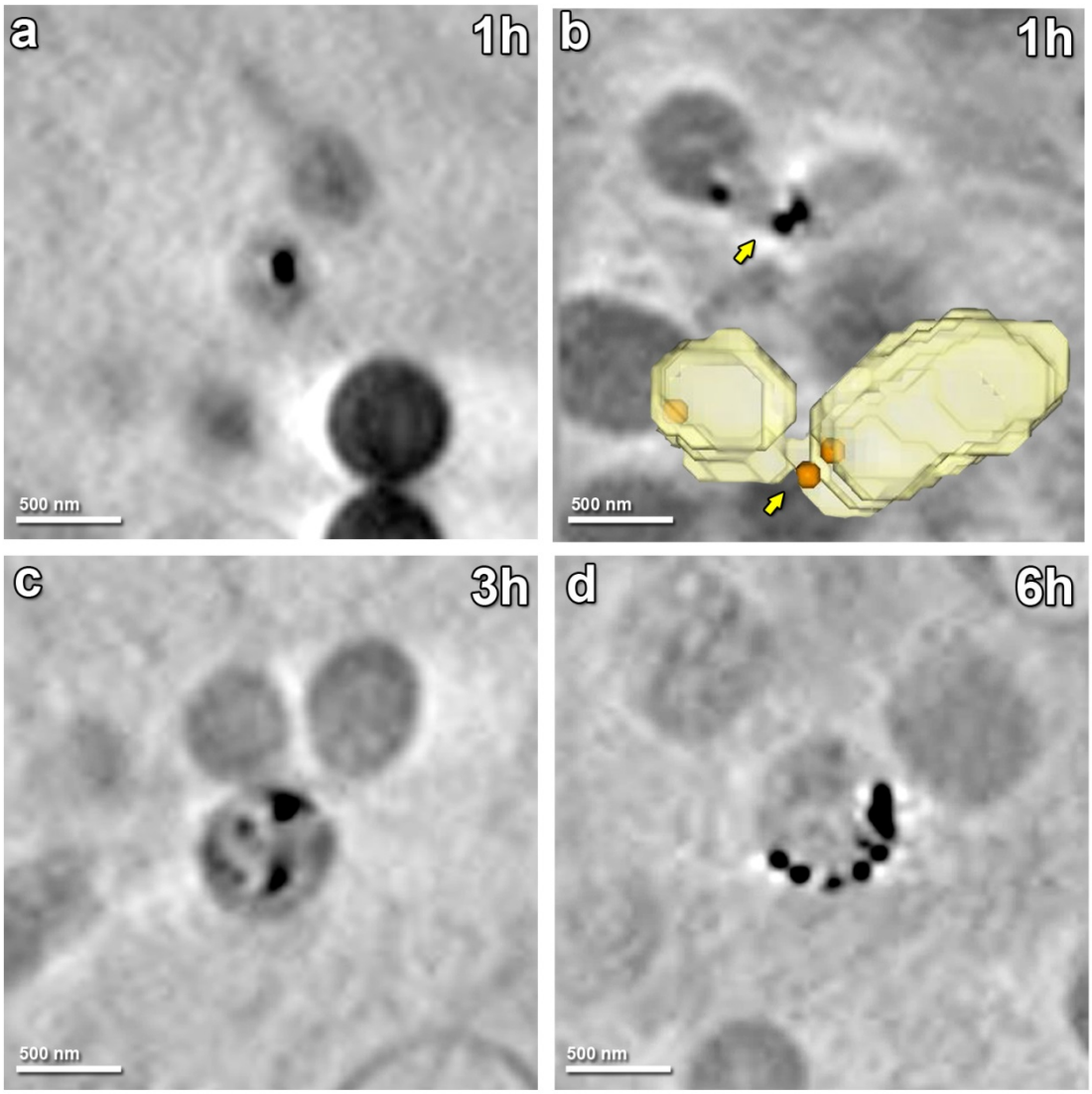

Figure 6.5 Possible fusion events are detected between uncoated vesicles via cryo-SXT. The cells are incubated with dPGS nanoparticles for 1 h, 3 h and 6 h. dPGS nanoparticles (yellow arrows) were found in uncoated vesicles. The cells are incubated with dPGS nanoparticles (yellow arrows) for 1 h, 3 h and 6 h. dPGS nanoparticles were found in uncoated vesicles. The size of these uncoated vesicles tended to increase as incubation time increased suggesting that these vesicles may mature by fusing with each other (a-d). During these fusion events, nanoparticles may escape to the cytoplasm, as suggested for example by images like those in (b) in which nanoparticles are at the intersection points of endosome fusion. Scale bars = 500 nm.

dPGS nanoparticles were also found in lysosomes (Fig. 6.6c). The lysosomes were identified as larger cytoplasmic vesicles containing a dense, granular interior with membrane whorls (Fig. 6.6c) [63, 462]. The nanoparticles were found at the inner, luminal edge of the vesicle membrane in lysosomes.

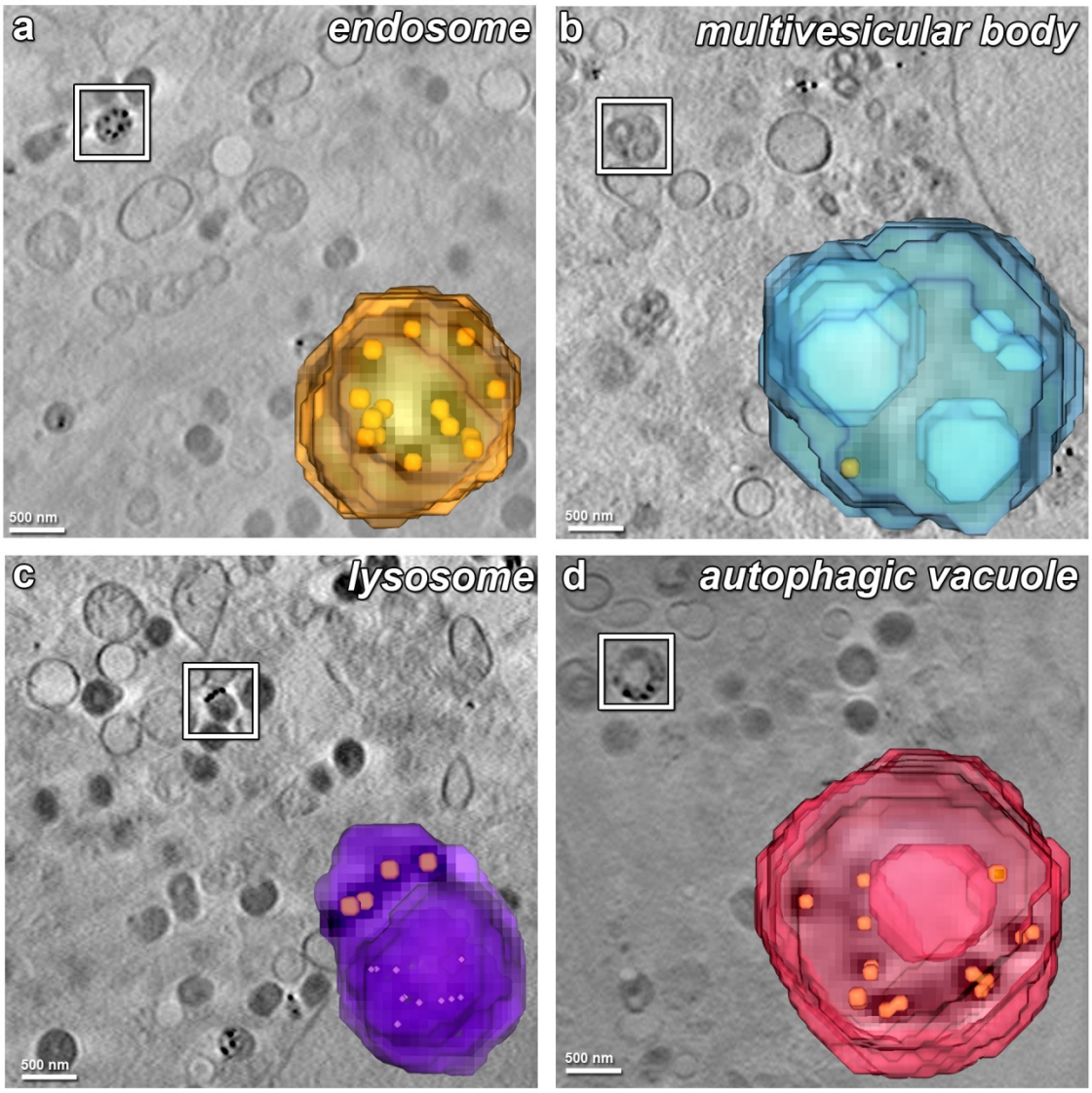

Figure 6.6 Intracellular trafficking of dPGS nanoparticles in A549 cells via cryo SXT. Nanoparticles were observed within endosomes (a), multivesicular bodies (b), lysosomes (c) and autophagic vacuoles (d). Scale bars = 500 nm.

In sum, the presence of dPGS nanoparticles in endosomes, MVB's and lysosomes shows that the endo/lysosomal pathway is involved in trafficking of dPGS nanoparticles (Fig. 6.6a-c). Note that this finding is consistent with many previous nanoparticle studies with a variety of different coatings [286, 463].

Another location where dPGS nanoparticles were found was in autophagic vacuoles (Fig. 6.6d). In this thesis, the autophagic vacuoles were identified as larger, hollow cytoplasmic vesicles containing a denser region surrounding an X-ray lucent inner core

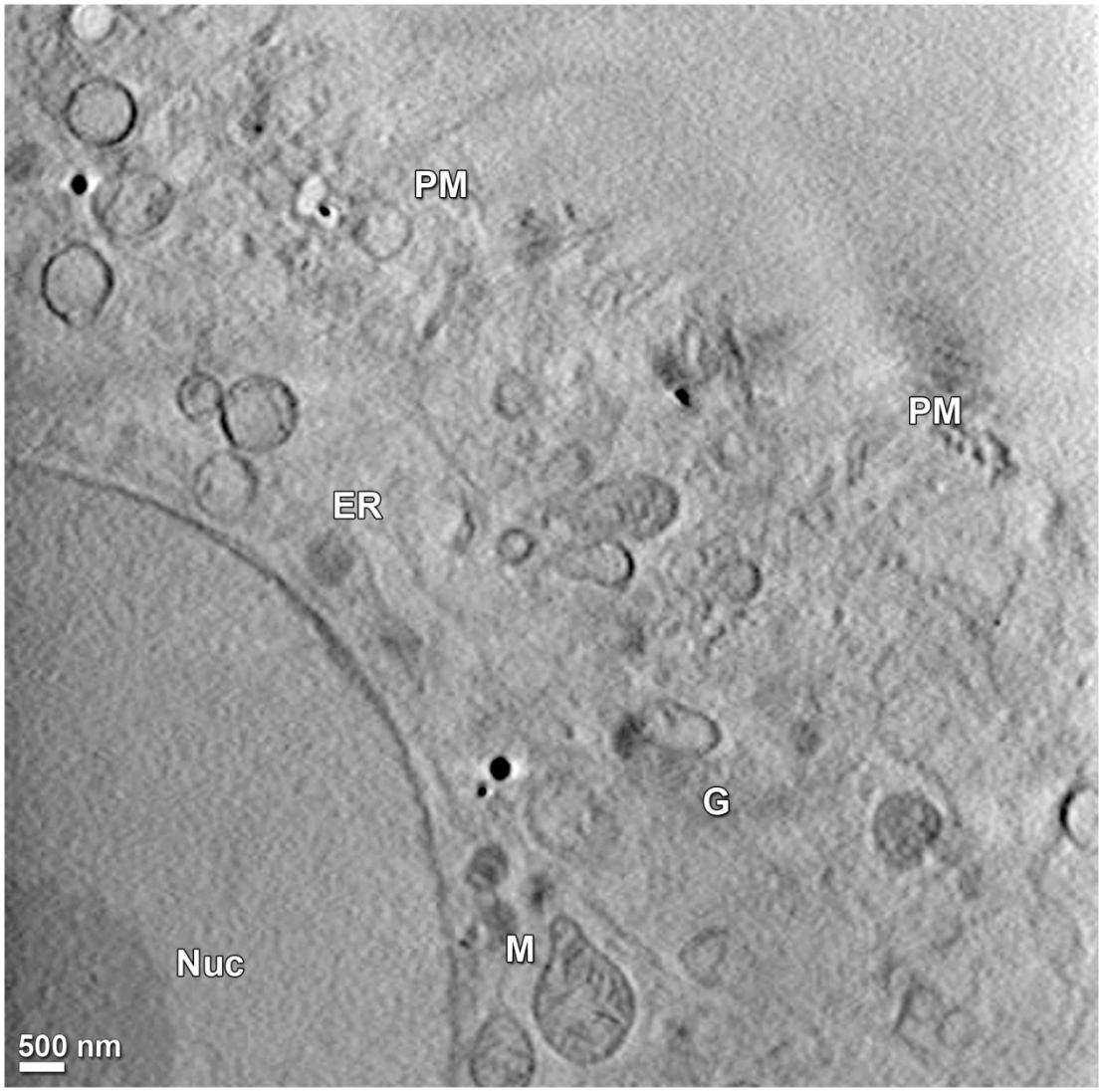

Figure 6.7 A number of organelles never contained any dPGS nanoparticles, including endoplasmic reticulum (ER), mitochondria (M) and Golgi (G). dPGS nanoparticles were also never found in the nucleus (Nuc). Scale bar = 500 nm.

(Fig. 6.6d) [464-467]. Note that the term autophagic vacuole includes a series of related organelles, namely autophagosomes, amphisomes and autolysosomes. Amphisomes and autolysosomes arise from the fusion of autophagosomes with other endocytic compartments, specifically MVB's and lysosomes respectively [466, 468, 469]. dPGS nanoparticles were found to localize either in the X-ray dense membranous region or in the X-ray lucent core of autophagic vacuoles. These findings show that autophagy is involved in the trafficking of dPGS nanoparticles, consistent with some other nanoparticle studies which also implicated autophagy in nanoparticle trafficking [470].

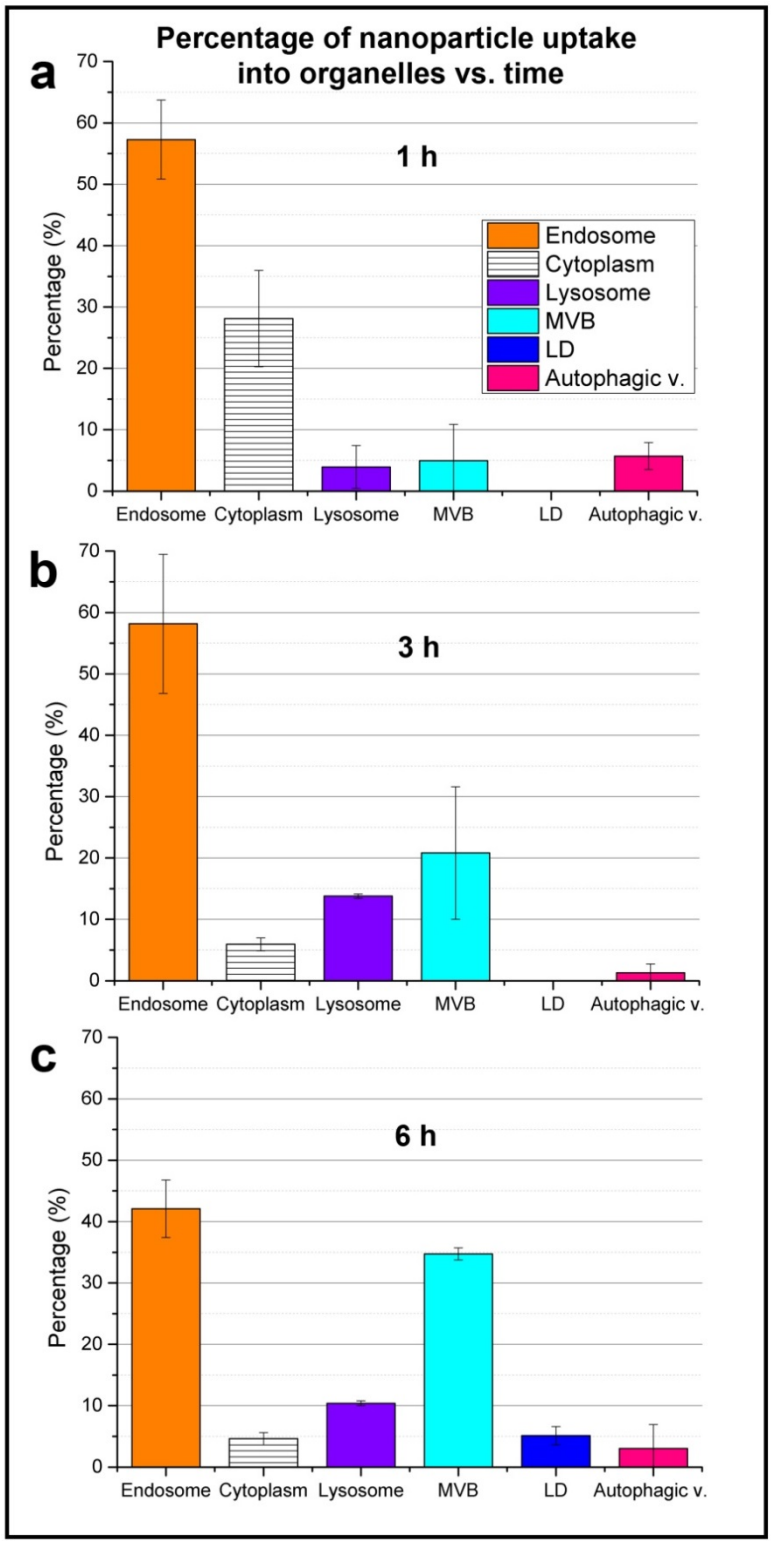

Figure 6.8 Fraction of total nanoparticles taken up by different organelles at 1 h ,3 h and 6 h of nanoparticle incubation. All counts were made using the 3D cryo SXT images. Error bars are standard deviation (n = 4). Note that endosomes contain the most nanoparticles at all time points, but that the fraction entering lysosomes, multivesicular bodies and lipid droplets increases at later time points.

dPGS nanoparticles were not detected in other cytoplasmic compartments such as mitochondria, the Golgi apparatus, ER or the nucleus, even though many of these organelles could be observed within the set of 3D reconstructions of the cells produced by cryo SXT in this thesis (Fig. 6.7). This shows that the dPGS nanoparticles rarely if ever enter into these other organelles. Thus these results indicate that dPGS nanoparticles are not processed with the retrograde pathway, which includes the Golgi apparatus and ER. Rather, dPGS nanoparticles are confined mostly to organelles of the endo/lysosomal pathway and autophagy.

To quantify the distribution of nanoparticles within the cells as a function of incubation time, the number of nanoparticles present in the different organelles was counted where they were detected. This quantification was done as before using a 3D sub-volume of the cytoplasm positioned midway between the nucleus and cytoplasm as explained in Chapter 12 (Fig. 12.2). Note that this sub-volume corresponds approximately to 1/7 of the whole cell volume (Fig. 12.3).

At all three time points (1 h ,3 h, 6 h) the majority of dPGS nanoparticles were found in the endosomes, namely from 42 - 68% of the internalized nanoparticles (Fig. 6.8). This is not surprising since endosomes are known to be the first organelle to which any cargo is trafficked and then sorted to other organelles [471]. The fraction of dPGS nanoparticles in endosomes decreased at 6 h, indicating that nanoparticles were sorted from endosomes to other organelles (Fig. 6.8c).

At 3 h and 6 h, 93% and 87% of the nanoparticles, respectively, were found in endosomes, lysosomes and multivesicular bodies, all of which are members of the endo/lysosomal pathway (Fig. 6.8b,c). This indicates that around 90% of dPGS nanoparticles were trafficked via this endo/lysosomal pathway. As noted above, autophagy is also involved in trafficking of dPGS nanoparticles, but the quantification, performed in this thesis shows that this is a small component. At 6 h, only 4% of dPGS nanoparticles were found in autophagic vacuoles (Fig. 6.8c). In sum, dPGS nanoparticles were mostly enclosed within membrane bound organelles of the endo/lysosomal pathway, and did not localize in most other vital organelles within the cell.

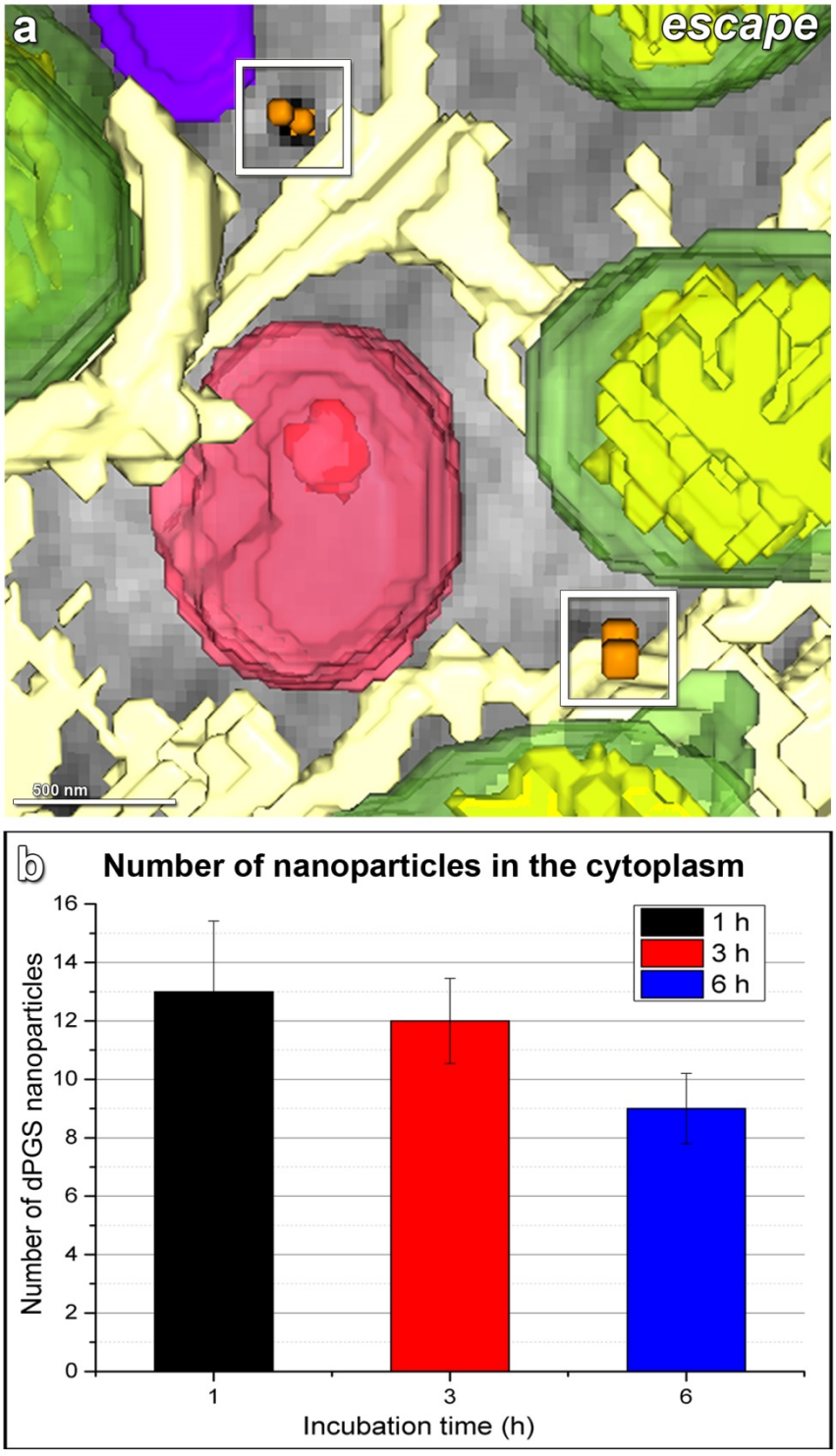

Figure 6.9 Cytoplasmic escape of dPGS nanoparticles in A549 cells via cryo SXT. Cells were incubated with dPGS nanoparticles at 1 h, 3 h and 6 h, and then imaged via cryo-SXT to obtain 3D volumes from an area of interest in the cells, which corresponds to approximately 1/7 of the whole cell volume. After investigating this area of interest, a limited amount of dPGS nanoparticles were found to be free in the cytoplasm (a). This escape was in the range of 9 - 13 nanoparticles at each incubation time point, indicating that cytoplasmic escape was limited (b). Error bars are standard deviation (n = 4). Scale bar of the gray scale image = 500 nm.

Additionally, note that the fraction of dPGS in MVB increased with time up to 35% at 6 h (Fig. 6.8c). Since some MVBs are known to excrete their cargo within exosomes to the extracellular environment by fusing with the plasma membrane as described in Chapter 4 [330, 332, 461], the localization of nanoparticles to these organelles suggests that some portion of dPGS nanoparticles may be excreted to the extracellular environment.

6.7 Some dPGS nanoparticles are found free in the cytoplasm

The membrane-bound organelles of the endo/lysosomal pathway and autophagy are not the only place where dPGS nanoparticles localize. Some dPGS nanoparticles were also found in the cytoplasm (Fig. 6.9a). The 3D capabilities of cryo-SXT allowed inspection of these isolated nanoparticles to confirm that there were no residual membranes associated with them (Fig. 6.9a). How these nanoparticles escape into the cytoplasm is unclear. No evidence for ruptured organelles was observed in the cytoplasm. However, note that nanoparticles were sometimes present in the thin membrane tunnels formed during vesicle fusion (Fig. 6.5b), and perhaps escape might occur during such fusion events. The number of nanoparticles free in the cytoplasm was only around ten (Fig. 6.9b), as measured within the 3D volume of interest which corresponds to approximately 1/7 of the whole cell volume as explained in Chapter 12 (Fig. 12.2, Fig. 12.3). Although the estimated number of cytoplasmic nanoparticles is relatively low (~70) per cell, they could still potentially interact with cytoplasmic proteins and yield unwanted cellular responses within the cell. On the positive side, there has also been some suggestion that cytoplasmic dPGS may have additional therapeutic effects in the cytoplasm. Specifically, some experimental data which are yet unpublished suggest that dPGS may have a suppressive effect on NF-κB and AP-1 activation which take part in the release of inflammatory cytokines [472]. Thus the cellular responses to dPGS nanoparticles within the cytoplasm should be investigated in future studies.

6.8 dPGS nanoparticles enter into lipid droplets

In addition to nanoparticles within the cytoplasm and the organelles of the endo/lysosomal pathway and autophagy, nanoparticles were also detected in a surprising location, namely within lipid droplets (Fig. 6.10). Lipid droplets were identified as round and very X-ray dense organelles within the cytoplasm (Fig. 6.10c-f). They exhibited a granular interior that could only be detected with low contrast levels at which the rest of

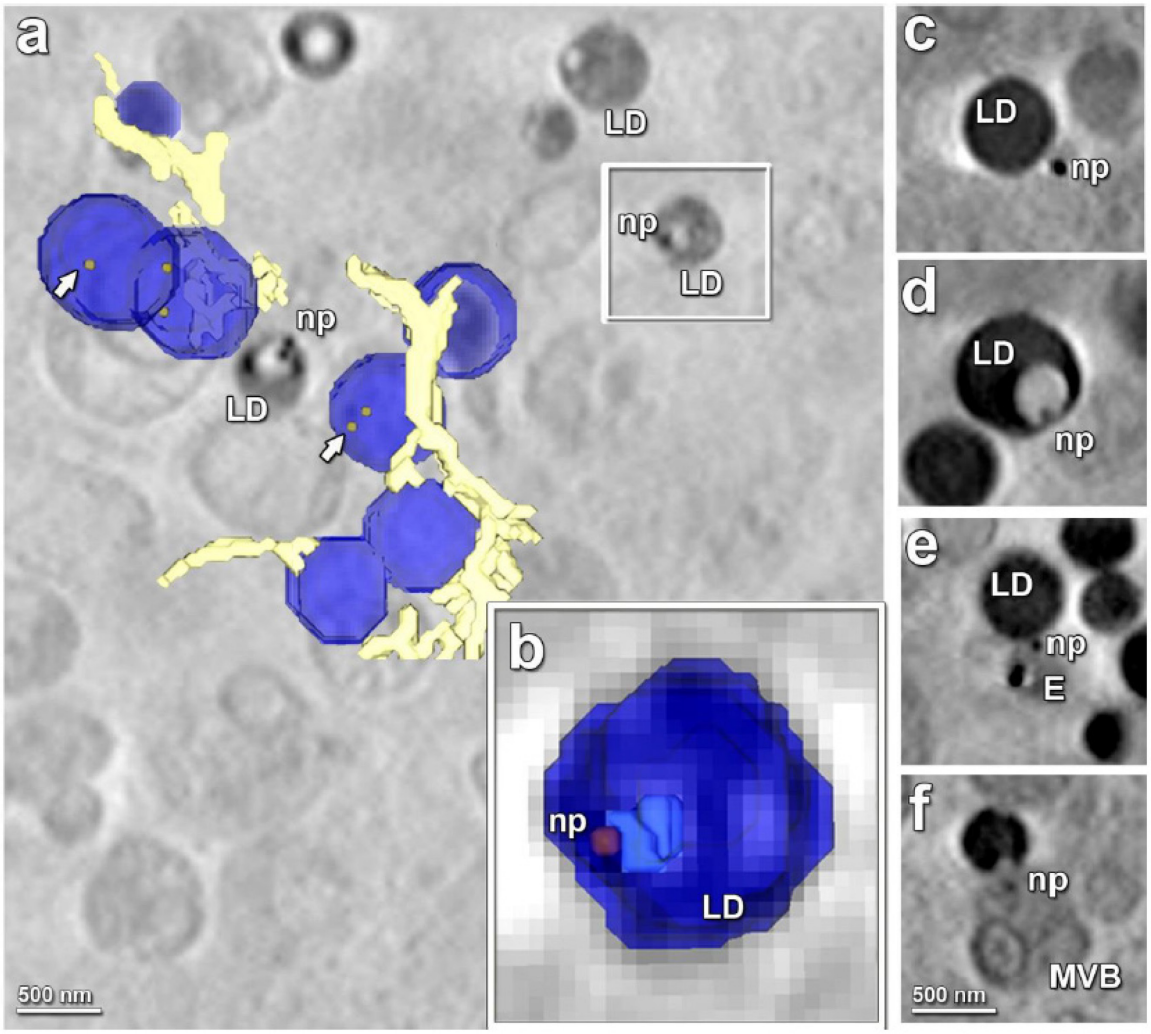

Figure 6.10 dPGS nanoparticle entry into lipid droplets. Selected sections from cryo SXT images are shown. The lipid droplets are spherical and X-ray dense (a). They often contain an X-ray lucent inclusion (a). The white square encloses a lipid droplet containing a nanoparticle, which is 3D rendered in (b). Several other lipid droplets (dark blue) and endoplasmic reticulum (cream) are also 3D rendered from the 3D data corresponding to (a) and overlaid onto the cryo SXT slice. Arrows (white) point to nanoparticles (gold) in the rendered images in (a). Possible intermediate stages of nanoparticle entry into lipid droplets are shown in (c-f). Lipid droplets were found to contact nanoparticles which are free in either the cytoplasm (c) or contained in endosomes (e) or multivesicular bodies (f). These contacts gave rise to X-ray lucent "holes" in the lipid droplet (f). These same X-ray lucent regions often contained nanoparticles in other lipid droplets (d). Scale bar = 500 nm.

the sub-cellular organelles appeared dim (Fig. 6.10a). About 5% of the dPGS nanoparticles (~70 per cell) were found to end up in lipid droplets by the 6 h time point (Fig. 6.8c). This observation of nanoparticles in lipid droplets is not unprecedented as only two other studies, to my knowledge, also observed this [322, 473]. However, the

vast majority of nanoparticle studies have not reported localization in lipid droplets. This relatively rare identification of nanoparticles in lipid droplets could arise because only a small number of surface coatings, such as dPGS, lead to incorporation into lipid droplets. Alternatively, it is also possible, that nanoparticle localization in lipid droplets has been missed in TEM studies since the relative numbers in lipid droplets are low and the lipid droplets are very intensely stained in standard TEM preparations, which could easily obscure the presence of nanoparticles.

Since very few studies have seen nanoparticles in lipid droplets, very little is known about how they might enter into these organelles. Lipid droplets are thought to originate from the endoplasmic reticulum (ER) membrane [474, 475]. However, dPGS nanoparticles were never observed in association with the ER, suggesting that the nanoparticles entered lipid droplets by a different route. Indeed, it was possible to identify three different plausible intermediate stages that could reflect dPGS nanoparticle entry into lipid droplets. Specifically, examples where lipid droplets associated closely with either endosomes (Fig. 6.10e) or multivesicular bodies (Fig. 6.10f) containing nanoparticles and with isolated nanoparticles free in the cytoplasm could be found (Fig. 6.10c,d). At such points of contact, the presence of an X-ray lucent hole within the lipid droplet, sometimes containing nanoparticles, could be observed, suggesting the possibility of a transfer of some of the X-ray lucent material from either the vesicles or cytoplasm (Fig. 6.10a,d,f). In sum, these observations suggest that the dPGS nanoparticles may enter lipid droplets by interactions with either endosomes or free nanoparticles in the cytoplasm, or both.

These observations of dPGS nanoparticles in lipid droplets were unexpected because dPGS itself is not known to be strongly lipophilic [157]. Rather, it seems likely that some other molecule on the nanoparticle surface is responsible for the interaction with lipid droplets, which are known to contain an outer membrane composed of a protein coated phospholipid monolayer that could mediate interactions with cellular components [476]. Some evidence suggests that dPGS interacts with apolipoprotein A-I [457], which was also suggested to be associated with lipid droplets in another study together with some other apolipoprotein types [477]. Indeed, lipoproteins are found in the protein corona of many nanoparticles, and so if these proteins are involved in targeting to lipid droplets

[478], then many other kinds of nanoparticles may also be found to localize to these droplets. Further work on the molecular mechanisms involved in dPGS targeting to lipid droplets will therefore be important. These data also raise questions about the long term fate of nanoparticles within lipid droplets, and whether there are any effects on cellular signaling and cellular metabolism, which are two key functions of lipid droplets. Further research on these questions will also be important.

6.9 dPGS nanoparticles cluster only within endosomes and are trafficked as single nanoparticles to other locations

As discussed in Chapter 4, clustering of nanoparticles can alter their behavior since clustering would create bigger nanoparticles with different surface properties [215, 216, 308]. Therefore, analysis of nanoparticle clustering is important for nanoparticle characterization. In general, it is extremely difficult to track clustering *in situ* within organelles. However, with the cryo SXT approach, the spatial distribution of nanoparticles relative to membrane bound organelles can be assessed, and clustered nanoparticles within the organelles can be detected. According to 3D images in this thesis, single nanoparticles were consistently observed at all cellular locations. The only exception to this was that clusters of nanoparticles could not be detected within small endosomes at early time points (1 h, 3 h) (Fig. 6.5a-c), but not at the later time point (6 h) (Fig. 6.5d, Fig. 6.6a), suggesting that the clusters disintegrated relatively quickly, perhaps due to fusion events of endosomes which are known to change the ionic conditions of the endosome [479, 480]. Outside of endosomes, all dPGS nanoparticles were found as single nanoparticles in multivesicular bodies, lysosomes, autophagic vacuoles (Fig. 6.6b-d), the cytoplasm (Fig. 6.9) and lipid droplets (Fig. 6.10). This demonstrates that dPGS nanoparticles are mostly single during their trafficking and therefore clustering does not significantly influence their cellular trafficking.

6.10 dPGS nanoparticles may be excreted by multivesicular bodies

Some morphological evidence for possible excretion of dPGS nanoparticles was found. First, dPGS nanoparticles localize to multivesicular bodies (Fig. 6.6b). Secondly, the percentage of nanoparticles in multivesicular bodies increased as the incubation time increased (Fig. 6.8). Third, the dPGS nanoparticles were found to shift their location within the multivesicular bodies from the limiting membrane region (Fig. 6.11a) to inner

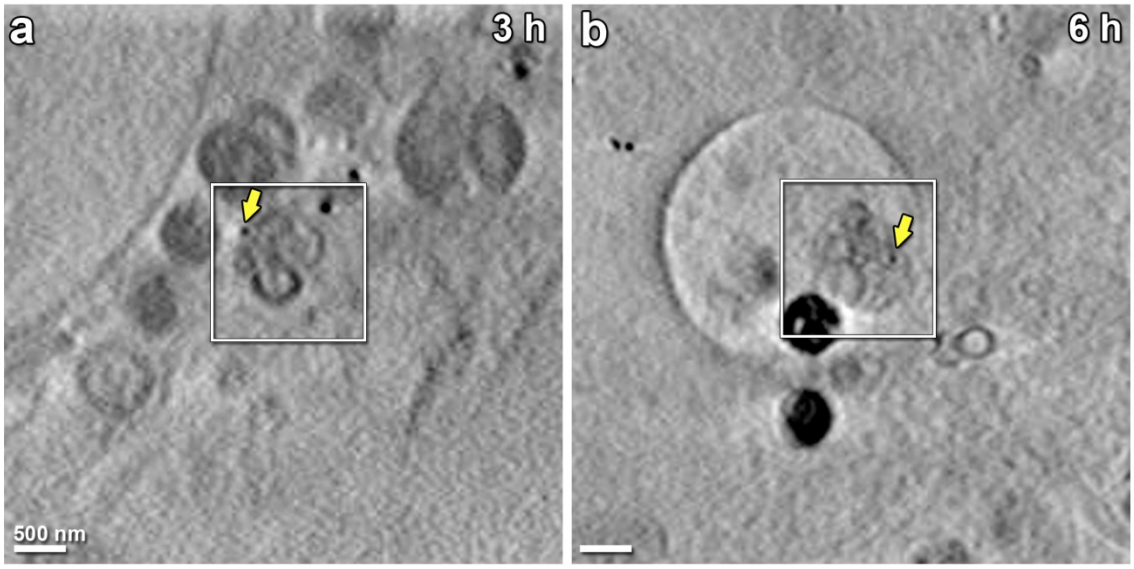

Figure 6.11 dPGS nanoparticles shift their positions within MVB's at later time points. At 3 h, dPGS nanoparticles are found within the luminal side of the outer membrane of MVB's (a), whereas at 6 h, dPGS nanoparticles are mostly found within the inner vesicles of MVB's (b). This shift in position suggests that dPGS nanoparticles may eventually be excreted from the cells via exosomes. Nanoparticles are indicated with yellow arrows. Scale bars = 500 nm.

vesicles (Fig. 6.11b). The limiting membrane region is between the outer membrane of multivesicular bodies and the inner vesicles. Specifically, at earlier time points, nanoparticles were observed to associate with this limiting membrane of the multivesicular body (Fig. 6.11a, Fig. 6.12a). At later time points, the nanoparticles were found to be sorted to the interior of the inner vesicles of the multivesicular body (Fig. 6.11b, Fig. 6.12b). The inner vesicles are known to be involved in excretion of the cargo contained within them when the multivesicular bodies fuse with the plasma membrane [330, 332, 461]. Therefore, localization of dPGS nanoparticles inside the inner vesicles of multivesicular bodies suggests that the nanoparticles will be excreted to the extracellular environment once multivesicular bodies fuse with the plasma membrane. Proof of this however will require examination of later time points to detect evidence for actual excretion of these inner vesicles.

6.11 Morphological markers of cell death pathways were not observed after dPGS nanoparticle incubation

Cell death can be classified according to its morphological appearance which may be apoptotic, necrotic or autophagic [64, 481]. Dying cells are engaged in a process that is

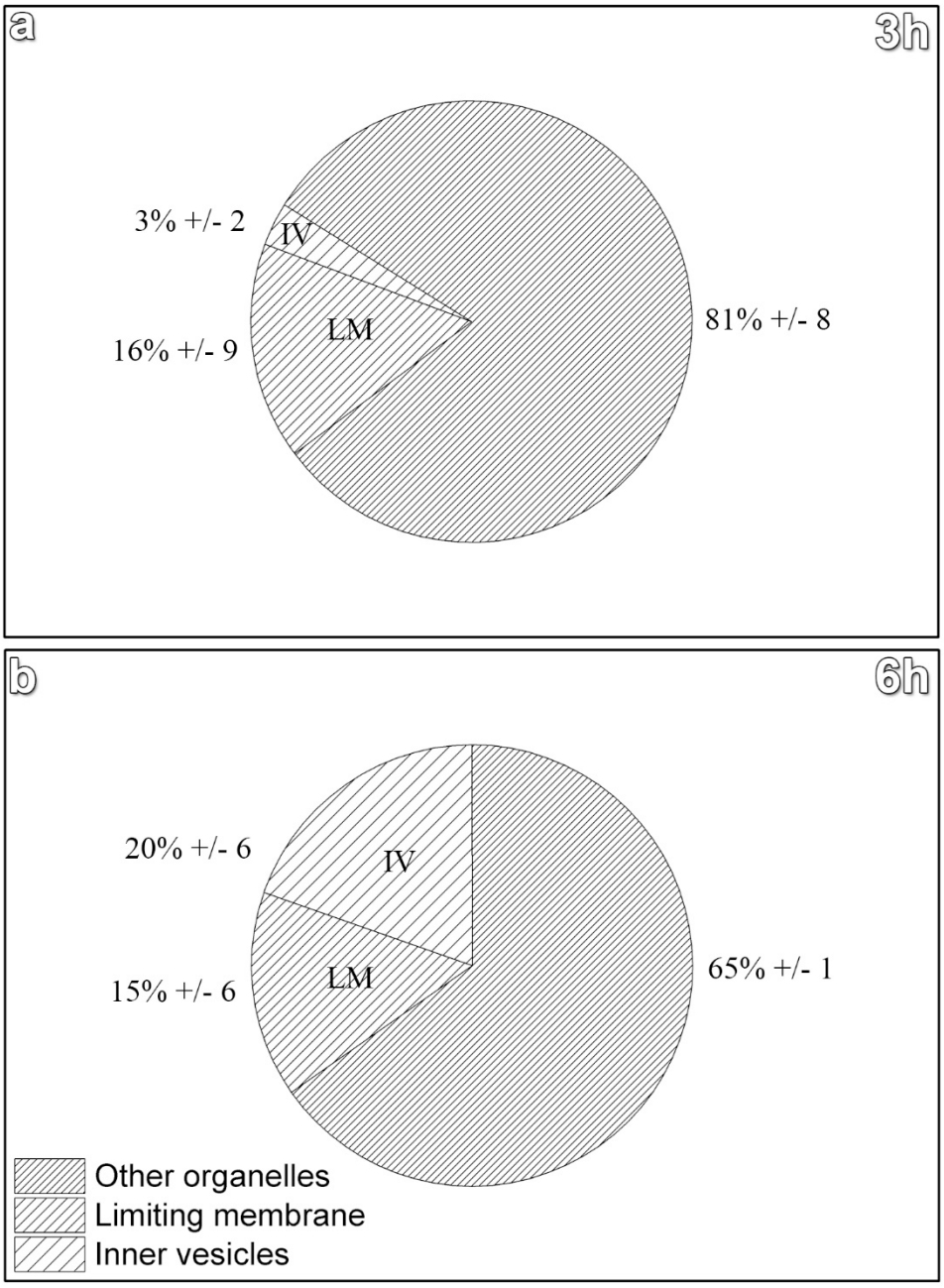

Figure 6.12 Sorting of dPGS nanoparticles to inner vesicles from the limiting membrane in multivesicular bodies. At 3 h, dPGS nanoparticles mostly localize to the limiting membrane (a). By 6 h, they are mostly localized to the inner vesicles of MVBs, suggesting that nanoparticles are sorted to the inner vesicles for excretion from the cells (b).

reversible until a point of no return is encountered in which the cell is completely dead [64, 481]. To investigate whether a cell is dead or dying and which cell death pathway is involved in this dying process, various assays including morphological and biochemical analysis can be performed. Biochemical assays often include assessment of caspase

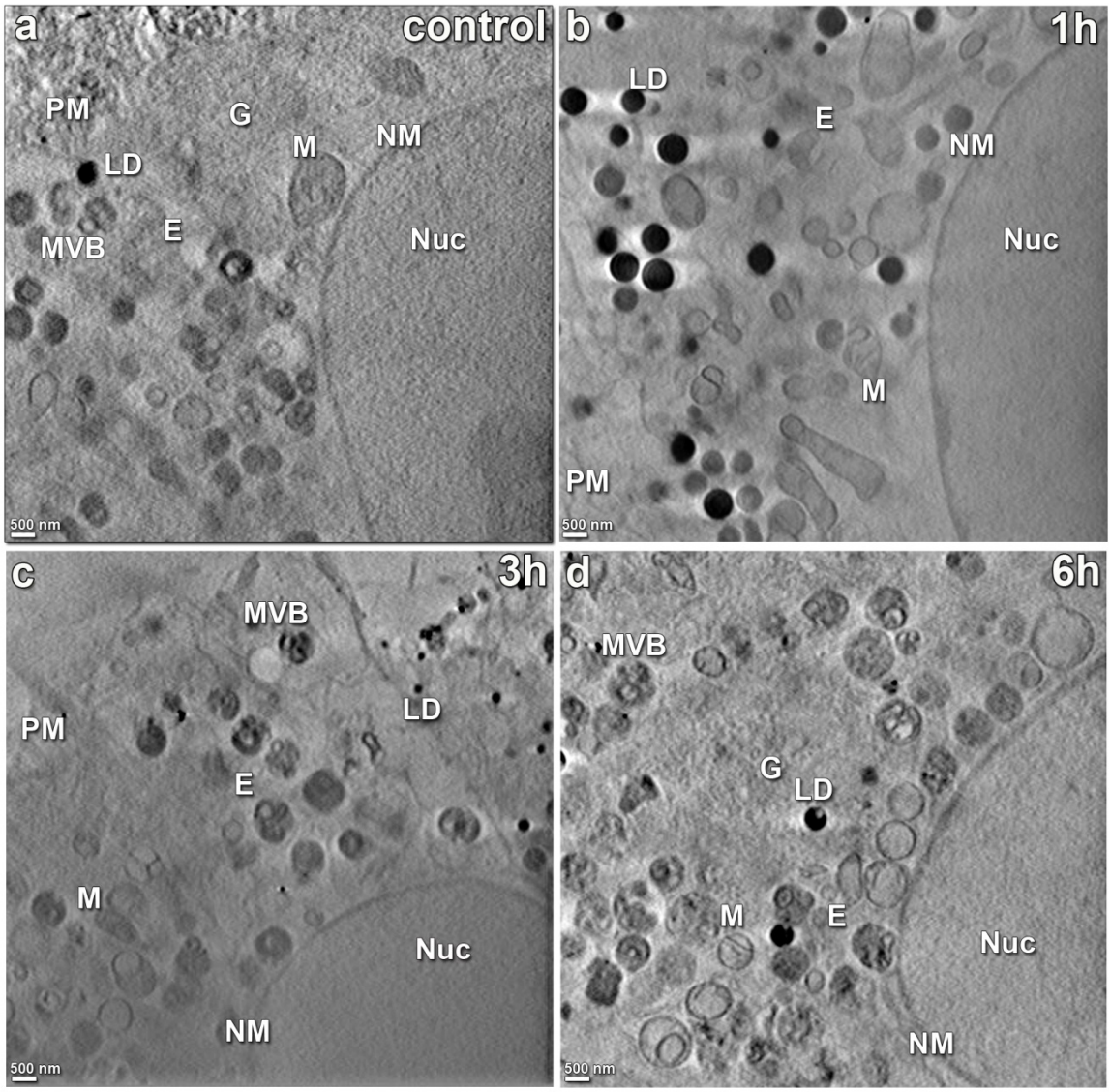

Figure 6.13 dPGS nanoparticles do not induce structural changes related to apoptotic and necrotic cell death pathways in A549 cells. Selected slices from 3D cryo X-ray tomography data from control A549 cells (a) and A549 cells incubated with dPGS nanoparticles for 1 h (b), 3 h (c) and 6 h (d). No evidence for blebbing in the plasma membrane (PM), fragmentation of the nuclear membrane (NM) or chromatin condensation in the nucleus (Nuc) (a-d) was found in any of the cells examined. After incubation with dPGS nanoparticles, the volume of the whole A549 cell and the volumes of organelles within it (b-d) remained similar to control cells (a). Specifically, the size of endosomes (E), multivesicular bodies (MVB), lipid droplets (LD), Golgi (G) and mitochondria (M) did not change after dPGS incubation. Furthermore, the plasma membrane (PM) did not rupture and cells remained intact (a-d). Scale bars = 500 nm.

cleavage, plasma membrane integrity and mitochondrial activity. In this thesis, cell viability was investigated with a morphological analysis since an apoptotic, necrotic

andautophagic cell can be distinguished by morphological hallmarks of these cell death pathways.

The cryo SXT observations showed that the morphological markers for cell viability were not markedly influenced by dPGS nanoparticle uptake (Fig. 6.13). No evidence for any of the hallmarks of apoptosis was observed, including no structural changes in the mitochondria, no plasma membrane blebbing, no nuclear fragmentation and no chromatin condensation. Furthermore, none of the morphological signs of another cell death pathway, namely necrosis, was observed. Specifically, there was no increase in cell volume, swelling of organelles or plasma membrane rupture. Thus the data suggest that the A549 cells remained viable after the nanoparticle incubation, consistent with previous analyses of dPGS which showed no evidence for induction of apoptotic and necrotic cell death pathways. However, to understand the exact mechanism behind this morphological signs, biochemical assays should be performed in the future [64].

6.12 Summary

dPGS is a compound designed to diagnose and treat inflammation by interacting with the plasma membrane of cells. Previous fluorescence microscopy studies had demonstrated that dPGS was internalized by cells yielding a punctate pattern of cytoplasmic fluorescence presumably reflecting endocytic vesicles [21-26]. Inhibitor studies had implicated roles for macropinocytosis and clathrin- and caveolae-mediated endocytosis in the cellular uptake of dPGS [168, 457]. Additionally, it was shown that dPGS compounds are not toxic to cells [23-26, 168]. However, the intracellular pathway of dPGS, including whether or not dPGS nanoparticles reach the cytoplasm, had not been studied. Defining the cellular locations and trafficking pathway of dPGS nanoparticles is important to understand their potential side effects and mode of action. Therefore, this chapter investigated both the distribution of dPGS nanoparticles on the plasma membrane and the endocytosis and intracellular trafficking pathway of dPGS nanoparticles using differential interference contrast (DIC) microscopy and cryo soft X-ray tomography (Fig. 6.14). Additionally, the effect of dPGS nanoparticles on cell viability was investigated through a morphological analysis. According to this investigation, dPGS nanoparticles were found to attach at widely dispersed locations on the plasma membrane, and then be internalized via two different pathways in a time-dependent manner. Two internalization

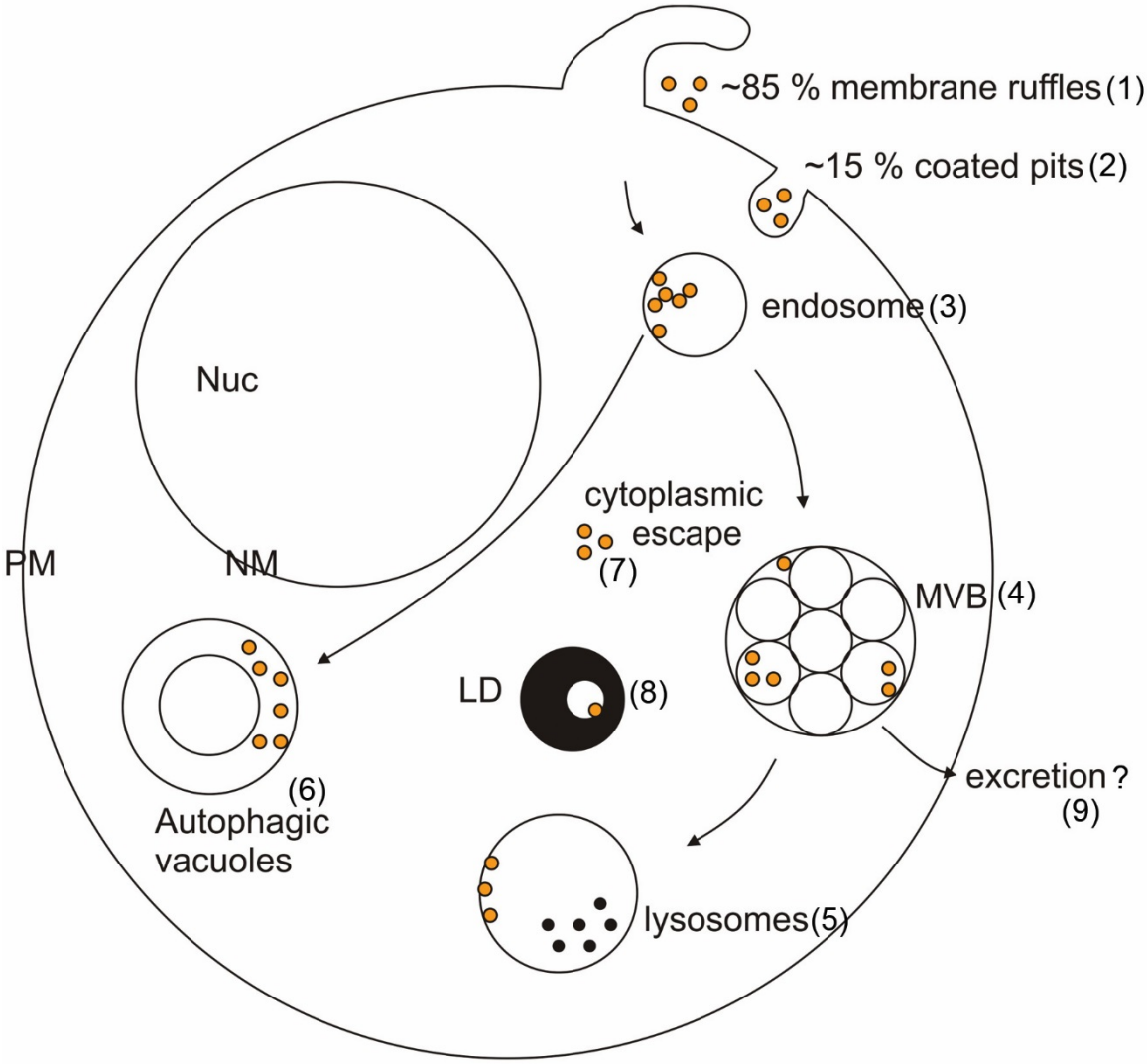

Figure 6.14 Model summarizes the observations about the endocytosis and intracellular trafficking pathway of dPGS nanoparticles. dPGS nanoparticles were endocytosed via at least two endocytosis pathways (1,2) which may be macropinocytosis (1) and a caveolae- or clathrin-mediated endocytosis (2). The predominant endocytosis pathway was macropinocytosis (1). The nanoparticles were first sorted to early endosomes (3). Later, dPGS nanoparticles were trafficked from endosomes to multivesicular bodies (4) and lysosomes (5) demonstrating that the endo/lysosomal pathway is involved in trafficking of dPGS nanoparticles. A small fraction of dPGS nanoparticles were also found in autophagic vacuoles, demonstrating that autophagy is involved in trafficking of dPGS nanoparticles (6). Additionally, a small portion of dPGS nanoparticles was found in the cytoplasm (7) and in lipid droplets (8). Morphological signs, which suggested that dPGS nanoparticles may be excreted via MVBs, were also detected (9).

pathways, macropinocytosis and a putative clathrin- or caveolae-mediated pathway, were suggested. The macropinocytosis pathway was found to be the predominant pathway accounting for ~85% of nanoparticle internalizations. However, these endocytosis

pathways can be further investigated by endocytosis markers and inhibitors to confirm the results. Moreover, once endocytosed, the dPGS nanoparticles were mostly trafficked to endosomes, multivesicular bodies and lysosomes which are the membrane bound organelles of the endo/lysosomal pathway. Approximately 90% of nanoparticles were enclosed within this endomembrane system at all incubation times. Only a limited number of dPGS nanoparticles appeared to be trafficked via autophagy, since ~4% of dPGS nanoparticles were found in autophagosomes. The retrograde pathway was not involved with dPGS nanoparticles. Specifically, dPGS nanoparticles were not detected in the Golgi apparatus or the endoplasmic reticulum. Nuclear and mitochondrial entry of dPGS nanoparticles was also not detected. A small amount of cytoplasmic escape (5%) was detected, which may still be enough to exert some effects on the cell such as interacting with NF-κB. The effect of nanoparticles within the cytoplasm on cell function and physiology should be investigated in future studies. A similar number of nanoparticles were also trafficked to a rather surprising location, lipid droplets (but only at the last time point, 6 h), and probably through contact with either free nanoparticles in the cytoplasm or with endosomes or multivesicular bodies containing nanoparticles. This finding shows that lipid droplets can be a trafficking site of nanoparticles. However, why and how nanoparticles interact with lipid droplets should be further investigated. Some signs that dPGS nanoparticles might be excreted by multivesicular bodies to the extracellular environment were found. Finally, consistent with previous biochemical viability assays, the morphological analysis showed that dPGS nanoparticles did not induce necrotic and apoptotic cell death mechanisms.

7. TRAFFICKING PATHWAY OF PEI NANOPARTICLES

The preceding chapter contained a detailed analysis of the interaction of dPGS nanoparticles with cells, including their internalization pathway, trafficking pathway, and some of their effects on the cell. The current chapter will now report the corresponding analysis using the other nanoparticle coating studied in this thesis, namely the PEI nanoparticles.

7.1 Motivation to study trafficking of PEI nanoparticles

PEI is now being used in many *in vitro* studies to transfect cells with various plasmid genes because PEI is an efficient gene delivery tool. It entraps DNA and also enhances its escape from vesicles into the cytoplasm [185, 186]. However, there are still conflicting issues about the trafficking of PEI. If these conflicts could be resolved, more efficient PEI nanoparticles could be developed which might one day be used in the clinic. The principal controversial points regarding the trafficking of PEI nanoparticles are their endocytosis pathway, whether they localize to lysosomes and whether they enter the nucleus. Each of these controversial points is discussed in more detail below.

First, the specific endocytosis pathway of PEI internalization is debated. Different studies report different pathways including macropinocytosis, and clathrin- and/or caveolae-mediated endocytosis [37-42]. One conceivable explanation for these different observations is that PEI internalization depends on different factors such as nanoparticle size and cell type [37-42]. It will be important to clarify which pathway(s) PEI nanoparticles utilize, and how the pathways might change dependent on cell type or nanoparticle size, since the pathway strongly influences nanoparticle localization. Notably, caveolae-mediated endocytosis is a pathway that in some cases avoids lysosomes, which therefore enables nanoparticles to escape the corrosive environment of these digestive organelles which could destroy the nanoparticle cargo [191-193].

The second controversial point is related to the first, and concerns the question of whether PEI enters into lysosomes. Many nanoparticles have been found to localize to lysosomes [42, 44-46], including PEI nanoparticles. In contrast, other studies suggests that PEI nanoparticles never localize to lysosomes [49, 50], although they are still found in endosomes [49] or enter into the nucleus [50]. In these cases, some hypothesize that

this occurs because the PEI nanoparticles induced endosomes to rupture before they could reach the lysosomes [49]. Others have hypothesized that these nanoparticles which did not enter into lysosomes may have been internalized via caveolae-mediated endocytosis [192]. However, none of these hypotheses have been directly tested. Understanding if PEI can avoid lysosomes and if so, how it avoids lysosomes is critical to engineer drug delivery vehicles that can bypass this corrosive organelle.

A third controversial point is whether or not PEI nanoparticles enter into the nucleus in order to deliver DNA [33, 482]. Ideally, for efficient DNA delivery, a vector should enter into the nucleus and unload the DNA [483]. The nuclear membrane is largely impermeable, but there are currently two well-defined entry routes for nanoparticles to get cargo into the nucleus. The first is during cell mitosis when the nuclear membrane breaks down, and the second is via small pores in the nuclear membrane which are known to transport larger cargos into the nucleus. Specifically, it is commonly argued that small particles (up to 9 nm) can passively diffuse through the nuclear pores, and larger particles up to ~30 - 40 nm can only be transported through the pores if they contain a small peptide known as the nuclear localization signal [42, 195, 200, 316, 355, 357, 484], even in cells which do not undergo mitosis [200]. Some other studies have shown that even 50 - 90 nm nanoparticles containing a nuclear localization signal can also enter the nucleus, but it is not clear whether these nanoparticles may have entered during mitosis [485-487]. Further complicating this picture are studies which show that in some cases larger nanoparticles can enter the nucleus even if they do not contain a nuclear localization signal [488]. Thus it is clear that in some cases nanoparticles can enter the nucleus, but this is not always true. The entry may depend on the size of the nanoparticle and the presence of nuclear localization signals. In sum, in many cases when nanoparticles are found in the nucleus, it remains unclear how they got there.

In addition to the preceding controversial questions, which have attracted the most attention in the PEI field, there is a relatively understudied area that is also important. This is the question of whether PEI nanoparticles are eventually excreted from the cell. This is critical to know because if the nanoparticles remain in the cell for extended periods their chances of causing adverse effects increase.

To address all of the preceding questions, cryo SXT was used to examine the distribution of 50 nm PEI coated gold nanoparticles at a concentration of 0.13 nM in A549 cells at 2 h, 3 h and 6 h. Additionally, at 6 h, nanoparticle incubation was stopped, and cryo SXT was used to observe the cells at 48 h in order to understand nanoparticle behavior at later time points. At each time point, 8 - 19 cells were examined.

7.2 PEI nanoparticle internalization in A549 cells appears to occur via two different routes

As done for dPGS in Chapter 6, cryo SXT was used to investigate the endocytosis pathways of the PEI nanoparticles. The PEI nanoparticles were consistently found within membrane pits (Fig. 7.1a,b), suggesting that the PEI nanoparticles were internalized via endocytosis like the dPGS nanoparticles, and also consistent with the model that nanoparticles enter cells mostly via endocytosis [255, 258, 259].

Then, as done for dPGS nanoparticles, the morphology of these membrane pits containing nanoparticles was analyzed, and similar structures were found. One of the invagination types appeared to be membrane ruffles (Fig. 7.1a). The other type invagination type was omega-shaped with a coat along the invagination (Fig. 7.1b). As with dPGS, these data suggested that these invaginations may again lead to formation of two different types of endocytic vesicles. PEI nanoparticles were observed in uncoated vesicles with a size ≥200 nm and an interior that was a mixture of X-ray dense and X-ray lucent material (Fig. 7.1c,e). These uncoated vesicles may have arisen from the uncoated membrane ruffles. Second, nanoparticles were also observed in coated vesicles with clear interiors and sizes around 100 - 150 nm (Fig. 7.1d,f). These coated vesicles could have arisen from the coated omega-shaped invaginations. Thus the two internalization pathways of the PEI nanoparticles appeared to be identical to the two internalization pathways of the dPGS nanoparticles.

As described in Chapter 4 and Chapter 6, membrane ruffles and uncoated vesicles are characteristics of macropinocytosis [259], and the omega-shaped invaginations and endocytic vesicles with a coat are characteristics of a clathrin- or a caveolae- mediated endocytosis [260, 266]. These morphological data do not clearly distinguish between caveolae and clathrin. Some additional findings for dPGS in Chapter 6 suggested that this second pathway was more likely to be caveolae-mediated endocytosis, since the coat of

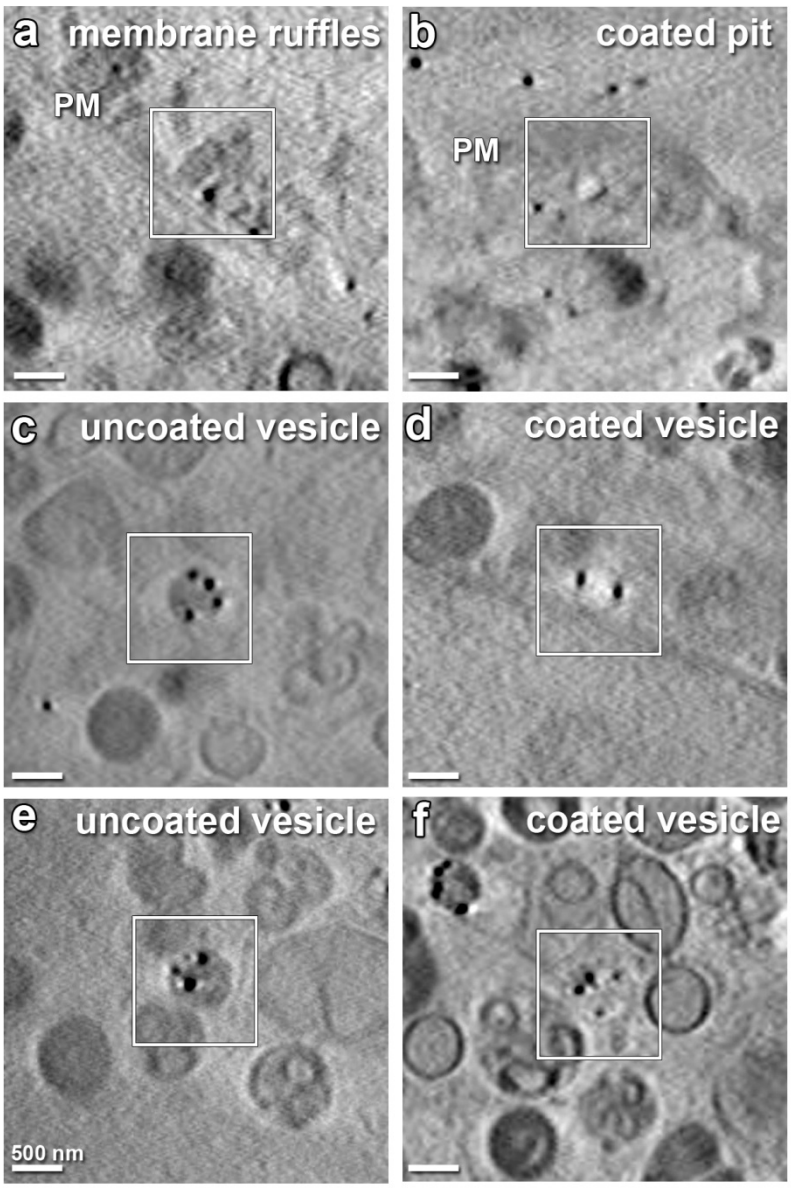

Figure 7.1 Internalization pathway of PEI nanoparticles via cryo-SXT. PEI nanoparticles were found in membrane ruffles (a) on the plasma membrane (PM) and also in uncoated endocytic vesicles within the cell (d,g). These observations suggest that the PEI nanoparticles were internalized via macropinocytosis. PEI nanoparticles were also found in coated pits in the plasma membrane (b), and in coated endocytic vesicles (e,h), which suggests that the PEI nanoparticles were also internalized via a clathrin- or caveolae- mediated endocytosis. Scale bars = 500 nm.

these vesicles did not disappear [260], and the vesicles sometimes appeared to form an accumulation of small vesicles [266]. The same two features were observed with PEI (Fig. 7.1d,f). However, the size of these coated vesicles (100 - 150 nm) was larger than typical caveolin coated vesicles (60 - 80 nm) [266], and more in the range of clathrin-coated vesicles (100 - 150 nm) [261]. Therefore, the morphological data do not

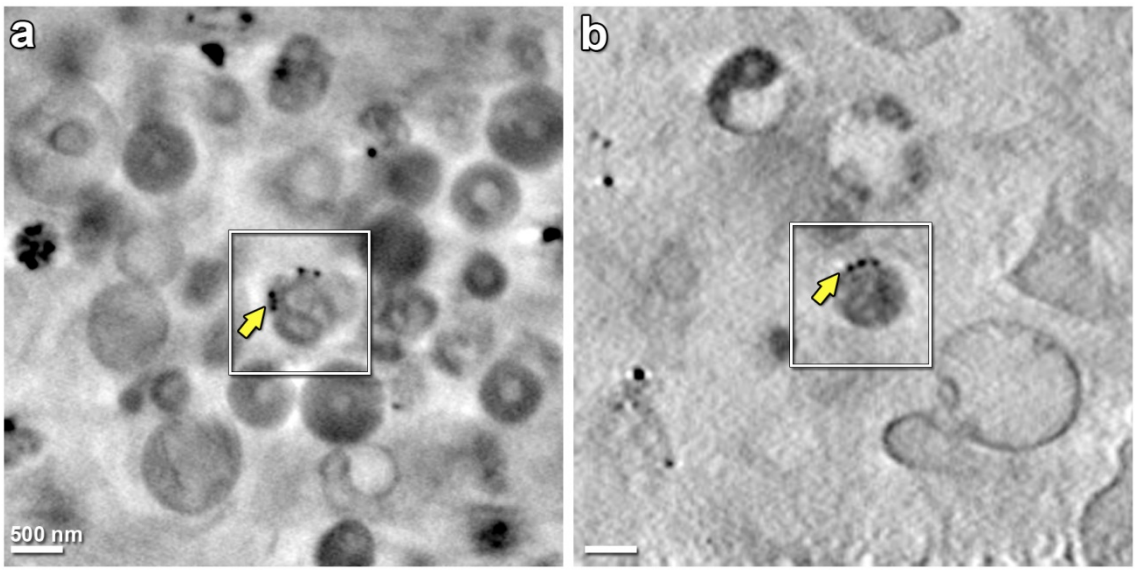

Figure 7.2 Intracellular trafficking of PEI nanoparticles via cryo-SXT. Besides uncoated and coated endocyctic vesiscles, PEI nanoparticles (yellow arrows) were found in multivesicular bodies (a) and lysosomes (b), as marked by the white squares. Scale bars = 500 nm.

definitively distinguish between these two possibilities, and so in this thesis this pathway will be referred to as a clathrin- or a caveolae- mediated endocytosis.

The fraction of PEI nanoparticles in the two types of endocytic vesicles was also quantified as done in Chapter 6 for dPGS nanoparticles according to the counting technique described in Chapter 12 (Fig. 12.2, Fig.12.3). Upon quantification, 77% of nanoparticles were found in the putative macropinosomes and 23% of nanoparticles were in coated vesicles, which could arise from either clathrin- or caveolae- mediated endocytosis. Note that these fractions were quite similar to the fractions measured for the dPGS nanoparticles (85% macropinocytosis and 15% putative clathrin- or caveolae-mediated endocytosis) demonstrating that the two types of nanoparticles were taken up by cells not only with the same two pathways, but also in similar proportions between the two pathways.

7.3 PEI nanoparticles are trafficked via the endo/lysosomal pathway

Next the intracellular trafficking of PEI nanoparticles was investigated to address conflicting views in the literature about lysosomal and nuclear localization of these nanoparticles and to understand whether or not these nanoparticles will be eventually

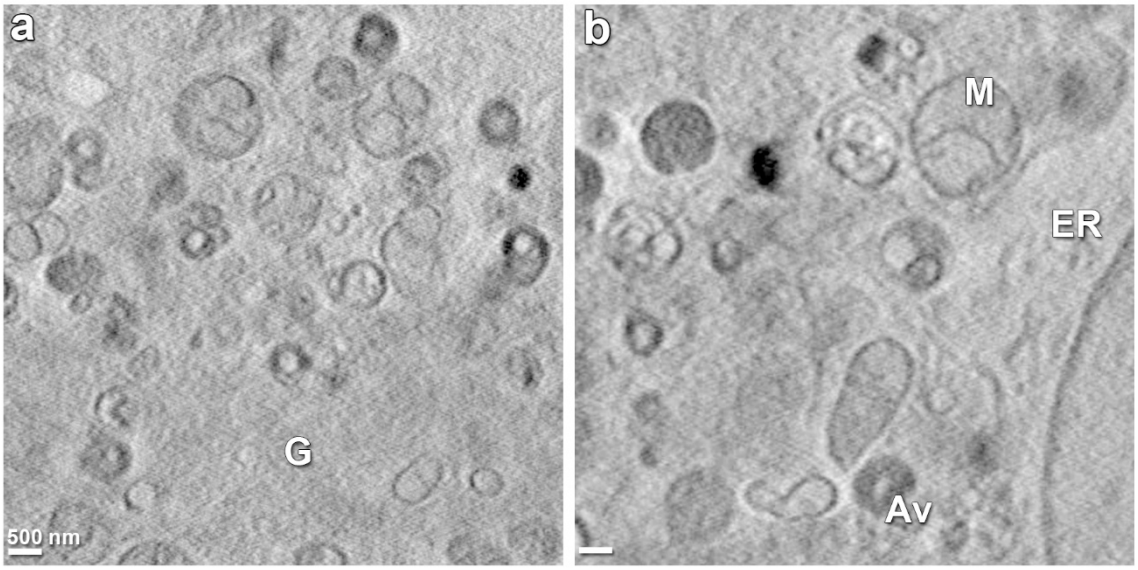

Figure 7.3 Intracellular trafficking of PEI nanoparticles via cryo-SXT. PEI nanoparticles were not detected at any time points in Golgi (G) (a), endoplasmic reticulum (ER), mitochondria (M) or autophagic vacuoles (Av) (b). Scale bars = 500 nm.

excreted from the cells. In addition to the endosome localization described above (Fig. 7.1c-f), PEI nanoparticles were also found within multivesicular bodies (Fig. 7.2a) and lysosomes (Fig. 7.2b). Now each of these localizations will be discussed in more detail.

First, PEI nanoparticles localized to endosomes. As discussed in Chapter 7.2, two different types of endosomes probably arose from two different endocytosis pathways. In each type of endosome, nanoparticles were found in a ring structure in close proximity to the luminal side of the endosomal membrane (Fig. 7.1c-f). Note that such a ring structure was not detected for the anionic dPGS nanoparticles, although the nanoparticle number per endosome is comparable for both nanoparticles, ranging from 1 to 15. This suggests that PEI nanoparticles form a strong interaction with endosomes probably due to their cationic nature. This ring structure, as observed here with PEI, was also reported in the literature for iron nanoparticles [10].

Another location, where PEI nanoparticles were found, was multivesicular bodies (Fig. 7.2a), which are clusters of small vesicles enclosed within a surrounding outer membrane, as discussed in Chapter 4 and Chapter 6. The nanoparticles were either found within the inner vesicles of multivesicular bodies or free within the lumen of the surrounding outer membrane, similar to what was observed for the dPGS nanoparticles. The number of

nanoparticles per multivesicular body was also similar to what was observed for dPGS nanoparticles, ranging from 1 to 14, suggesting that the trafficking of PEI nanoparticles and dPGS nanoparticles to multivesicular bodies follows a similar trend. Multivesicular bodies are known to excrete some of their cargo to the extracellular space. Therefore, the localization of PEI nanoparticles to this organelle suggests that they will be eventually excreted from the cells.

PEI nanoparticles were also detected in lysosomes (Fig. 7.2b), which were identified (Chapter 4, 6) as larger vesicles with a granular interior and membrane whorls. Recall that lysosomes are controversial trafficking sites for PEI nanoparticles. According to the measurements in this thesis, from 1 - 23 PEI nanoparticles enter into lysosomes, consistent with some previous studies which have also localized PEI to lysosomes [45]. It is worth to note here that lysosomes, which contained more than three nanoparticles, exhibited a ruptured morphology (Fig. 8.1a-c, Fig. 8.4b). This finding will be analyzed further in Chapter 8, where the cytoplasmic escape mechanism of PEI nanoparticles is described.

In sum, the presence of PEI nanoparticles in endosomes, MVBs and lysosomes indicates that the endo/lysosomal pathway is involved in trafficking of PEI nanoparticles. This finding is consistent with many other nanoparticles [286, 463], and also with the dPGS nanoparticles that were investigated in Chapter 6.

At all of the incubation time points, PEI nanoparticles could not be found in mitochondria, Golgi, ER, lipid droplets or autophagosomes, although many of these organelles could be imaged in the 3D reconstructions of cells (Fig. 7.3). This demonstrates that at best PEI nanoparticles interact only very rarely with these organelles. The absence of PEI nanoparticles in the Golgi, ER or autophagosomes shows that neither the retrograde pathway nor autophagy was involved in trafficking of PEI nanoparticles. Recall that dPGS nanoparticles were found within lipid droplets at the 6 h time point (Chapter 6), but no such localization was observed for the PEI nanoparticles. This indicates that lipid droplet entry is a nanoparticle dependent event.

In sum, PEI nanoparticles were found in endosomes, multivesicular bodies and lysosomes and excluded from Golgi, ER, autophagosomes and lipid droplets, suggesting

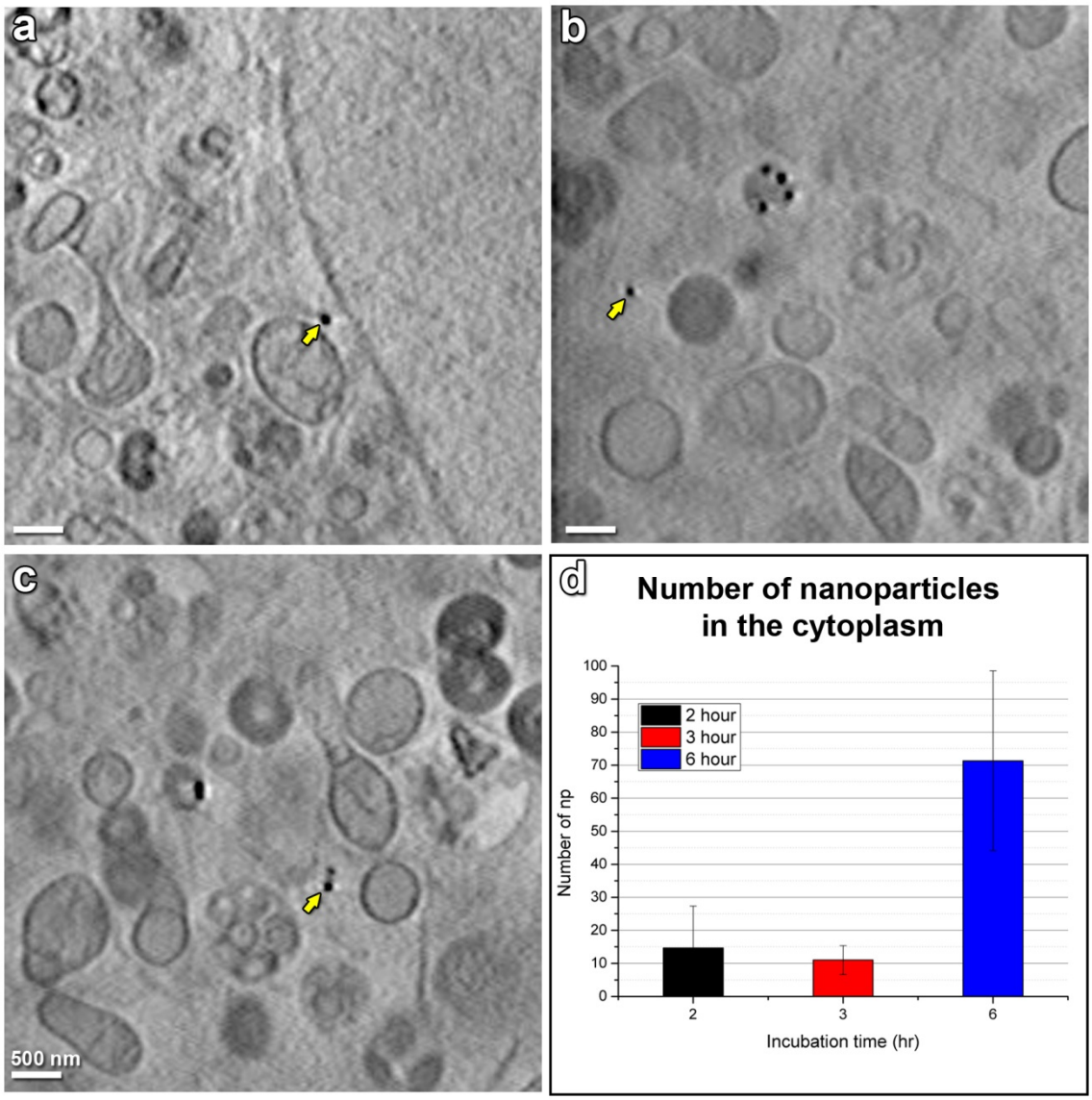

Figure 7.4 Many PEI nanoparticles are found free in the cytoplasm via cryo-SXT. The cells were incubated with PEI nanoparticles for 2 h, 3 h and 6 h. At each time point, PEI nanoparticles (yellow arrows) were detected in the cytoplasm. These nanoparticles did not contain any membranes around them. Nanoparticles in the cytoplasm are indicated with yellow arrows (a-c). The number of free PEI nanoparticle in the cytoplasm was around 15 at early incubation time points. However, at the 6 h time point, the cytoplasmic PEI nanoparticle number increased up to around 100 nanoparticles with an average number of 72 in the area of interest, which corresponds approximately to 1/7 of the total cell volume (d). Scale bars = 500 nm.

that PEI nanoparticles are trafficked only via the endo/lysosomal pathway. Autophagy and the retrograde pathway were not involved in trafficking of PEI nanoparticles. In contrast, autophagy was involved in trafficking of approximately 3% of dPGS nanoparticles.

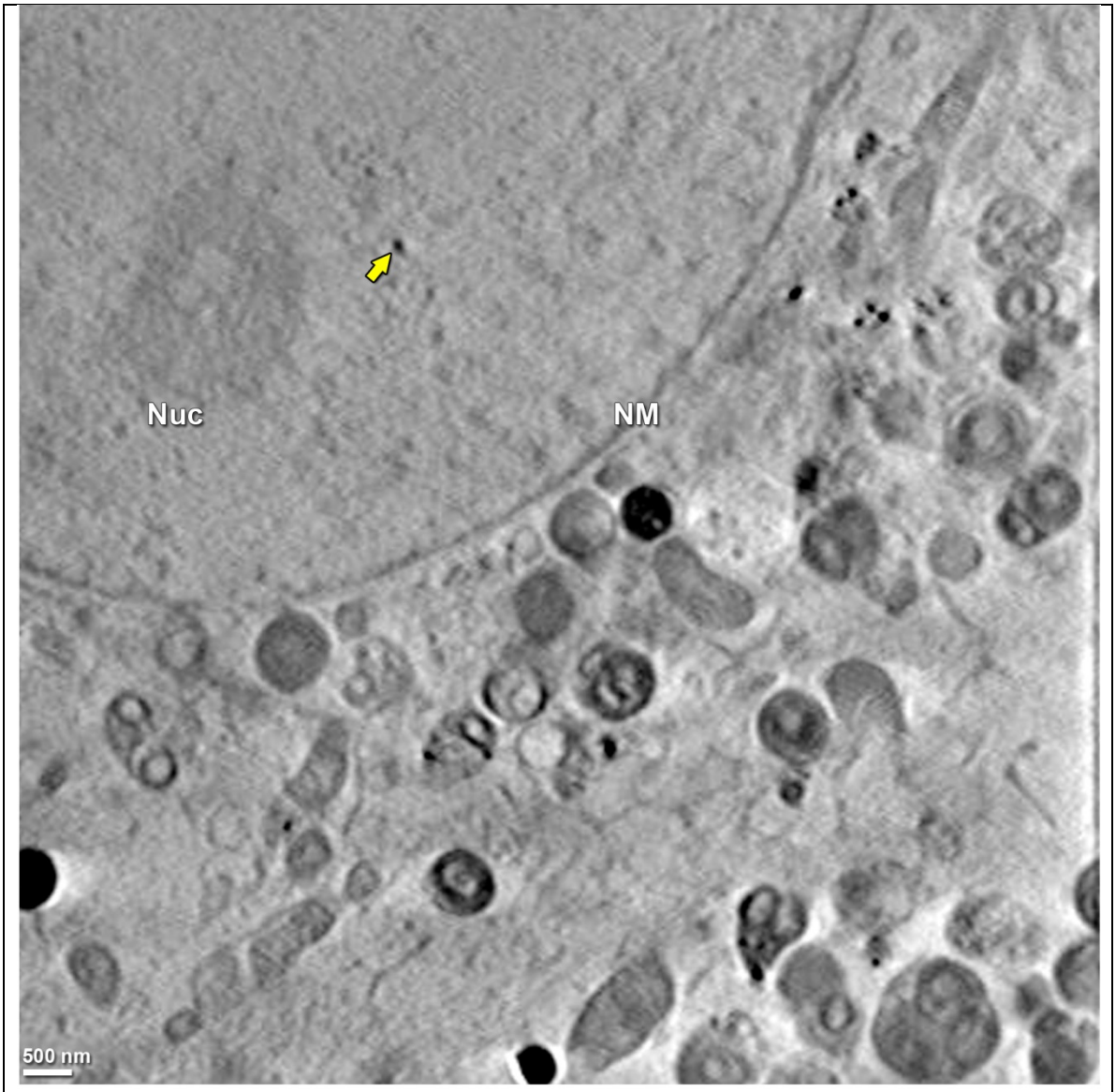

Figure 7.5 At 6 h PEI nanoparticle incubation, a limited amount of nanoparticles (yellow arrows) were found in the nucleus (Nuc) of A549 cells. Scale bar = 500 nm.

7.4 Many PEI nanoparticles were found in the cytoplasm

Organelles of the endo/lysosomal pathway were not the only location where PEI nanoparticles were detected. Many PEI nanoparticles were also found in the cytoplasm (Fig. 7.4a-c). At early time points (e.g. 2 h and 3 h), the number of nanoparticles in the cytoplasm was on average around 15 in the 3D volume of interest (Fig. 7.4d), which approximately corresponds to 1/7 of the whole cell volume as explained in Chapter 12 (Fig. 12.2, Fig. 12.3). At the 6 h time point, the number of nanoparticles in this region

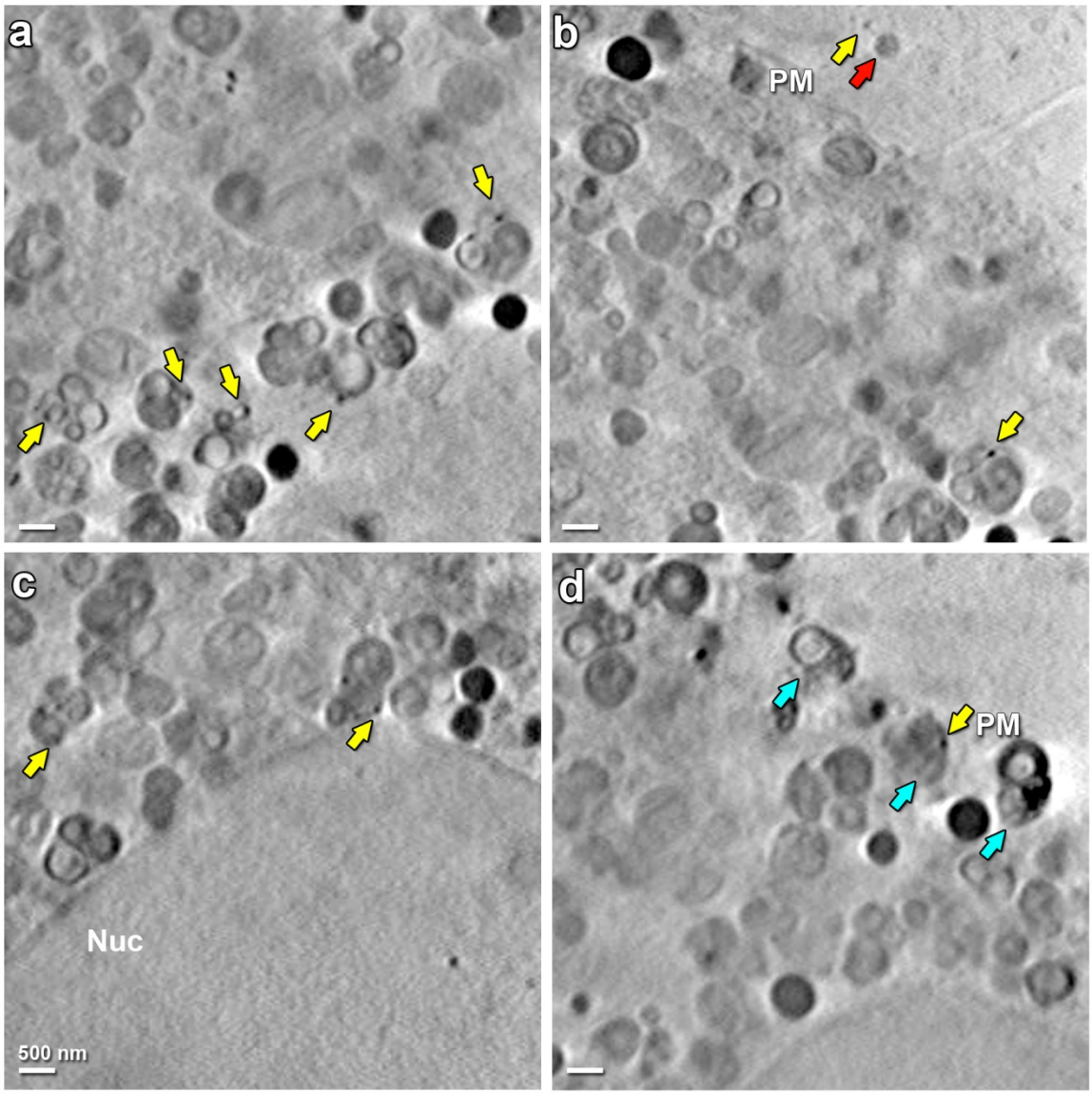

Figure 7.6 The excretion of PEI nanoparticles via multivesicular bodies at 48 h via cryo-SXT. At this late time point, the majority of PEI nanoparticles (yellow arrows) were detected in MVBs rather than other organelles (a-d). Additionally, many MVBs were found in close vicinity to the plasma membrane (blue arrows), suggesting that they will fuse with the plasma membrane to excrete their cargo into the extracellular environment (d). Indeed, nanoparticles (yellow arrow) and one vesicle (red arrow), which may be an exosome, were detected outside of the cell (b). Scale bars = 500 nm.

increased up to an average of 72 (Fig. 7.4d). At this time point, the number of cytoplasmic PEI nanoparticles was estimated to be around 500 per cell. Recall that this estimated number was only 70 for dPGS nanoparticles, indicating that PEI enhances the cytoplasmic escape of nanoparticles by around seven-fold. Note that this finding is

consistent with many PEI studies which suggest an enhanced cytoplasmic escape compared to studies which utilize vectors that do not contain a PEI coat [489].

7.5 A limited amount of PEI nanoparticles were found in the nucleus

For gene therapy, PEI nanoparticles need to carry DNA to the nucleus. However, as discussed in Chapter 3.4.2, Chapter 4.6 and Chapter 7.1, there is no consensus about whether PEI nanoparticles enter into the nucleus. According to the investigation of the 3D volumes of cells, a limited amount of PEI nanoparticles (1 - 5) was found to enter into the nucleus of every cell examined (Fig. 7.5a). This demonstrates that PEI nanoparticles can enter the nucleus even though they did not contain a nuclear localization signal. Entry cannot be due to nuclear envelope breakdown during mitosis, as only a small fraction of the cells would be expected to have gone through mitosis. The current hypothesis in this thesis is that entry occurred through nuclear pores. Consistent with this, the nanoparticles in the nucleus appeared to be smaller than those in the cytoplasm, suggesting that only smaller nanoparticles could pass through the nuclear pores. However, the pixel size in these images was not small enough to permit an accurate measurement of nanoparticle size, so further work will be needed to determine whether there is a size limit for nuclear entry in these cells.

7.6 PEI nanoparticles are excreted by multivesicular bodies

In the nanomedicine field, excretion of nanoparticles after exerting their therapeutic effects is desired to eliminate long term effects of nanoparticles on the patient. Therefore, signs of nanoparticle excretion were sought.

In previous sections, PEI nanoparticles were reported to enter into multivesicular bodies. Since multivesicular bodies are known to excrete some of their cargo to the extracellular environment, this is a good sign that PEI nanoparticles may be excreted at some point. To further investigate the possibility of excretion, the cells were imaged at 48 h after the nanoparticle incubation was stopped at 6 h. By washing away the nanoparticles at 6 h, nanoparticles present outside of the cells at 48 h could be safely assumed to reflect excretion.

At 48 h, the nanoparticle number within cells was reduced, and about 90% of the nanoparticles remaining were in multivesicular bodies. The remaining 10% of the

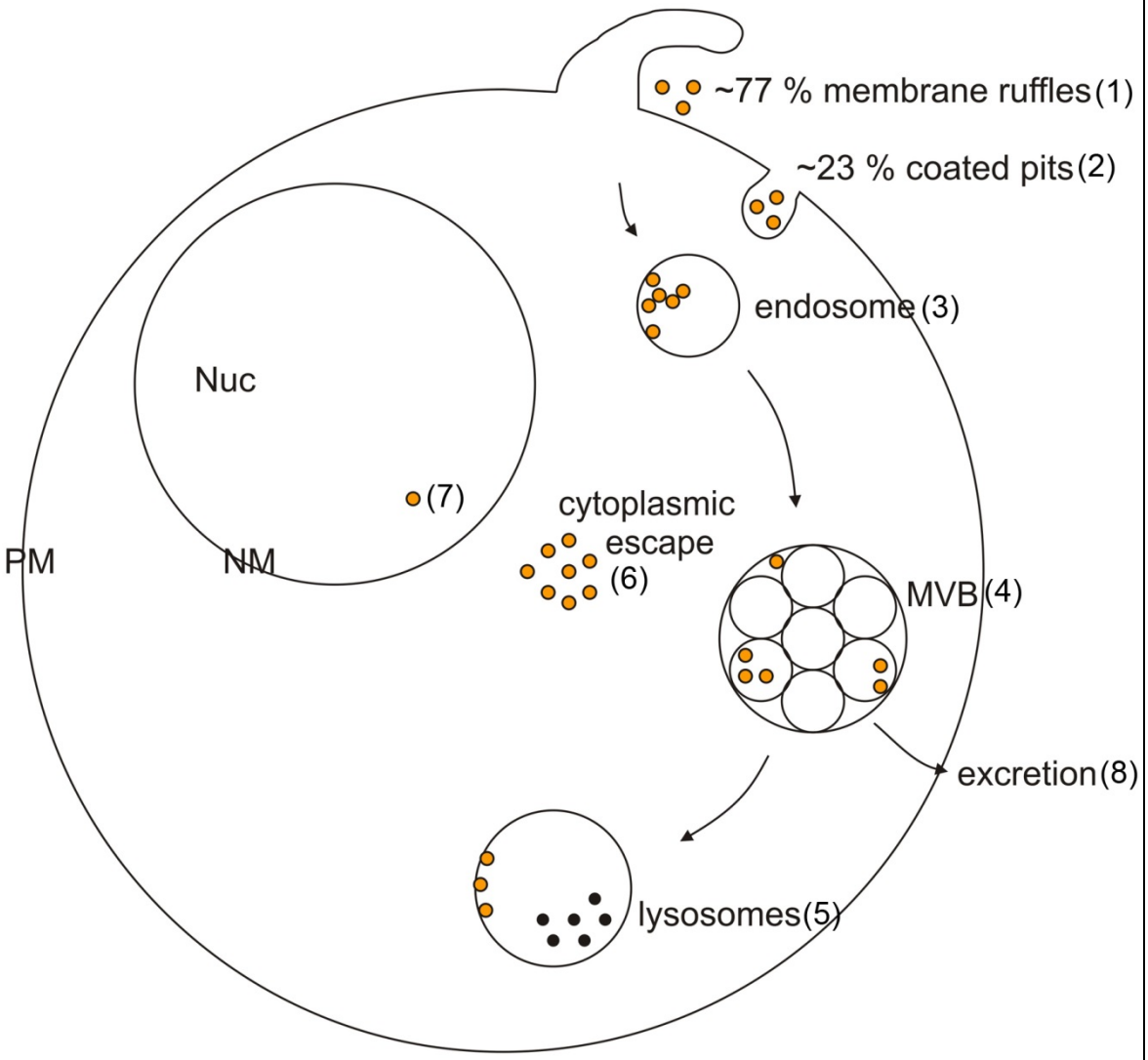

Figure 7.7 Model summarizing the observations about the endocytosis and intracellular trafficking pathway of PEI nanoparticles. PEI nanoparticles were endocytosed via at least two endocytosis pathways, which may be macropinocytosis (1) and a caveolae- or clathrin-mediated endocytosis (2). The predominant endocytosis pathway was macropinocytosis (1). The nanoparticles were first sorted to early endosomes (3). Later, PEI nanoparticles were trafficked from endosomes to multivesicular bodies (4) and lysosomes (5), demonstrating that the endo/lysosomal pathway is involved in trafficking of PEI nanoparticles at this concentration. Additionally, many free PEI nanoparticles were found in the cytoplasm (6), and a small number of PEI nanoparticles were found in the nucleus (7). The morphological findings also suggested that some PEI nanoparticles were excreted to the extracellular environment via MVBs (8).

nanoparticles were in endosomes. The nanoparticles were not found in ER, Golgi, autophagosomes and lipid droplets consistent with the early time points, suggesting that these organelles were not involved in trafficking of PEI nanoparticles at any incubation

time. Surprisingly, no nanoparticles could be detected in the cytoplasm and nucleus (Fig. 7.6a-d), although some were present at earlier time points.

Many multivesicular bodies were found to be in close proximity to the plasma membrane (Fig. 7.6d). Additionally, some excreted nanoparticles and one excreted vesicle (exosome) could be detected outside of the cell (Fig. 7.6b). Note that such an event is expected to be detected rarely since these objects quickly diffuse in the incubation medium following excretion. These findings are in agreement with the fact that multivesicular bodies fuse with the plasma membrane to excrete their inner vesicles into the extracellular environment [330, 332, 461]. Thus these morphological data suggest that many nanoparticles are likely to be excreted from the cells via multivesicular bodies.

7.7 Summary

In this chapter, a morphological investigation of the endocytosis pathway and the intracellular trafficking pathway of PEI nanoparticles was performed (Fig. 7.8). This investigation provides answers to debated questions about whether PEI nanoparticles ever localize into lysosomes, whether PEI nanoparticles enter the nucleus, and if and how PEI nanoparticles will eventually be excreted from the cells. By using cryo soft X-ray tomography, PEI nanoparticles were found to be internalized predominantly via macropinocytosis with a lesser contribution from a putative clathrin- or caveolae-mediated endocytosis. Moreover, PEI nanoparticles were found to be trafficked to endosomes, multivesicular bodies and eventually lysosomes, consistent with some previous studies indicating that PEI nanoparticles could enter into lysosomes. Many PEI nanoparticles were found to escape to the cytoplasm. Only a limited number (1-5 PEI nanoparticles per cell) could enter into the nucleus. Moreover, PEI nanoparticles were also found to be excreted from the cells via multivesicular bodies.

8. CYTOPLASMIC ESCAPE MECHANISM OF PEI NANOPARTICLES

8.1 Motivation for studying cytoplasmic escape mechanism of PEI nanoparticles

As demonstrated in Chapter 7, PEI nanoparticles are internalized via endocytosis which would enclose these nanoparticles within vesicles. To be able to exert their effects like many other nanoparticles, endocytosed nanoparticles need to escape from these vesicles. PEI is known to enhance this cytoplasmic escape of nanoparticles by destabilizing the membrane of vesicles. However, the mechanism by which PEI nanoparticles escape to the cytoplasm is still elusive as briefly discussed in Chapter 3.4.1 and Chapter 7.1. In the literature, there are diverse ideas about how PEI may escape from vesicles into the cytoplasm. Some studies argue that PEI is trafficked to lysosomes and escapes to the cytoplasm from these organelles [42, 44-46]. However, lysosomes are degradative organelles of the cell. Therefore, localization of PEI into lysosomes is not desired. However, other studies argue that PEI does not localize to lysosomes [49, 50]. Rather, PEI may instead escape quickly from endosomes by membrane destabilization before they are trafficked to lysosomes [49]. Moreover, the extent of this membrane destabilization is not clear. According to current views, cytoplasmic escape occurs either by pore formation [43, 45] or vesicle rupture [35]. The pore formation mechanism is explained as a temporary destabilization of the vesicle membrane due to the cationic nature of PEI resulting in leakage of molecules from the vesicle to the cytoplasm. Vesicle rupture refers to the complete bursting of a vesicle releasing its contents [347]. The most commonly accepted explanation for vesicle rupture is the ‘’proton sponge’’ hypothesis, although it is not yet proven [44]. According to this hypothesis, PEI exhibits a buffering capability in vesicles at low pH values. The unprotonated amine groups of PEI start to be protonated at this low pH and they act as a proton pump creating an increased flux of protons into vesicles. Cl^- ions and water molecules also enter into the vesicles alongside with protons, resulting in an increased osmotic swelling and eventual rupture of these vesicles [35].

To address these clashing ideas in the literature, cells were incubated with 0.13 nM PEI-coated gold nanoparticles for different incubation time points (2 h, 3 h and 6 h) and 6 - 19 cells were observed via cryo-SXT. Since cryo-SXT is a high resolution 3D technique,

relatively rare events can be detected in a cell and the clashing ideas can potentially be resolved.

8.2 Cryo soft X-ray tomography can help address the conflicting views about the cytoplasmic escape mechanism of PEI nanoparticles

Ideally, to address these clashing points in the literature, one would like to be able to detect both pore formation and vesicle rupture events within cells, and this might require observation of many cells if either of these events is relatively rare. Since cryo soft X-ray tomography is a 3D technique enabling the imaging of hundreds of slices from multiple cells, in principle relatively rare events should be detected in a cell. Additionally, cryo soft X-ray tomography provides a 40 nm spatial resolution which is sufficient to detect endosomes and lysosomes. In control cells, the endosome size is around 100 nm and the lysosome size is around 500 nm. If these vesicles rupture and have a distorted morphology due to this rupture, these events should be observed by comparing these organelles to control cells. However, pores that allow nanoparticles to penetrate the membrane should be around the size of the nanoparticle, and are likely to close after nanoparticle passage. Thus one might hope to see a nanoparticle caught in the act of passing through the membrane, but such events would be very difficult to distinguish from nanoparticles simply bound to the inner or outer membrane of a vesicle, since these are all at the resolution limit of the X-ray microscope. In sum, cryo soft X-ray tomography should be able to detect ruptured endosomes or lysosomes, but not the passage of nanoparticles through membrane pores.

8.3 PEI nanoparticles escape to the cytoplasm via lysosomal rupture

According to the cryo-SXT analysis performed for this chapter, many ruptured lysosomes could be detected upon PEI nanoparticle incubation. In this thesis, ruptured lysosomes are identified as lysosomes which lost their circular appearance and became enlarged and distorted (a burst morphology) or in some cases looked like they were divided into two (Fig. 8.1a-c). However, the distinct morphology of lysosomes was still present in these ruptured organelles such as small black dots and membrane whorls.

These observations are in striking contrast to what was observed with dPGS (as described in Chapter 6), where lysosomal rupture was not detected. In contrast, PEI

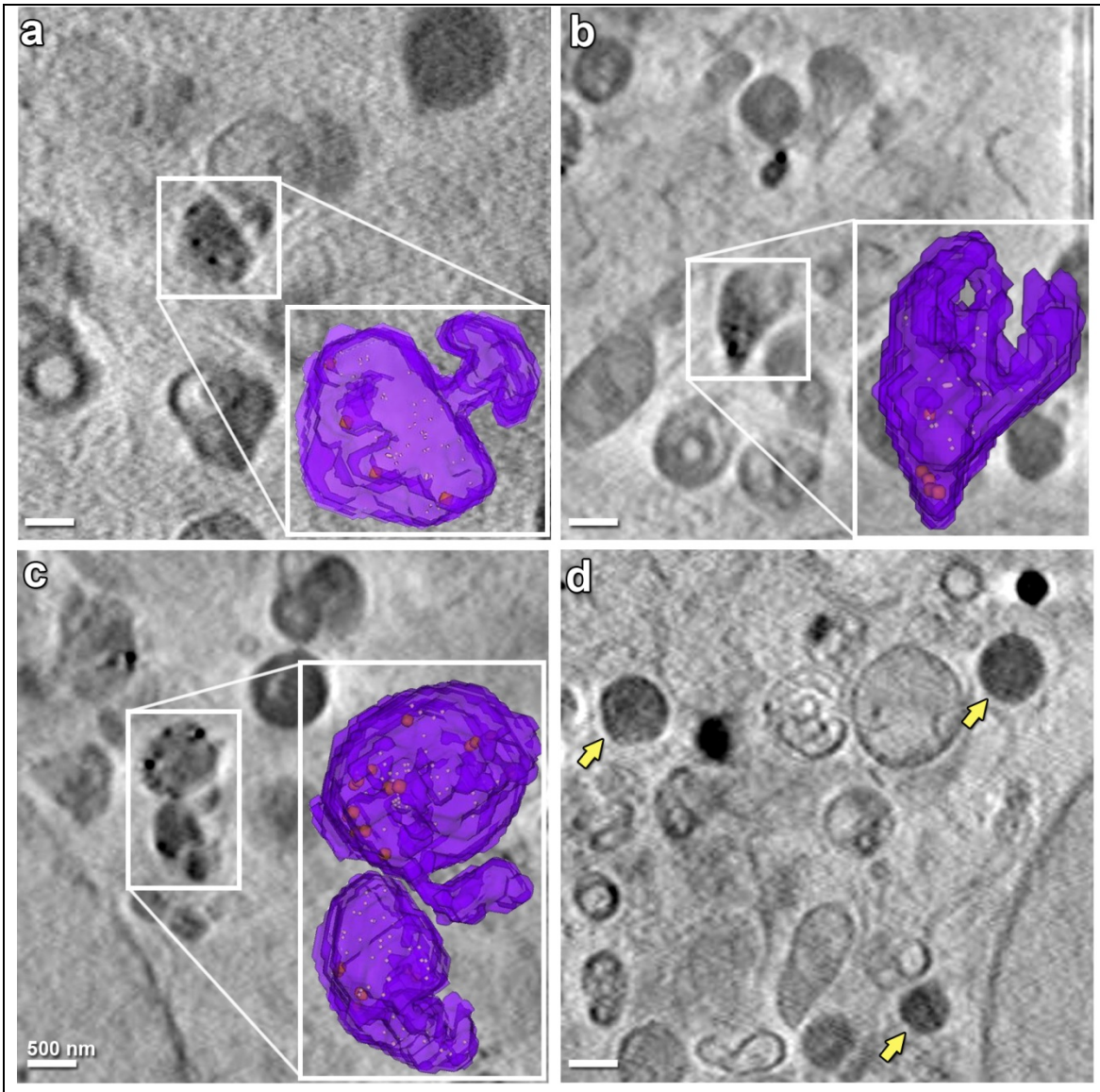

Figure 8.1 PEI nanoparticles rupture lysosomes to escape to the cytoplasm. PEI nanoparticles are incubated at 2 h, 3 h and 6 h with A549 cells. At early time points, lysosomal rupture was mild. However, at 6 h, approximately 60% of the lysosomes lost their circular appearance and presented a burst morphology (a-c). The rupture of lysosomes (purple) upon nanoparticle (orange) incubation can be seen in 3D in the rendered images taken from the regions within white squares (a-c). In lysosomes lacking nanoparticles (yellow arrows), no evidence for bursting was found and instead the lysosomes retained their circular appearance (d). Scale bars = 500 nm.

nanoparticles caused lysosomes to rupture at each incubation time point (e.g 2 h, 3 h and 6 h). Rupture was highest at 6 h where ~60% of the lysosomes appeared to be ruptured. Note that many nanoparticles were also found to remain attached to the membranes of the ruptured lysosomes, which may limit their access to cellular target sites.

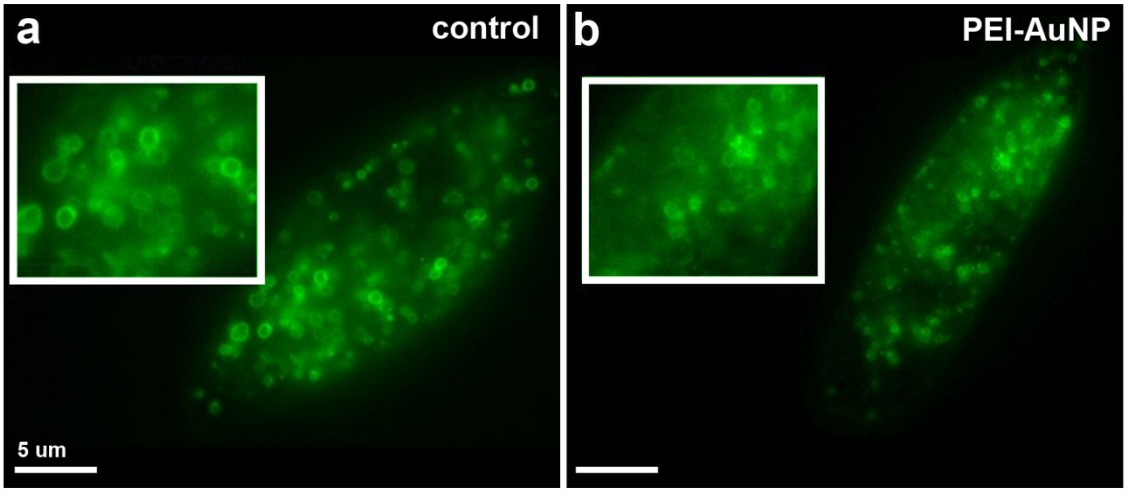

Figure 8.2 Live-cell fluorescence imaging showed that lysosomes lost their circular appearance upon PEI nanoparticle incubation. When the lysosomes of A549 cells were labeled with CellLight® Lysosomes-GFP, lysosomes presented a circular appearance in control cells (zoomed-in views (a)). Upon PEI- nanoparticle incubation for 6 h, the circular appearance of lysosomes was lost and the background fluorescence increased suggesting that lysosomes may be ruptured (zoomed-in views (b)). Scale bars = 5 μm.

Additionally, the lysosomal rupture morphology was only associated with the presence of PEI nanoparticles within these organelles. Lysosomes which did not contain any nanoparticles maintained their circular appearance (Fig. 8.1d).

Moreover, two fluorescence microscopy experiments were performed to confirm this lysosomal rupture in living cells. In the first experiment, lysosomes of control cells and cells treated with PEI nanoparticles for 6 h were labeled with green fluorescence protein (GFP) using CellLight® Lysosomes-GFP. In the labeled control cells, lysosomes looked round and intact (Fig. 8.2a). In the cells treated with PEI nanoparticles for 6 h, lysosomes lost their circular appearance and the background fluorescence increased (Fig. 8.2b). This finding confirms that PEI nanoparticles distort the lysosomal morphology.

In the second fluorescence microscopy experiment, a caspase test was performed to confirm lysosomal rupture, similar to what has been done before for prickly gold nanoparticles to explore whether they rupture vesicles or not [183]. For this assay, control cells and cells treated with PEI nanoparticles for 6 h were incubated with a caspase staining kit. Caspase is an enzyme, which resides in lysosomes in its inactive form. In

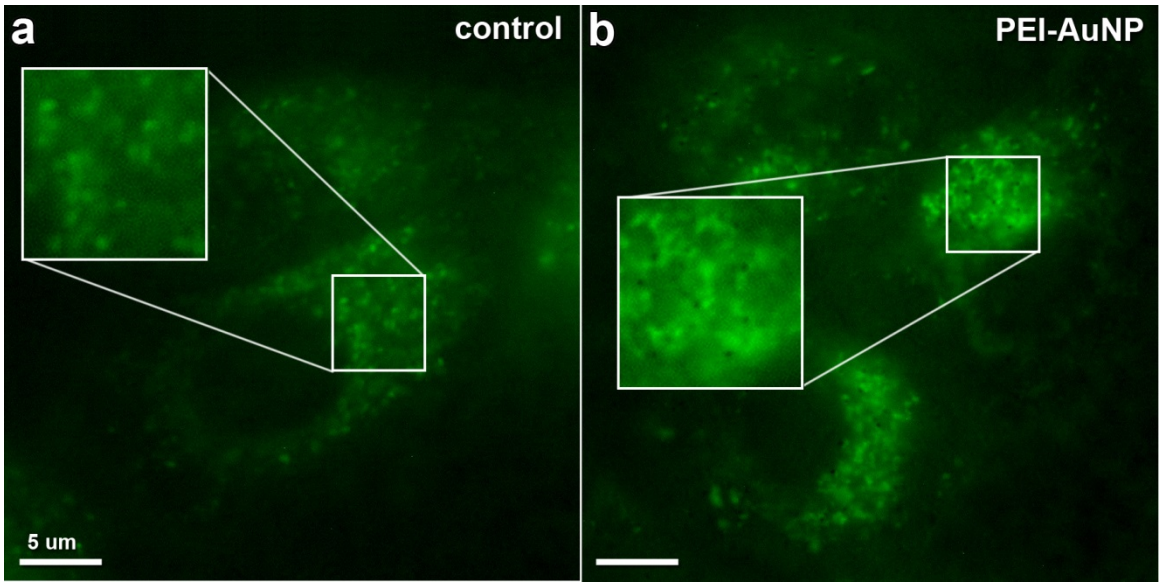

Figure 8.3 Live-cell fluorescence imaging showed that lysosomal content diffused throughout the cytoplasm upon PEI nanoparticle incubation. Cells were stained with a caspase kit. In control cells, the caspase stain presented a punctated appearance (a). Upon PEI nanoparticle incubation for 6 h, this punctated appearance of caspase staining was lost and background fluorescence increased, suggesting that the contents of lysosomes had diffused throughout the cytoplasm upon PEI nanoparticle incubation (b). Scale bars = 5 μm.

the control cells, caspase was found within lysosomes yielding a punctated appearance in the cytoplasm (Fig. 8.3a). However, when the cells were incubated with PEI nanoparticles for 6 h, caspase staining lost its punctated appearance and was instead spread throughout the cytoplasm (Fig. 8.3b), suggesting that lysosomes ruptured and their content diffused throughout the cytoplasm. In sum, cryo soft X-ray microscopy and two fluorescence microscopy experiments show that PEI nanoparticles escape to the cytoplasm by rupturing lysosomes. This result is supported by a TEM study which also provided evidence that PEI ruptures lysosomes [45].

8.4 At least four PEI nanoparticles are required to enter into lysosomes to rupture them

How lysosomal rupture might occur was also investigated. Lysosomes were found to be ruptured only if the number of nanoparticles internalized by the lysosomes exceeded three ($n>3$). Whenever the nanoparticle number was three or lower, lysosomes were found to be intact (Fig. 8.4a). Whenever this nanoparticle number exceeded three, the lysosomes

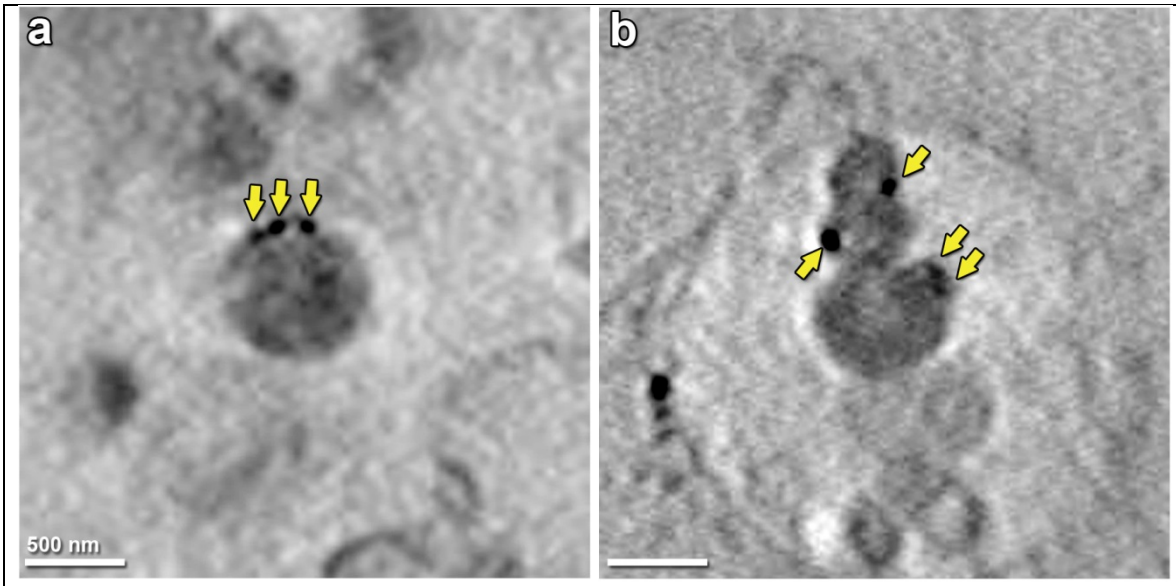

Figure 8.4 Three PEI nanoparticles is the critical limit to surpass for lysosomal rupture. Specifically, lysosomes were found to maintain their circular appearance if they contained three or less nanoparticles (a). Whenever the nanoparticle number increased above three nanoparticles, the circular appearance of the lysosomes was lost (b). Scale bars = 500 nm.

were found to be ruptured (Fig. 8.4b). This finding indicates that three nanoparticles is a critical limit to surpass for lysosomal rupture.

Additionally, internalized PEI nanoparticles did not alter the size of lysosomes significantly. This is in agreement with the hypothesis which suggests that for vesicles to lose their membrane integrity, only a 2 - 4% area expansion would be sufficient [33]. Such a size increase is very small and cannot be detected by cryo-SXT.

8.5 PEI nanoparticle incubation did not cause endosomal rupture

Although lysosomal rupture was easily detected, no evidence for fragmented endosomes could be found. Conceivably, detection of fragmented endosomes could be more difficult than detection of lysosomal rupture because endosomes are smaller and do not contain membrane whorls. Still, one might have expected to detect at least some membrane fractions around a nanoparticle cluster in the cytoplasm if the nanoparticles had escaped from an endosome. However, such events were never observed. Instead, many intact endosomes were found containing 1 - 10 PEI nanoparticles (Fig. 8.5). Overall these data are consistent with the hypothesis that PEI nanoparticles do not cause endosomes to rupture, or if they do, then this event is quite rare.

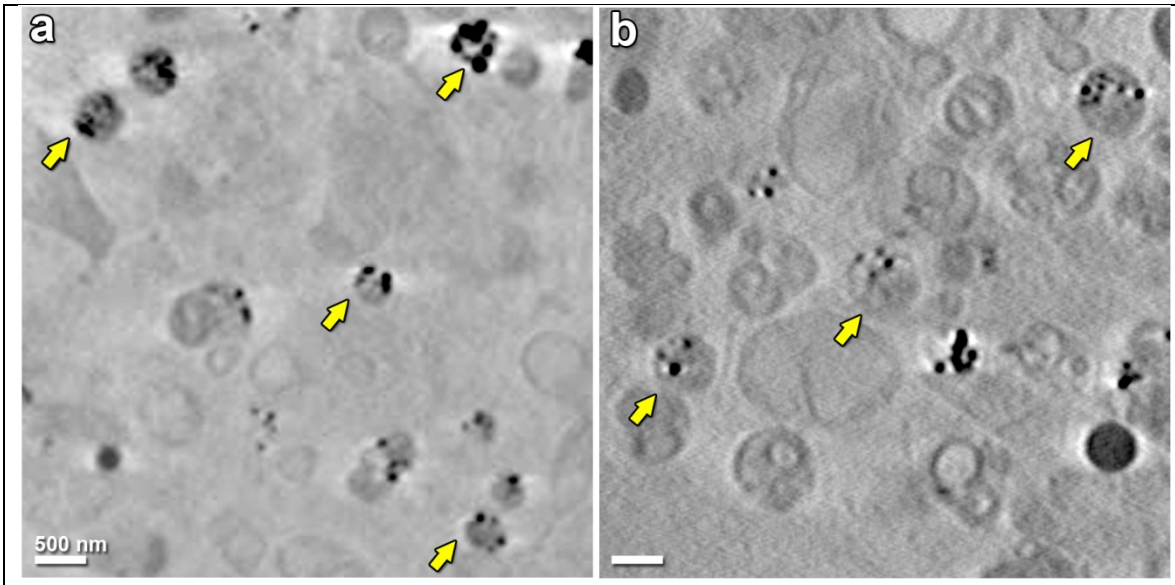

Figure 8.5 PEI nanoparticles do not cause endosomal rupture or this is a very rare event. Fragmented endosomes were not detected. Instead, many PEI nanoparticles (1-10) were found trapped in a large number of endosomes (arrows) which showed no signs of rupture (a,b). Scale bars = 500 nm.

Interestingly, it was found that the volume of endosomes increased in proportion to the number of nanoparticles within the endosomes. It was observed that endosomal size increased significantly, up to 350 nm, upon PEI nanoparticle incubation (Fig. 8.6a). On the surface at least, this finding is in agreement with the protein sponge hypothesis which predicts that each nanoparticle would be responsible for a certain amount of water influx to neutralize its presence [35]. However, a similar increase in the volume of endosomes was detected upon dPGS nanoparticle incubation even through dPGS does not have any buffering abilities (Fig. 8.6b). Therefore, these findings suggest that the increasing volume of endosomes in proportion to the number of nanoparticles within endosomes is more likely to occur due to nanoparticle-mediated fusion events between endosomes rather than osmotic swelling.

In sum, these findings suggest that PEI nanoparticles do not rupture endosomes to escape to the cytoplasm, or if endosomes are ruptured, this event is quite rare. These findings also suggest that the increase in the size of endosomes does not directly reflect osmotic swelling and is not correlated with the rupture of endosomes.

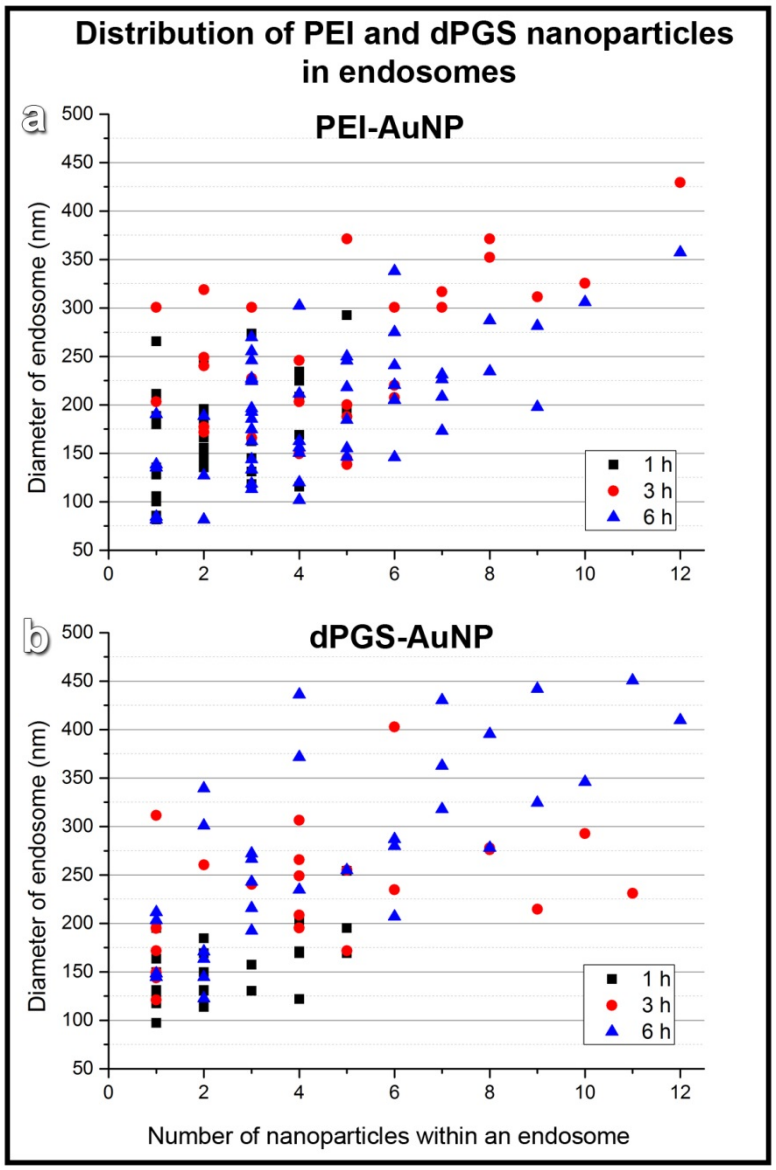

Figure 8.6 The diameter of endosomes increased proportionally with the number of nanoparticles within the endosomes. This proportional increase was similar both for PEI nanoparticles (a) and dPGS nanoparticles (b).

8.6 The amount of cytoplasmic escape observed can be reasonably accounted for by lysosomal rupture

As noted in Chapter 8.1 and Chapter 8.2, cytoplasmic escape could occur by vesicle rupture or by membrane pore formation, with the latter event being very difficult to detect by cryo soft X-ray tomography. To see if the escape that was detected in this thesis could

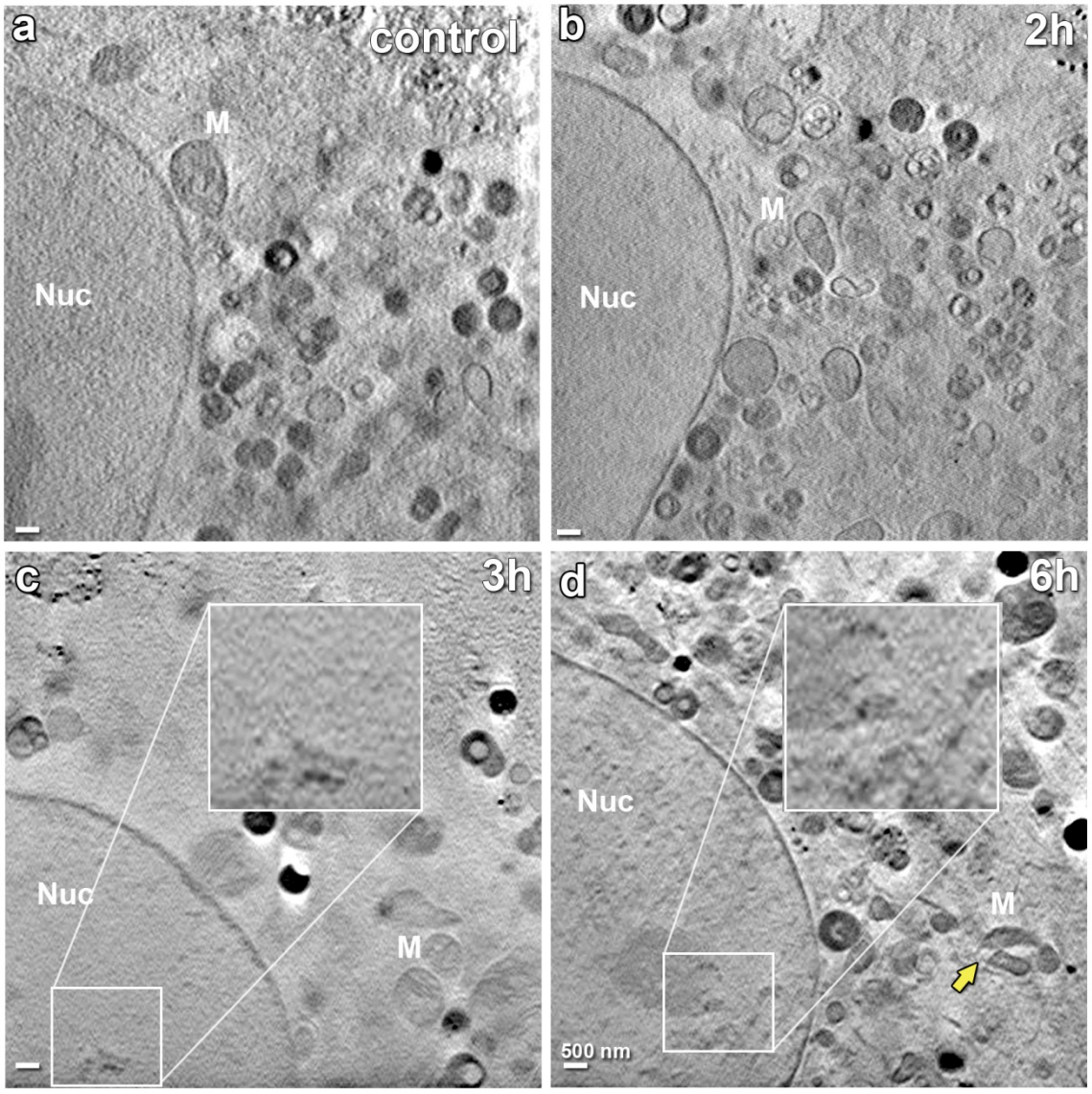

Figure 8.7 PEI nanoparticles yielded adverse effects on the cells probably due to lysosomal rupture. Specifically, chromatin condensation gradually increased at 2 h (b), 3 h (c) and 6 h (d) incubation time points compared to control cells (a). Also elongated mitochondria began to be observed at 6 h (yellow arrows) (d). Scale bars = 500 nm.

be explained solely by the lysosomal rupture that was observed, an estimate was made for the amount of escape to be expected based on the number of burst lysosomes in the measured volume (~12) and the average number of nanoparticles in a lysosome (~10). This predicted that ~120 nanoparticles should have escaped within this volume, compared to the actual number of escaped nanoparticles of 72 $\pm$ 21.4 that was measured in this volume. Thus, the data suggest that the cytoplasmic escape of the PEI nanoparticles can be adequately explained by the rupture of lysosomes.

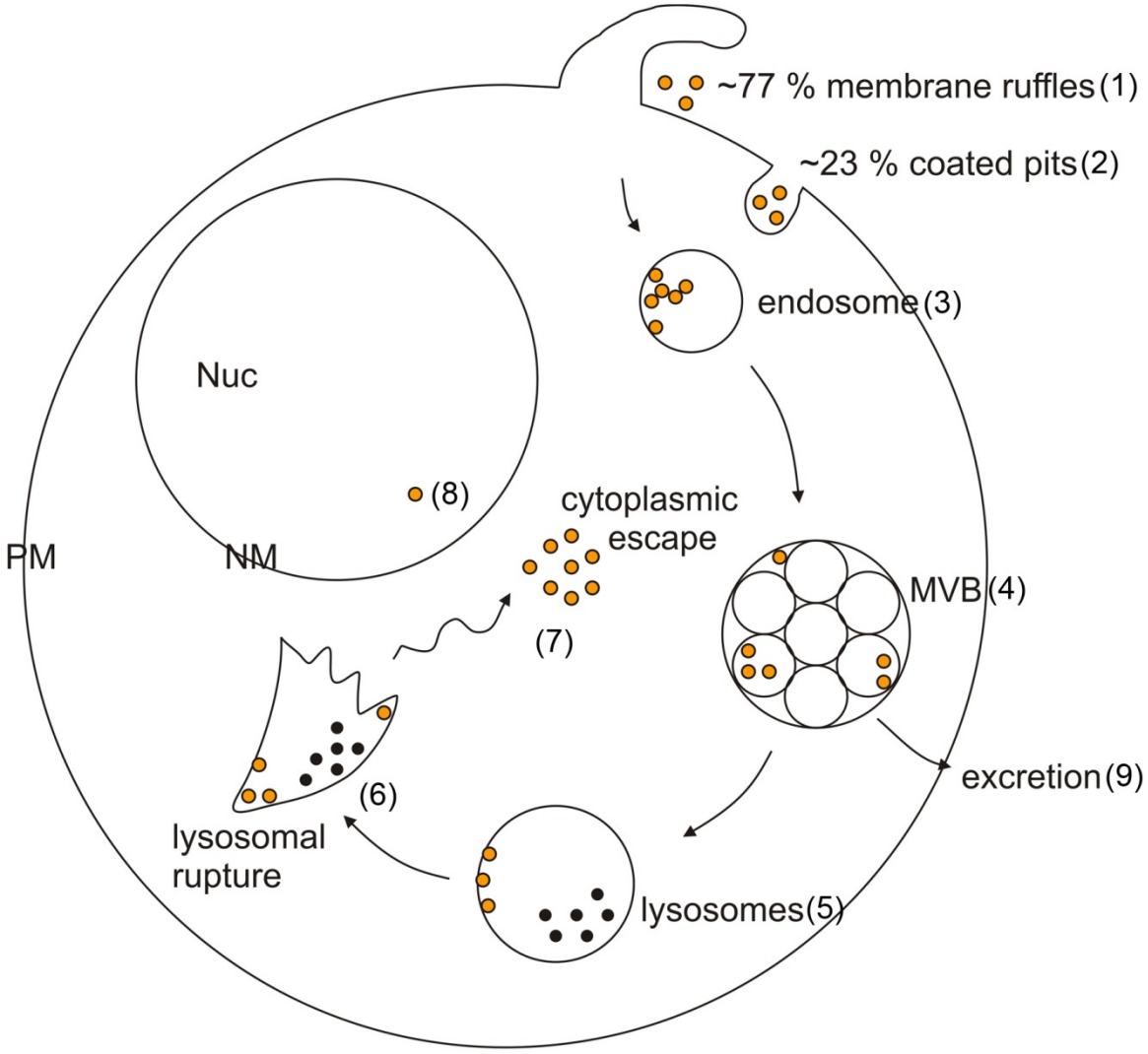

Figure 8.8 Model summarizes the observations about the endocytosis and intracellular trafficking pathway of PEI nanoparticles. PEI nanoparticles were endocytosed via at least two endocytosis pathways which may be macropinocytosis (1) and a caveolae- or clathrin-mediated endocytosis (2). The predominant endocytosis pathway was macropinocytosis (1). The nanoparticles were first sorted to early endosomes (3). Later, dPGS nanoparticles were trafficked from endosomes to multivesicular bodies (4) and lysosomes (5) demonstrating that the endo/lysosomal pathway is involved in trafficking of PEI nanoparticles at this concentration. Additionally, PEI nanoparticles were found to rupture lysosomes (6) to escape into the cytoplasm (7). Moreover, a small portion of PEI nanoparticles were found in the nucleus (8). Morphological findings also indicated that some of the PEI nanoparticles are excreted to the extracellular environment via MVBs (9).

8.7 PEI nanoparticles induce signs of cell stress probably due to lysosomal rupture

Lysosomes are highly acidic and contain many proteolytic enzymes [194], so their rupture can cause adverse effects on cells [304]. Consistent with this, various morphological signs of cell stress were observed. Some chromatin condensation in the cell nucleus, which increased with PEI incubation time, was observed (Fig. 8.7b-d). An increased number of autophagic vacuoles and some elongated mitochondria were also observed (Fig.8.7d). All of these features are indicative of some cell stress [490]. However, by 48 h, all of these alterations had disappeared (Fig. 7.6 in Chapter 7), suggesting that the cells had largely recovered from the effects of the PEI-nanoparticles following their removal from the incubation medium at the 6 h time point.

8.8 Summary

A trafficking pathway for PEI nanoparticles was defined in A549 cells. The nanoparticles when applied at a concentration of 0.13 nM were demonstrated to escape to the cytoplasm via rupture of lysosomes (Fig. 8.8). This rupture was observed to create adverse effects in the cells that included mild chromatin condensation, increase in autophagic vacuole numbers and mitochondrial elongation, although these effects disappeared at 48 h following removal of the nanoparticles from the incubation medium at 6 h. Additionally, after lysosome rupture, many nanoparticles were found to stay attached to lysosomal membranes, which is likely to prevent nanoparticles from reaching their target in the cytoplasm and certainly would prohibit nuclear entry. Therefore, these findings demonstrate that lysosomal rupture is not an optimal pathway for delivery of PEI nanoparticles, and consequently other trafficking pathways that bypass lysosomes should be sought for PEI nanoparticles.

9. dPGS AND PEI NANOPARTICLES INDUCE SIMILAR GLOBAL CYTOPLASMIC REORGANIZATIONS

In the previous chapter, the endocytosis and intracellular trafficking pathways of both dPGS and PEI nanoparticles were identified. Both were shown to be internalized via a combination of macropinocytosis and a putative clathrin- and caveolae-mediated endocytosis. These nanoparticles differed in their cytoplasmic escape tendency. Only a limited amount of dPGS nanoparticles were found in the cytoplasm while many PEI nanoparticles could escape to the cytoplasm by rupturing lysosomes.

9.1 Motivation for investigation of morphological changes exerted by dPGS and PEI nanoparticles

A cell's subcellular morphology includes its size, shape, and the quantity and location of its organelles. Subcellular morphology is cell type specific and changes drastically upon cell differentiation, mitosis, mechanical stimulation, starvation and viral infections [439, 491-493]. Morphology is also a sensitive indicator for the initiation of cell death [494]. All of these conditions have distinct morphological hallmarks. For instance, Hepatitis C virus (HCV) infection is known to stress cells causing ER cisternae alterations, aberrant mitochondria and multiple membrane vesicles, as observed by TEM studies and X-ray tomography [439]. Alternatively, during nutrient starvation, cells adapt by shifting their metabolism from glucose-dependent to mitochondrial fatty acid oxidation. Starvation causes an initial increase in lipid droplet (LD) numbers, and this is followed by shrinkage in the size and number of the LDs, since LDs are converted to fatty acids via lipolysis and lipophagy. During starvation conditions, mitochondria are often found in a highly connected network arising from fission and fusion dynamics. They are also in close proximity to LDs to receive fatty acids from the LDs [491]. The preceding examples illustrate the importance of cytoplasmic organization in understanding the functional behavior of a cell.

Some morphological alterations have already been identified upon nanoparticle incubation. Some of the changes induced by nanoparticles include alterations in the cell surface [371, 495] and the shapes of either mitochondria, Golgi, ER, lysosomes or chromatin [66, 360]. However, most studies have focused on specific organelles and used specific nanoparticle coatings, so it is not clear if there are any common changes induced

by nanoparticles within cells. Furthermore, no studies to date have focused on the potential effects of nanoparticles on the global sub-cellular organization. In this thesis, it is hypothesized that just like infection and starvation, nanoparticles may induce some global morphological changes in the cell, which might be dependent on the nanoparticle type.

One reason why previous studies have not analyzed the effects of nanoparticles on the global cellular organization may be due to the limitations of the techniques which are often utilized in nanoparticle studies, such as TEM and confocal fluorescence microscopy. TEM can only evaluate thin slices of cells. This provides information about the shape of individual organelles. However, the global 3D subcellular organization cannot be observed [57, 58, 417]. Confocal fluorescence microscopy enables imaging of cells in 3D. However, this is limited to the subset of organelles that are fluorescently tagged. Untagged organelles cannot be observed [59]. Using the 3D X-ray technique, a systematic study was performed in this thesis to determine the global subcellular effect of nanoparticles on cells.

To do this, the 50 nm gold nanoparticles coated with either dPGS or PEI were used as described in the previous chapters, and 6 – 19 A549 cells were examined at time points from 1 - 6 h.

9.2 dPGS nanoparticles induce significant global cytoplasmic alterations

In control cells, the cytoplasm was found to be dominated by multivesicular bodies (Fig. 9.1a). This presumably reflects some significant normal function of these A549 cells, which may use the multivesicular bodies for the production and recycling of lung surfactant proteins [496]. The control cells also contained endosomes, lysosomes, autophagic vacuoles, lipid droplets and mitochondria.

After 1 h and 3 h of nanoparticle treatment, multivesicular bodies almost completely disappeared from the cytoplasm (Fig. 9.1b,c, Fig. 9.2b), while the numbers of endosomes first doubled and then quintupled (Fig. 9.1b,c, Fig. 9.2a). Additionally, significant changes in mitochondrial number, and in lipid body number and morphology at the 1 and

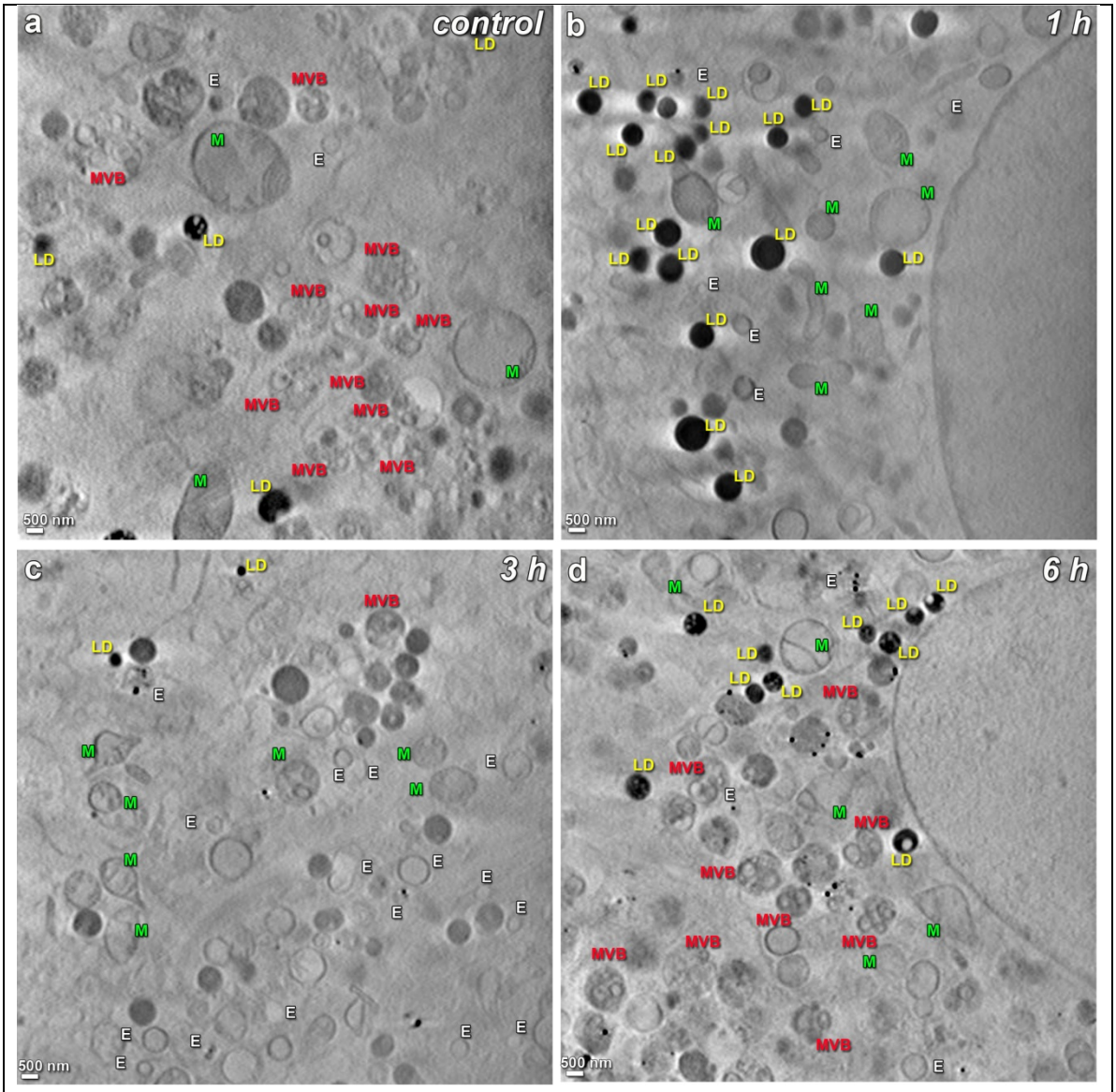

Figure 9.11 A significant cellular re-organization occurs upon dPGS nanoparticle incubation in A549 cells. Control cells (a) exhibit many multivesicular bodies (red, MVB) throughout their cytoplasm. These virtually disappear after 1 h and 3 h incubations with dPGS nanoparticles (b,c), but then begin to return to normal levels after a 6 h incubation (d). Conversely, endosomes (white, E) and mitochondria (green, M) show marked increases following the dPGS nanoparticle treatment, but then also begin to return to normal levels after a 6 h incubation. Lipid droplets (yellow, LD) first increase in number, then decrease and shrink dramatically, followed again by a return to normal levels and morphology after a 6 h incubation. Scale bars = 500 nm.

3 h time points were observed. The mitochondria number was found to significantly increase, almost tripling, during the incubation time (Fig. 9.1b,c, Fig. 9.2d), and lipid droplet number was significantly reduced accompanied by a significant shrinkage in their

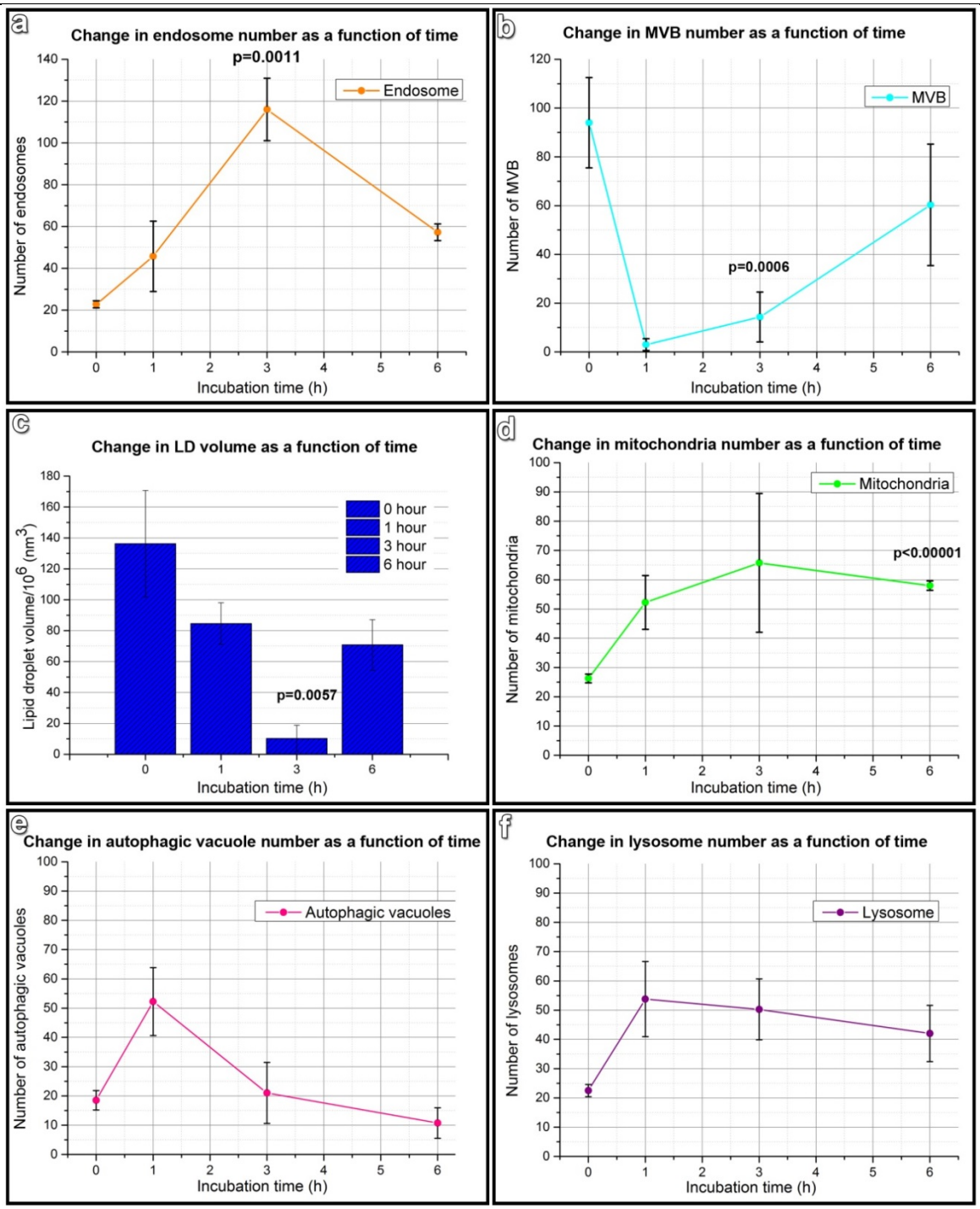

Figure 9.2 Quantification of cellular re-organization upon dPGS nanoparticle incubation. Shown are changes in endosome number (a), multivesicular body number (b), lipid droplet number (c), mitochondria number (d), autophagic vacuole number (e) and lysosome number (f) as a function of time after incubation with dPGS nanoparticles for 1 h ,3 h and 6 h. The organelles were counted at each time point using 3D cryo SXT images from 4 cells (a total of ~800 slices counted per time point). Error bars are standard deviations. Endosome number, MVB number, lipid droplet size and mitochondria number showed significant changes over the course of nanoparticle incubation (p values are indicated at selected time points).

volume (Fig. 9.1b,c, Fig. 9.2c). Significantly, some of these cytoplasmic alterations were already reversing themselves at the 6 h time point, despite the fact that nanoparticles were still present both within cells and within the incubation medium (Fig. 9.1d, Fig. 9.2). At this time point, the endosome number had begun to decrease, multivesicular bodies had begun to increase, and lipid droplet size had returned to almost normal levels (Fig. 9.1d, Fig. 9.2a-d). To be sure, none of the organelle counts had fully returned to control levels, but the observations suggest that by 6 h of incubation, the cells were beginning to revert to a more basal state. No significant changes in the lysosome and autophagic vacuole numbers or morphology could be detected at any of the incubation time points (Fig. 9.1b-d, Fig. 9.2e,f).

In sum, dPGS induced significant changes in global cell ultrastructure. The dramatic increase in endosomes probably reflects the transformation of the cell from its default state to an alternate state in response to the substantial endocytic demands imposed by the dPGS nanoparticle incubation. The nearly complete disappearance of MVB's may reflect some functional loss in these cells, since MVB's are the predominant component of the cytoplasm before nanoparticle incubation. One function of the MVB's in these A549 lung epithelial cells is the production of surfactant proteins, which is vital for lung function and survival [497]. A transient loss of the MVB's might lead to a temporary loss of secreted surfactant proteins, which might have consequences for normal respiration in a patient treated with the dPGS nanoparticles. Clearly, further tests are necessary to determine if the changes in MVB number have any functional consequences.

The significant changes in lipid droplet and mitochondria numbers after dPGS nanoparticle incubation resemble those seen in the cell starvation response. In a starving cell, lipid droplets also shrink dramatically in size and are often found in close proximity to mitochondria where they deliver fatty acids for energy production [498]. Interestingly, the changes that were observed in lipid droplets and mitochondria were not directly induced by contact with nanoparticles, as nanoparticles were never observed in mitochondria, and nanoparticles were observed only in lipid droplets at the 6 h time point. Rather, the changes in mitochondria and lipid droplets most likely reflect the indirect response to dPGS nanoparticle uptake, which appears to induce a significant cellular reorganization that requires energy resources comparable to cell starvation.

9.3 PEI nanoparticles induce significant global cytoplasmic alterations similar to those with dPGS nanoparticles

The global cytoplasmic organization was examined after incubation with PEI nanoparticles for 2 h, 3 h and 6 h (Fig. 9.3). 6-19 cells were analyzed per time point, and

	Change in the organelle number upon np incubation	
	dPGS nanoparticle	PEI nanoparticle
Endosome numbers	x 5	x 3
MVB numbers	x 1/30	x 1/2
LD numbers	x 1/2	x 1/2
Mitochondria numbers	x 3	x 2

Table 2 Maximum observed change in organelle number upon nanoparticle incubation. Note that the trend in alterations is similar for dPGS and PEI nanoparticles, namely, endosomes and mitochondria increase, multivesicular bodies and lipid droplets decrease. However, the alterations induced by PEI nanoparticles were not as pronounced as those induced by dPGS nanoparticles.

these exhibited a cytoplasmic reorganization that resembled what was seen after incubation with dPGS nanoparticles. To quantify this, the number of organelles of each type was counted using the 3D images of the cytoplasm at the three different time points. These measurements on 3 - 6 cells per time point confirmed the visual impressions derived from the larger collection of 6 - 19 cells per time point. Specifically, upon PEI nanoparticle incubation, endosome numbers tripled (Fig. 9.4a) and multivesicular body and lipid droplet numbers were almost reduced by half (Fig. 9.4b,c). Additionally, mitochondria numbers approximately doubled (Fig. 9.4d). No significant changes in lysosome numbers could be observed (note the counts included the deformed lysosomes which presented a burst morphology) (Fig. 9.4f). The magnitude of all these alterations was less significant than for dPGS nanoparticles. However, the trend for each organelle was almost identical (Table. 2). This demonstrates that each nanoparticle induces a similar subcellular reorganization regardless of the surface coating.

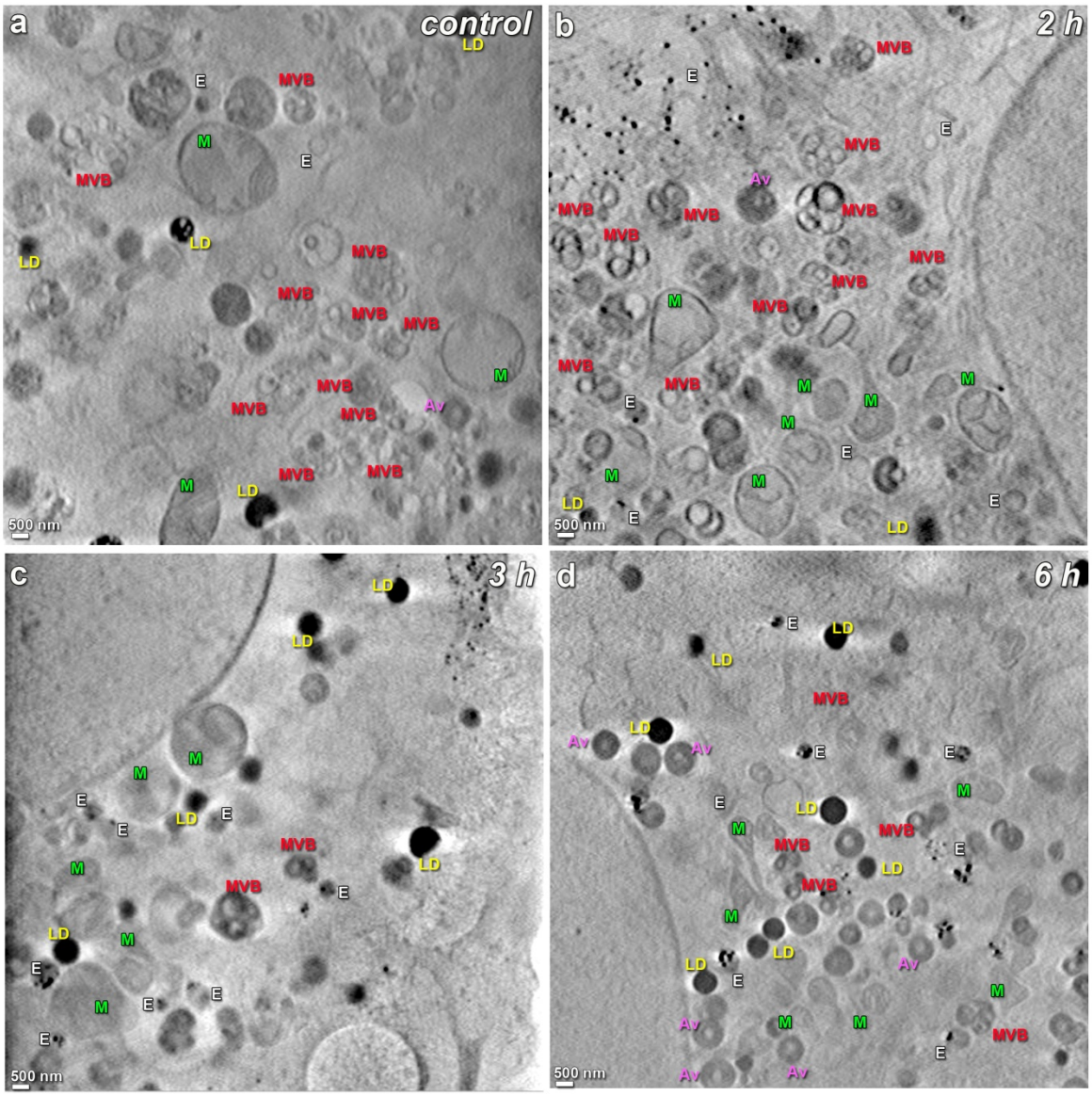

Figure 9.3 A significant cellular re-organization occurs upon PEI nanoparticle incubation in A549 cells. Control cells (a) exhibit many multivesicular bodies (red, MVB) throughout their cytoplasm. These multivesicular bodies are reduced in number after a 3 h incubation with PEI nanoparticles (c), but then begin to return to normal levels after a 6 h incubation (d). Conversely, endosomes (white, E) and mitochondria (green, M) increase after a 2 h PEI nanoparticle incubation (b-d). Lipid droplets (yellow, LD) decrease in number after 2-6 h PEI nanoparticle incubation (b-d). Autophagosome numbers (pink, Av) increased markedly after a 6 h PEI nanoparticle incubation (d). Scale bars = 500 nm.

Nevertheless, the surface coating showed some effects on the subcellular reorganization. Specifically, autophagic vacuole numbers were significantly altered upon PEI nanoparticle incubation, whereas no alteration was observed with dPGS

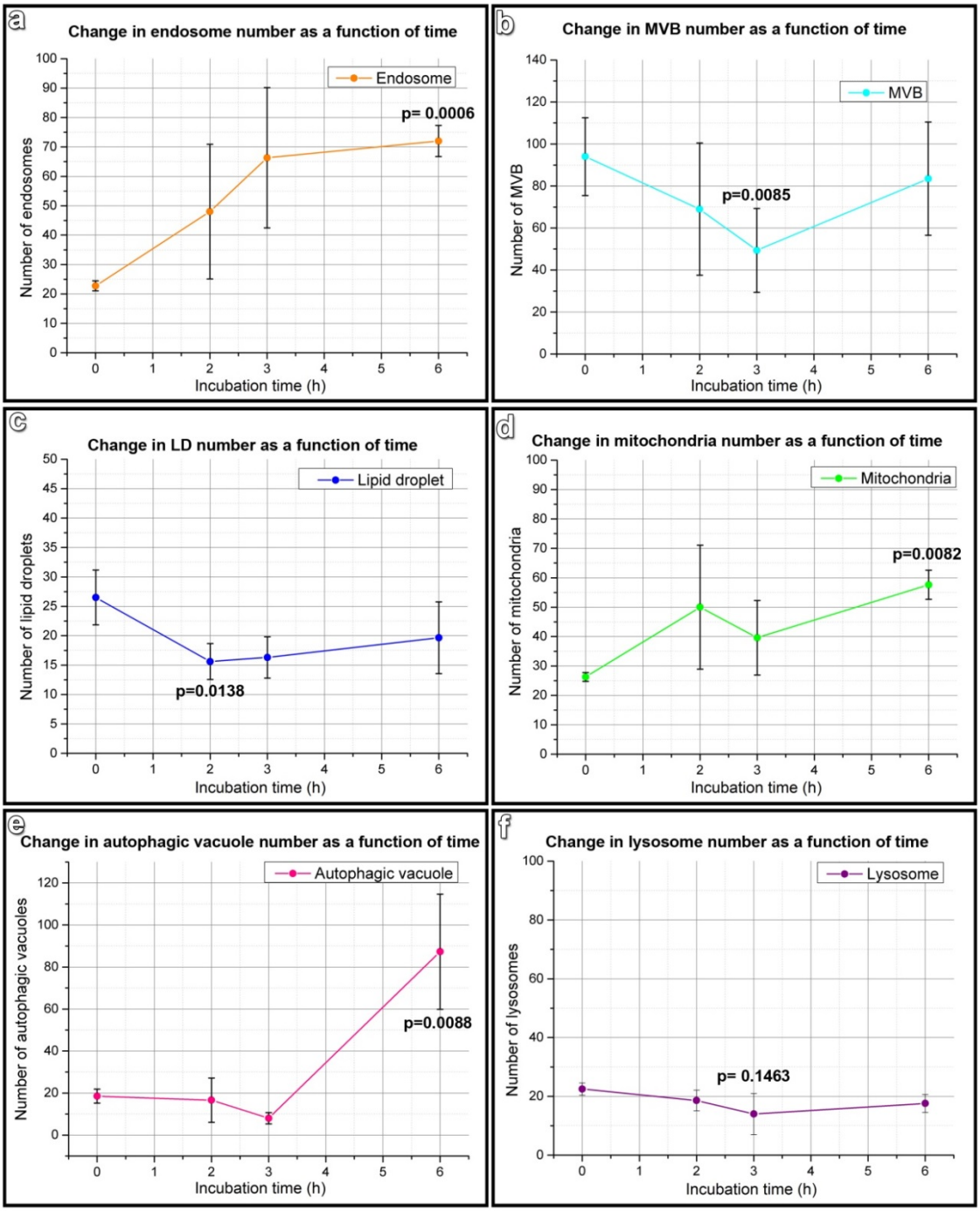

Figure 9.4 Quantification of cellular re-organization upon PEI nanoparticle incubation. Shown are changes in endosome number (a), multivesicular body number (b), lipid droplet number (c), mitochondria number (d), autophagic vacuole number (e) and lysosome number (f) as a function of time after incubation with PEI nanoparticles for 2 h ,3 h and 6 h. The organelles were counted at each time point using 3D cryo SXT images from 3 cells for (a,c-f) (a total of ~600 slices counted per time point) and from 6 cells for b (a total of ~1200 slices counted per time point). Error bars are standard deviations. Endosome number, MVB number, lipid droplet number, mitochondria number and autophagosome number showed significant changes over the course of nanoparticle incubation (p values are indicated at selected time points).

nanoparticles. According to the quantification, autophagic vacuole numbers had more than quadrupled at 6 h upon PEI nanoparticle treatment, which indicates that PEI nanoparticles induce autophagy unlike dPGS nanoparticles. This difference probably arises due to the fact that at these concentrations, PEI nanoparticles caused lysosomes to rupture releasing their corrosive content to the cytoplasm. This is likely to induce an autophagic process to protect the cell, which would lead to an increase in autophagosome numbers. Note, however, as discussed in Chapter 8, this response was transient because autophagosome numbers appeared to return to normal by the 48 h time point after the PEI nanoparticles were removed at 6 h.

9.4 Summary

Both dPGS and PEI nanoparticles induced similar global cytoplasmic alterations within A549 cells. Significant decreases in the number of MVB's and significant increases in the number of endosomes were found. The increase in endosome numbers probably reflects the increased endocytic demands imposed by nanoparticle incubation. It is not clear why MVB numbers drop significantly, but this reduction may have functional consequences since the MVB is the predominant organelle in the cytoplasm of the A549 cells. In the future, it would be interesting to perform more direct functional tests during nanoparticle incubation, such as measurement of the levels of secreted surfactant proteins since MVB's are reported to be a critical step during the production of these proteins [497]. Both nanoparticle incubations caused mitochondrial numbers to increase and lipid droplet numbers and volume to decrease. These significant changes in lipid droplets and mitochondria after nanoparticle incubation resembled those previously reported for the cell starvation response, suggesting that the nanoparticle incubations required significant amounts of cellular energy reserves. All of the alterations were found to be more significant upon dPGS nanoparticle incubation than PEI nanoparticle incubation. However, the trend was similar. This raises the possibility that regardless of their coat, nanoparticles might induce similar cytoplasmic reorganizations. This should be tested in the future by using the techniques which were developed here to examine more nanoparticle types. These results also show the power of this 3D global analysis as a more sensitive measure of cell state than conventional cell toxicity assays.

10. A TEN-FOLD REDUCTION IN PEI NANOPARTICLE CONCENTRATION DIRECTS NANOPARTICLES TO A MORE EFFECTIVE PATHWAY IN WHICH LYSOSOMES DO NOT RUPTURE

10.1 Motivation for studying trafficking at lower PEI nanoparticle concentrations

As shown in Chapter 7, when cells were incubated with the commonly used concentration of PEI nanoparticles (0.13 nM), a great deal of cytoplasmic escape was achieved (~7x greater than dPGS nanoparticle escape). However, as demonstrated in Chapter 8, PEI nanoparticles exerted adverse effects, including autophagic cell death most likely due to lysosomal rupture. Previously, it was reported that the harmful effects of PEI on cell viability were reduced when low molecular weight PEI was used, as determined from viability assays such as measuring cell proliferation and plasma membrane integrity [499, 500]. However, low molecular weights yielded less efficient DNA transfection [500, 501]. These lower molecular weight forms of PEI have less unprotonated amines, so in an attempt to mimic these results, the concentrations of PEI nanoparticles were reduced in the experiments described in this Chapter. Specifically, A549 cells were treated with a ten-fold lower concentration of PEI nanoparticles (0.013 nM) for 6 h and inspected for morphological signs of cell stress to analyze whether lower concentrations were less harmful to the cells. Moreover, this Chapter also investigates whether the lower concentration had an effect on the cellular uptake mechanism, trafficking mechanism or cytoplasmic escape mechanism within the cells. Additionally, to understand whether lower concentrations reduced the efficiency of PEI nanoparticles analogous to lower molecular weight PEI, the cytoplasmic escape and nuclear entry efficiency was analyzed by quantifying the nanoparticle number in the cytoplasm and nucleus.

10.2 At ten-fold lower concentrations, morphological signs of cell stress diminished

After a 6 h incubation with a ten-fold lower concentration of PEI nanoparticles, no morphological signs of cell stress were observed (Fig. 10.1), consistent with previous studies performed with lower molecular weight PEI [500]. Specifically, plasma membrane blebbing, chromatic condensation, an increase in autophagic vacuole numbers or mitochondrial elongation were not observed. These results show that in contrast to the

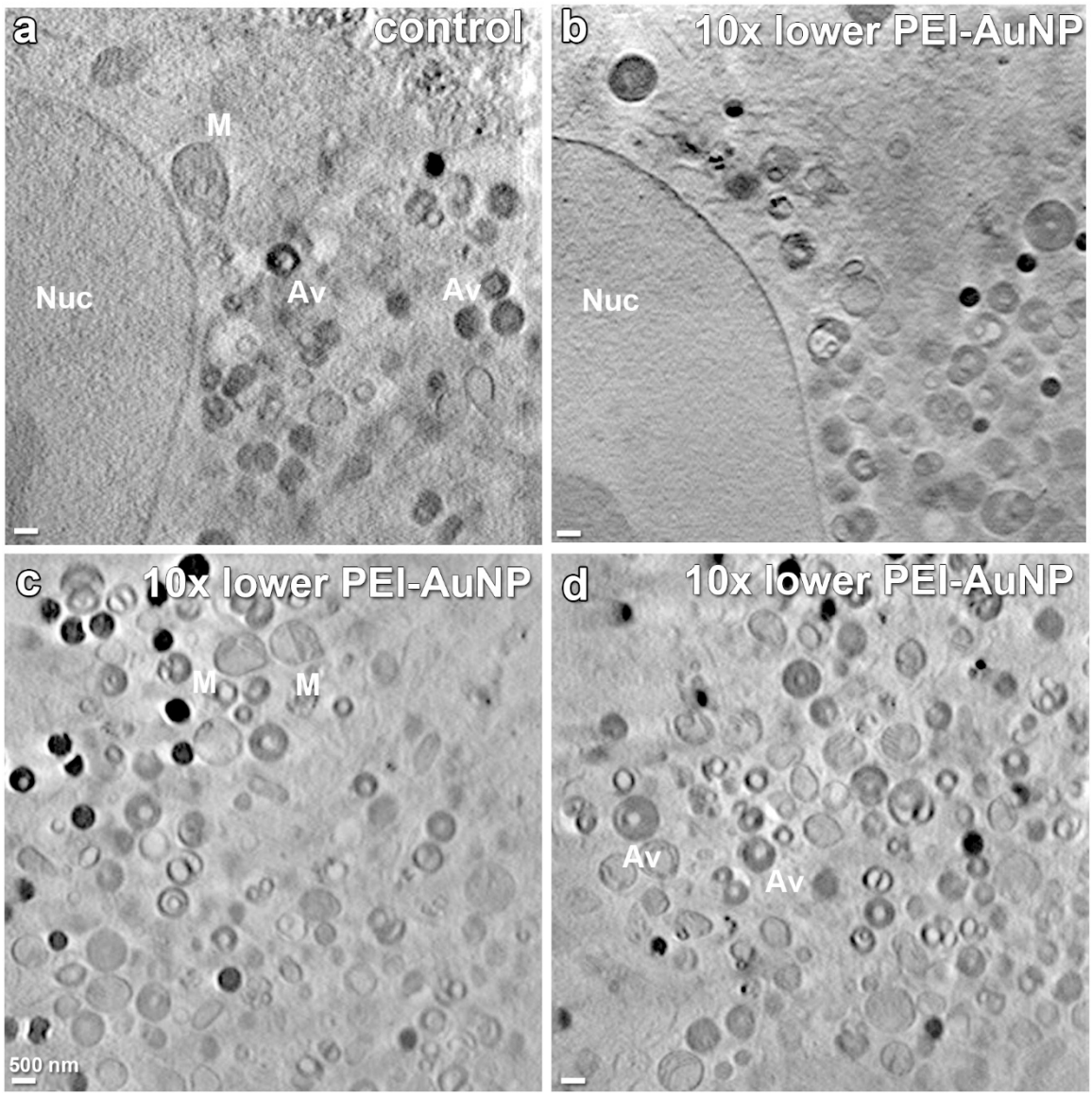

Figure 10.1 Lowering the concentration of PEI nanoparticles ten-fold reduced the adverse effects of these nanoparticles. No chromatin condensation was detected in the nucleus (Nuc) (b). Mitochondria (M) were not elongated (c) and autophagic vacuole (Av) numbers (d) were similar to control cells (a). Scale bars = 500 nm.

higher concentration, the lower concentrations of PEI nanoparticles did not significantly affect cell homeostasis.

10.3 At ten-fold lower concentrations, the predominant endocytosis pathway of PEI nanoparticles was altered

As described in Chapter 7, at standard concentrations PEI nanoparticles were found to be internalized predominantly via macropinocytosis and with a small fraction internalized by a putative caveolae-mediated endocytosis.

When ten-fold lower concentrations of PEI nanoparticles were used, the predominant uptake mechanism of PEI nanoparticles was found to change. Specifically, membrane ruffles were not observed, which were prominent on the plasma membrane at the higher PEI nanoparticle concentration. Additionally, when the endocytic vesicles containing nanoparticles were quantified, only 11% of these endocytic vesicles containing nanoparticles matched the characteristics of macropinocytosis, namely vesicles that were uncoated and around 200 nm and bigger (Fig. 10.2c). At the higher concentration, 77% of the nanoparticles in endosomes were found to be in macropinosomes. These results indicate that internalization of the nanoparticles via the macropinocytosis pathway was significantly reduced at the lower concentration of PEI nanoparticles.

In contrast, 89% of endocytic vesicles containing PEI nanoparticles were found to be coated and had a diameter of 100 - 150 nm (Fig. 10.2a-b). These coated invaginations and endocytic vesicles are characteristics of either a clathrin- or a caveolae- mediated endocytosis [266], as described in Chapter 6 and Chapter 7. Recall that at the higher concentration of PEI nanoparticles this clathrin or caveolae-mediated pathway had only accounted for 23% of the endocytic vesicles containing PEI.

It is not clear how this switch in the endocytosis pathway could occur due solely to the difference in PEI nanoparticle concentration. One possible hypothesis for this switch could be the different distributions of PEI nanoparticles on the plasma membrane at the different concentrations. At high concentrations, PEI nanoparticles were found to be very closely spaced along the plasma membrane. Conceivably, such a distribution may appear to the cell as a larger cargo. Since cells internalize larger cargos through macropinocytosis, this may have favored uptake via macropinocytosis at the high PEI nanoparticle concentration. However, at the low concentration, PEI nanoparticles were found to be more widely spaced. Since cells internalize smaller cargos through

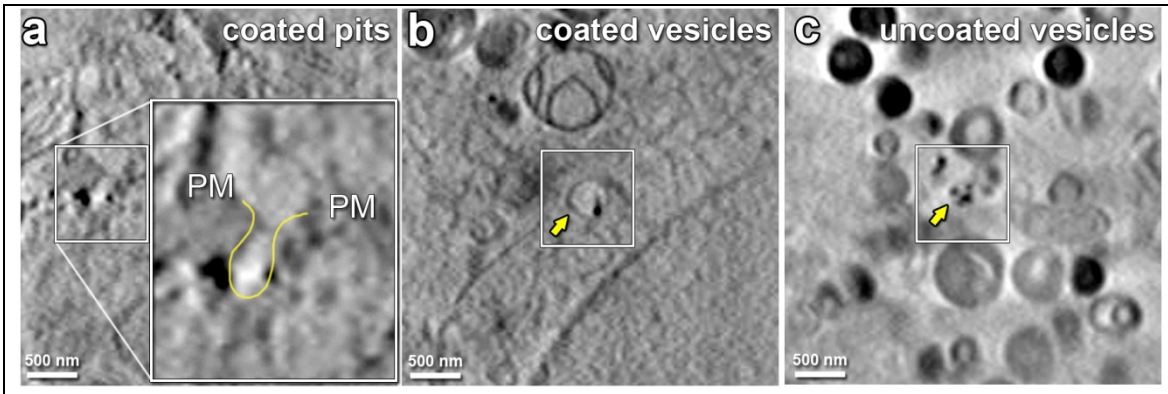

Figure 10.2 Internalization pathway of PEI nanoparticles at ten-fold lower concentrations via cryo-SXT. PEI nanoparticles were found within uncoated endocytic vesicles as shown in zoomed in views with a yellow line (a) and in coated endocytic vesicles (arrow) (b) which suggests that the PEI nanoparticles were internalized via a clathrin- or caveolae-mediated endocytosis. The nanoparticles were also found in a limited amount of uncoated endocytic vesicles within the cell (arrow) (c), suggesting that macropinocytosis is also involved in internalization of PEI nanoparticles at 10x lower concentrations. Scale bars = 500 nm.

either clathrin- or caveolae-mediated endocytosis [282-284], this may have favored uptake by these pathways at the low PEI nanoparticle concentration.

10.4 At ten-fold lower concentrations, the intracellular pathway of PEI nanoparticles was altered: they bypassed lysosomes

The effect of PEI nanoparticle concentration on nanoparticle localization was also examined within the cell. At ten-fold lower concentrations, PEI nanoparticles were found to be mostly localized to similar places in the cells, namely endosomes (Fig. 10.2b,c), multivesicular bodies (Fig. 10.3a,b), cytoplasm (Fig. 10.3c) and the nucleus (Fig. 10.4a). Consistent with what was observed at the high concentration, nanoparticles were not detected in autophagic vacuoles (Fig. 10.3d).

However, one significant difference was detected in the intracellular locations of PEI nanoparticles at the low concentration. Although lysosomes were still clearly present within the cells, PEI nanoparticles were never detected within these lysosomes (Fig. 10.3d). Furthermore, these lysosomes exhibited normal morphology and were not enlarged or fragmented as observed at the high PEI concentration. These observations indicate that the PEI nanoparticles bypassed lysosomes at the low PEI concentration, and

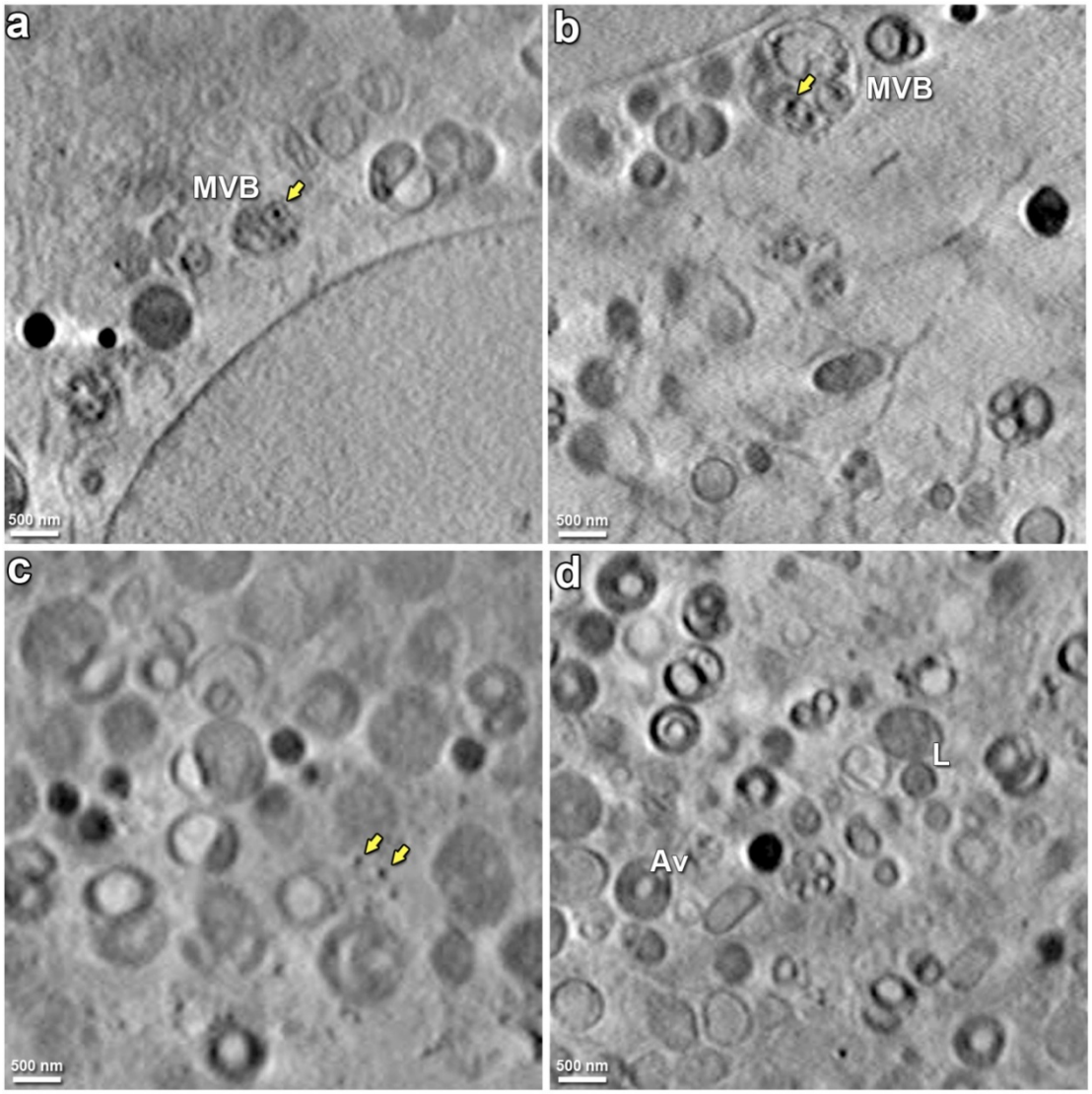

Figure 10.3 Intracellular trafficking of PEI nanoparticles at ten-fold lower concentration via cryo-SXT. Besides uncoated and coated endocyc vesiscles, PEI nanoparticles (yellow arrows) were found in multivesicular bodies (MVB) (a,b) and free in the cytoplasm (c). PEI nanoparticles were not found in autophagic vacuoles (Av) or lysosomes (L), and lysosome morphology appeared to be normal (d). Scale bars = 500 nm.

further they suggest that the vast majority of lysosomes do not rupture at the low PEI nanoparticle concentration.

In sum, PEI nanoparticles at high concentrations are internalized predominantly through macropinocytosis, which leads to trafficking through lysosomes and subsequent rupture of many lysosomes. At ten-fold lower concentrations, the nanoparticles were internalized

predominantly through a putative clathrin- or caveolae-mediated endocytosis in which nanoparticles were not trafficked to lysosomes and most lysosomes were not ruptured.

Overall the results about PEI nanoparticle uptake are consistent with some previous inhibition studies which came to the conclusion that PEI polyplexes were taken up by a combination of macropinocytosis, clathrin- and caveolae-mediated endocytosis [37-42]. However, up until now, no one has directly studied how PEI concentration influences the choice of these uptake pathways.

Note that the observation that lysosomes are bypassed when the nanoparticles are taken up by this clathrin- or caveolae- mediated endocytosis suggests that this pathway may be caveolae- mediated, since several previous studies have demonstrated that lysosomes are bypassed in the caveolar pathway [269, 270]. To confirm this, future studies with the PEI nanoparticles should use molecular stains for the clathrin and caveolar pathways at the two different PEI nanoparticle concentrations to better characterize the nature of these pathways.

10.5 At ten-fold lower concentrations, PEI nanoparticles still escape to the cytoplasm and nuclear entry is more efficient

The preceding observations in Chapter 10.2 demonstrate that lower PEI nanoparticle concentrations lead to significantly less signs of cell stress, presumably because the uptake pathway of the nanoparticles changes. The new pathway bypasses lysosomes, which do not rupture, and this prevents release of the corrosive contents of the lysosomes. Next, whether this lower concentration would still allow nanoparticles to escape to the cytoplasm and nucleus was investigated.

At ten-fold lower concentrations, free PEI nanoparticles could be detected in the cytoplasm (Fig. 10.3c). Specifically, within the defined standard measurement volume at 6 h of incubation, an average of 21 $\pm$ 11 nanoparticles could be counted at the low concentration and 72 $\pm$ 21 nanoparticles at the high concentration. Thus nanoparticles escaped to the cytoplasm at the low concentration, but at about 1/3 of the number found at the high concentration. Recall, that the standard measurement volume is about 1/7 of the total cell volume, so at the low concentration approximately 120 nanoparticles per cell were estimated to escape. This is still probably enough to deliver nucleic acids to the cell,

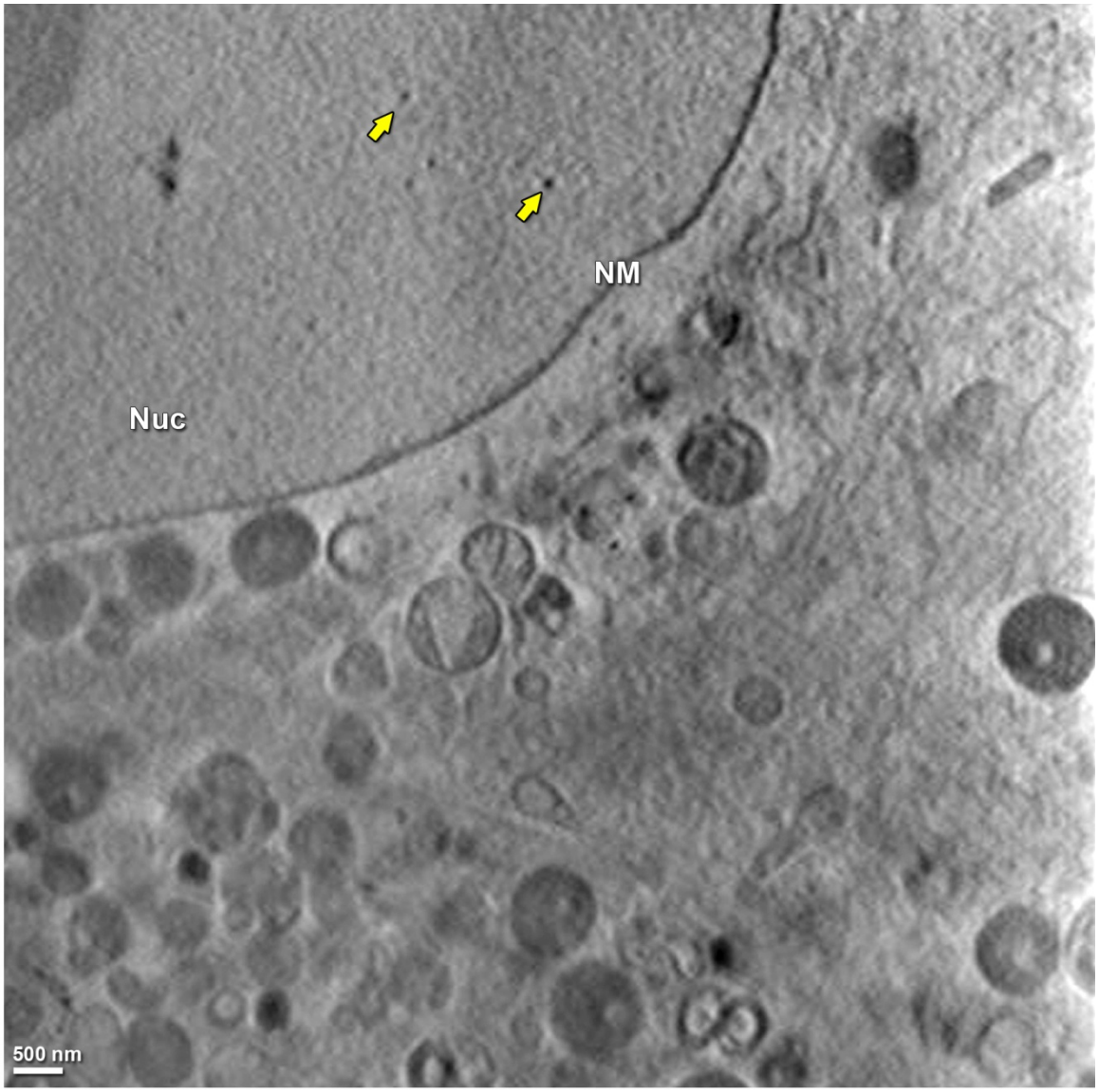

Figure 10.4 At ten-fold lower concentrations, PEI nanoparticles were found in the nucleus (Nuc). A549 cells were treated with PEI nanoparticles (yellow arrows) for 6 h and PEI nanoparticles were detected in the nucleus. Scale bar = 500 nm.

but this should be tested directly in future studies using a functional assay such as mRNA knockdown or nuclear DNA delivery.

Functional tests for nucleic acid delivery would also be important since the effects may not scale with the number of escaped nanoparticles. Specifically, nanoparticles which pass through the corrosive environment of the lysosome may have their DNA digested. Indeed, previous studies have suggested that passage through the lysosome can reduce or

even eliminate transfection efficiency via PEI [192], so the larger number of escaped nanoparticles at the high PEI concentration may not mean that gene delivery is more efficient. In addition, at the higher concentration, many PEI nanoparticles were observed to remain attached to lysosomal fragments, which could prevent them from entering the nucleus. In fact, the preliminary data suggest that more nanoparticles were found in the nucleus after the incubation at the low concentration, but confirmation of this will require more data.

Interestingly, the nanoparticles that entered the nucleus, at either concentration, appeared to be smaller than the nanoparticles found in the cytoplasm. The current pixel size in the images is too small to directly measure this, but future work should investigate this observation more thoroughly, since it could imply a size cutoff for nuclear entry of nanoparticles.

Unfortunately, these cryo-SXT data do not allow conclusions to be drawn about how the nanoparticles escape to the cytoplasm at the low concentration. As noted, no evidence for ruptured lysosomes was found. Also, no evidence for rupture of other vesicles could be detected, although it might be difficult to clearly detect rupture of smaller vesicles. At the moment, the observations favor the hypothesis that escape at this low concentration may have occurred through pore formation in the endosomes, since this transient event would be difficult to detect by cryo SXT. Further work should use alternative techniques [348] to investigate the escape mechanism at the low concentration of PEI nanoparticles.

10.6 Summary

As described in Chapter 8, PEI nanoparticles at standard concentrations (~0.13 nM) were internalized predominantly via macropinocytosis which led nanoparticles to lysosomes. When ten-fold lower concentrations (~0.013 nM) of PEI nanoparticles were used, differences in the endocytosis and intracellular pathway of nanoparticles were observed (Fig. 10.5) compared to high concentrations. Specifically, PEI nanoparticles at low concentration were internalized predominantly via a putative caveolae-mediated endocytosis that could have been favored due to a wider distribution of nanoparticles along the plasma membrane compared to high concentrations. This alternate uptake mechanism prevented PEI nanoparticles from reaching lysosomes, thereby yielding a positive, practical consequence. Since nanoparticles were not trafficked to lysosomes,

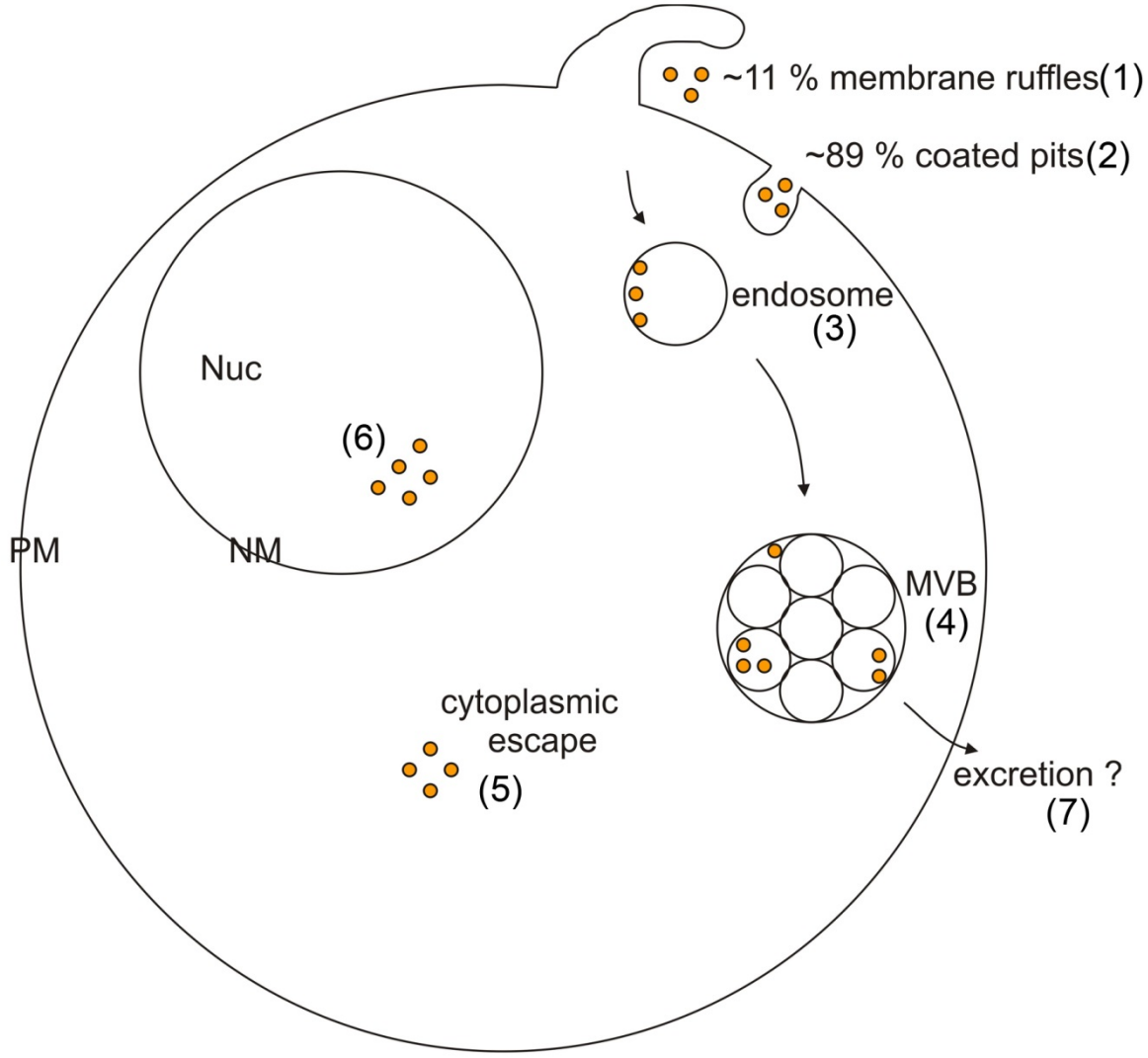

Figure 10.5 Model summarizing the observations about the endocytosis and intracellular trafficking pathway of PEI nanoparticles at 10x lower concentration. PEI nanoparticles were endocytosed via at least two endocytosis pathways which may be macropinocytosis (1) and a caveolae- or clathrin-mediated endocytosis (2). The predominant endocytosis pathway was caveolae- or clathrin-mediated endocytosis (2). The nanoparticles were first sorted to early endosomes (3). Later, the PEI nanoparticles were trafficked from endosomes to multivesicular bodies (4). They bypassed lysosomes, suggesting that the internalization pathway could be caveolae-mediated endocytosis. Additionally, many free PEI nanoparticles were found in the cytoplasm (5) and in the nucleus (6). The location of many PEI nanoparticles within MVB's suggests that at least a portion of the nanoparticles will be excreted from the cells (7).

lysosomes did not rupture and PEI nanoparticles did not appear to exert any harmful effects on the cells. Specifically, morphological signs of cell stress could not be detected such as chromatin condensation, plasma membrane blebbing, increase in autophagic vacuole numbers and mitochondrial elongation. Furthermore, at this lower concentration,

a reasonable amount of cytoplasmic escape was still detected. These findings indicate that lowering the concentration of PEI nanoparticles may be a practical solution to reduce the harmful effects of PEI nanoparticles on cells, however functional assays for nucleic acid delivery should be performed to confirm this, and the result should be tested in other cell types to see if similar conclusions hold.

11. CONCLUSION

In order to treat and diagnose diseases, nanoparticles are good alternatives to bulk medications and medical contrast agents, which are not site specific [2-4]. Biologically relevant nanoparticles can potentially target specific unhealthy cells without interacting with healthy cells. If this potential can be achieved, the side effects of treatments on healthy cells can be minimized, yielding a break-through in the medical field. However, to achieve this potential is not straightforward since the rules which govern the cellular interactions of nanoparticles are still not known. Especially elusive are the rules governing the endocytosis pathway, intracellular trafficking pathway, cellular end-points and the excretion tendency of a specific nanoparticle [2-4, 11]. Therefore, researchers in the nanomedicine field have typically focused on a particular type of biologically relevant nanoparticle of interest to them and investigated this nanoparticle.

Similarly, in this thesis, two biologically relevant nanoparticles were examined, namely dPGS-coated gold nanoparticles and PEI-coated gold nanoparticles. Specifically, dPGS nanoparticles are designed for simultaneous diagnosis and treatment of inflammation by binding to cell surface receptors which are enhanced in inflamed regions [12, 19, 20]. PEI nanoparticles are designed as targeted gene delivery tools, since they can enhance cytoplasmic escape within the cells [13, 14, 35, 184]. Both nanoparticles are promising for use in biomedical applications. However, they cannot be utilized due to many unknowns about their interactions with biological systems.

To answer some of the unknown questions about dPGS and PEI nanoparticles, a collaboration was established with two different groups. The group of Prof. Haag at the Free University in Berlin designed and synthesized dPGS-coated gold nanoparticles with a core size of 50 nm. The group of Prof. Breunig at Regensburg University synthesized PEI-coated gold nanoparticles with a core size of 50 nm. These nanoparticles (0.13 nM) were incubated with A549 cells for various time points and observed the cells with cryo-SXT to investigate cellular interactions of dPGS and PEI nanoparticles. Note that using cryo-SXT enabled imaging the nanoparticle - cell interactions in 3D within near-native state cells at 40 nm spatial resolution [62, 63]. Therefore, rare events within the cells could be discovered, which led to interesting findings about the cellular interactions of dPGS and PEI nanoparticles. Moreover, since the same core size and concentration were

used, the cellular interactions of dPGS and PEI nanoparticles could be systematically compared to understand the effect of the biologically relevant coat on nanoparticle - cell interactions.

Although dPGS nanoparticles are designed to function at the cell surface, they were previously found to enter into cells [21-26]. What happens next to dPGS nanoparticles within the cell was a mystery. Specific unknowns included the endocytosis pathway and organellar localization sites, and also whether dPGS escaped to the cytoplasm, entered the nucleus and eventually was excreted from cells. In this thesis, some of these questions could be answered via cryo-SXT analysis. Specifically, dPGS nanoparticles were found to be endocytosed predominantly via macropinocytosis (~85%). The majority of nanoparticles were trafficked to endosomes, multivesicular bodies and lysosomes, which are all membrane bound organelles of the endo/lysosomal system. A small portion of endocytosed nanoparticles (~70 np per cell) were found in the cytoplasm. However, no nuclear entry was detected. Moreover, some morphological signs were detected suggesting that dPGS nanoparticles might eventually be excreted from the cells. Specifically, dPGS nanoparticles were sequestered to the inner vesicles of multivesicular bodies, which are known to be excreted to the extracellular environment when multivesicular bodies fuse with the plasma membrane. Overall, these findings suggest that most dPGS nanoparticles stay enclosed within membrane bound organelles and may eventually be excreted from the cells. These are desirable properties for medical usage.

Two observations made in this thesis, however, raise some questions about the impact of dPGS on cells. First, as noted above, some cytoplasmic escape of dPGS nanoparticles could be detected. This may have a positive effect, as it is possible that dPGS could exert therapeutic effects not only at the cell surface, but also from within the cytoplasm [166]. But it is also conceivable that the presence of the dPGS nanoparticles in the cytoplasm may have some unwanted consequences. Further work is required to investigate these possibilities. Second, dPGS nanoparticles were also found within lipid droplets at later time points. Lipid droplets are not a commonly reported trafficking site for nanoparticles, as only two other studies report nanoparticles localizing to lipid droplets [322, 473]. Combined with these reports, the observations in this thesis now highlight the need to examine lipid droplets more carefully as possible localization sites for nanoparticles, and

also to determine how the nanoparticles enter lipid droplets and whether they eventually leave. Related to this is a need to determine whether the presence of nanoparticles in lipid droplets has consequences for the function of this organelle, which is known to play key roles in cellular signaling and energy metabolism.

PEI nanoparticles were also investigated in this thesis. PEI is known to enhance cytoplasmic escape due to its ability to destabilize membranes [13, 35], and so it has been proposed as a tool for targeted gene delivery. However, the mechanism of PEI-induced cytoplasmic escape is still elusive [33, 43]. Clarification of this mechanism will help develop more efficient gene delivery tools. A related controversial point is whether PEI nanoparticles localize to lysosomes [42, 44-50]. This is a critical issue, since lysosomes have digestive enzymes which can digest nucleic acids, which in turn will reduce or eliminate PEI-mediated gene delivery. If it is known that PEI nanoparticles will localize to lysosomes, then the gene will need to be protected from the lysosomal enzymes [14, 184]. Another uncertain issue is whether PEI nanoparticles enter into the nucleus [33]. This would be desirable for nuclear delivery of DNA [483]. More generally, it would also be useful to determine if the nuclear membrane is a barrier for nanoparticles [299].

In this thesis, these questions were addressed by analyzing PEI nanoparticle uptake at the standard concentration used in most previous studies and also at a ten-fold reduced concentration. At the high concentration, PEI nanoparticles were found to be mainly endocytosed by macropinocytosis (like dPGS nanoparticles) and trafficked by the endo/lysosomal pathway, where they localized to endosomes, MVB and lysosomes. At this high concentration, PEI nanoparticles predominantly escaped to the cytoplasm via rupturing lysosomes. Rupture appeared to require a minimum of four nanoparticles per lysosome, and led to multiple signs of cellular stress, including mild chromatin condensation, mitochondrial elongation and an increase in autophagic vacuole numbers. These adverse effects disappeared at later time points when the nanoparticle incubation had ended. At this high concentration, ~500 PEI nanoparticles per cell were estimated to escape to the cytoplasm and a few PEI nanoparticles (1 - 5) could enter into the nucleus. Finally, morphological evidence was found suggesting that at later time points PEI nanoparticles were excreted from the cells via multivesicular bodies.

At the low PEI nanoparticle concentrations, the adverse effects of PEI nanoparticles were found to be eliminated. The data suggest this beneficial effect is due to an altered endocytosis and intracellular trafficking pathway of PEI nanoparticles at the low concentration. Specifically, the predominant endocytosis pathway of PEI nanoparticles was found to be switched to a putative caveolae-mediated endocytosis which bypassed lysosomes. Since no lysosomal rupture occurred, the morphological signs of cellular stress were eliminated. This finding shows that reducing the concentration of PEI nanoparticles alters both the endocytosis and intracellular pathway of nanoparticles. This suggests that it can also reduce cytotoxic effects and increase efficiency of gene delivery.

Then, the effects of the dPGS and PEI nanoparticles on cells were compared. Nanoparticles were discovered to alter the global cytoplasmic organization. Specifically, the organelle content of A549 cells was significantly changed upon nanoparticle incubation. Remarkably, the trend of this subcellular reorganization was similar for both dPGS and PEI nanoparticles, although the effects were consistently stronger with dPGS. Specifically, endosome numbers were found to increase significantly, while multivesicular body numbers decreased significantly. Lipid droplet numbers also decreased accompanied by a significant decrease in their volume, while mitochondria numbers increased. This reorganization does not reflect a cell death response, since in the case of dPGS no evidence for any conventional signs of cell stress could be detected. Rather the reorganization is more likely to reflect a cellular adaptation required to internalize a large number of nanoparticles, and the requirements for energy and lipid utilization to meet these endocytic demands. Although previous studies have described the morphological effects of nanoparticles on cell surface morphology or on individual organelle morphology [66, 371, 377], the observations in this thesis are the first to describe this global cytoplasmic reorganization. These new observations in this thesis were enabled by cryo SXT because previous studies using electron or fluorescence microscopy could not observe the complete 3D morphology of the cell [57-59].

This finding suggests that it may not be sufficient to merely test the cytotoxicity of nanoparticles. An examination of overall cell morphology is likely to provide a much more sensitive assay of the potential physiological effects of nanoparticles on cells. These morphological assays can and should be supplemented by biochemical / functional

assays. For example, future work with dPGS or PEI nanoparticles could investigate the physiological effects of reduced multivesicular body numbers by investigating whether this reduction impacts secretion of lung surfactant proteins since multivesicular bodies are reported to be a critical step during the production of these proteins [497]. Other future directions should include molecular studies using fluorescent tagging techniques to provide corroborative evidence for the structures that were identified based on their morphology in cryo X-ray tomography. This would include in particular tagging for macropinosomes, caveolar vesicles and clathrin coated vesicles to help identify the different potential endocytosis pathways. It could also include alternate approaches to detect and quantify the global cytoplasmic organization, such as fluorescent tagging of different organelles and then examination of the cells in 3D by fluorescent microscopy to count the organelles of different types before and after nanoparticle incubation. Here, it is also important to note that the quantifications in this thesis were performed manually for a small sample size of cells and for a sub-volume which corresponds approximately to 1/7 of the total cell volume. With development of automated organelle recognition software and automated data acquisition in cryo SXT, organelle quantification could be greatly facilitated to obtain much better statistics.

It is striking that the global cytoplasmic reorganization in the A549 cells induced by either dPGS or PEI nanoparticles was very similar, even though dPGS and PEI are completely different biologically relevant coatings. This was not the only similarity. The two nanoparticle types were also found to share the same predominant endocytosis pathway, intracellular trafficking pathway and excretion mechanisms. Furthermore, the predominant endocytosis pathway for PEI nanoparticles could be switched from macropinocytosis to a putative clathrin- or caveolae- mediated endocytosis. A hint was also found which suggests that the same switch might happen for dPGS nanoparticles, where in this case the switch was triggered by the presence and absence of serum proteins (see the Appendix, Chapter 13). Note that the capability to switch uptake to a pathway that bypasses lysosomes has great potential in nanomedicine because it is much more beneficial for the nanoparticle cargo [270].

It is important to point out that some differences between these nanoparticles were also detected such as their higher cytoplasmic escape tendency (PEI) and their lipid droplet

localization (dPGS). This demonstrates that the surface coat of the nanoparticle does influence its behavior. Nevertheless, the considerable number of similarities between the behavior of the two nanoparticles suggests that there may be patterns and rules which govern nanoparticle - cell interactions and that they can be discovered through such systematic studies by limiting the independent variable to only one. A better understanding of these rules which govern nanoparticle - cell interactions, should greatly aid in the synthesis of nanoparticles targeted to a specific disease, and then maybe at some point, even for a specific patient with a defined protein and genomic map. Then, one day, personalized nanoparticle treatment can be a reality for a healthier future.

12. EXPERIMENTAL TECHNIQUES

Characterization of dPGS nanoparticles and PEI nanoparticles. dPGS nanoparticles and PEI nanoparticles were prepared by our collaborators with previously described techniques (Chapter 3). The hydrodynamic radius of the nanoparticles was measured in water and in cell culture medium using a Zetasizer (Malvern Zetasizer Nano ZS ZEN 3500). The size measurement was performed both before and after incubating cells with the nanoparticles. To analyze the shape of the nanoparticles, TEM images were obtained with a JEOL JEM-2100 at 200kV. The particle concentration was calculated via gravimetric analysis [502].

Cell Culture. Both cell lines (A549, HeLa) were routinely propagated in Dulbecco's Modified Eagle Medium (DMEM), with penicillin/streptomycin and 10% fetal calf serum at 37 °C with 5% CO_2, and were sub-cultured twice a week. To analyze the escape mechanism of PEI nanoparticles, a caspase assay was performed and endosomes and lysosomes were stained respectively with CellLight® Early Endosomes-GFP and CellLight® Lysosomes-GFP tags.

DIC Microscopy. 400 µl of cells were seeded on cover slips within 48-well plate chambers for fixed cell experiments and on eight-well Lab-Tek® II Chamber Slides™ at 1×10^5 cells mL^{-1} for live cell experiments. The cells were incubated for 24 h to achieve 60%-70% confluency. Then, the cell culture medium was replaced with 400 µl of nanoparticles in either the presence or the absence of serum. The nanoparticles were incubated with the cells for different durations, namely for 1 h, 3 h, 6 h and 12 h. After the defined incubation time, for fixed cell experiments, the cells were fixed with 4% PFA and washed with PBS multiple times. After washing, the coverslips were mounted on glass slides. The fixed cells glass slides and the live cells on chambers were then examined with a Leica DMI 6000B microscope with a 100x oil objective and 0.28 NA condenser.

Nanoparticle quantification in DIC images. DIC images were filtered with a Gaussian filter and contrast adjusted using ImageJ such that the nanoparticles were bright and the rest of the cell dark. The total remaining brightness of these images was then measured to provide an estimate of the total amount of nanoparticles within the cells at the different

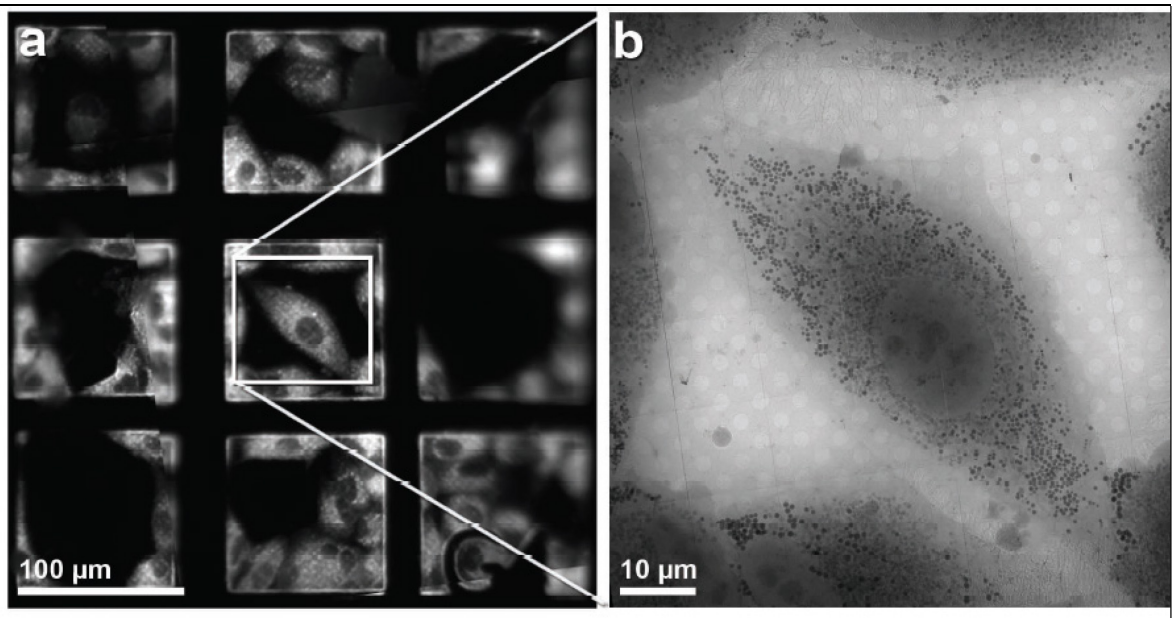

Figure 12.1 Map of the cells (a) obtained by cryo fluorescence microscopy. This was used to evaluate the ice quality and also to effectively find the cell of interest on the X-ray microscope, first at low magnification (b). Then a region of interest was selecting for higher magnification X-ray imaging at a series of tilt angles. Scale bars = 100 µm for (a) and 10 µm for (b).

time points. Then, these cumulative brightness values at different time points were compared to determine whether the number of nanoparticles within the cell was changing.

Sample Preparation for cryo SXT. For cryo SXT, cells were grown on perforated carbon-foil-coated gold-finder grids from Quantifoil (QUANTIFOIL R 2/2 on Au G200F1). First, grids were treated with plasma for 10 sec in an evacuated chamber to increase the hydrophilicity prior to cell adhesion. Next, the grids were transferred to six-well Corning® Costar® cell culture plates and treated with cell culture medium with 10% FBS for 30 min to enhance the attachment of cells on the grid. Then, 1×10^5 cells mL^{-1} were seeded on grids and incubated at 37°C with 5% CO_2 for 24 h. After 60% confluency was reached, the cells were fluorescently labeled with 100 nM MitoTracker® Green for 30 min to stain mitochondria. After washing the cells with PBS twice to get rid of excess mitochondria tracker, cells were incubated with 0.13 nM colloidal dPGS nanoparticles or dPG nanoparticles suspension for 1 h, 3 h and 6 h. At the end of the incubation time, the colloidal suspension was rinsed with 1x PBS, and the cells on the grids were vitrified immediately.

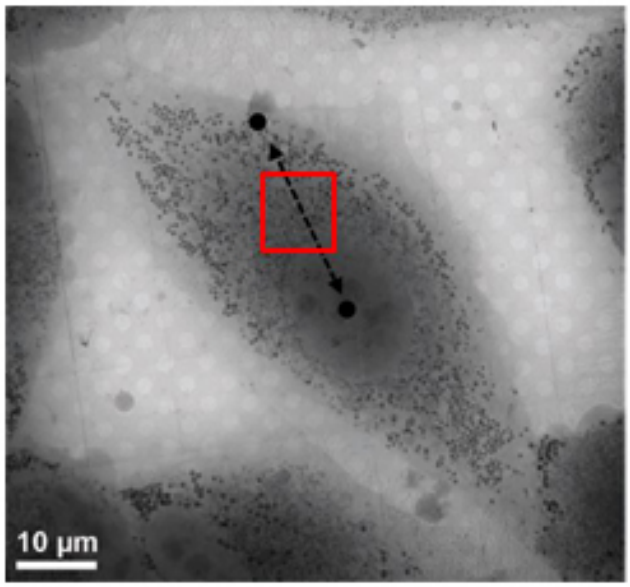

Figure 12.2 Low magnification X-ray tomography image of the cell at a 0° tilt angle. The red square shows the selected region for organelle quantification. In this case, the area of interest encompasses a region at the mid-way between the center of nucleus and the plasma membrane. Scale bar = 10 µm.

Vitrification via manual plunge freezer. The grid with attached cells was attached to a manual plunge freezer with a cryo-transfer holder. The grid was blotted by applying a hardened filter paper to the non-coated part of the grid for 2 sec to remove excess liquid around the cell, but not so long as to dry out the cell. The grid was dipped into liquid ethane for 8 sec and transferred to liquid nitrogen directly and stored there until data acquisition.

Evaluation of the freezing. The vitrified grids were prescreened with a fluorescence microscope equipped with a Linkam cryo stage to obtain a map of cells on the grids via a 5x objective, and also to evaluate the quality of freezing via 10x and 100x objectives. This helped to select the grids which contain a suitable ice layer, namely a 2-4 µm ice layer on top of the cell. This thickness of ice was sufficient to protect the cells against radiation damage during data acquisition, but also thin enough to allow sufficient X-ray penetration.

Data acquisition. The map of the cells on the grid from the cryo fluorescence microscope was used to efficiently find the cell of interest on the same grid during cryo SXT (Fig.12.1). Later, the cell of interest was examined on the X-ray microscope using 510 eV X-rays, either at BESSY II in Berlin or at ALBA in Barcelona, with typical exposure times of 1 - 4 sec. with tilt angles ranging either from -60° to +60° or -70° to +70°. A 40

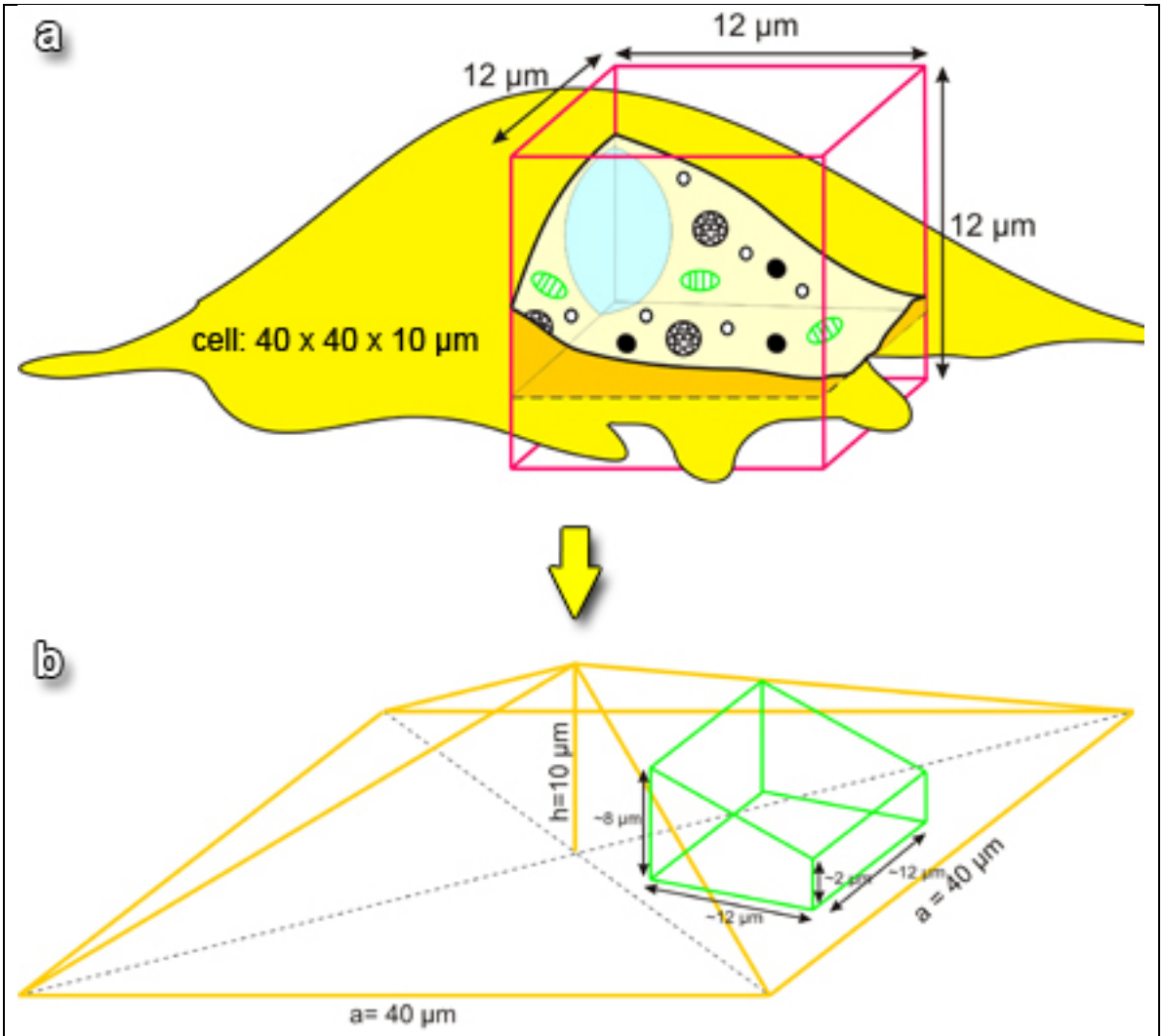

Figure 12.3 Schematic showing selection of the sub-volume used for quantification by cryo-SXT. A549 cells have approximate dimensions of 40 x 40 x 10 µm. Since the field of view of cryo-SXT is 12 x 12 x 12 µm, only a sub-region of the cell can be imaged (a). The volume of this sub-region (b) can be roughly calculated by approximating the shape of the cell as a pyramid (orange lines), and then computing the volume of the sub-region (green lines). This volume of interest corresponds approximately to 1/7 of the total cell volume.

nm zone plate was used for the dPGS nanoparticle experiments, and a 25 nm zone plate for the PEI nanoparticles experiments. After the tilt series, flat field corrections were recorded.

Data reconstruction. For reconstruction of the 3D volume, the images from each tilt angle later were aligned with Bsoft [448, 449, 503] and reconstructed via TomoJ [504, 505] via weighted back projection algorithm.

Quantification of organelles and nanoparticles from cryo SXT reconstructions. First, A549 cells were grown on multiple grids. Each grid was incubated either with dPGS or

PEI nanoparticles for different time periods as described above, and then the samples were vitrified and selected cells (Fig. 12.1) were imaged by cryo SXT. At least 6-19 reconstructions were obtained from selected cells at a series of different time points and for each of the two nanoparticle types. Typical reconstructions had a field of view of 12x12x12 μm (Fig.12.2, Fig.12.3a), which was not large enough to visualize an entire cell. To quantify nanoparticle localization within the cell, manual counts were performed in all focal planes of the 3D reconstruction. Since this is a time consuming and laborious practice, the sample size was limited to 4 out of 6-19 reconstructions at each time point. For consistency, cells were selected for counting only if the reconstruction contained a specific part of the cell, namely a region bordering the nuclear membrane and extending approximately halfway towards the plasma membrane (Fig. 12.2). Then, within this region either the number of nanoparticles within different organelles or the different types of organelles present within the 3D volume were counted. The quantified organelles were endosomes, multivesicular bodies, lysosomes, autophagic vacuoles, lipid droplets and mitochondria. Note that the sub-volume where the quantification was performed corresponds approximately to 1/7 of the total cell volume. This is calculated assuming that the 3D cell shape can be approximated as a pyramid with dimensions of (40 x 40 x 10 μm) (Fig. 12.3b).

13. APPENDIX

13.1. Effect of protein corona on dPGS nanoparticle uptake and trafficking

In Chapter 6, dPGS nanoparticle trafficking was investigated in the presence of serum which leads to formation of a protein corona, and a trafficking pathway was identified that mostly involved the endo/lysosomal pathway and autophagy, but also included some cytoplasmic escape and localization to lipid droplets. In this chapter, the cellular localization of dPGS nanoparticles was investigated in the absence of serum in order to understand the effect of serum on cellular trafficking of dPGS nanoparticles.

13.2 Motivation for understanding the effect of serum proteins on dPGS nanoparticles internalization

As discussed in the overview in Chapter 4 and also at the start of Chapter 6, nanoparticles develop a protein corona when they are exposed to any biological media. The corona arises because proteins within the media absorb to the surface of the nanoparticles. It is known that this corona can alter the behavior of the nanoparticles, including the cellular uptake efficiency, the cellular receptors to which nanoparticles bind [506, 507] and the uptake mechanism of nanoparticles [5, 276, 508, 509]. However, there is still no consensus about how the protein corona leads to these alterations, and so it is difficult to predict how the presence or absence of a corona will influence the behavior of the dPGS nanoparticles.

If dPGS would someday reach clinical approval, it might be used in different ways that could lead in some cases to the presence of serum proteins, and in other cases to the absence of serum proteins. For example, dPGS nanoparticles could be injected into the blood stream to treat arthritis of a joint, in which case serum proteins would attach on the nanoparticle surface. Alternatively, dPGS nanoparticles might be inhaled to treat asthma, in which case nanoparticles would not be exposed to serum proteins before they are internalized into cells. Thus it is of interest to examine how dPGS nanoparticles behave in the presence and the absence of serum proteins. This chapter then investigates how the absence of serum proteins influences the internalization rate of dPGS nanoparticles, the localization of dPGS nanoparticles in the cell and the uptake mechanism of dPGS nanoparticles.

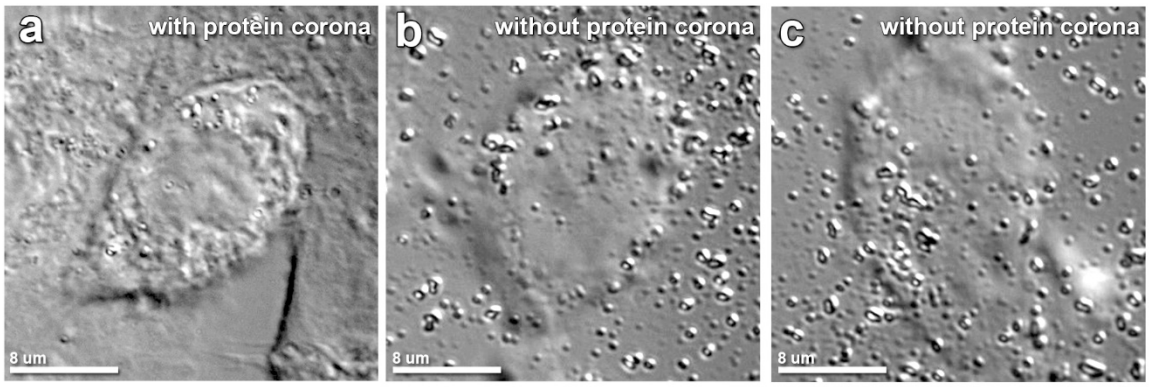

Figure 13.1 dPGS nanoparticle uptake in the presence and absence of serum. Cells were incubated with dPGS nanoparticles in the presence (a) and absence (b) of serum for 1 h. Considerably more nanoparticles interact with cells in the absence of serum (i.e. without protein corona)(b,c). Red arrows point to examples of nanoparticles. Scale bar = 10 μm.

To ensure that the dPGS nanoparticles do not contain serum proteins before they are internalized into cells, the nanoparticles were not pre-incubated with serum (as was done in Chapter 6), and furthermore serum was removed from the cell culture medium. This latter requirement constrained the experiments to a 1 h incubation time, since cell behavior begins to change when serum is omitted from the medium for longer times. Nevertheless, this 1 h time point enabled a direct comparison to the 1 h time point in the presence of serum already discussed in Chapter 6.

Unfortunately, cryo SXT data is obtained at the moment from only one cell in the absence of serum, and so further investigation is needed to confirm the observations reported in this chapter. These observations may be representative since consistent results were obtained from cell to cell in all of the other cryo SXT experiments in this thesis. One other caveat about the data in this chapter is that nanoparticles can acquire a protein corona once they get inside of the cell, so the observations in this Chapter reflect the behavior of nanoparticles which do not acquire serum proteins from the cell culture medium.

13.3 Nanoparticle internalization rate significantly increased in the absence of serum proteins

To understand the effect of the protein corona on the internalization rate of dPGS nanoparticles, Cells were incubated with the dPGS nanoparticles in the absence of serum for 1 h using a procedure similar to that previously described [457], and then nanoparticle uptake was monitored using DIC microscopy. Next, the internalization rate was compared

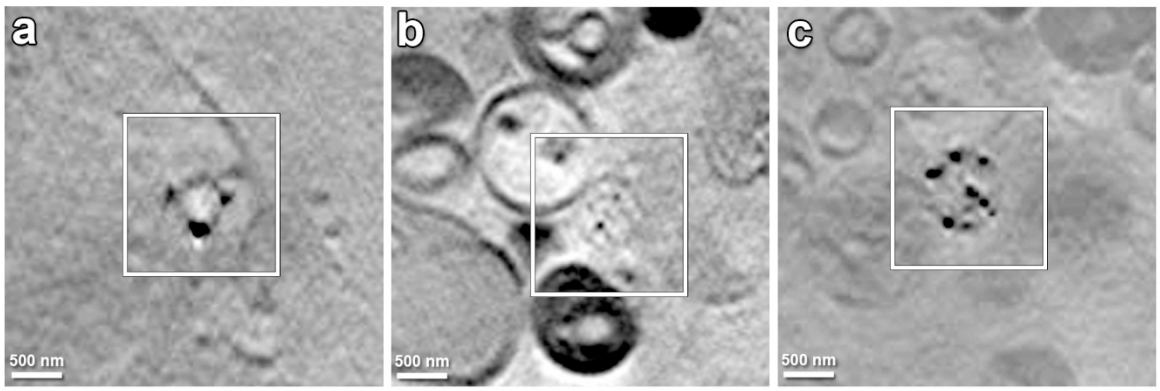

Figure 13.2 Endocytosis of dPGS nanoparticles in the absence of serum. dPGS nanoparticles were internalized via membrane pits with a coat (a) and enclosed into vesicles with a coat and X-ray lucent interior characteristic of clathrin- or caveolae-mediated endocytosis (b). The nanoparticles were also found in a small number of uncoated vesicles (c), characteristic of macropinocytosis. Scale bars = 500 nm.

to that measured after 1 h in the presence of serum (Chapter 6). Significantly more dPGS nanoparticles were found to be internalized by cells in the absence of serum (Fig. 13.1).

These results suggest that serum proteins in some way inhibit the uptake of dPGS nanoparticles. A simple model for this is that the protein corona partially obscures the sulfate moieties of dPGS. This model is consistent with the observation in Chapter 6 that dPG, which completely lacks the sulfate moiety, shows no uptake whatsoever and no interaction with the cells (Fig. 6.2g,h). This model is also consistent with the general model that proteins reduce the binding affinity of nanoparticles to the cell surface, thereby leading to reduced uptake [5, 219, 225, 226].

13.4 The predominant nanoparticle internalization pathway changes in the absence of the protein corona

As discussed in Chapter 6, dPGS nanoparticles in the presence of serum appeared to be internalized via two different pathways. As suggested in Chapter 6, the dominant endocytosis pathway might reflect macropinocytosis based on the presence of membrane ruffles (Fig. 6.4a,b) and the subsequent incorporation into uncoated vesicles with a diameter of 200 nm or greater (Fig. 6.4e). The data also suggested that the other pathway might reflect clathrin- or caveolae-mediated endocytosis based on the presence of omega shaped plasma membrane invaginations (Fig. 6.4b) and the subsequent formation of coated vesicles of 100 - 150 nm in diameter (Fig. 6.4d,f).

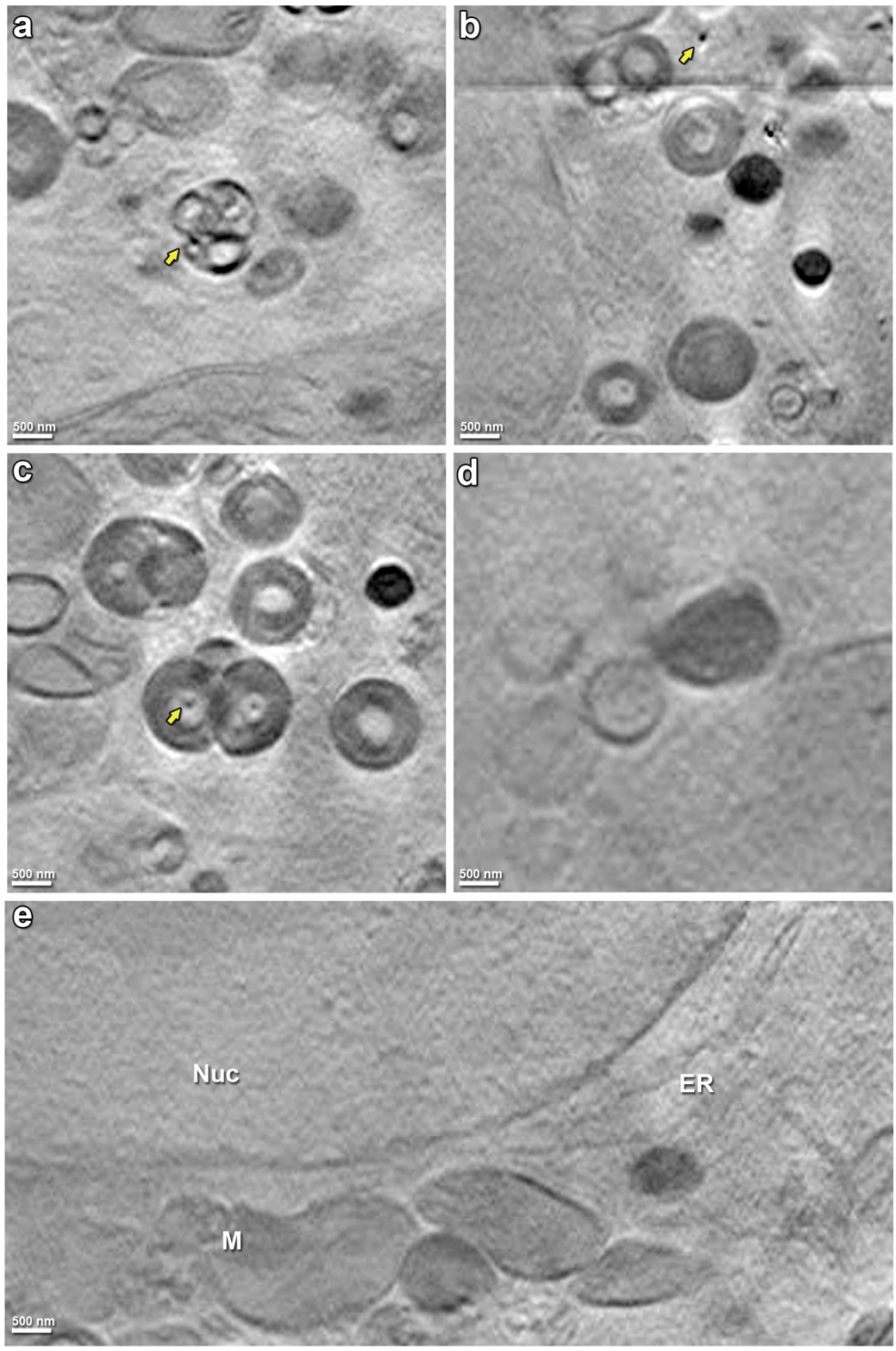

Figure 13.3 Intracellular location of dPGS nanoparticles in the absence of serum. Cells were incubated with dPGS nanoparticles in the absence of serum for 1 h. In addition to endosomes, a small number of dPGS nanoparticles were also found in multivesicular bodies (a) and free in the cytoplasm (b). The black dots inside the X-ray lucent region of autophagic vacuoles may also reflect dPGS nanoparticles (c). dPGS nanoparticles were not found in lysosomes (d), endoplasmic reticulum (ER), mitochondria (M) or in the nucleus (Nuc) (e). Scale bars = 500 nm.

To see if these routes were altered in the absence of the protein corona, cryo-SXT was used to examine a cell volume from a cell incubated for 1 h with dPGS nanoparticles.

Strikingly, in the absence of serum proteins, the predominant pathway was observed to switch from macropinocytosis to a putative caveolae- or clathrin-mediated endocytosis. Specifically, the formation of membrane ruffles associated with dPGS nanoparticles on the plasma membrane was not observed, and only 17% of the endocytic vesicles containing dPGS nanoparticles were found to be in putative macropinosomes, namely uncoated vesicles with diameters 200 nm and larger (Fig 13.2c). Therefore, it was concluded that macropinocytosis had reduced from 85% to 17%.

In contrast, in the absence of serum, dPGS nanoparticles were predominantly internalized via the second uptake pathway, the putative caveolae-mediated endocytosis pathway. Thus, dPGS nanoparticles were observed in omega-shaped membrane invaginations with a thin coat and they were mostly internalized into membrane vesicles with a consistent thin coat with diameters of 100 - 150 nm with a clear X-ray lucent interior (Fig 13.2a,b).

Thus these results demonstrate that the presence or absence of the protein corona can influence the uptake pathways of the nanoparticles. However, it is worth to note that the analysis is done only on one early time point and in one cell. To make sure that these changes are consistent, more experiments need to be performed.

13.5 Nanoparticle localization within the cell changes in the absence of a protein corona: lysosomes are bypassed

Given that an effect of the protein corona was seen on the endocytic uptake pathways, it was also of interest to determine whether this led to any effects on nanoparticle localization within the cell. In the absence of serum, nanoparticles were mostly found to localize to similar places in the cell after a 1 h incubation, namely to endosomes (Fig. 13.2b,c), multivesicular bodies(Fig. 13.3a), autophagosomes (Fig. 13.3c) and the cytoplasm (Fig. 13.3b), consistent with what was observed in the presence of serum in Chapter 6. The nanoparticles were not found in lipid droplets, but this was also the case in the presence of serum at the 1 h time point. dPGS nanoparticles were also not detected in

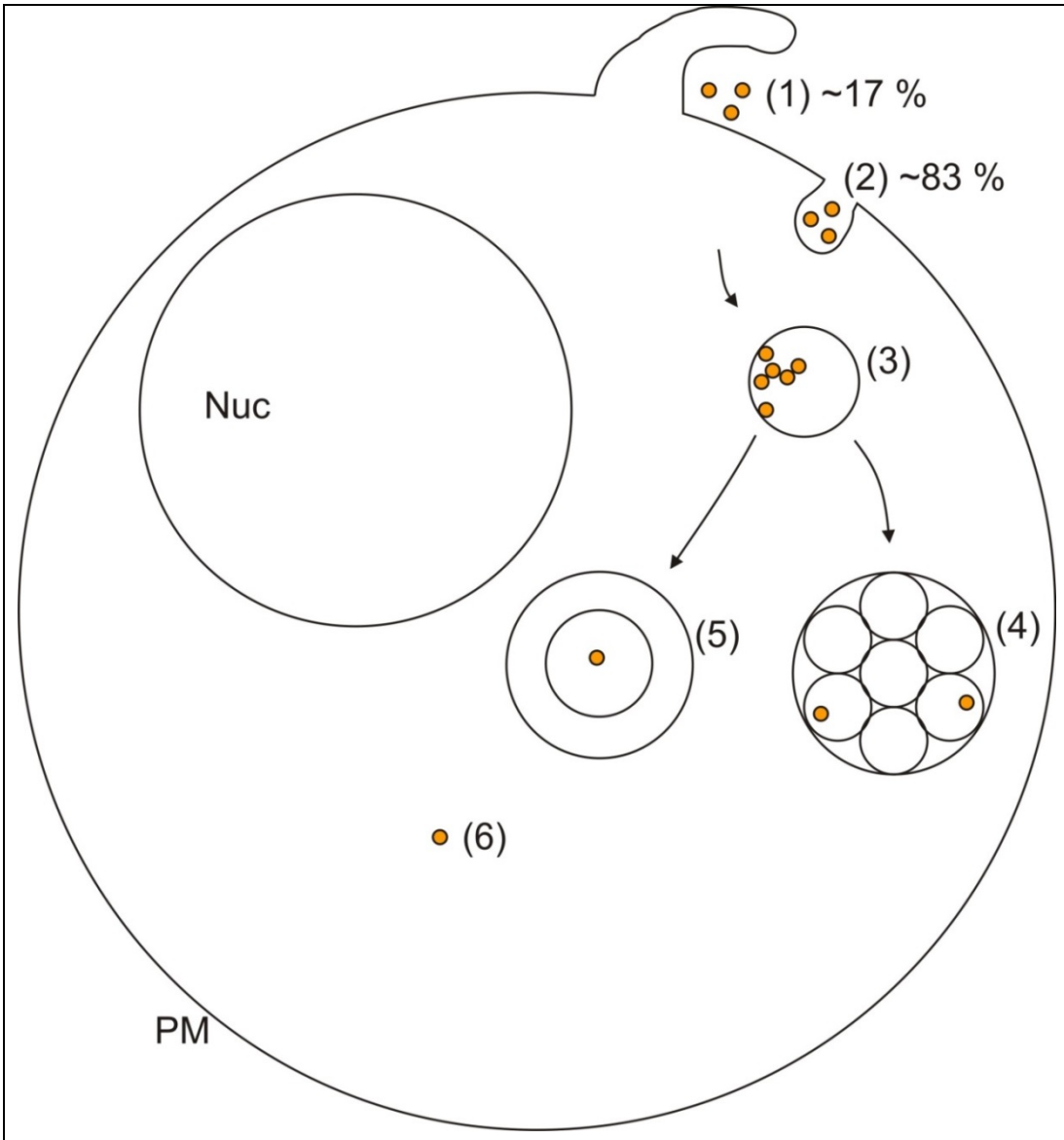

Figure 13.4 Model summarizing the findings about the endocytosis and intracellular trafficking pathway of dPGS nanoparticles in the absence of serum at the 1 h incubation time point. dPGS nanoparticles were endocytosed via at least two pathways (1,2), which may be macropinocytosis (1) and a clathrin- or caveolae-mediated endocytosis This suggests that the predominant endocytosis pathway switched from macropinocytosis in the presence of serum (Chapter 6) to a clathrin- or caveolae-mediated endocytosis in the absence of serum. In the absence of serum, the nanoparticles were first sorted to early endosomes (3). Later, dPGS nanoparticles were trafficked to multivesicular bodies (4) and autophagosomes (5), but no nanoparticles were detected in lysosomes, suggesting that in the absence of serum, dPGS nanoparticles bypass the lysosome. Note that nanoparticle numbers in multivesicular bodies (4) and autophagosomes (5) were limited. Additionally, cytoplasmic escape of dPGS nanoparticles in the absence of serum appeared to be less than what was observed in the presence of serum (6). At 1 h, the dPGS nanoparticles did not localize to lipid droplets, which was also the case at 1 h in the presence of serum. Later time points would be required to assess lipid droplet localization, and whether the nanoparticles might be excreted by MVB's.

ER, mitochondria or the nucleus, consistent with what was observed in the presence of serum (Fig. 13.3e).

One key difference in the absence of serum was that dPGS nanoparticles were not found in the lysosomes of this cell (Fig. 13.3d). These findings suggest that the protein corona has an effect on the intracellular trafficking of dPGS nanoparticles in the cell.

13.6 Summary

Whether the protein corona alters the endocytosis and intracellular trafficking pathway of dPGS nanoparticles was investigated. Endocytosis of dPGS nanoparticles was found to be shifted from macropinocytosis to a putative caveolae-mediated endocytosis pathway, which did not lead dPGS nanoparticles to lysosomes (Fig. 13.4). Note that a similar shift was observed with similar proportions for the PEI nanoparticles in Chapter 10 based there on the concentration of the nanoparticles. These observations suggest that nanoparticle behavior can be predictably altered by changing the physicochemical properties of the nanoparticles. However, the experiments reported in this chapter should be performed for more cells to confirm these findings.

REFERENCES

1. Buzea, C., I.I. Pacheco, and K. Robbie, *Nanomaterials and nanoparticles: Sources and toxicity.* Biointerphases, 2007. **2**(4): p. Mr17-Mr71.
2. Yameen, B., et al., *Insight into nanoparticle cellular uptake and intracellular targeting.* Journal of Controlled Release, 2014. **190**: p. 485-499.
3. Albanese, A., P.S. Tang, and W.C. Chan, *The effect of nanoparticle size, shape, and surface chemistry on biological systems.* Annu Rev Biomed Eng, 2012. **14**: p. 1-16.
4. Abadeer, N.S. and C.J. Murphy, *Recent Progress in Cancer Thermal Therapy Using Gold Nanoparticles.* Journal of Physical Chemistry C, 2016. **120**(9): p. 4691-4716.
5. Cheng, X.J., et al., *Protein Corona Influences Cellular Uptake of Gold Nanoparticles by Phagocytic and Nonphagocytic Cells in a Size-Dependent Manner.* Acs Applied Materials & Interfaces, 2015. **7**(37): p. 20568-20575.
6. Chithrani, B.D., A.A. Ghazani, and W.C. Chan, *Determining the size and shape dependence of gold nanoparticle uptake into mammalian cells.* Nano Lett, 2006. **6**(4): p. 662-8.
7. Jiang, W., et al., *Nanoparticle-mediated cellular response is size-dependent.* Nature Nanotechnology, 2008. **3**(3): p. 145-150.
8. Liu, X.S., et al., *Surface and Size Effects on Cell Interaction of Gold Nanoparticles with Both Phagocytic and Nonphagocytic Cells.* Langmuir, 2013. **29**(29): p. 9138-9148.
9. Duan, X.P. and Y.P. Li, *Physicochemical Characteristics of Nanoparticles Affect Circulation, Biodistribution, Cellular Internalization, and Trafficking.* Small, 2013. **9**(9-10): p. 1521-1532.
10. Drescher, D., et al., *Specific biomolecule corona is associated with ring-shaped organization of silver nanoparticles in cells.* Nanoscale, 2013. **5**(19): p. 9193-9198.
11. Sahay, G., D.Y. Alakhova, and A.V. Kabanov, *Endocytosis of nanomedicines.* Journal of Controlled Release, 2010. **145**(3): p. 182-195.
12. Vonnemann, J., et al., *Polyglycerolsulfate functionalized gold nanorods as optoacoustic signal nanoamplifiers for in vivo bioimaging of rheumatoid arthritis.* Theranostics, 2014. **4**(6): p. 629-41.
13. Song, W.J., et al., *Gold Nanoparticles Capped with Polyethyleneimine for Enhanced siRNA Delivery.* Small, 2010. **6**(2): p. 239-246.
14. Elbakry, A., et al., *Layer-by-Layer Assembled Gold Nanoparticles for siRNA Delivery.* Nano Letters, 2009. **9**(5): p. 2059-2064.
15. Min, Y.Z., et al., *Clinical Translation of Nanomedicine.* Chemical Reviews, 2015. **115**(19): p. 11147-11190.
16. Dykman, L.A. and N.G. Khlebtsov, *Gold Nanoparticles in Biology and Medicine: Recent Advances and Prospects.* Acta Naturae, 2011. **3**(2): p. 34-55.
17. Kim, E.Y., et al., *Recent advances in gold nanoparticle-based bioengineering applications.* Journal of Materials Chemistry B, 2015. **3**(43): p. 8433-8444.
18. Turk, H., R. Haag, and S. Alban, *Dendritic polyglycerol sulfates as new heparin analogues and potent inhibitors of the complement system.* Bioconjug Chem, 2004. **15**(1): p. 162-7.
19. Dernedde, J., et al., *Dendritic polyglycerol sulfates as multivalent inhibitors of inflammation.* Proc Natl Acad Sci U S A, 2010. **107**(46): p. 19679-84.
20. Weinhart, M., et al., *Synthesis of dendritic polyglycerol anions and their efficiency toward L-selectin inhibition.* Biomacromolecules, 2011. **12**(7): p. 2502-11.
21. Maysinger, D., et al., *Dendritic Polyglycerol Sulfate Inhibits Microglial Activation and Reduces Hippocampal CA1 Dendritic Spine Morphology Deficits.* Biomacromolecules, 2015. **16**(9): p. 3073-82.

22. Bewersdorff, T., et al., *The influence of surface charge on serum protein interaction and cellular uptake: studies with dendritic polyglycerols and dendritic polyglycerol-coated gold nanoparticles.* Int J Nanomedicine, 2017. **12**: p. 2001-2019.
23. Heek, T., et al., *Synthesis, Photophysical, and Biological Evaluation of Sulfated Polyglycerol Dendronized Perylenebisimides (PBIs)-A Promising Platform for Anti-Inflammatory Theranostic Agents?* Bioconjugate Chemistry, 2016. **27**(3): p. 727-736.
24. Groger, D., et al., *Synthesis and biological evaluation of radio and dye labeled amino functionalized dendritic polyglycerol sulfates as multivalent anti-inflammatory compounds.* Bioconjug Chem, 2013. **24**(9): p. 1507-14.
25. Licha, K., et al., *Fluorescence imaging with multifunctional polyglycerol sulfates: novel polymeric near-IR probes targeting inflammation.* Bioconjug Chem, 2011. **22**(12): p. 2453-60.
26. Paulus, F., et al., *Structure related transport properties and cellular uptake of hyperbranched polyglycerol sulfates with hydrophobic cores.* Polymer Chemistry, 2014. **5**(17): p. 5020-5028.
27. Heek, T., et al., *Synthesis, Photophysical, and Biological Evaluation of Sulfated Polyglycerol Dendronized Perylenebisimides (PBIs)--A Promising Platform for Anti-Inflammatory Theranostic Agents?* Bioconjug Chem, 2016. **27**(3): p. 727-36.
28. Zhong, Y., et al., *Micelles with Sheddable Dendritic Polyglycerol Sulfate Shells Show Extraordinary Tumor Targetability and Chemotherapy in Vivo.* ACS Appl Mater Interfaces, 2016.
29. Dey, P., et al., *Mimicking of Chondrocyte Microenvironment Using In Situ Forming Dendritic Polyglycerol Sulfate-Based Synthetic Polyanionic Hydrogels.* Macromol Biosci, 2016. **16**(4): p. 580-90.
30. Chen, Q.Z., et al., *An elastomeric patch derived from poly(glycerol sebacate) for delivery of embryonic stem cells to the heart.* Biomaterials, 2010. **31**(14): p. 3885-93.
31. Sousa-Herves, A., et al., *Dendritic polyglycerol sulfate as a novel platform for paclitaxel delivery: pitfalls of ester linkage.* Nanoscale, 2015. **7**(9): p. 3923-32.
32. Yen, J., L.C. Yin, and J.J. Cheng, *Enhanced non-viral gene delivery to human embryonic stem cells via small molecule-mediated transient alteration of the cell structure.* Journal of Materials Chemistry B, 2014. **2**(46): p. 8098-8105.
33. Won, Y.Y., R. Sharma, and S.F. Konieczny, *Missing pieces in understanding the intracellular trafficking of polycation/DNA complexes.* Journal of Controlled Release, 2009. **139**(2): p. 88-93.
34. Ding, Y., et al., *Gold Nanoparticles for Nucleic Acid Delivery.* Molecular Therapy, 2014. **22**(6): p. 1075-1083.
35. Behr, J.P., *The proton sponge: A trick to enter cells the viruses did not exploit.* Chimia, 1997. **51**(1-2): p. 34-36.
36. Thomas, M. and A.M. Klibanov, *Conjugation to gold nanoparticles enhances polyethylenimine's transfer of plasmid DNA into mammalian cells.* Proceedings of the National Academy of Sciences of the United States of America, 2003. **100**(16): p. 9138-9143.
37. van der Aa, M.A., et al., *Cellular uptake of cationic polymer-DNA complexes via caveolae plays a pivotal role in gene transfection in COS-7 cells.* Pharm Res, 2007. **24**(8): p. 1590-8.
38. Huth, S., et al., *Insights into the mechanism of magnetofection using PEI-based magnetofectins for gene transfer.* Journal of Gene Medicine, 2004. **6**(8): p. 923-936.
39. Rejman, J., A. Bragonzi, and M. Conese, *Role of clathrin- and caveolae-mediated endocytosis in gene transfer mediated by lipo- and polyplexes.* Molecular Therapy, 2005. **12**(3): p. 468-474.

40. Grosse, S., et al., *Potocytosis and cellular exit of complexes as cellular pathways for gene delivery by polycations.* Journal of Gene Medicine, 2005. **7**(10): p. 1275-1286.
41. Hufnagel, H., et al., *Fluid Phase Endocytosis Contributes to Transfection of DNA by PEI-25.* Molecular Therapy, 2009. **17**(8): p. 1411-1417.
42. Das, J., et al., *Efficient delivery of C/EBP beta gene into human mesenchymal stem cells via polyethylenimine-coated gold nanoparticles enhances adipogenic differentiation (vol 6, 33784, 2016).* Scientific Reports, 2016. **6**.
43. Rehman, Z.U., D. Hoekstra, and I.S. Zuhorn, *Mechanism of Polyplex- and Lipoplex-Mediated Delivery of Nucleic Acids: Real-Time Visualization of Transient Membrane Destabilization without Endosomal Lysis.* Acs Nano, 2013. **7**(5): p. 3767-3777.
44. Benjaminsen, R.V., et al., *The Possible "Proton Sponge" Effect of Polyethylenimine (PEI) Does Not Include Change in Lysosomal pH.* Molecular Therapy, 2013. **21**(1): p. 149-157.
45. Bieber, T., et al., *Intracellular route and transcriptional competence of polyethylenimine-DNA complexes.* Journal of Controlled Release, 2002. **82**(2-3): p. 441-454.
46. Ferrati, S., et al., *Cellular communication via nanoparticle-transporting biovesicles.* Nanomedicine, 2014. **9**(5): p. 581-592.
47. Bieber, T., et al., *Intracellular route and transcriptional competence of polyethylenimine-DNA complexes.* J Control Release, 2002. **82**(2-3): p. 441-54.
48. Godbey, W.T., K.K. Wu, and A.G. Mikos, *Tracking the intracellular path of poly(ethylenimine)/DNA complexes for gene delivery.* Proc Natl Acad Sci U S A, 1999. **96**(9): p. 5177-81.
49. Akinc, A., et al., *Exploring polyethylenimine-mediated DNA transfection and the proton sponge hypothesis.* Journal of Gene Medicine, 2005. **7**(5): p. 657-663.
50. Godbey, W.T., et al., *Poly(ethylenimine)-mediated transfection: A new paradigm for gene delivery.* Journal of Biomedical Materials Research, 2000. **51**(3): p. 321-328.
51. Hu, C., et al., *Low Molecular Weight Polyethylenimine Conjugated Gold Nanoparticles as Efficient Gene Vectors.* Bioconjugate Chemistry, 2010. **21**(5): p. 836-843.
52. Ye, D., et al., *Immunogold labeling reveals subcellular localisation of silica nanoparticles in a human blood-brain barrier model.* Nanoscale, 2015. **7**(22): p. 10050-10058.
53. Gilleron, J., et al., *Image-based analysis of lipid nanoparticle-mediated siRNA delivery, intracellular trafficking and endosomal escape.* Nat Biotechnol, 2013. **31**(7): p. 638-46.
54. Srikar, R., et al., *Three-Dimensional Nanocomposites: Fluidics Driven Assembly of Metal Nanoparticles on Protein Nanostructures and Their Cell-Line-Dependent Intracellular Trafficking Pattern.* Langmuir, 2016. **32**(19): p. 4877-4885.
55. Chu, Z.Q., et al., *Unambiguous observation of shape effects on cellular fate of nanoparticles.* Scientific Reports, 2014. **4**.
56. Chu, Z., et al., *Rapid endosomal escape of prickly nanodiamonds: implications for gene delivery.* Sci Rep, 2015. **5**: p. 11661.
57. Weston, A.E., H.E. Armer, and L.M. Collinson, *Towards native-state imaging in biological context in the electron microscope.* J Chem Biol, 2009. **3**(3): p. 101-12.
58. Yusuf, M., et al., *Procedures for cryogenic X-ray ptychographic imaging of biological samples.* IUCrJ, 2017. **4**(Pt 2): p. 147-151.
59. Tantra, R. and A. Knight, *Cellular uptake and intracellular fate of engineered nanoparticles: A review on the application of imaging techniques.* Nanotoxicology, 2011. **5**(3): p. 381-392.
60. Benyair, R. and G.Z. Lederkremer, *Common fixation-permeabilization methods cause artifactual localization of a type II transmembrane protein.* Microscopy, 2016. **65**(6): p. 517-521.
61. Ott, C. and J. Lippincott-Schwartz, *Visualization of live primary cilia dynamics using fluorescence microscopy.* Curr Protoc Cell Biol, 2012. **Chapter 4**: p. Unit 4 26.

62. Schneider, G., et al., *Three-dimensional cellular ultrastructure resolved by X-ray microscopy.* Nature Methods, 2010. **7**(12): p. 985-U116.
63. Muller, W.G., et al., *Towards an atlas of mammalian cell ultrastructure by cryo soft X-ray tomography.* J Struct Biol, 2012. **177**(2): p. 179-92.
64. Kroemer, G., et al., *Classification of cell death: recommendations of the Nomenclature Committee on Cell Death 2009.* Cell Death and Differentiation, 2009. **16**(1): p. 3-11.
65. Tinari, A., et al., *Analyzing morphological and ultrastructural features in cell death.* Programmed Cell Death, General Principles for Studying Cell Death, Pt A, 2008. **442**: p. 1-26.
66. Ma, X., et al., *Colloidal Gold Nanoparticles Induce Changes in Cellular and Subcellular Morphology.* ACS Nano, 2017.
67. Astruc, D., *Introduction to Nanomedicine.* Molecules, 2016. **21**(1).
68. Min, Y.J., et al., *The role of interparticle and external forces in nanoparticle assembly.* Nature Materials, 2008. **7**(7): p. 527-538.
69. Pelaz, B., et al., *Diverse Applications of Nanomedicine.* Acs Nano, 2017. **11**(3): p. 2313-2381.
70. Anselmo, A.C. and S. Mitragotri, *A Review of Clinical Translation of Inorganic Nanoparticles.* Aaps Journal, 2015. **17**(5): p. 1041-1054.
71. Rogosnitzky, M. and S. Branch, *Gadolinium-based contrast agent toxicity: a review of known and proposed mechanisms.* Biometals, 2016. **29**(3): p. 365-76.
72. Chen, H.Y., M.M. Rogalski, and J.N. Anker, *Advances in functional X-ray imaging techniques and contrast agents.* Physical Chemistry Chemical Physics, 2012. **14**(39): p. 13469-13486.
73. Wang, H., et al., *Folic acid-modified dendrimer-entrapped gold nanoparticles as nanoprobes for targeted CT imaging of human lung adencarcinoma.* Biomaterials, 2013. **34**(2): p. 470-480.
74. Sun, I.C., et al., *Heparin-Coated Gold Nanoparticles for Liver-Specific CT Imaging.* Chemistry-a European Journal, 2009. **15**(48): p. 13341-13347.
75. Zhou, Z.J., et al., *Folic acid-conjugated silica capped gold nanoclusters for targeted fluorescence/X-ray computed tomography imaging.* Journal of Nanobiotechnology, 2013. **11**.
76. Cormode, D.P., et al., *Atherosclerotic Plaque Composition: Analysis with Multicolor CT and Targeted Gold Nanoparticles.* Radiology, 2010. **256**(3): p. 774-782.
77. Chinen, A.B., et al., *Nanoparticle Probes for the Detection of Cancer Biomarkers, Cells, and Tissues by Fluorescence.* Chem Rev, 2015. **115**(19): p. 10530-74.
78. MacLaughlin, C.M., et al., *Surface-Enhanced Raman Scattering Dye-Labeled Au Nanoparticles for Triplexed Detection of Leukemia and Lymphoma Cells and SERS Flow Cytometry.* Langmuir, 2013. **29**(6): p. 1908-1919.
79. Bilan, R., et al., *Quantum-dot-based suspension microarray for multiplex detection of lung cancer markers: preclinical validation and comparison with the Luminex xMAP(R) system.* Sci Rep, 2017. **7**: p. 44668.
80. Dong, H.F., et al., *Multifunctional Poly(L-lactide)-Polyethylene Glycol-Grafted Graphene Quantum Dots for Intracellular MicroRNA Imaging and Combined Specific-Gene-Targeting Agents Delivery for Improved Therapeutics.* Acs Applied Materials & Interfaces, 2015. **7**(20): p. 11015-11023.
81. Nagasaki, Y., et al., *Novel molecular recognition via fluorescent resonance energy transfer using a biotin-PEG/polyamine stabilized CdS quantum dot.* Langmuir, 2004. **20**(15): p. 6396-400.
82. Dong, H., et al., *Multifunctional Poly(L-lactide)-Polyethylene Glycol-Grafted Graphene Quantum Dots for Intracellular MicroRNA Imaging and Combined Specific-Gene-*

Targeting Agents Delivery for Improved Therapeutics. ACS Appl Mater Interfaces, 2015. **7**(20): p. 11015-23.
83. Cheng, W., et al., *Cascade signal amplification strategy for subattomolar protein detection by rolling circle amplification and quantum dots tagging.* Anal Chem, 2010. **82**(8): p. 3337-42.
84. van Tilborg, G.A., et al., *Annexin A5-conjugated quantum dots with a paramagnetic lipidic coating for the multimodal detection of apoptotic cells.* Bioconjug Chem, 2006. **17**(4): p. 865-8.
85. Kneipp, J., *Interrogating Cells, Tissues, and Live Animals with New Generations of Surface-Enhanced Raman Scattering Probes and Labels.* Acs Nano, 2017. **11**(2): p. 1136-1141.
86. McQueenie, R., et al., *Detection of inflammation in vivo by surface-enhanced Raman scattering provides higher sensitivity than conventional fluorescence imaging.* Anal Chem, 2012. **84**(14): p. 5968-75.
87. Matschulat, A., D. Drescher, and J. Kneipp, *Surface-enhanced Raman scattering hybrid nanoprobe multiplexing and imaging in biological systems.* ACS Nano, 2010. **4**(6): p. 3259-69.
88. Mura, S., J. Nicolas, and P. Couvreur, *Stimuli-responsive nanocarriers for drug delivery.* Nat Mater, 2013. **12**(11): p. 991-1003.
89. Han, H.S., et al., *Gold-Nanoclustered Hyaluronan Nano-Assemblies for Photothermally Maneuvered Photodynamic Tumor Ablation.* ACS Nano, 2016. **10**(12): p. 10858-10868.
90. Sercombe, L., et al., *Advances and Challenges of Liposome Assisted Drug Delivery.* Front Pharmacol, 2015. **6**: p. 286.
91. Hua, S. and S.Y. Wu, *The use of lipid-based nanocarriers for targeted pain therapies.* Frontiers in Pharmacology, 2013. **4**.
92. Sercombe, L., et al., *Advances and Challenges of Liposome Assisted Drug Delivery.* Frontiers in Pharmacology, 2015. **6**.
93. Gabizon, A., et al., *In vivo fate of folate-targeted polyethylene-glycol liposomes in tumor-bearing mice.* Clinical Cancer Research, 2003. **9**(17): p. 6551-6559.
94. Hua, S. and P.J. Cabot, *Targeted Nanoparticles that Mimic Immune Cells in Pain Control Inducing Analgesic and Anti-inflammatory Actions: A Potential Novel Treatment of Acute and Chronic Pain Conditions.* Pain Physician, 2013. **16**(3): p. E199-E216.
95. Huang, X.H., et al., *Gold nanoparticles: interesting optical properties and recent applications in cancer diagnostic and therapy.* Nanomedicine, 2007. **2**(5): p. 681-693.
96. Jain, P.K., et al., *Calculated absorption and scattering properties of gold nanoparticles of different size, shape, and composition: Applications in biological imaging and biomedicine.* Journal of Physical Chemistry B, 2006. **110**(14): p. 7238-7248.
97. Anker, J.N., et al., *Biosensing with plasmonic nanosensors.* Nature Materials, 2008. **7**(6): p. 442-453.
98. Lane, L.A., X.M. Qian, and S.M. Nie, *SERS Nanoparticles in Medicine: From Label-Free Detection to Spectroscopic Tagging.* Chemical Reviews, 2015. **115**(19): p. 10489-10529.
99. Hu, W.Q., et al., *Surface plasmon resonance and field enhancement in #-shaped gold wires metamaterial.* Optics Express, 2009. **17**(24): p. 21843-21849.
100. Polte, J., *Fundamental growth principles of colloidal metal nanoparticles - a new perspective.* Crystengcomm, 2015. **17**(36): p. 6809-6830.
101. Behari, J., *Principles of nanoscience: An overview.* Indian Journal of Experimental Biology, 2010. **48**(10): p. 1008-1019.
102. Turkevich, J., P.C. Stevenson, and J. Hillier, *A Study of the Nucleation and Growth Processes in the Synthesis of Colloidal Gold.* Discussions of the Faraday Society, 1951(11): p. 55-&.

103. Vonnemann, J., et al., *Size dependence of steric shielding and multivalency effects for globular binding inhibitors.* J Am Chem Soc, 2015. **137**(7): p. 2572-9.
104. Nakamura, Y., et al., *Nanodrug Delivery: Is the Enhanced Permeability and Retention Effect Sufficient for Curing Cancer?* Bioconjugate Chemistry, 2016. **27**(10): p. 2225-2238.
105. Giner-Casares, J.J., et al., *Inorganic nanoparticles for biomedicine: where materials scientists meet medical research.* Materials Today, 2016. **19**(1): p. 19-28.
106. Juliano, R.L., *The delivery of therapeutic oligonucleotides.* Nucleic Acids Res, 2016. **44**(14): p. 6518-48.
107. Danhier, F., O. Feron, and V. Preat, *To exploit the tumor microenvironment: Passive and active tumor targeting of nanocarriers for anti-cancer drug delivery.* Journal of Controlled Release, 2010. **148**(2): p. 135-146.
108. Morachis, J.M., E.A. Mahmoud, and A. Almutairi, *Physical and Chemical Strategies for Therapeutic Delivery by Using Polymeric Nanoparticles.* Pharmacological Reviews, 2012. **64**(3): p. 505-519.
109. Vonnemann, J., et al., *Polyglycerolsulfate Functionalized Gold Nanorods as Optoacoustic Signal Nanoamplifiers for In Vivo Bioimaging of Rheumatoid Arthritis.* Theranostics, 2014. **4**(6): p. 629-641.
110. Vonnemann, J., et al., *Virus inhibition induced by polyvalent nanoparticles of different sizes.* Nanoscale, 2014. **6**(4): p. 2353-2360.
111. Fernandez-Sanles, A., et al., *Functional Information Stored in the Conserved Structural RNA Domains of Flavivirus Genomes.* Frontiers in Microbiology, 2017. **8**.
112. Zhang, Z.W., et al., *Conjugating folic acid to gold nanoparticles through glutathione for targeting and detecting cancer cells.* Bioorganic & Medicinal Chemistry, 2010. **18**(15): p. 5528-5534.
113. Tabas, I. and C.K. Glass, *Anti-Inflammatory Therapy in Chronic Disease: Challenges and Opportunities.* Science, 2013. **339**(6116): p. 166-172.
114. Heneka, M.T., et al., *Neuroinflammation in Alzheimer's disease.* Lancet Neurology, 2015. **14**(4): p. 388-405.
115. Mantovani, A., et al., *Cancer-related inflammation.* Nature, 2008. **454**(7203): p. 436-444.
116. Donath, M.Y., *Targeting inflammation in the treatment of type 2 diabetes: time to start.* Nature Reviews Drug Discovery, 2014. **13**(6): p. 465-476.
117. Karin, M., T. Lawrence, and V. Nizet, *Innate immunity gone awry: Linking microbial infections to chronic inflammation and cancer.* Cell, 2006. **124**(4): p. 823-835.
118. Pearlman, D.S., *Pathophysiology of the inflammatory response.* Journal of Allergy and Clinical Immunology, 1999. **104**(4): p. S132-S137.
119. Brochner, A.C. and P. Toft, *Pathophysiology of the systemic inflammatory response after major accidental trauma.* Scandinavian Journal of Trauma Resuscitation & Emergency Medicine, 2009. **17**.
120. Levi, M. and T. van der Poll, *Inflammation and coagulation.* Critical Care Medicine, 2010. **38**(2): p. S26-S34.
121. Cruz-Adalia, A., et al., *T cells kill bacteria captured by transinfection from dendritic cells and confer protection in mice.* Cell Host Microbe, 2014. **15**(5): p. 611-22.
122. Stevenson, R., et al., *Nanoparticles and Inflammation.* Thescientificworldjournal, 2011. **11**: p. 1300-1312.
123. Daniels, R., *Surviving the first hours in sepsis: getting the basics right (an intensivist's perspective).* Journal of Antimicrobial Chemotherapy, 2011. **66**: p. Ii11-Ii23.
124. Johnson, S.B., et al., *Gene expression profiles differentiate between sterile SIRS and early sepsis.* Annals of Surgery, 2007. **245**(4): p. 611-621.
125. Sanz, J. and Z.A. Fayad, *Imaging of atherosclerotic cardiovascular disease.* Nature, 2008. **451**(7181): p. 953-957.

126. Bjarnason, I., et al., *Side effects of nonsteroidal anti-inflammatory drugs on the small and large intestine in humans.* Gastroenterology, 1993. **104**(6): p. 1832-47.
127. Schacke, H., W.D. Docke, and K. Asadullah, *Mechanisms involved in the side effects of glucocorticoids.* Pharmacol Ther, 2002. **96**(1): p. 23-43.
128. Nosratabadi, R., et al., *Hyperforin-loaded gold nanoparticle alleviates experimental autoimmune encephalomyelitis by suppressing Th1 and Th17 cells and upregulating regulatory T cells.* Nanomedicine, 2016. **12**(7): p. 1961-1971.
129. Hua, S., *Targeting sites of inflammation: intercellular adhesion molecule-1 as a target for novel inflammatory therapies.* Frontiers in Pharmacology, 2013. **4**.
130. Cormode, D.P., et al., *Nanocrystal Core High-Density Lipoproteins: A Multimodality Contrast Agent Platform.* Nano Letters, 2008. **8**(11): p. 3715-3723.
131. Cormode, D.P., et al., *Atherosclerotic plaque composition: analysis with multicolor CT and targeted gold nanoparticles.* Radiology, 2010. **256**(3): p. 774-82.
132. Wilson, D.S., et al., *Orally delivered thioketal nanoparticles loaded with TNF-alpha-siRNA target inflammation and inhibit gene expression in the intestines.* Nature Materials, 2010. **9**(11): p. 923-928.
133. Lee, H., et al., *Synthesis, characterization, and in vivo diagnostic applications of hyaluronic acid immobilized gold nanoprobes.* Biomaterials, 2008. **29**(35): p. 4709-18.
134. Sul, O.J., et al., *Gold nanoparticles inhibited the receptor activator of nuclear factor-kappab ligand (RANKL)-induced osteoclast formation by acting as an antioxidant.* Biosci Biotechnol Biochem, 2010. **74**(11): p. 2209-13.
135. Chen, H., et al., *In vivo study of spherical gold nanoparticles: inflammatory effects and distribution in mice.* PLoS One, 2013. **8**(2): p. e58208.
136. Bhattacharya, R., et al., *Gold nanoparticles inhibit VEGF165-induced proliferation of HUVEC cells.* Nano Letters, 2004. **4**(12): p. 2479-2481.
137. Lee, H., et al., *Hyaluronate-gold nanoparticle/tocilizumab complex for the treatment of rheumatoid arthritis.* ACS Nano, 2014. **8**(5): p. 4790-8.
138. Ju, Y., et al., *Improving Targeting of Metal-Phenolic Capsules by the Presence of Protein Coronas.* ACS Appl Mater Interfaces, 2016. **8**(35): p. 22914-22.
139. Khan, H.A., et al., *Transient increase in IL-1beta, IL-6 and TNF-alpha gene expression in rat liver exposed to gold nanoparticles.* Genet Mol Res, 2013. **12**(4): p. 5851-7.
140. Reynolds, P.R., et al., *Detection of vascular expression of E-selectin in vivo with MR imaging.* Radiology, 2006. **241**(2): p. 469-76.
141. Ma, S., et al., *E-selectin-targeting delivery of microRNAs by microparticles ameliorates endothelial inflammation and atherosclerosis.* Sci Rep, 2016. **6**: p. 22910.
142. Southworth, R., et al., *Renal vascular inflammation induced by Western diet in ApoE-null mice quantified by (19)F NMR of VCAM-1 targeted nanobeacons.* Nanomedicine, 2009. **5**(3): p. 359-67.
143. Zern, B.J., et al., *Reduction of nanoparticle avidity enhances the selectivity of vascular targeting and PET detection of pulmonary inflammation.* ACS Nano, 2013. **7**(3): p. 2461-9.
144. Shao, X., et al., *I-125-Labeled Gold Nanorods for Targeted Imaging of Inflammation.* Acs Nano, 2011. **5**(11): p. 8967-8973.
145. Dong, X., D. Chu, and Z. Wang, *Leukocyte-mediated Delivery of Nanotherapeutics in Inflammatory and Tumor Sites.* Theranostics, 2017. **7**(3): p. 751-763.
146. Koeberle, A., et al., *Hyperforin, an Anti-Inflammatory Constituent from St. John's Wort, Inhibits Microsomal Prostaglandin E(2) Synthase-1 and Suppresses Prostaglandin E(2) Formation in vivo.* Front Pharmacol, 2011. **2**: p. 7.
147. Lorusso, G., et al., *Mechanisms of Hyperforin as an anti-angiogenic angioprevention agent.* Eur J Cancer, 2009. **45**(8): p. 1474-84.

148. Dernedde, J., et al., *Dendritic polyglycerol sulfates as multivalent inhibitors of inflammation.* Proceedings of the National Academy of Sciences of the United States of America, 2010. **107**(46): p. 19679-19684.
149. Wu, Y., K. Briley, and X. Tao, *Nanoparticle-based imaging of inflammatory bowel disease.* Wiley Interdiscip Rev Nanomed Nanobiotechnol, 2016. **8**(2): p. 300-15.
150. Wang, H., et al., *Prevention of acute vascular rejection by a functionally blocking anti-C5 monoclonal antibody combined with cyclosporine.* Transplantation, 2005. **79**(9): p. 1121-7.
151. Khullar, P., et al., *Bovine Serum Albumin Bioconjugated Gold Nanoparticles: Synthesis, Hemolysis, and Cytotoxicity toward Cancer Cell Lines.* Journal of Physical Chemistry C, 2012. **116**(15): p. 8834-8843.
152. Mastrobattista, E., et al., *Cellular uptake of liposomes targeted to intercellular adhesion molecule-1 (ICAM-1) on bronchial epithelial cells.* Biochimica Et Biophysica Acta-Biomembranes, 1999. **1419**(2): p. 353-363.
153. Sakhalkar, H.S., et al., *Leukocyte-inspired biodegradable particles that selectively and avidly adhere to inflamed endothelium in vitro and in vivo.* Proc Natl Acad Sci U S A, 2003. **100**(26): p. 15895-900.
154. Nordmeyer, D., et al., *Iron oxide nanoparticles stabilized with dendritic polyglycerols as selective MRI contrast agents.* Nanoscale, 2014. **6**(16): p. 9646-9654.
155. Reimann, S., et al., *Shell Cleavable Dendritic Polyglycerol Sulfates Show High Anti-Inflammatory Properties by Inhibiting L-Selectin Binding and Complement Activation.* Advanced Healthcare Materials, 2015. **4**(14): p. 2154-2162.
156. Schneider, T., et al., *Effects of dendritic polyglycerol sulfate on articular chondrocytes.* Inflammation Research, 2015. **64**(11): p. 917-928.
157. Turk, H., R. Haag, and S. Alban, *Dendritic polyglycerol sulfates as new heparin analogues and potent inhibitors of the complement system.* Bioconjugate Chemistry, 2004. **15**(1): p. 162-167.
158. Weinhart, M., et al., *Synthesis of Dendritic Polyglycerol Anions and Their Efficiency Toward L-Selectin Inhibition.* Biomacromolecules, 2011. **12**(7): p. 2502-2511.
159. Quadir, M.A. and R. Haag, *Biofunctional nanosystems based on dendritic polymers.* Journal of Controlled Release, 2012. **161**(2): p. 484-495.
160. Groger, D., et al., *Synthesis and Biological Evaluation of Radio and Dye Labeled Amino Functionalized Dendritic Polyglycerol Sulfates as Multivalent Anti-Inflammatory Compounds.* Bioconjugate Chemistry, 2013. **24**(9): p. 1507-1514.
161. Virginia Wycisk, K.A., Paul Hillmann, Ole Hirsch, Christian Kuehne, Jens Dernedde; Rainer Haag, Kai Licha, *Responsive Contrast Agents: Synthesis and Characterization of a Tunable Series of pH-Sensitive Near_Infrared Pentamethines.* ACS Omega, 2016. **1**(5): p. 808-817.
162. Holzhausen, C., et al., *Biodistribution, cellular localization, and in vivo tolerability of S-35-labeled antiinflammatory dendritic polyglycerol sulfate amine.* Journal of Nanoparticle Research, 2015. **17**(3).
163. Pant, K., et al., *Synthesis and Biodistribution Studies of H-3- and Cu-64-Labeled Dendritic Polyglycerol and Dendritic Polyglycerol Sulfate.* Bioconjugate Chemistry, 2015. **26**(5): p. 906-918.
164. Licha, K., et al., *Fluorescence Imaging with Multifunctional Polyglycerol Sulfates: Novel Polymeric near-IR Probes Targeting Inflammation.* Bioconjugate Chemistry, 2011. **22**(12): p. 2453-2460.
165. Biffi, S., et al., *Dendritic Polyglycerolsulfate Near Infrared Fluorescent (NIRF) Dye Conjugate for Non-Invasively Monitoring of Inflammation in an Allergic Asthma Mouse Model.* Plos One, 2013. **8**(2).

166. Schneider, T., et al., *Influence of dendritic polyglycerol sulfates on knee osteoarthritis: an experimental study in the rat osteoarthritis model.* Bmc Musculoskeletal Disorders, 2015. **16**.
167. Khandare, J., et al., *Structure-biocompatibility relationship of dendritic polyglycerol derivatives.* Biomaterials, 2010. **31**(15): p. 4268-4277.
168. Maysinger, D., et al., *Dendritic Polyglycerol Sulfate Inhibits Microglial Activation and Reduces Hippocampal CA1 Dendritic Spine Morphology Deficits.* Biomacromolecules, 2015. **16**(9): p. 3073-3082.
169. Heald, R. and O. Cohen-Fix, *Morphology and function of membrane-bound organelles.* Current Opinion in Cell Biology, 2014. **26**: p. 79-86.
170. Emlen, W. and M. Mannik, *Kinetics and Mechanisms for Removal of Circulating Single-Stranded-DNA in Mice.* Journal of Experimental Medicine, 1978. **147**(3): p. 684-699.
171. Yin, H., et al., *Non-viral vectors for gene-based therapy.* Nat Rev Genet, 2014. **15**(8): p. 541-55.
172. Mendes, R., A.R. Fernandes, and P.V. Baptista, *Gold Nanoparticle Approach to the Selective Delivery of Gene Silencing in Cancer-The Case for Combined Delivery?* Genes (Basel), 2017. **8**(3).
173. Cervia, L.D., et al., *Distinct effects of endosomal escape and inhibition of endosomal trafficking on gene delivery via electrotransfection.* Plos One, 2017. **12**(2).
174. Qian, Z.Q., et al., *Early Endosomal Escape of a Cyclic Cell-Penetrating Peptide Allows Effective Cytosolic Cargo Delivery.* Biochemistry, 2014. **53**(24): p. 4034-4046.
175. Juliano, R.L., *The delivery of therapeutic oligonucleotides.* Nucleic Acids Research, 2016. **44**(14): p. 6518-6548.
176. Liu, L., et al., *Poly(cationic lipid)-mediated in vivo gene delivery to mouse liver.* Gene Therapy, 2003. **10**(2): p. 180-187.
177. Panyam, J., et al., *Rapid endo-lysosomal escape of poly(DL-lactide-co-glycolide) nanoparticles: implications for drug and gene delivery.* FASEB J, 2002. **16**(10): p. 1217-26.
178. Yang, Y., et al., *A novel gene delivery composite system based on biodegradable folate-poly (ester amine) polymer and thermosensitive hydrogel for sustained gene release.* Scientific Reports, 2016. **6**.
179. Davtyan, H., et al., *Delivery of a DNA Vaccine for Alzheimer's Disease by Electroporation versus Gene Gun Generates Potent and Similar Immune Responses.* Neurodegenerative Diseases, 2012. **10**(1-4): p. 261-264.
180. Giljohann, D.A., et al., *Gene Regulation with Polyvalent siRNA-Nanoparticle Conjugates.* Journal of the American Chemical Society, 2009. **131**(6): p. 2072-+.
181. Giljohann, D.A., et al., *Oligonucleotide loading determines cellular uptake of DNA-modified gold nanoparticles.* Nano Letters, 2007. **7**(12): p. 3818-3821.
182. Panyam, J., et al., *Rapid endo-lysosomal escape of poly(DL-lactide-co-glycolide) nanoparticles: implications for drug and gene delivery.* Faseb Journal, 2002. **16**(10).
183. Chu, Z.Q., et al., *Rapid endosomal escape of prickly nanodiamonds: implications for gene delivery.* Scientific Reports, 2015. **5**.
184. Elbakry, A., et al., *Layer-by-Layer Coated Gold Nanoparticles: Size-Dependent Delivery of DNA into Cells.* Small, 2012. **8**(24): p. 3847-3856.
185. Utsuno, K. and H. Uludag, *Thermodynamics of Polyethylenimine-DNA Binding and DNA Condensation.* Biophysical Journal, 2010. **99**(1): p. 201-207.
186. Maemoto, Y., et al., *Involvement of calpain-7 in epidermal growth factor receptor degradation via the endosomal sorting pathway.* Febs Journal, 2014. **281**(16): p. 3642-3655.
187. Schafer, J., et al., *Liposome-polyethylenimine complexes for enhanced DNA and siRNA delivery.* Biomaterials, 2010. **31**(26): p. 6892-6900.

188. Moffatt, S., S. Wiehle, and R.J. Cristiano, *A multifunctional PEI-based cationic polyplex for enhanced systemic p53-mediated gene therapy.* Gene Therapy, 2006. **13**(21): p. 1512-1523.
189. Peng, S.F., et al., *Novel PEI/Poly--Gutamic Acid Nanoparticles for High Efficient siRNA and Plasmid DNA Co-Delivery.* Molecules, 2017. **22**(1).
190. Schiffelers, R.M., et al., *Cancer siRNA therapy by tumor selective delivery with ligand-targeted sterically stabilized nanoparticle.* Nucleic Acids Research, 2004. **32**(19).
191. Gabrielson, N.P. and D.W. Pack, *Efficient polyethylenimine-mediated gene delivery proceeds via a caveolar pathway in HeLa cells.* Journal of Controlled Release, 2009. **136**(1): p. 54-61.
192. van der Aa, M.A.E.M., et al., *Cellular uptake of cationic polymer-DNA complexes via caveolae plays a pivotal role in gene transfection in COS-7 cells.* Pharmaceutical Research, 2007. **24**(8): p. 1590-1598.
193. Rejman, J., M. Conese, and D. Hoekstra, *Gene transfer by means of lipo- and polyplexes: Role of clathrin and caveolae-mediated endocytosis.* Journal of Liposome Research, 2006. **16**(3): p. 237-247.
194. Lodish, H., et al., *Organelles of the Eukaryotic Cell*, in *Molecular Cell Biology.* 2000, W. H. Freeman: New York.
195. Cebrian, V., et al., *Size-dependent transfection efficiency of PEI-coated gold nanoparticles.* Acta Biomaterialia, 2011. **7**(10): p. 3645-3655.
196. Huo, S.D., et al., *Ultrasmall Gold Nanoparticles as Carriers for Nucleus-Based Gene Therapy Due to Size-Dependent Nuclear Entry.* Acs Nano, 2014. **8**(6): p. 5852-5862.
197. Shahbazi, R., et al., *Functionalized gold nanoparticles manifested as potent carriers for nucleolar targeting.* Nanotechnology, 2017. **28**(2).
198. Hinde, E., et al., *Pair correlation microscopy reveals the role of nanoparticle shape in intracellular transport and site of drug release.* Nat Nanotechnol, 2017. **12**(1): p. 81-89.
199. Tkachenko, A.G., et al., *Cellular trajectories of peptide-modified gold particle complexes: Comparison of nuclear localization signals and peptide transduction domains.* Bioconjugate Chemistry, 2004. **15**(3): p. 482-490.
200. Feldherr, C.M. and D. Akin, *The permeability of the nuclear envelope in dividing and nondividing cell cultures.* J Cell Biol, 1990. **111**(1): p. 1-8.
201. Lin, P.C., et al., *Techniques for physicochemical characterization of nanomaterials.* Biotechnology Advances, 2014. **32**(4): p. 711-726.
202. Lim, J., et al., *Characterization of magnetic nanoparticle by dynamic light scattering.* Nanoscale Res Lett, 2013. **8**(1): p. 381.
203. Moore, T.L., et al., *Nanoparticle colloidal stability in cell culture media and impact on cellular interactions.* Chemical Society Reviews, 2015. **44**(17): p. 6287-6305.
204. Treuel, L., X. Jiang, and G.U. Nienhaus, *New views on cellular uptake and trafficking of manufactured nanoparticles.* J R Soc Interface, 2013. **10**(82): p. 20120939.
205. Albanese, A. and W.C.W. Chan, *Effect of Gold Nanoparticle Aggregation on Cell Uptake and Toxicity.* Acs Nano, 2011. **5**(7): p. 5478-5489.
206. Gatoo, M.A., et al., *Physicochemical Properties of Nanomaterials: Implication in Associated Toxic Manifestations.* Biomed Research International, 2014.
207. Drescher, D., et al., *In situ Characterization of SiO2 Nanoparticle Biointeractions Using BrightSilica.* Advanced Functional Materials, 2014. **24**(24): p. 3765-3775.
208. Pyrgiotakis, G., C.O. Blattmann, and P. Demokritou, *Real-Time Nanoparticle-Cell Interactions in Physiological Media by Atomic Force Microscopy.* Acs Sustainable Chemistry & Engineering, 2014. **2**(7): p. 1681-1690.

209. Hotze, E.M., T. Phenrat, and G.V. Lowry, *Nanoparticle aggregation: challenges to understanding transport and reactivity in the environment.* J Environ Qual, 2010. **39**(6): p. 1909-24.
210. Nel, A.E., et al., *Understanding biophysicochemical interactions at the nano-bio interface.* Nat Mater, 2009. **8**(7): p. 543-57.
211. Pilon, L., H.N. Wang, and A. d'Entremont, *Recent Advances in Continuum Modeling of Interfacial and Transport Phenomena in Electric Double Layer Capacitors.* Journal of the Electrochemical Society, 2015. **162**(5): p. A5158-A5178.
212. Halamoda-Kenzaoui, B., et al., *Dispersion Behaviour of Silica Nanoparticles in Biological Media and Its Influence on Cellular Uptake.* Plos One, 2015. **10**(10).
213. Hotze, E.M., J.Y. Bottero, and M.R. Wiesner, *Theoretical framework for nanoparticle reactivity as a function of aggregation state.* Langmuir, 2010. **26**(13): p. 11170-5.
214. Rivera-Gil, P., et al., *The challenge to relate the physicochemical properties of colloidal nanoparticles to their cytotoxicity.* Acc Chem Res, 2013. **46**(3): p. 743-9.
215. Liu, M.M., et al., *Real-time visualization of clustering and intracellular transport of gold nanoparticles by correlative imaging.* Nature Communications, 2017. **8**.
216. Kaizuka, Y., et al., *Cytosolic Transport of Nanoparticles through Pressurized Plasma Membranes for Molecular Delivery and Amplification of Intracellular Fluorescence.* Langmuir, 2016. **32**(50): p. 13534-13545.
217. Adkins, J.N., et al., *Toward a human blood serum proteome: analysis by multidimensional separation coupled with mass spectrometry.* Mol Cell Proteomics, 2002. **1**(12): p. 947-55.
218. Mortensen, N.P., et al., *Dynamic development of the protein corona on silica nanoparticles: composition and role in toxicity.* Nanoscale, 2013. **5**(14): p. 6372-6380.
219. Treuel, L., et al., *Impact of Protein Modification on the Protein Corona on Nanoparticles and Nanoparticle-Cell Interactions.* Acs Nano, 2014. **8**(1): p. 503-513.
220. Min, Y., et al., *The role of interparticle and external forces in nanoparticle assembly.* Nat Mater, 2008. **7**(7): p. 527-38.
221. Monopoli, M.P., et al., *Physical-Chemical Aspects of Protein Corona: Relevance to in Vitro and in Vivo Biological Impacts of Nanoparticles.* Journal of the American Chemical Society, 2011. **133**(8): p. 2525-2534.
222. Walkey, C.D., et al., *Nanoparticle Size and Surface Chemistry Determine Serum Protein Adsorption and Macrophage Uptake.* Journal of the American Chemical Society, 2012. **134**(4): p. 2139-2147.
223. Wang, X., et al., *Chiral Surface of Nanoparticles Determines the Orientation of Adsorbed Transferrin and Its Interaction with Receptors.* ACS Nano, 2017.
224. Lundqvist, M., et al., *Nanoparticle size and surface properties determine the protein corona with possible implications for biological impacts.* Proc Natl Acad Sci U S A, 2008. **105**(38): p. 14265-70.
225. Docter, D., et al., *The protein corona protects against size- and dose-dependent toxicity of amorphous silica nanoparticles.* Beilstein Journal of Nanotechnology, 2014. **5**: p. 1380-1392.
226. Schottler, S., et al., *Protein adsorption is required for stealth effect of poly(ethylene glycol)- and poly(phosphoester)-coated nanocarriers.* Nature Nanotechnology, 2016. **11**(4): p. 372-377.
227. Yallapu, M.M., et al., *Implications of protein corona on physico-chemical and biological properties of magnetic nanoparticles.* Biomaterials, 2015. **46**: p. 1-12.
228. Shang, L., et al., *Nanoparticles Interacting with Proteins and Cells: A Systematic Study of Protein Surface Charge Effects.* Advanced Materials Interfaces, 2014. **1**(2).
229. Ritz, S., et al., *Protein Corona of Nanoparticles: Distinct Proteins Regulate the Cellular Uptake.* Biomacromolecules, 2015. **16**(4): p. 1311-1321.

230. Tenzer, S., et al., *Rapid formation of plasma protein corona critically affects nanoparticle pathophysiology.* Nat Nanotechnol, 2013. **8**(10): p. 772-81.
231. Caracciolo, G., O.C. Farokhzad, and M. Mahmoudi, *Biological Identity of Nanoparticles In Vivo: Clinical Implications of the Protein Corona.* Trends Biotechnol, 2017. **35**(3): p. 257-264.
232. Deng, Z.J., et al., *Nanoparticle-induced unfolding of fibrinogen promotes Mac-1 receptor activation and inflammation.* Nat Nanotechnol, 2011. **6**(1): p. 39-44.
233. Chen, H.W., et al., *Reducing non-specific binding and uptake of nanoparticles and improving cell targeting with an antifouling PEO-b-P gamma MPS copolymer coating.* Biomaterials, 2010. **31**(20): p. 5397-5407.
234. Aggarwal, P., et al., *Nanoparticle interaction with plasma proteins as it relates to particle biodistribution, biocompatibility and therapeutic efficacy.* Adv Drug Deliv Rev, 2009. **61**(6): p. 428-37.
235. Huang, J., et al., *Effects of Nanoparticle Size on Cellular Uptake and Liver MRI with Polyvinylpyrrolidone-Coated Iron Oxide Nanoparticles.* Acs Nano, 2010. **4**(12): p. 7151-7160.
236. Rejman, J., et al., *Size-dependent internalization of particles via the pathways of clathrin- and caveolae-mediated endocytosis.* Biochemical Journal, 2004. **377**: p. 159-169.
237. Herd, H., et al., *Nanoparticle Geometry and Surface Orientation Influence Mode of Cellular Uptake.* Acs Nano, 2013. **7**(3): p. 1961-1973.
238. Penaloza, J.P., et al., *Intracellular trafficking and cellular uptake mechanism of PHBV nanoparticles for targeted delivery in epithelial cell lines.* Journal of Nanobiotechnology, 2017. **15**.
239. Kim, J.A., et al., *Role of cell cycle on the cellular uptake and dilution of nanoparticles in a cell population.* Nature Nanotechnology, 2012. **7**(1): p. 62-68.
240. Tan, S.J., et al., *Surface-Ligand-Dependent Cellular Interaction, Subcellular Localization, and Cytotoxicity of Polymer-Coated Quantum Dots.* Chemistry of Materials, 2010. **22**(7): p. 2239-2247.
241. Xu, Q., et al., *Anti-tumor activity of paclitaxel through dual-targeting carrier of cyclic RGD and transferrin conjugated hyperbranched copolymer nanoparticles.* Biomaterials, 2012. **33**(5): p. 1627-1639.
242. Gratton, S.E., et al., *The effect of particle design on cellular internalization pathways.* Proc Natl Acad Sci U S A, 2008. **105**(33): p. 11613-8.
243. Qiu, Y., et al., *Surface chemistry and aspect ratio mediated cellular uptake of Au nanorods.* Biomaterials, 2010. **31**(30): p. 7606-19.
244. Chithrani, B.D. and W.C. Chan, *Elucidating the mechanism of cellular uptake and removal of protein-coated gold nanoparticles of different sizes and shapes.* Nano Lett, 2007. **7**(6): p. 1542-50.
245. Muro, S., et al., *Control of endothelial targeting and intracellular delivery of therapeutic enzymes by modulating the size and shape of ICAM-1-targeted carriers.* Molecular Therapy, 2008. **16**(8): p. 1450-1458.
246. Green, J.J., et al., *Electrostatic ligand coatings of nanoparticles enable ligand-specific gene delivery to human primary cells.* Nano Letters, 2007. **7**(4): p. 874-879.
247. Decuzzi, P. and M. Ferrari, *The role of specific and non-specific interactions in receptor-mediated endocytosis of nanoparticles.* Biomaterials, 2007. **28**(18): p. 2915-22.
248. Bruce Alberts, A.J., Julian Lewis, Martin Raff, Keith Roberts, and Peter Walter., *Molecular Biology of the Cell*. 4 ed. 2002, New York: Garland Science.
249. Wang, T.T., et al., *Cellular Uptake of Nanoparticles by Membrane Penetration: A Study Combining Confocal Microscopy with FTIR Spectroelectrochemistry.* Acs Nano, 2012. **6**(2): p. 1251-1259.

250. Fiorentino, I., et al., *Energy independent uptake and release of polystyrene nanoparticles in primary mammalian cell cultures.* Experimental Cell Research, 2015. **330**(2): p. 240-247.
251. Zhao, Y.N., et al., *Interaction of mesoporous silica nanoparticles with human red blood cell membranes: Size and surface functionality effects.* Abstracts of Papers of the American Chemical Society, 2011. **241**.
252. Rothen-Rutishauser, B.M., et al., *Interaction of fine particles and nanoparticles with red blood cells visualized with advanced microscopic techniques.* Environmental Science & Technology, 2006. **40**(14): p. 4353-4359.
253. Leroueil, P.R., et al., *Wide varieties of cationic nanoparticles induce defects in supported lipid bilayers.* Nano Letters, 2008. **8**(2): p. 420-424.
254. Lin, J.Q., et al., *Penetration of Lipid Membranes by Gold Nanoparticles: Insights into Cellular Uptake, Cytotoxicity, and Their Relationship.* Acs Nano, 2010. **4**(9): p. 5421-5429.
255. Nel, A.E., et al., *Understanding biophysicochemical interactions at the nano-bio interface.* Nature Materials, 2009. **8**(7): p. 543-557.
256. Gao, H., W. Shi, and L.B. Freund, *Mechanics of receptor-mediated endocytosis.* Proc Natl Acad Sci U S A, 2005. **102**(27): p. 9469-74.
257. Decuzzi, P. and M. Ferrari, *The receptor-mediated endocytosis of nonspherical particles.* Biophys J, 2008. **94**(10): p. 3790-7.
258. Sahay, G., D.Y. Alakhova, and A.V. Kabanov, *Endocytosis of nanomedicines.* J Control Release, 2010. **145**(3): p. 182-95.
259. Longfa Kou, J.S., Yinglei Zhai, Zhonggui He, *The endocytosis and intracellular fate of nanomedicines: Implication for rational design.* Asian Journal of Pharmaceutical Sciences, 2013.
260. Rappoport, J.Z., *Focusing on clathrin-mediated endocytosis.* Biochem J, 2008. **412**(3): p. 415-23.
261. Kirchhausen, T., D. Owen, and S.C. Harrison, *Molecular structure, function, and dynamics of clathrin-mediated membrane traffic.* Cold Spring Harb Perspect Biol, 2014. **6**(5): p. a016725.
262. Mayor, S. and R.E. Pagano, *Pathways of clathrin-independent endocytosis.* Nature Reviews Molecular Cell Biology, 2007. **8**(8): p. 603-612.
263. Benmerah, A. and C. Lamaze, *Clathrin-coated pits: vive la difference?* Traffic, 2007. **8**(8): p. 970-82.
264. Chithrani, B.D. and W.C.W. Chan, *Elucidating the mechanism of cellular uptake and removal of protein-coated gold nanoparticles of different sizes and shapes.* Nano Letters, 2007. **7**(6): p. 1542-1550.
265. Ng, C.T., et al., *Clathrin-Mediated Endocytosis of Gold Nanoparticles In Vitro.* Anatomical Record-Advances in Integrative Anatomy and Evolutionary Biology, 2015. **298**(2): p. 418-427.
266. Parton, R.G. and K. Simons, *The multiple faces of caveolae.* Nat Rev Mol Cell Biol, 2007. **8**(3): p. 185-94.
267. Nichols, B.J., *A distinct class of endosome mediates clathrin-independent endocytosis to the Golgi complex.* Nat Cell Biol, 2002. **4**(5): p. 374-8.
268. Pelkmans, L. and M. Zerial, *Kinase-regulated quantal assemblies and kiss-and-run recycling of caveolae.* Nature, 2005. **436**(7047): p. 128-133.
269. Botos, E., et al., *Caveolin-1 is transported to multi-vesicular bodies after albumin-induced endocytosis of caveolae in HepG2 cells.* Journal of Cellular and Molecular Medicine, 2008. **12**(5A): p. 1632-1639.

270. Tiruppathi, C., et al., *Gp60 activation mediates albumin transcytosis in endothelial cells by tyrosine kinase-dependent pathway.* Journal of Biological Chemistry, 1997. **272**(41): p. 25968-25975.
271. Suen, W.L.L. and Y. Chau, *Size- dependent internalisation of folate- decorated nanoparticles via the pathways of clathrin and caveolae- mediated endocytosis in ARPE-19 cells.* Journal of Pharmacy and Pharmacology, 2014. **66**(4): p. 564-573.
272. Mayor, S., R.G. Parton, and J.G. Donaldson, *Clathrin-independent pathways of endocytosis.* Cold Spring Harb Perspect Biol, 2014. **6**(6).
273. Kerr, M.C. and R.D. Teasdale, *Defining Macropinocytosis.* Traffic, 2009. **10**(4): p. 364-371.
274. Kalia, M., et al., *Arf6-independent GPI-anchored protein-enriched early endosomal compartments fuse with sorting endosomes via a Rab5/phosphatidylinositol-3 '-kinase-dependent machinery.* Molecular Biology of the Cell, 2006. **17**(8): p. 3689-3704.
275. Gupta, G.D., et al., *Analysis of Endocytic Pathways in Drosophila Cells Reveals a Conserved Role for GBF1 in Internalization via GEECs.* Plos One, 2009. **4**(8).
276. Kokkinopoulou, M., et al., *Visualization of the protein corona: towards a biomolecular understanding of nanoparticlecell- interactions.* Nanoscale, 2017. **9**(25): p. 8858-8870.
277. Otto, G.P. and B.J. Nichols, *The roles of flotillin microdomains - endocytosis and beyond.* Journal of Cell Science, 2011. **124**(23): p. 3933-3940.
278. Meister, M. and R. Tikkanen, *Endocytic trafficking of membrane-bound cargo: a flotillin point of view.* Membranes (Basel), 2014. **4**(3): p. 356-71.
279. Kasper, J., et al., *Interactions of silica nanoparticles with lung epithelial cells and the association to flotillins.* Archives of Toxicology, 2013. **87**(6): p. 1053-1065.
280. Lim, J.P. and P.A. Gleeson, *Macropinocytosis: an endocytic pathway for internalising large gulps.* Immunology and Cell Biology, 2011. **89**(8): p. 836-843.
281. Dolat, L. and E.T. Spiliotis, *Septins promote macropinosome maturation and traffic to the lysosome by facilitating membrane fusion.* Journal of Cell Biology, 2016. **214**(5): p. 517-527.
282. Mercer, J. and A. Helenius, *Gulping rather than sipping: macropinocytosis as a way of virus entry.* Current Opinion in Microbiology, 2012. **15**(4): p. 490-499.
283. Garcia-Perez, B.E., et al., *Macropinocytosis is responsible for the uptake of pathogenic and non-pathogenic mycobacteria by B lymphocytes (Raji cells).* Bmc Microbiology, 2012. **12**.
284. Meng, H., et al., *Aspect Ratio Determines the Quantity of Mesoporous Silica Nanoparticle Uptake by a Small GTPase-Dependent Macropinocytosis Mechanism.* Acs Nano, 2011. **5**(6): p. 4434-4447.
285. Park, S., et al., *Cellular Uptake Pathway and Drug Release Characteristics of Drug-Encapsulated Glycol Chitosan Nanoparticles in Live Cells.* Microscopy Research and Technique, 2010. **73**(9): p. 857-865.
286. Gilleron, J., et al., *Image-based analysis of lipid nanoparticle-mediated siRNA delivery, intracellular trafficking and endosomal escape.* Nature Biotechnology, 2013. **31**(7): p. 638-U102.
287. Dong, Y.Z., et al., *Lipopeptide nanoparticles for potent and selective siRNA delivery in rodents and nonhuman primates (vol 111, pg 3955, 2014).* Proceedings of the National Academy of Sciences of the United States of America, 2014. **111**(15): p. 5753-5753.
288. Harush-Frenkel, O., et al., *Targeting of nanoparticles to the clathrin-mediated endocytic pathway.* Biochemical and Biophysical Research Communications, 2007. **353**(1): p. 26-32.
289. Jiang, X.E., et al., *Specific Effects of Surface Amines on Polystyrene Nanoparticles in their Interactions with Mesenchymal Stem Cells.* Biomacromolecules, 2010. **11**(3): p. 748-753.

290. Dausend, J., et al., *Uptake Mechanism of Oppositely Charged Fluorescent Nanoparticles in HeLa Cells.* Macromolecular Bioscience, 2008. **8**(12): p. 1135-1143.
291. Huang, M., et al., *Uptake of FITC-chitosan nanoparticles by a549 cells.* Pharmaceutical Research, 2002. **19**(10): p. 1488-1494.
292. Xia, T., et al., *Cationic polystyrene nanosphere toxicity depends on cell-specific endocytic and mitochondrial injury pathways.* Acs Nano, 2008. **2**(1): p. 85-96.
293. Chang, J., et al., *Characterization of endocytosis of transferrin-coated PLGA nanoparticles by the blood-brain barrier.* International Journal of Pharmaceutics, 2009. **379**(2): p. 285-292.
294. Singh, S., et al., *Unveiling the mechanism of uptake and sub-cellular distribution of cerium oxide nanoparticles.* Molecular Biosystems, 2010. **6**(10): p. 1813-1820.
295. Nam, H.Y., et al., *Cellular uptake mechanism and intracellular fate of hydrophobically modified glycol chitosan nanoparticles.* Journal of Controlled Release, 2009. **135**(3): p. 259-267.
296. Gunduz, N., et al., *Intracellular Accumulation of Gold Nanoparticles Leads to Inhibition of Macropinocytosis to Reduce the Endoplasmic Reticulum Stress.* Scientific Reports, 2017. **7**.
297. Vercauteren, D., et al., *The Use of Inhibitors to Study Endocytic Pathways of Gene Carriers: Optimization and Pitfalls.* Molecular Therapy, 2010. **18**(3): p. 561-569.
298. Frohlich, E., *The role of surface charge in cellular uptake and cytotoxicity of medical nanoparticles.* Int J Nanomedicine, 2012. **7**: p. 5577-91.
299. Sakhrani, N.M. and H. Padh, *Organelle targeting: third level of drug targeting.* Drug Design Development and Therapy, 2013. **7**: p. 585-599.
300. Kwon, H.J., et al., *Mitochondria-Targeting Ceria Nanoparticles as Antioxidants for Alzheimer's Disease.* Acs Nano, 2016. **10**(2): p. 2860-2870.
301. Wongrakpanich, A., et al., *Mitochondria-targeting particles.* Nanomedicine, 2014. **9**(16): p. 2531-2543.
302. Trudeau, K.M., et al., *Lysosome acidification by photoactivated nanoparticles restores autophagy under lipotoxicity.* Journal of Cell Biology, 2016. **214**(1): p. 25-34.
303. Hu, W.B., et al., *Engineering Lysosome-Targeting BODIPY Nanoparticles for Photoacoustic Imaging and Photodynamic Therapy under Near-Infrared Light.* Acs Applied Materials & Interfaces, 2016. **8**(19): p. 12039-12047.
304. Domenech, M., et al., *Lysosomal Membrane Permeabilization by Targeted Magnetic Nanoparticles in Alternating Magnetic Fields.* Acs Nano, 2013. **7**(6): p. 5091-5101.
305. Chou, L.Y.T., K. Ming, and W.C.W. Chan, *Strategies for the intracellular delivery of nanoparticles.* Chemical Society Reviews, 2011. **40**(1): p. 233-245.
306. Sahay, G., et al., *Efficiency of siRNA delivery by lipid nanoparticles is limited by endocytic recycling.* Nature Biotechnology, 2013. **31**(7): p. 653-U119.
307. Kadiu, I., et al., *Macrophage endocytic trafficking of antiretroviral nanoparticles.* Nanomedicine, 2011. **6**(6): p. 975-994.
308. Liu, M., et al., *Real-time visualization of clustering and intracellular transport of gold nanoparticles by correlative imaging.* Nat Commun, 2017. **8**: p. 15646.
309. Zhou, K., et al., *Tunable, ultrasensitive pH-responsive nanoparticles targeting specific endocytic organelles in living cells.* Angew Chem Int Ed Engl, 2011. **50**(27): p. 6109-14.
310. Chu, Z., et al., *Unambiguous observation of shape effects on cellular fate of nanoparticles.* Sci Rep, 2014. **4**: p. 4495.
311. Cartiera, M.S., et al., *The uptake and intracellular fate of PLGA nanoparticles in epithelial cells.* Biomaterials, 2009. **30**(14): p. 2790-2798.
312. Asati, A., et al., *Surface-charge-dependent cell localization and cytotoxicity of cerium oxide nanoparticles.* ACS Nano, 2010. **4**(9): p. 5321-31.

313. Zeng, X.H., R. Morgenstern, and A.M. Nystrom, *Nanoparticle-directed sub-cellular localization of doxorubicin and the sensitization breast cancer cells by circumventing GST-Mediated drug resistance.* Biomaterials, 2014. **35**(4): p. 1227-1239.
314. Zhang, J.X., et al., *Intracellular Trafficking Network of Protein Nanocapsules: Endocytosis, Exocytosis and Autophagy.* Theranostics, 2016. **6**(12): p. 2099-2113.
315. Zeng, X., Y. Zhang, and A.M. Nystrom, *Endocytic uptake and intracellular trafficking of bis-MPA-based hyperbranched copolymer micelles in breast cancer cells.* Biomacromolecules, 2012. **13**(11): p. 3814-22.
316. Tkachenko, A.G., et al., *Multifunctional gold nanoparticle-peptide complexes for nuclear targeting.* Journal of the American Chemical Society, 2003. **125**(16): p. 4700-4701.
317. Pan, L.M., et al., *Nuclear-Targeted Drug Delivery of TAT Peptide-Conjugated Monodisperse Mesoporous Silica Nanoparticles.* Journal of the American Chemical Society, 2012. **134**(13): p. 5722-5725.
318. Burd, C.G., *Physiology and Pathology of Endosome-to-Golgi Retrograde Sorting.* Traffic, 2011. **12**(8): p. 948-955.
319. Chou, L.Y., K. Ming, and W.C. Chan, *Strategies for the intracellular delivery of nanoparticles.* Chem Soc Rev, 2011. **40**(1): p. 233-45.
320. He, B., et al., *The transport pathways of polymer nanoparticles in MDCK epithelial cells.* Biomaterials, 2013. **34**(17): p. 4309-26.
321. Mathiowitz, E., et al., *Biologically erodable microspheres as potential oral drug delivery systems.* Nature, 1997. **386**(6623): p. 410-4.
322. Zhang, J., et al., *Intracellular Trafficking Network of Protein Nanocapsules: Endocytosis, Exocytosis and Autophagy.* Theranostics, 2016. **6**(12): p. 2099-2113.
323. Zhao, F., et al., *Cellular uptake, intracellular trafficking, and cytotoxicity of nanomaterials.* Small, 2011. **7**(10): p. 1322-37.
324. Lakadamyali, M., M.J. Rust, and X. Zhuang, *Ligands for clathrin-mediated endocytosis are differentially sorted into distinct populations of early endosomes.* Cell, 2006. **124**(5): p. 997-1009.
325. Dautry-Varsat, A., A. Ciechanover, and H.F. Lodish, *pH and the recycling of transferrin during receptor-mediated endocytosis.* Proc Natl Acad Sci U S A, 1983. **80**(8): p. 2258-62.
326. Herbst, J.J., et al., *Regulation of postendocytic trafficking of the epidermal growth factor receptor through endosomal retention.* J Biol Chem, 1994. **269**(17): p. 12865-73.
327. Piper, R.C. and J.P. Luzio, *Late endosomes: sorting and partitioning in multivesicular bodies.* Traffic, 2001. **2**(9): p. 612-21.
328. Von Bartheld, C.S. and A.L. Altick, *Multivesicular bodies in neurons: Distribution, protein content, and trafficking functions.* Progress in Neurobiology, 2011. **93**(3): p. 313-340.
329. Piper, R.C. and D.J. Katzmann, *Biogenesis and function of multivesicular bodies.* Annual Review of Cell and Developmental Biology, 2007. **23**: p. 519-547.
330. Boulanger, C.M., et al., *Extracellular vesicles in coronary artery disease.* Nature Reviews Cardiology, 2017. **14**(5): p. 259-272.
331. Buschow, S.I., et al., *MHC class II-associated proteins in B-cell exosomes and potential functional implications for exosome biogenesis.* Immunology and Cell Biology, 2010. **88**(8): p. 851-856.
332. Buschow, S.I., et al., *MHC II in Dendritic Cells is Targeted to Lysosomes or T Cell-Induced Exosomes Via Distinct Multivesicular Body Pathways.* Traffic, 2009. **10**(10): p. 1528-1542.
333. Alexander, M., et al., *Exosome-delivered microRNAs modulate the inflammatory response to endotoxin.* Nature Communications, 2015. **6**.
334. Hergenreider, E., et al., *Atheroprotective communication between endothelial cells and smooth muscle cells through miRNAs.* Nat Cell Biol, 2012. **14**(3): p. 249-56.

335. Bazer, F.W. and G.A. Johnson, *Pig blastocyst-uterine interactions.* Differentiation, 2014. **87**(1-2): p. 52-65.
336. Gruenberg, J., *The endocytic pathway: A mosaic of domains.* Nature Reviews Molecular Cell Biology, 2001. **2**(10): p. 721-730.
337. Geoffrey, C.M., *Part III. Cell Structure and Function*, in *The Cell: A molecular approach*. 2000, Sinauer Associates: Sunderland (MA).
338. Saftig, P. and J. Klumperman, *Lysosome biogenesis and lysosomal membrane proteins: trafficking meets function.* Nature Reviews Molecular Cell Biology, 2009. **10**(9): p. 623-635.
339. Li, Y., et al., *The lysosomal membrane protein SCAV-3 maintains lysosome integrity and adult longevity.* Journal of Cell Biology, 2016. **215**(2): p. 167-185.
340. Amaya, C., C.M. Fader, and M.I. Colombo, *Autophagy and proteins involved in vesicular trafficking.* Febs Letters, 2015. **589**(22): p. 3343-3353.
341. Stolz, A., A. Ernst, and I. Dikic, *Cargo recognition and trafficking in selective autophagy.* Nature Cell Biology, 2014. **16**(6): p. 495-501.
342. Szatmari, Z., et al., *Rab11 facilitates cross-talk between autophagy and endosomal pathway through regulation of Hook localization.* Molecular Biology of the Cell, 2014. **25**(4): p. 522-531.
343. Krukemeyer, M.G., et al., *Mitoxantrone-Iron Oxide Biodistribution in Blood, Tumor, Spleen, and Liver-Magnetic Nanoparticles in Cancer Treatment.* Journal of Surgical Research, 2012. **175**(1): p. 35-43.
344. Yum, K., et al., *Mechanochemical Delivery and Dynamic Tracking of Fluorescent Quantum Dots in the Cytoplasm and Nucleus of Living Cells.* Nano Letters, 2009. **9**(5): p. 2193-2198.
345. Zelphati, O. and F.C. Szoka, Jr., *Mechanism of oligonucleotide release from cationic liposomes.* Proc Natl Acad Sci U S A, 1996. **93**(21): p. 11493-8.
346. Zuris, J.A., et al., *Cationic lipid-mediated delivery of proteins enables efficient protein-based genome editing in vitro and in vivo.* Nat Biotechnol, 2015. **33**(1): p. 73-80.
347. Martens, T.F., et al., *Intracellular delivery of nanomaterials: How to catch endosomal escape in the act.* Nano Today, 2014. **9**(3): p. 344-364.
348. Zhan, X., et al., *Controlled Endolysosomal Release of Agents by pH-responsive Polymer Blend Particles.* Pharmaceutical Research, 2015. **32**(7): p. 2280-2291.
349. Hu, Y., et al., *Cytosolic delivery of membrane-impermeable molecules in dendritic cells using pH-responsive core-shell nanoparticles.* Nano Lett, 2007. **7**(10): p. 3056-64.
350. Gemeinhart, R.A., D. Luo, and W.M. Saltzman, *Cellular fate of a modular DNA delivery system mediated by silica nanoparticles.* Biotechnology Progress, 2005. **21**(2): p. 532-537.
351. Beck, M., et al., *Nuclear pore complex structure and dynamics revealed by cryoelectron tomography.* Science, 2004. **306**(5700): p. 1387-1390.
352. Patel, S.S., et al., *Natively unfolded nucleoporins gate protein diffusion across the nuclear pore complex.* Cell, 2007. **129**(1): p. 83-96.
353. Seibel, N.M., et al., *Nuclear localization of enhanced green fluorescent protein homomultimers.* Analytical Biochemistry, 2007. **368**(1): p. 95-99.
354. Popken, P., et al., *Size-dependent leak of soluble and membrane proteins through the yeast nuclear pore complex.* Molecular Biology of the Cell, 2015. **26**(7): p. 1386-1394.
355. Lenart, P. and J. Ellenberg, *Monitoring the permeability of the nuclear envelope during the cell cycle.* Methods, 2006. **38**(1): p. 17-24.
356. Dworetzky, S.I., R.E. Lanford, and C.M. Feldherr, *The effects of variations in the number and sequence of targeting signals on nuclear uptake.* J Cell Biol, 1988. **107**(4): p. 1279-87.

357. Feldherr, C.M., E. Kallenbach, and N. Schultz, *Movement of a karyophilic protein through the nuclear pores of oocytes.* J Cell Biol, 1984. **99**(6): p. 2216-22.
358. Shi, Z.L., et al., *Size effect of hydroxyapatite nanoparticles on proliferation and apoptosis of osteoblast-like cells.* Acta Biomaterialia, 2009. **5**(1): p. 338-345.
359. Yao, Y., X. Shi, and F. Chen, *The effect of gold nanoparticles on the proliferation and differentiation of murine osteoblast: a study of MC3T3-E1 cells in vitro.* J Nanosci Nanotechnol, 2014. **14**(7): p. 4851-7.
360. Hou, Y.H., et al., *Effects of titanium nanoparticles on adhesion, migration, proliferation, and differentiation of mesenchymal stem cells.* International Journal of Nanomedicine, 2013. **8**: p. 3619-3630.
361. Liu, D.D., et al., *The effects of gold nanoparticles on the proliferation, differentiation, and mineralization function of MC3T3-E1 cells in vitro.* Chinese Science Bulletin, 2010. **55**(11): p. 1013-1019.
362. Wu, Y.C., et al., *Intrinsic effects of gold nanoparticles on proliferation and invasion activity in SGC-7901 cells.* Oncology Reports, 2016. **35**(3): p. 1457-1462.
363. Tran, K.N., et al., *Effect of pH on the Synthesis of Fucoidan-coated Magnetic Iron Oxide Nanoparticles for Biomedical Applications.* 5th International Conference on Biomedical Engineering in Vietnam, 2015. **46**: p. 71-74.
364. Liu, H., et al., *The promotion of bone regeneration by nanofibrous hydroxyapatite/chitosan scaffolds by effects on integrin-BMP/Smad signaling pathway in BMSCs.* Biomaterials, 2013. **34**(18): p. 4404-17.
365. Zhao, Y., et al., *Differential Regulation of Gene and Protein Expression by Zinc Oxide Nanoparticles in Hen's Ovarian Granulosa Cells: Specific Roles of Nanoparticles.* PLoS One, 2015. **10**(10): p. e0140499.
366. Devanabanda, M., S.A. Latheef, and R. Madduri, *Immunotoxic effects of gold and silver nanoparticles: Inhibition of mitogen-induced proliferative responses and viability of human and murine lymphocytes in vitro.* J Immunotoxicol, 2016. **13**(6): p. 897-902.
367. Wan, R., et al., *DNA damage caused by metal nanoparticles: involvement of oxidative stress and activation of ATM.* Chem Res Toxicol, 2012. **25**(7): p. 1402-11.
368. Li, N., et al., *Ultrafine particulate pollutants induce oxidative stress and mitochondrial damage.* Environ Health Perspect, 2003. **111**(4): p. 455-60.
369. Napierska, D., et al., *Oxidative stress induced by pure and iron-doped amorphous silica nanoparticles in subtoxic conditions.* Chem Res Toxicol, 2012. **25**(4): p. 828-37.
370. Chung, T.H., et al., *Iron Oxide Nanoparticle-Induced Epidermal Growth Factor Receptor Expression in Human Stem Cells for Tumor Therapy.* Acs Nano, 2011. **5**(12): p. 9807-9816.
371. Guo, Z., et al., *Titanium Dioxide Nanoparticle Ingestion Alters Nutrient Absorption in an In Vitro Model of the Small Intestine.* NanoImpact, 2017. **5**: p. 70-82.
372. Lovric, J., et al., *Unmodified cadmium telluride quantum dots induce reactive oxygen species formation leading to multiple organelle damage and cell death.* Chem Biol, 2005. **12**(11): p. 1227-34.
373. Yu, K.N., et al., *Titanium Dioxide Nanoparticles Induce Endoplasmic Reticulum Stress-Mediated Autophagic Cell Death via Mitochondria-Associated Endoplasmic Reticulum Membrane Disruption in Normal Lung Cells.* Plos One, 2015. **10**(6).
374. Simon, M., et al., *In situ quantification of diverse titanium dioxide nanoparticles unveils selective endoplasmic reticulum stress-dependent toxicity.* Nanotoxicology, 2017. **11**(1): p. 134-145.
375. Christen, V. and K. Fent, *Silica nanoparticles and silver-doped silica nanoparticles induce endoplasmatic reticulum stress response and alter cytochrome P4501A activity.* Chemosphere, 2012. **87**(4): p. 423-34.

376. Oo, M.K.K., et al., *Gold Nanoparticle-Enhanced and Size-Dependent Generation of Reactive Oxygen Species from Protoporphyrin IX.* Acs Nano, 2012. **6**(3): p. 1939-1947.
377. Grady, M.E., et al., *Intracellular nanoparticle dynamics affected by cytoskeletal integrity.* Soft Matter, 2017. **13**(9): p. 1873-1880.
378. Wang, J., et al., *Silica nanoparticles induce autophagy dysfunction via lysosomal impairment and inhibition of autophagosome degradation in hepatocytes.* International Journal of Nanomedicine, 2017. **12**: p. 809-825.
379. Ma, X.W., et al., *Gold Nanoparticles Induce Autophagosome Accumulation through Size-Dependent Nanoparticle Uptake and Lysosome Impairment.* Acs Nano, 2011. **5**(11): p. 8629-8639.
380. Khatchadourian, A. and D. Maysinger, *Lipid Droplets: Their Role in Nanoparticle-induced Oxidative Stress.* Molecular Pharmaceutics, 2009. **6**(4): p. 1125-1137.
381. Heng, B.C., et al., *Evaluation of the cytotoxic and inflammatory potential of differentially shaped zinc oxide nanoparticles.* Arch Toxicol, 2011. **85**(12): p. 1517-28.
382. Li, Y., et al., *Mechanism of Photogenerated Reactive Oxygen Species and Correlation with the Antibacterial Properties of Engineered Metal-Oxide Nanoparticles.* Acs Nano, 2012. **6**(6): p. 5164-5173.
383. Yi, C., et al., *Gold nanoparticles promote osteogenic differentiation of mesenchymal stem cells through p38 MAPK pathway.* ACS Nano, 2010. **4**(11): p. 6439-48.
384. Oh, K., et al., *In Vivo Differentiation of Therapeutic Insulin-Producing Cells from Bone Marrow Cells via Extracellular Vesicle-Mimetic Nanovesicles.* ACS Nano, 2015. **9**(12): p. 11718-27.
385. Santos, T., et al., *Polymeric nanoparticles to control the differentiation of neural stem cells in the subventricular zone of the brain.* ACS Nano, 2012. **6**(12): p. 10463-74.
386. Sengstock, C., et al., *Effect of silver nanoparticles on human mesenchymal stem cell differentiation.* Beilstein J Nanotechnol, 2014. **5**: p. 2058-69.
387. Xu, F.L., et al., *Silver nanoparticles (AgNPs) cause degeneration of cytoskeleton and disrupt synaptic machinery of cultured cortical neurons.* Molecular Brain, 2013. **6**.
388. Gupta, A.K., et al., *Effect of cellular uptake of gelatin nanoparticles on adhesion, morphology and cytoskeleton organisation of human fibroblasts.* Journal of Controlled Release, 2004. **95**(2): p. 197-207.
389. Lipski, A.M., et al., *The effect of silica nanoparticle-modified surfaces on cell morphology, cytoskeletal organization and function.* Biomaterials, 2008. **29**(28): p. 3836-3846.
390. Hussain, S., et al., *Cerium Dioxide Nanoparticles Induce Apoptosis and Autophagy in Human Peripheral Blood Monocytes.* Acs Nano, 2012. **6**(7): p. 5820-5829.
391. Khan, M.I., et al., *Induction of ROS, mitochondrial damage and autophagy in lung epithelial cancer cells by iron oxide nanoparticles.* Biomaterials, 2012. **33**(5): p. 1477-88.
392. Ha, S.W., M.N. Weitzmann, and G.R. Beck, Jr., *Bioactive silica nanoparticles promote osteoblast differentiation through stimulation of autophagy and direct association with LC3 and p62.* ACS Nano, 2014. **8**(6): p. 5898-910.
393. Peynshaert, K., et al., *Exploiting Intrinsic Nanoparticle Toxicity: The Pros and Cons of Nanoparticle-Induced Autophagy in Biomedical Research.* Chemical Reviews, 2014. **114**(15): p. 7581-7609.
394. Khan, M.I., et al., *Induction of ROS, mitochondrial damage and autophagy in lung epithelial cancer cells by iron oxide nanoparticles.* Biomaterials, 2012. **33**(5): p. 1477-1488.
395. Periyasamy-Thandavan, S., et al., *Autophagy: molecular machinery, regulation, and implications for renal pathophysiology.* American Journal of Physiology-Renal Physiology, 2009. **297**(2): p. F244-F256.

396. Kherlopian, A.R., et al., *A review of imaging techniques for systems biology.* Bmc Systems Biology, 2008. **2**.
397. van der Zwaag, D., et al., *Super Resolution Imaging of Nanoparticles Cellular Uptake and Trafficking.* Acs Applied Materials & Interfaces, 2016. **8**(10): p. 6391-6399.
398. Buchner, T., et al., *Biomolecular environment, quantification, and intracellular interaction of multifunctional magnetic SERS nanoprobes.* Analyst, 2016. **141**(17): p. 5096-5106.
399. Lengyel, J.S., J.L.S. Milne, and S. Subramaniam, *Electron tomography in nanoparticle imaging and analysis.* Nanomedicine, 2008. **3**(1): p. 125-131.
400. Chiappi, M., et al., *Cryo-soft X-ray tomography as a quantitative three-dimensional tool to model nanoparticle:cell interaction.* Journal of Nanobiotechnology, 2016. **14**.
401. Gibbs-Flournoy, E.A., et al., *Darkfield-Confocal Microscopy detection of nanoscale particle internalization by human lung cells.* Particle and Fibre Toxicology, 2011. **8**.
402. Tkachenko, A.G., et al., *Multifunctional gold nanoparticle-peptide complexes for nuclear targeting.* J Am Chem Soc, 2003. **125**(16): p. 4700-1.
403. Sun, W., et al., *Endocytosis of a single mesoporous silica nanoparticle into a human lung cancer cell observed by differential interference contrast microscopy.* Analytical and Bioanalytical Chemistry, 2008. **391**(6): p. 2119-2125.
404. Luo, Y., et al., *Wavelength-Dependent Differential Interference Contrast Microscopy: Multiplexing Detection Using Nonfluorescent Nanoparticles.* Analytical Chemistry, 2010. **82**(15): p. 6675-6679.
405. Tse, Y.C., et al., *Identification of multivesicular bodies as prevacuolar compartments in Nicotiana tabacum BY-2 cells.* Plant Cell, 2004. **16**(3): p. 672-693.
406. Hemmerich, P.H. and A.H. von Mikecz, *Defining the Subcellular Interface of Nanoparticles by Live-Cell Imaging.* Plos One, 2013. **8**(4).
407. White R.A, K.K.J., Wampler J.E., *Fundamentals of Fluorescence Microscopy*, in *Topics in Fluorescence Spectroscopy*, L. J.R, Editor. 2002, Springer: Boston, MA.
408. Semwogerere, D.W., Eric, *Confocal Microscopy.* Encyclopedia of Biomaterials and Biomedical Engineering, 2005.
409. Rombouts, K., et al., *Effect of Covalent Fluorescence Labeling of Plasmid DNA on Its Intracellular Processing and Transfection with Lipid-Based Carriers.* Molecular Pharmaceutics, 2014. **11**(5): p. 1359-1368.
410. Kuhn, D.A., et al., *Different endocytotic uptake mechanisms for nanoparticles in epithelial cells and macrophages.* Beilstein Journal of Nanotechnology, 2014. **5**: p. 1625-1636.
411. Orsi, A., et al., *Dynamic and transient interactions of Atg9 with autophagosomes, but not membrane integration, are required for autophagy.* Molecular Biology of the Cell, 2012. **23**(10): p. 1860-1873.
412. Hell, S.W., *Microscopy and its focal switch.* Nature Methods, 2009. **6**(1): p. 24-32.
413. van der Zwaag, D., et al., *Super Resolution Imaging of Nanoparticles Cellular Uptake and Trafficking.* ACS Appl Mater Interfaces, 2016. **8**(10): p. 6391-9.
414. Brandenberger, C., et al., *Quantitative Evaluation of Cellular Uptake and Trafficking of Plain and Polyethylene Glycol-Coated Gold Nanoparticles.* Small, 2010. **6**(15): p. 1669-1678.
415. Gao, H.L., et al., *Ligand modified nanoparticles increases cell uptake, alters endocytosis and elevates glioma distribution and internalization.* Scientific Reports, 2013. **3**.
416. Goldstein, J.I., *Electron Beam-Specimen Interaction*, in *Practical Scanning Electron microscopy*, H.Z. J. I. Goldstein, Editor. 1975, Springer US. p. 49-94.
417. Hurbain, I. and M. Sachse, *The future is cold: cryo-preparation methods for transmission electron microscopy of cells.* Biology of the Cell, 2011. **103**(9): p. 405-420.

418. Wilson, S.M. and A. Bacic, *Preparation of plant cells for transmission electron microscopy to optimize immunogold labeling of carbohydrate and protein epitopes.* Nature Protocols, 2012. **7**(9): p. 1716-1727.
419. Thompson, R.F., et al., *An introduction to sample preparation and imaging by cryo-electron microscopy for structural biology.* Methods, 2016. **100**: p. 3-15.
420. Ostrowski, A., et al., *Overview about the localization of nanoparticles in tissue and cellular context by different imaging techniques.* Beilstein Journal of Nanotechnology, 2015. **6**: p. 263-280.
421. Dubochet, J., et al., *Cryo-Electron Microscopy of Vitrified Biological Specimens.* Trends in Biochemical Sciences, 1985. **10**(4): p. 143-146.
422. Dubochet, J., et al., *Cryo-Electron Microscopy of Vitrified Specimens.* Quarterly Reviews of Biophysics, 1988. **21**(2): p. 129-228.
423. Henderson, R., *Cryoprotection of Protein Crystals against Radiation-Damage in Electron and X-Ray-Diffraction.* Proceedings of the Royal Society B-Biological Sciences, 1990. **241**(1300): p. 6-8.
424. Marziale Milani, D.D., Francesco Tatu, *How to study biological samples by FIB/SEM?* Modern Reseach and Educational Topics in Microscopy., 2007.
425. Schneider, G., et al., *Cryo X-ray microscope with flat sample geometry for correlative fluorescence and nanoscale tomographic imaging.* Journal of Structural Biology, 2012. **177**(2): p. 212-223.
426. Delgado, F.F., et al., *Intracellular Water Exchange for Measuring the Dry Mass, Water Mass and Changes in Chemical Composition of Living Cells.* Plos One, 2013. **8**(7).
427. White , J., *Variation in water content of yeast cells caused by varying temperatures of growth and by other cultural conditions.* J. Inst. Brew., 1952. **58**: p. 47-50.
428. Wolter, H., *Spiegel systeme streifenden Einfalls als abbildende Optiken für Röntgenstrahlen.* Ann. Physik., 1952. **6**(10): p. 94-114.
429. Schneider, G., *Cryo X-ray microscopy with high spatial resolution in amplitude and phase contrast.* Ultramicroscopy, 1998. **75**(2): p. 85-104.
430. Chapman, H.N. and K.A. Nugent, *Coherent lensless X-ray imaging.* Nature Photonics, 2010. **4**(12): p. 833-839.
431. Sakdinawat, A. and D. Attwood, *Nanoscale X-ray imaging.* Nature Photonics, 2010. **4**(12): p. 840-848.
432. Nelson, J., et al., *High-resolution x-ray diffraction microscopy of specifically labeled yeast cells.* Proceedings of the National Academy of Sciences of the United States of America, 2010. **107**(16): p. 7235-7239.
433. Rose, M., et al., *Water window ptychographic imaging with characterized coherent X-rays.* Journal of Synchrotron Radiation, 2015. **22**: p. 819-827.
434. Giewekemeyer, K., et al., *Ptychographic coherent x-ray diffractive imaging in the water window.* Optics Express, 2011. **19**(2): p. 1037-1050.
435. Rodenburg, J.M. and H.M.L. Faulkner, *A phase retrieval algorithm for shifting illumination.* Applied Physics Letters, 2004. **85**(20): p. 4795-4797.
436. Deng, J.J., et al., *X-ray ptychographic and fluorescence microscopy of frozen-hydrated cells using continuous scanning.* Scientific Reports, 2017. **7**.
437. McDermott, G., M.A. Le Gros, and C.A. Larabell, *Visualizing Cell Architecture and Molecular Location Using Soft X-Ray Tomography and Correlated Cryo-Light Microscopy.* Annual Review of Physical Chemistry, Vol 63, 2012. **63**: p. 225-239.
438. Chiappi, M., et al., *Cryo-soft X-ray tomography as a quantitative three-dimensional tool to model nanoparticle:cell interaction.* J Nanobiotechnology, 2016. **14**: p. 15.
439. Perez-Berna, A.J., et al., *Structural Changes In Cells Imaged by Soft X-ray Cryo-Tomography During Hepatitis C Virus Infection.* ACS Nano, 2016. **10**(7): p. 6597-611.

440. Kapishnikov, S., et al., *Unraveling heme detoxification in the malaria parasite by in situ correlative X-ray fluorescence microscopy and soft X-ray tomography.* Scientific Reports, 2017. **7**.
441. Sorrentino, A., et al., *MISTRAL: a transmission soft X-ray microscopy beamline for cryo nano-tomography of biological samples and magnetic domains imaging.* Journal of Synchrotron Radiation, 2015. **22**: p. 1112-1117.
442. Zeng, X.H., et al., *Ellipsoidal and parabolic glass capillaries as condensers for x-ray microscopes.* Applied Optics, 2008. **47**(13): p. 2376-2381.
443. Bjeoumikhov, A., S. Bjeoumikhova, and R. Wedell, *Capillary optics in X-ray analytics.* Particle & Particle Systems Characterization, 2006. **22**(6): p. 384-390.
444. Carrascosa, J.L., et al., *Cryo-X-ray tomography of vaccinia virus membranes and inner compartments.* J Struct Biol, 2009. **168**(2): p. 234-9.
445. Werner, S., et al., *Towards high diffraction efficiency zone plates for X-ray microscopy.* Microelectronic Engineering, 2010. **87**(5-8): p. 1557-1560.
446. Hagen, C., et al., *Correlative VIS-fluorescence and soft X-ray cryo-microscopy/tomography of adherent cells.* Journal of Structural Biology, 2012. **177**(2): p. 193-201.
447. Frank, J., *Electron Tomograhy*. 2005, New York, NY 10013, USA: Springer.
448. Heymann, J.B., et al., *Computational resources for cryo-electron tomography in Bsoft.* Journal of Structural Biology, 2008. **161**(3): p. 232-242.
449. Heymann, J.B. and D.M. Belnap, *Bsoft: Image processing and molecular modeling for electron microscopy.* Journal of Structural Biology, 2007. **157**(1): p. 3-18.
450. Heymann, J.B., *Bsoft: Image and molecular processing in electron microscopy.* Journal of Structural Biology, 2001. **133**(2-3): p. 156-169.
451. Schneider, G., et al., *Three-dimensional cellular ultrastructure resolved by X-ray microscopy.* Nat Methods, 2010. **7**(12): p. 985-7.
452. Weiner, A., et al., *Vitrification of thick samples for soft X-ray cryo-tomography by high pressure freezing.* Journal of Structural Biology, 2013. **181**(1): p. 77-81.
453. Mayer, E., *New Method for Vitrifying Water and Other Liquids by Rapid Cooling of Their Aerosols.* Journal of Applied Physics, 1985. **58**(2): p. 663-667.
454. Mcdonald, K.L., *A review of high-pressure freezing preparation techniques for correlative light and electron microscopy of the same cells and tissues.* Journal of Microscopy-Oxford, 2009. **235**(3): p. 273-281.
455. Sun, W., et al., *Endocytosis of a single mesoporous silica nanoparticle into a human lung cancer cell observed by differential interference contrast microscopy.* Analytical and Bioanalytical Chemistry, 2008. **391**(6 %@ 1618-2650): p. 2119-2125.
456. Mehta, S.B. and C.J.R. Sheppard, *Partially coherent image formation in differential interference contrast (DIC) microscope.* Optics Express, 2008. **16**(24): p. 19462-19479.
457. Bewersdorff, T., et al., *The influence of surface charge on serum protein interaction and cellular uptake: studies with dendritic polyglycerols and dendritic polyglycerol-coated gold nanoparticles.* International Journal of Nanomedicine, 2017. **12**: p. 2001-2019.
458. Duke, E.M., et al., *Imaging endosomes and autophagosomes in whole mammalian cells using correlative cryo-fluorescence and cryo-soft X-ray microscopy (cryo-CLXM).* Ultramicroscopy, 2014. **143**: p. 77-87.
459. Palade, G.E., *A Small Particulate Component of the Cytoplasm.* Anatomical Record, 1954. **118**(2): p. 432-433.
460. Nanney, L.B., et al., *Visualization of Epidermal Growth-Factor Receptors in Human-Epidermis.* Journal of Investigative Dermatology, 1984. **82**(2): p. 165-169.
461. Piper, R.C. and J.P. Luzio, *Late endosomes: Sorting and partitioning in multivesicular bodies.* Traffic, 2001. **2**(9): p. 612-621.

462. Mullock, B.M., et al., *Fusion of lysosomes with late endosomes produces a hybrid organelle of intermediate density and is NSF dependent.* Journal of Cell Biology, 1998. **140**(3): p. 591-601.
463. Grant, B.D. and J.G. Donaldson, *Pathways and mechanisms of endocytic recycling.* Nature Reviews Molecular Cell Biology, 2009. **10**(9): p. 597-608.
464. Mizushima, N., T. Yoshimori, and B. Levine, *Methods in mammalian autophagy research.* Cell, 2010. **140**(3): p. 313-26.
465. Wang, R., et al., *Stellettin B Induces G1 Arrest, Apoptosis and Autophagy in Human Non-small Cell Lung Cancer A549 Cells via Blocking PI3K/Akt/mTOR Pathway.* Sci Rep, 2016. **6**: p. 27071.
466. Klionsky, D.J., et al., *Guidelines for the use and interpretation of assays for monitoring autophagy (3rd edition).* Autophagy, 2016. **12**(1): p. 1-222.
467. Duke, E.M.H., et al., *Imaging endosomes and autophagosomes in whole mammalian cells using correlative cryo-fluorescence and cryo-soft X-ray microscopy (cryo-CLXM).* Ultramicroscopy, 2014. **143**: p. 77-87.
468. Mizushima, N., Y. Ohsumi, and T. Yoshimori, *Autophagosome formation in mammalian cells.* Cell Structure and Function, 2002. **27**(6): p. 421-429.
469. Mizushima, N., *Autophagy: process and function.* Genes Dev, 2007. **21**(22): p. 2861-73.
470. Zhang, J.X., et al., *Systematic investigation on the intracellular trafficking network of polymeric nanoparticles.* Nanoscale, 2017. **9**(9): p. 3269-3282.
471. Jovic, M., et al., *The early endosome: a busy sorting station for proteins at the crossroads.* Histology and Histopathology, 2010. **25**(1): p. 99-112.
472. Schneider, T., et al., *Influence of dendritic polyglycerol sulfates on knee osteoarthritis: an experimental study in the rat osteoarthritis model.* BMC Musculoskelet Disord, 2015. **16**: p. 387.
473. Behrendt, M., et al., *Imaging and organelle distribution of fluorescent InGaP/ZnS nanoparticles in glial cells.* Nanomedicine, 2009. **4**(7): p. 747-761.
474. Jacquier, N., et al., *Lipid droplets are functionally connected to the endoplasmic reticulum in Saccharomyces cerevisiae.* Journal of Cell Science, 2011. **124**(14): p. 2424-2437.
475. Ohsaki, Y., et al., *Lipid droplets are arrested in the ER membrane by tight binding of lipidated apolipoprotein B-100.* Journal of Cell Science, 2008. **121**(14): p. 2415-2422.
476. Thiam, A.R., R.V. Farese, and T.C. Walther, *The biophysics and cell biology of lipid droplets.* Nature Reviews Molecular Cell Biology, 2013. **14**(12): p. 775-786.
477. Zhang, H.N., et al., *Proteome of Skeletal Muscle Lipid Droplet Reveals Association with Mitochondria and Apolipoprotein A-I.* Journal of Proteome Research, 2011. **10**(10): p. 4757-4768.
478. Corbo, C., et al., *The impact of nanoparticle protein corona on cytotoxicity, immunotoxicity and target drug delivery.* Nanomedicine, 2016. **11**(1): p. 81-100.
479. Luzio, J.P., P.R. Pryor, and N.A. Bright, *Lysosomes: fusion and function.* Nat Rev Mol Cell Biol, 2007. **8**(8): p. 622-32.
480. Rink, J., et al., *Rab conversion as a mechanism of progression from early to late endosomes.* Cell, 2005. **122**(5): p. 735-749.
481. Galluzzi, L., et al., *Cell death modalities: classification and pathophysiological implications.* Cell Death and Differentiation, 2007. **14**(7): p. 1237-1243.
482. Chen, Z.Z., et al., *Sandwich-Type Au-PEI/DNA/PEI-Dexa Nanocomplex for Nucleus-Targeted Gene Delivery in Vitro and in Vivo.* Acs Applied Materials & Interfaces, 2014. **6**(16): p. 14196-14206.
483. Lam, A.P. and D.A. Dean, *Progress and prospects: nuclear import of nonviral vectors.* Gene Therapy, 2010. **17**(4): p. 439-447.

484. Feldherr, C.M., D. Akin, and R.J. Cohen, *Regulation of functional nuclear pore size in fibroblasts.* Journal of Cell Science, 2001. **114**(24): p. 4621-4627.
485. Xu, J., W.D. Xiang, and F.T. Hu, *Preparation of monodisperse polystyrene spheres and inorganic porous films.* Rare Metal Materials and Engineering, 2008. **37**: p. 196-200.
486. Nitin, N., et al., *Tat Peptide Is Capable of Importing Large Nanoparticles Across Nuclear Membrane in Digitonin Permeabilized Cells.* Annals of Biomedical Engineering, 2009. **37**(10): p. 2018-2027.
487. Tammam, S.N., et al., *Chitosan Nanoparticles for Nuclear Targeting: The Effect of Nanoparticle Size and Nuclear Localization Sequence Density.* Molecular Pharmaceutics, 2015. **12**(12): p. 4277-4289.
488. Hinde, E., et al., *Pair correlation rnicroscopy reveals the role of nanoparticle shape in intracellular transport and site of drug release.* Nature Nanotechnology, 2017. **12**(1): p. 81-89.
489. Xia, T.A., et al., *Polyethyleneimine Coating Enhances the Cellular Uptake of Mesoporous Silica Nanoparticles and Allows Safe Delivery of siRNA and DNA Constructs.* Acs Nano, 2009. **3**(10): p. 3273-3286.
490. Ghavami, S., et al., *Autophagy and apoptosis dysfunction in neurodegenerative disorders.* Progress in Neurobiology, 2014. **112**: p. 24-49.
491. Rambold, A.S., S. Cohen, and J. Lippincott-Schwartz, *Fatty Acid Trafficking in Starved Cells: Regulation by Lipid Droplet Lipolysis, Autophagy, and Mitochondrial Fusion Dynamics.* Developmental Cell, 2015. **32**(6): p. 678-692.
492. van Bergeijk, P., C.C. Hoogenraad, and L.C. Kapitein, *Right Time, Right Place: Probing the Functions of Organelle Positioning.* Trends Cell Biol, 2016. **26**(2): p. 121-34.
493. He, B., *Viruses, endoplasmic reticulum stress, and interferon responses.* Cell Death Differ, 2006. **13**(3): p. 393-403.
494. Ziegler, U. and P. Groscurth, *Morphological features of cell death.* News in Physiological Sciences, 2004. **19**: p. 124-128.
495. Fanizza, C., et al., *Human epithelial cells exposed to functionalized multiwalled carbon nanotubes: interactions and cell surface modifications.* Journal of Microscopy, 2015. **259**(3): p. 173-184.
496. Perez-Gil, J. and T.E. Weaver, *Pulmonary surfactant pathophysiology: current models and open questions.* Physiology (Bethesda), 2010. **25**(3): p. 132-41.
497. Weaver, T.E. and J.J. Conkright, *Functions of surfactant proteins B and C.* Annual Review of Physiology, 2001. **63**: p. 555-578.
498. Rambold, A.S., S. Cohen, and J. Lippincott-Schwartz, *Fatty acid trafficking in starved cells: regulation by lipid droplet lipolysis, autophagy, and mitochondrial fusion dynamics.* Dev Cell, 2015. **32**(6): p. 678-92.
499. Beyerle, A., et al., *Toxicity Pathway Focused Gene Expression Profiling of PEI-Based Polymers for Pulmonary Applications.* Molecular Pharmaceutics, 2010. **7**(3): p. 727-737.
500. Neamnark, A., et al., *Aliphatic Lipid Substitution on 2 kDa Polyethylenimine Improves Plasmid Delivery and Transgene Expression.* Molecular Pharmaceutics, 2009. **6**(6): p. 1798-1815.
501. Fernandes, J.C., et al., *Linear polyethylenimine produced by partial acid hydrolysis of poly(2-ethyl-2-oxazoline) for DNA and siRNA delivery in vitro.* International Journal of Nanomedicine, 2013. **8**: p. 4091-4102.
502. Shang, J. and X.H. Gao, *Nanoparticle counting: towards accurate determination of the molar concentration.* Chemical Society Reviews, 2014. **43**(21): p. 7267-7278.
503. Heymann, J.B., *Bsoft: An integrated rational approach to software development for structural biology.* Biophysical Journal, 2001. **80**(1): p. 322A-+.

504. Schneider, C.A., W.S. Rasband, and K.W. Eliceiri, *NIH Image to ImageJ: 25 years of image analysis.* Nature Methods, 2012. **9**(7): p. 671-675.
505. Messaoudil, C., et al., *TomoJ: tomography software for three-dimensional reconstruction in transmission electron microscopy.* Bmc Bioinformatics, 2007. **8**.
506. Fleischer, C.C. and C.K. Payne, *Nanoparticle surface charge mediates the cellular receptors used by protein-nanoparticle complexes.* J Phys Chem B, 2012. **116**(30): p. 8901-7.
507. Fleischer, C.C. and C.K. Payne, *Secondary structure of corona proteins determines the cell surface receptors used by nanoparticles.* J Phys Chem B, 2014. **118**(49): p. 14017-26.
508. Lunov, O., et al., *Differential Uptake of Functionalized Polystyrene Nanoparticles by Human Macrophages and a Monocytic Cell Line.* Acs Nano, 2011. **5**(3): p. 1657-1669.
509. Doorley, G.W. and C.K. Payne, *Nanoparticles act as protein carriers during cellular internalization.* Chemical Communications, 2012. **48**(24): p. 2961-2963.

TABLE OF FIGURES

TABLE OF TABLES

ACKNOWLEDGEMENTS

My doctoral study has been a great journey and I benefited from the help of many people during this journey. I would like to mention some of them. I would like to express my sincere gratitude to my advisors Prof. Dr. Schneider and Prof. Dr. Ballauff for providing me the opportunity to pursue a doctoral degree within a wonderful scientific environment with cutting-edge techniques. Together with my colleague Dr. James McNally, they have provided me continuous guidance and wisdom during my doctoral studies. My colleagues especially Dr. Stephan Werner, Dr. Peter Guttmann, Dr. Sergey Kapishnikov, Alexandra Gräbert, Dr. Stefan Rehbein, and Dr. Katja Henzler have always supported me scientifically and personally. Thanks to my advisors and colleagues, performing this interdisciplinary project has been educational, fulfilling and fun. Thanks to their supports, I grew intellectually and emotionally.

I also received great support from the beamline scientists of ALBA, especially Eva Pereiro, Ana Perez and Tanja Ducic for cryo-SXT data collection. It was very fun to work with them. I also thank group of Prof. Dr. Rainer Haag at Freie Universität and group of Prof. Dr. Miriam Breunig at University of Regensburg for their collaboration in analysis of the cellular interactions of nanoparticles. I would also like to thank Prof. Dr. Helge Ewers and Prof. Janina Kneipp for their insightful comments and encouragements.

This thesis work was financially supported by Helmholtz Zentrum Berlin (HZB) and School of Analytical Sciences Adlershof (SALSA). Additionally, my beamtime in ALBA Syncrothon was funded by BioStruct-X. Many thanks also go to the administrative staff in HZB and SALSA for their continuous efforts to provide wonderful working conditions.

I would like to thank my dear friends, Evelyn, Shun, Gregor, Martin, Richard, Nahla, Sasha, Dimitra, Dorota, Benita, Recep, Xinpei, Cansu and Gauri for their support and patience. I would also like to thank my family and sister for their support and love.

‘I declare that I have produced this doctor’s thesis independently using only the tools I have specified, in accordance with section 7 para. 3 of the Faculty of Mathematics and Natural Sciences PhD regulations, published in the Official Gazette of Humboldt-Universität zu Berlin (Amtliches Mitteilungsblatt) no. 126/2014 on 18/11/2014.

I have not applied for a doctoral degree in the doctoral subject of Chemistry elsewhere and do not hold a doctoral degree in the doctoral subject of Chemistry.

I have taken due note of the Faculty of Mathematics and Natural Sciences PhD Regulations, published in the Official Gazette of Humboldt-Universität zu Berlin (Amtliches Mitteilungsblatt) no. 126/2014 on 18/11/2014.’